

012

CCM-80-24

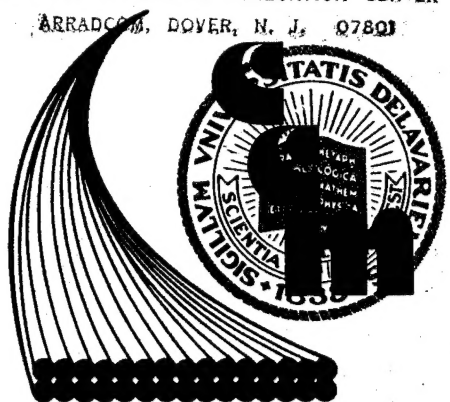
Center for Composite Materials

THE INFLUENCE OF EXTERNAL PLASTICIZERS
ON THE LONG TERM PERFORMANCE
OF CARBON FIBER COMPOSITE MATRICES

DATA QUALITY INSPECTED BY KENNETH R. MAY

DEPARTMENT OF DEFENSE
PLASTICS TECHNICAL EVALUATION CENTER
ARRADCOM, DOVER, N. J. 07801

19960215 069



**College of Engineering
University of Delaware
Newark, Delaware**

DISTRIBUTION STATEMENT
Approved for public release
Distribution Unlimited

PLASTIC 39407

THE INFLUENCE OF EXTERNAL PLASTICIZERS
ON THE LONG TERM PERFORMANCE
OF CARBON FIBER COMPOSITE MATRICES

By

Kenneth R. May

Sponsored By

Department of the Navy
Naval Air Development Center
Warminster, Pennsylvania

Issued By

Center for Composite Materials
University of Delaware
Newark, Delaware

December, 1980

ABSTRACT

Fiber reinforced polymeric composites intended for structural applications are expected to suffer exposure to a variety of plasticizing solvents which can degrade their long term mechanical performance. Procedures are reported for characterizing and predicting the influence of such external plasticizing agents on the viscoelastic behavior of high performance carbon fiber reinforced epoxy composites. Primary attention was directly focused on characterizing the behavior of the polymeric component.

Plasticization effects were examined for typical components of a stripping solvent (e.g., phenol, methylene chloride, water) as well as combinations of the components. The qualitative influence of the plasticization agent was determined from weight gain, swelling, and the time required for perceptible color changes to occur. Quantitative effects were determined by comparing the viscoelastic properties of the exposed resin to unexposed control specimens.

It was shown that phenol caused serious degradation at elevated temperatures. Water caused appreciable degrada-

tion while the isolated methylene chloride component caused only minor degradation. A mixture of phenol, water and methylene chloride with a small amount of surfactant proved to be the most aggressive solvent system considered. Further studies are suggested to identify the nature of this synergistic effect.

Dynamic mechanical spectra, obtained from a Rheovibron (DDV-II-B), were shown to be a quantitative means of detecting plasticization effects. In particular, shifts in certain peaks of the loss tangent spectrum and characteristic changes in the loss compliance spectrum were shown to be sensitive indicators of degradation due to plasticization.

Long term mechanical behavior was characterized by standard creep measurements. These data demonstrated that the time-temperature superposition principle tends to underestimate creep response. A power law model was shown to overestimate creep response. These two models can serve to predict upper and lower limits which bracket creep response over extended periods of time.

TABLE OF CONTENTS

Abstract.	ii
List of Figuresviii
List of Tables.	xv
Acknowledgements.xvii
 Chapter 1. INTRODUCTION	 1
 Chapter 2. DEVELOPMENT OF ANALYTICAL MODELS . . .	 9
2.1 Creep Models	9
2.1.1 Introduction.	9
2.1.2 Linear Viscoelastic Models. . .	11
2.1.3 Nonlinear Viscoelastic Models .	17
2.2 Dynamic Mechanical Models.	19
2.3 The Prediction of Creep from Dynamic Mechanical Measurements.	24
 Chapter 3. EXPERIMENTAL PROCEDURES AND RESULTS. .	 28
3.1 Sample Preparation and Character- ization.	28
3.2 Creep Testing Procedures	38

3.3	Dynamic Mechanical Testing Procedures.	52
3.4	The Absorption of Paint Stripper Solvents	65
3.5	Characteristics of Desorption.	74
Chapter 4.	ANALYSIS OF THE CREEP RESULTS.	82
4.1	Introduction	82
4.2	Creep of the Virgin Resin.	84
4.2.1.A	General Trends.	84
4.2.1.B	Comparison of the Creep of the 3501-6 with Other Epoxy Resins.	106
4.2.2	The Application of Visco- elastic Models.	112
4.2.2.A	The Voigt-Kelvin Model.	114
4.2.2.B	Power Law Model	132
4.2.3	Time-Temperature Super- position.	138
4.3	The Creep of Plasticized 3501-6 Resin.	152
Chapter 5.	ANALYSIS OF THE DYNAMIC MECHANICAL TEST RESULTS	160
5.1	Introduction	160
5.2	Dynamic Mechanical Behavior of the Virgin Resin	162
5.3	Dynamic Mechanical Behavior of the Plasticized Resin.	185
5.3.1	Introduction.	185

5.3.2	Comparison of the Plasticized and Virgin Resin.	186
5.3.2.A	Paint Stripper MIL-81294. . .	186
5.3.2.B	Water-Phenol Solution	196
5.3.2.C	Absorption of Other Solvents.	204
5.3.3	Summary	214
Chapter 6.	CONCLUSIONS AND RECOMMENDATIONS. . . .	217
Symbols		230
References.		235
Appendix A.	SUMMARY OF DATA.	241
A.1	Creep Data	242
A.2	Dynamic Mechanical Data.	248
A.3	Results of the Tensile Test on the 3501-6 Resin	259
Appendix B.	DIAGRAMS OF EXPERIMENTAL APPARATUS . .	263
Appendix C.	SOLVENT ABSORPTION INTO THE 3501-6 RESIN.	266
Appendix D.	MASTER CURVE CONSTRUCTION.	274
D.1	Example Calculations	277
D.1.1	Vertical Shift Factor	277

D.1.2	Activation Energy, ΔH	280
D.2	Predicting Creep Behavior from Master Curves	281
Appendix E.	ERROR ANALYSIS	284
Appendix F.	EFFECTS OF AGING ON CREEP.	300
Appendix G.	COMPARISONS OF VISCOELASTIC MODELS . .	305

LIST OF FIGURES

Figure 2.1.2-1	Schematic diagram of the Voigt-Kelvin four parameter model. . . .	13
Figure 3.1-1	The approximate chemical structure of the 3501-6 epoxy resin: (a) tetraglycidyl amine linear polymer (b) DDS crosslinking agent . .	29
Figure 3.1-2	The chemical structure of the diglycidyl ether of bis-phenol A epoxy resins (DGEBA)	31
Figure 3.1-3	Diagram of the injection molding device	35
Figure 3.2-1	Diagram of creep apparatus	39
Figure 3.2-2	The room temperature creep of the 3501-6 resin	47
Figure 3.2-3	The creep of batch no. 6-29-79-00 at different temperatures.	49
Figure 3.2-4	The creep of the 3501-6 resin plasticized with water-phenol (50/50) vs. the virgin resin (same batch) at room temperature	51
Figure 3.3-1	Schematic diagram of the Rheovibron DDV-II-B.	53
Figure 3.3-2	Complex dynamic modulus of the 3501-6 virgin resin for two different specimens	60
Figure 3.3-3	The loss tangent of the 3501-6 virgin resin for two different specimens.	61

Figure 3.4-1	Water absorption into the 3501-6 resin.	69
Figure 3.4-2	Diagram of the immersion apparatus used to swell the 3501-6 resin . .	72
Figure 3.4-3	Water-phenol (50/50) absorption into the 3501-6 resin at 75°C. . .	73
Figure 3.5-1	The desorption of water-phenol (50/50) from the 3501-6 resin above room temperature	76
Figure 4.2.1-1	The creep of 3501-6 epoxy resin at room temperature vs. time.	86
Figure 4.2.1-2	Creep of 3501-6 epoxy resin at higher temperatures.	91
Figure 4.2.1-3	The room temperature creep of 3501-6 resin in the viscoelastic zone	92
Figure 4.2.1-4	Reduced creep compliance of 3501-6 resin at room temperature in the viscoelastic zone.	101
Figure 4.2.1-5	Long term reduced creep compliance of the 3501-6 resin at room temperature (different batches) . . .	102
Figure 4.2.1-6	Reduced compliance vs. time for batch no. 6-29-79-00 at three different temperatures in the viscoelastic zone	104
Figure 4.2.1-7	Reduced creep of the virgin resin at other temperatures.	105
Figure 4.2.1-8	The creep of tetraglycidyl amine epoxy resins at room temperature .	108
Figure 4.2.1-9	The creep of the 3501-6 resin vs. the 5208 resin above room temperature.	111

Figure 4.2.2-1	Representation of the Voigt-Kelvin model on different time coordinates.	117
Figure 4.2.2-2	The Voigt-Kelvin model vs. the creep data of the 3501-6 resin in the viscoelastic zone.	121
Figure 4.2.2-3	J_0 vs. temperature for all batches	123
Figure 4.2.2-4	J_1 vs. temperature for all batches	124
Figure 4.2.2-5	J_0 vs. temperature for batch 6-29-79-00	125
Figure 4.2.2-6	J_1 vs. temperature for batch 6-29-79-00	126
Figure 4.2.2-7	The representation of the power law model on different time coordinates.	133
Figure 4.2.2-8	The power law model vs. the creep data of the 3501-6 resin in the viscoelastic zone.	135
Figure 4.2.3-1	The creep curves of batch 6-29-79-00 shifted vertically for temperature. The reference temperature is 23°C.	142
Figure 4.2.3-2	The room temperature master creep curves for some tetraglycidyl amine epoxy resins and their composites	144
Figure 4.2.3-3	The Arrhenian type dependence of the shift factor, a_T , on temperature.	145
Figure 4.2.3-4	Comparison of various analytical models and the actual creep data vs. the master creep at room temperature.	150
Figure 4.3-1	The effect of water-phenol (50/50) plasticization on the long term creep of the 3501-6 resin . .	154

Figure 4.3-2	The transverse master creep curves of carbon fiber composites plasticized by water at room temperature	157
Figure 5.2-1	The complex dynamic modulus of the virgin resin at 11 hz: the mean virgin resin data was taken without any instrument improvements and batch no. 1-2-80-00 data was taken with improvements.	163
Figure 5.2-2	The loss tangent of the 3501-6 resin at 11 hz without improvements.	167
Figure 5.2-3	Tan Delta as a function of temperature for two independent tests on the 3501-6 resin.	174
Figure 5.2-4	The complex dynamic modulus vs. temperature for two independent tests on the 3501-6 resin.	175
Figure 5.2-5	The mean loss and storage modulus for the virgin 3501-6 resin.	178
Figure 5.2-6	The mean loss and storage compliances for the 3501-6 virgin resin.	180
Figure 5.3.2-1	The effect of paint stripper, MIL-81294, on the complex dynamic modulus of the 3501-6 resin.	188
Figure 5.3.2-2	The effect of the paint stripper, MIL-81294, on the loss tangent of the 3501-6 resin.	189
Figure 5.3.2-3	The effect of the paint stripper, MIL-81294, on the loss compliance of the 3501-6 resin.	190
Figure 5.3.2-4	The glass transition temperature as a function of the percentage weight gain, M, for MIL-81294 plasticization	194

Figure 5.3.2-5	The effect of water-phenol (50/50) on the complex dynamic modulus of the 3501-6 resin	198
Figure 5.3.2-6	The effect of water-phenol (50/50) on the loss tangent of the 3501-6 resin.	199
Figure 5.3.2-7	The effect of water-phenol (50/50) on the loss compliance of the 3501-6 resin	200
Figure 5.3.2-8	The glass transition temperature as a function of the percentage weight gain, M, for water-phenol plasticization	203
Figure 5.3.2-9	The effect of methylene chloride on the loss compliance of the 3501-6 resin	206
Figure 5.3.2-10	The effect of water on the loss compliance of the 3501-6 resin . .	209
Figure 5.3.2-11	The effect of water-methylene chloride-phenol solution on the loss compliance of the 3501-6 resin.	212
Figure A.3-1	Stress-strain data for the tensile test on the Blake sample of the 3501-6 resin	261
Figure B-1	Right end and front view of the creep grips.	264
Figure B-2	Top view of the creep grips. . . .	265
Figure C-1	The absorption curves for the paint stripper and methylene chloride for the 3501-6 resin. . .	269
Figure C-2	The absorption curves for water-phenol at various temperatures. The saturation concentrations are: (29/71) at 25°C, (33/67) at 40°C, (50/50) at 64°C	270

Figure D.1-1	Master creep curve for the 3501-6 resin ($T_0 = 23^\circ\text{C}$)	276
Figure D.2-1	The creep of the virgin resin at 116°C versus the prediction of the master curve	283
Figure E-1	Worst case misalignment for the maximum strain error in creep experiments.	288
Figure E-2	Two computations for the value of the force constant, K , for the 3501-6 resin (tests without improvements).	295
Figure E-3	The computation for the value of the force constant, K , for the 3501-6 resin (tests with the new improvements).	296
Figure F-1	The retardation time plotted against the aging time of the specimen	304
Figure F-2	The creep compliance at 60 sec. plotted against aging time	304
Figure G-1	Retardation time vs. temperature for all batches.	310
Figure G-2	The parallel dashpot viscosity vs. temperature for all batches. . . .	311
Figure G-3	The long term dashpot viscosity vs. temperature for all batches. .	312
Figure G-4	Retardation time vs. temperature for batch 6-29-79-00	313
Figure G-5	The parallel dashpot viscosity vs. temperature for batch 6-29-79-00 .	314
Figure G-6	The long term viscosity vs. temperature for batch 6-29-79-00. . .	315

Figure G-7	The Voigt-Kelvin model vs. the creep data of the 3501-6 resin over the entire time range of the test	317
Figure G-8	The power law model vs. the creep data of the 3501-6 resin over the entire time range of the test. . .	319

LIST OF TABLES

Table 3.1-1	Physical Properties of the 3501-6 Resin at 25°C	37
Table 3.2-1	List of Creep Tests Performed on the 3501-6 Resin.	42
Table 3.3-1	List of Dynamic Mechanical Experiments.	64
Table 3.5-1	Results of the Experimental Simulation Desorption Tests	77
Table 4.2.2-1	Parameters of the Voigt-Kelvin Model	119
Table 4.2.2-2	Parameters of the Power Law Model	134
Table 4.2.3-1	Activation Energies of the Arrhenian Type Equation	148
Table 5.2-1	Room Temperature Tensile Moduli for the 3501-6 Resin.	170
Table 5.2-2	Summary of the Dynamic Mechanical Testing Results	184
Table A-1	Run Numbers of the Creep Experiments	243
Table A-2	Experimental Creep Data	244
Table A-3	Run Numbers of the Dynamic Mechanical Experiments	250
Table A-4	Dynamic Mechanical Data of the Virgin Resin.	251
Table A-5	Dynamic Mechanical Data of the MIL-81294 Plasticized Resin	255

Table A-6	Dynamic Mechanical Data of All Other Plasticized Resins	257
Table C-1	Summary of Absorption Tests	267
Table E-1	Data for the Sample Calculation of the Fixed Experimental Error in the Dynamic Modulus	298
Table F-1	Age of Room Temperature Creep Specimens	302
Table G-1	Summary of F-Score Tests.	308

ACKNOWLEDGEMENTS

This work was funded by the Naval Air Development Center in Warminster, Pennsylvania, and this report has been issued by the Center for Composite Materials, University of Delaware. In addition, the donation of two quarts of the 3501-6 epoxy resin by Hercules Incorporated of Wilmington, Delaware is greatly appreciated.

CHAPTER 1

INTRODUCTION

The expanded use of epoxy polymers as a matrix for carbon fiber composites has led to an increasing interest in the evaluation of their mechanical properties. The advanced composites are primarily used for structural applications in high performance military aircraft which experience a broad range of thermal, stress, and solvent environments. The composite must be resistant to these environments like the heavier metal parts they replace. Many of the static stiffness, strength, and thermal characteristics of the composite and the resin have been determined already. However, research into the effect of solvent plasticization on the mechanical properties has been limited to water. The variation of the tensile, shear, and flexural properties with different levels of moisture absorption has been well documented in a general review by Springer (1979). The time dependent behavior of the composite and the resin has been characterized to a lesser extent, but rarely has the effect of the external plasticization on these time-dependent properties been investigated. The

term external plasticization is used to denote the absorption of an external solvent which implies a degradation of the properties of the absorbent. In the case of composites, exposure to solvents (ranging from atmospheric moisture to stripping solvents which remove paint from aircraft) usually swells the composite by diffusing into the epoxy resin matrix thereby diminishing its mechanical properties. In the available reports, the investigation has centered around the properties of the composite and not the resin. The investigation presented in this thesis is intended to fill part of a void in the existing knowledge of the effect of external plasticizers on the long term performance of epoxy resins. The long term performance of a particular neat resin, the Hercules 3501-6 resin used in the AS/3501-6 carbon fiber composite, is characterized by the time-dependent variables of creep and dynamic mechanical testing.

Two objectives were identified and attained. The first objective was to document and analyze the creep behavior of the 3501-6 resin. The accumulated creep data not only provided information necessary for design applications of the resin, but it also provided the ability to project the creep behavior of other epoxy resins used in carbon fiber composites. The 3501-6 resin is representative of a unique class of polymers which provide high strength and excellent thermal properties. These resins are superior to

other common epoxy resins used for adhesive and molding applications. The chemical structure of the two types of epoxy resins is different. These differences are described in section 3.1. Many previous works on the creep of the carbon fiber matrix resins presented the data, but did not analyze the creep behavior. The second objective concerned the measuring of the changes in the time-dependent properties of the creep and dynamic mechanical behavior of the resin caused by the plasticization of external solvents. The changes in the creep and dynamic mechanical behavior of the resin are related to the microstructural changes in the network. A basic understanding of the viscoelastic behavior of the resin is achieved by monitoring the transition in the dynamic mechanical properties with increasing temperature. The transitions (see sections 3.3 and 5.2) in the properties are particularly sensitive to certain microstructural rearrangements in the resin, especially when the resin is plasticized. In addition, this work provides data which can be used to predict the performance of the composite under similar environmental conditions. The effects of external plasticization on the time-dependent properties of the composite manifest themselves through changes in the viscoelastic response of the resin phase. Under this view, the reinforcing fibers are simply load directors, inert to

the presence of the absorbed solvent. This view is particularly true of the transverse properties of the composite. Knowing the amount of change in the time-dependent properties of the resin caused by a particular solvent (at various levels of plasticization), the design engineer can make appropriate decisions on the structural applications of the composite.

The creep of the virgin resin was characterized for a variety of temperatures below the glass transition temperature. Before testing, the resin was cured and stored under conditions encountered by the composite system during fabrication. To simulate the normal storage environment of the composite, these practices enhanced the assumption that the creep of the virgin resin would simulate the creep of the resin in the composite. The creep testing of the virgin resin (i) provided a data base for the resin, (ii) determined the viscoelastic nature of the time-dependent properties, (iii) provided a comparison to the plasticized resin data, (iv) and provided an expectation on how the composite would perform under similarly stressed conditions.

The 3501-6 resin was plasticized to varying levels of absorption by a paint stripping solvent, MIL-81294, as suggested by the Naval Air Development Center (NADC) in

Warminster, Pennsylvania. Components of the stripping solvent were also used to plasticize the resin which provided an opportunity to examine the effects of plasticization by other solvents (chlorinated hydrocarbon, aromatic-protic, and long chain aliphatic solvents). Plasticized resin specimens were tested by dynamic mechanical methods using a commercially available Rheovibron DDV-II-B. All tests were performed at a constant frequency of 11 Hz and over a temperature range of 25° to 260°C. Characterizing the plasticized resin via dynamic mechanical experiments instead of creep experiments is preferred because of the shorter time needed to conduct an experiment on the Rheovibron. The virgin resin was also characterized by dynamic mechanical measurements so that a comparison to the plasticized resin results could be made (see section 5.2). The accomplishments of the dynamic mechanical testing of the plasticized resin were (i) the measurement of the degradation of the time-dependent properties of the resin, (ii) the determination of the qualitative effect on the static properties of the resin at room temperature, (iii) and which solvents plasticized the resin and to what degree.

A number of secondary considerations emerged as the investigation progressed. Among these were (i) the evaluation of the Rheovibron as an adequate method of determining

the effects of plasticization on the dynamic mechanical properties of polymers below their glass transition temperature (see section 5.3), (ii) a qualitative description of the diffusional characteristics (see appendix C) of a few solvents that absorb into the resin, (iii) and a review of the existing work on the creep and dynamic behavior of epoxy resins (see sections 4.2 and 5.2).

In chapter 2, a review of the viscoelastic models and equations used to analyze the time-dependent properties of creep and dynamic mechanical behavior is given. In section 2.1, two analytical models for the creep are presented, a linear viscoelastic and a nonlinear viscoelastic model. In section 2.2, the viscoelastic properties associated with dynamic mechanical testing are defined. In section 2.3, the connection between creep and dynamic mechanical behavior is explored.

In chapter 3, the experimental methods used to make resin specimens and to test them in creep and dynamic mechanical devices are presented. Section 3.1 reviews the chemistry and curing procedures of the 3501-6 resin. A list of its mechanical properties has also been compiled. In section 3.2, the procedures used to test the resin in creep tension are given. Some examples of the results are given; complete

data is given for all creep experiments in appendix A. A list of problems incurred during the creep testing and their solutions are provided. In section 3.3, the operating principles of dynamic mechanical testing on the Rheovibron model DDV-II-B are briefly reviewed. Examples of the experimental results are shown for a few cases, but the majority of the data and the results of the experiments on the plasticized resin are presented in sections 5.2 and 5.3 and appendix A. In section 3.4, the procedures used to plasticize the resin are described. The absorption curves which result as an outgrowth of the search for a specific soaking routine are presented in appendix C. In section 3.5, the desorption of the solvents from the plasticized resin is explored. The problems of desorption during the experiments are discussed.

In chapters 4 and 5, the results of the creep and dynamic mechanical testing are discussed and analyzed. Conclusions regarding the effect of certain solvents on the time-dependent properties are also given. In section 4.2, the creep of the virgin resin is analyzed. The data is compared to the results of other researchers, and the data is fit to the analytical models of section 2.1. In section 4.3, the creep of the plasticized resin is presented based on the results of one long term creep experiment. In section 5.2,

the dynamic mechanical behavior of the virgin resin is discussed. One other investigation into the dynamic mechanical behavior of the 3501-6 resin has been performed (Carpenter, 1978). Those results are compared to the current work. In section 5.3, the dynamic mechanical behavior of the plasticized resin is presented using the data of section 5.2 as a comparison in order to measure the changes in the behavior. The changes in the time-dependent properties caused by the paint stripper and its components are presented. The raw data is compiled in appendix A.

CHAPTER 2

DEVELOPMENT OF ANALYTICAL MODELS

2.1 CREEP MODELS

2.1.1 INTRODUCTION

The creep behavior of a material characterizes the extent to which the material deforms as a function of time at a constant stress level. The information supplied by a creep test is directly useful for design purposes as well as fundamental studies concerning the viscoelastic nature of the material. Creep tests can be conducted in tension, compression, shear, and torsion. The creep tests performed in this work are all tension tests. An alternate time dependent test, stress relaxation, is the inverse of creep testing. A stress relaxation experiment measures force as a function of time at a constant strain level. These tests are complimentary in the sense that a knowledge of one behavior means the other can be predicted by methods described in section 2.3. Creep is preferred over stress relaxation because it is a much simpler test to conduct and it is directly applicable to design considerations.

The theory of time-dependent deformation under an imposed external stress is described in terms of viscoelastic flow. Viscoelasticity as applied to isotropic solid polymers is reviewed elsewhere (Flügge, 1975; Ferry, 1961). The time-dependent deformation, $\epsilon(t)$, is modeled by either linear or nonlinear viscoelastic models. One kind of linear viscoelastic model chosen to represent the creep behavior of the 3501-6 resin is based on a mechanical analogue of combinations of springs and dashpots. The spring represents an instantaneous elastic deformation represented by the Hookian spring modulus, E . The time-dependent deformation is related through the dashpot which represents a pure viscous flow exhibited in liquids. The viscosity of the dashpot is represented by η . Any combination of these springs and dashpots can be used to model the creep of most polymers. Where linear viscoelastic models are not satisfactory nonlinear models must be used. Nonlinear models are generally empirical because satisfactory theoretical models have not been developed. The linear and nonlinear models are respectively discussed in sections 2.1.2 and 2.1.3.

2.1.2 LINEAR VISCOELASTIC MODELS

A linear viscoelastic model uses the basic assumption of Boltzmann superposition (Billmeyer, 1969; Ferry, 1961; Bird, et al, 1977; Alfrey and Gurnee, 1967). Under this assumption, stresses caused by a past history of strains can be added together in order to define the stress at any time, t . Therefore, stresses can be determined by summing up a number of small step strains. In integral form, the Boltzmann superposition principle is defined as

$$\sigma(t) = - \int_{-\infty}^t E(t-t') \dot{\epsilon}(t') dt' \quad (2.1.2-1)$$

in which $E(t-t')$ is the relaxation modulus. This same principle can be applied to the strain by adding a number of small step stresses together. This last approach more closely approximates the creep experiment. The integration shown in equation 2.1.2-1 is accomplished by using the creep compliance, $J(t-t')$. In either approach, stress or strain can be modeled as a linear combination of past stresses or strains.

The simple model chosen to represent the linear viscoelastic creep of the epoxy resin was the four parameter

Voigt-Kelvin model. The model in terms of springs and dashpots is shown in figure 2.1.2-1 (Nielsen, 1974; Alfrey and Gurnee, 1967). The basic deformation due to creep is represented by the Voigt-Kelvin element consisting of the spring, E_1 , and the dashpot, η_1 , in parallel. The initial spring, E_0 , accounts for the instantaneous elastic deformation at zero time when the load is applied. The final dashpot, η_0 , accounts for a long term, pure viscous flow behavior. Usually the spring and dashpot models omit the final dashpot for crosslinked polymers, but for reasons pointed out later the dashpot was retained for the current study. The spring moduli are generally represented by the Hookian modulus, E_i . The modulus is the reciprocal of the compliance, J_i .

$$J_i = 1/E_i \quad (2.1.2-2)$$

The viscosity of the dashpot is represented by the symbol, η_i . The normal constitutive equation relating the rate of strain to the stress of the viscoelastic solid is

$$\sigma_i = \eta_i \dot{\epsilon}_i \quad (2.1.2-3)$$

Equation 2.1.2-3 represents all dashpots in the model.

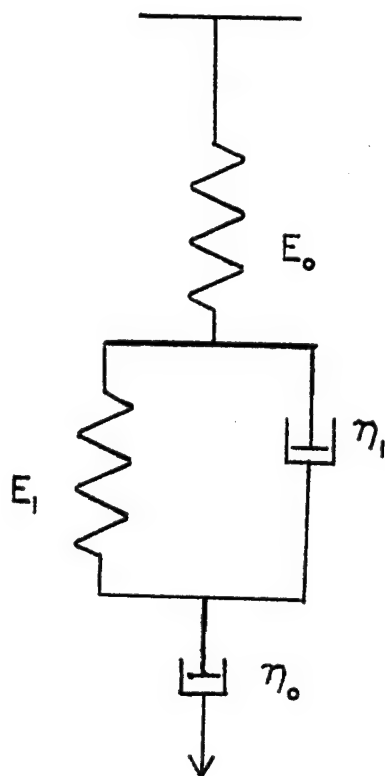


Figure 2.1.2-1 Schematic diagram of the Voigt-Kelvin four parameter model

To analytically represent the deformation of the entire model, the individual strains representing the three modes of deformation in series (the spring, E_0 , the spring and dashpot in parallel, and the dashpot, η_0) are summed according to the Boltzmann superposition principle (under a constant stress),

$$\epsilon(t) = \epsilon_1 + \epsilon_2 + \epsilon_3 . \quad (2.1.2-4)$$

The first term, ϵ_1 , is the instantaneous deformation of the material. The strain is related to a constant stress, σ_0 , through the modulus of the spring.

$$\epsilon_1 = J_0 \sigma_0 \quad (2.1.2-5)$$

In equation 2.1.2-5, the modulus, E_0 , has been replaced by its compliance, J_0 , as defined in equation 2.1.2-2 .

The deformation, ϵ_2 , must be determined from the spring and dashpot in parallel. Parallel terms indicate that constant strain (ϵ_2) is imposed on both components with the stress partitioned as follows:

$$\sigma_0 = \sigma_1 + \sigma_2 \quad (2.1.2-6)$$

where

$$\sigma_1 = \epsilon_2/J_1 \quad (2.1.2-7)$$

$$\sigma_2 = \eta_1 \dot{\epsilon}_2 \quad (2.1.2-8)$$

Solving these equations simultaneously yields

$$\epsilon_2 = J_1 \sigma_0 (1 - \exp(-t/\tau_1)) . \quad (2.1.2-9)$$

The retardation time, τ_1 , is the product of the dashpot viscosity and spring compliance,

$$\tau_1 = J_1 \eta_1 \quad (2.1.2-10)$$

The third deformation, ϵ_3 , is found by solving equation 2.1.2-3 . Parameter η_0 is the ultimate viscosity of the long term creep (linear creep).

$$\epsilon_3 = \sigma_0 t / \eta_0 \quad (2.1.2-11)$$

Adding the three strains together gives the final representation of the four parameter Voigt-Kelvin model. The stress, σ_0 , has been divided into the time-dependent

strain, $\varepsilon(t)$, to define the creep compliance, $J(t)$, in equation 2.1.2-12.

$$J(t) = \frac{\varepsilon(t)}{\sigma_0} = J_0 + J_1(1 - \exp(-t/\tau_1)) + t/\eta_0 \quad (2.1.2-12)$$

The model represented in equation 2.1.2-12 has only one retardation time, τ_1 . In actuality, a polymer has a distribution of relaxation times (Schultz, 1974; Nielsen, 1974; Alfrey and Gurnee, 1967). The total creep compliance represented by an infinite number of Voigt-Kelvin elements would have the following relationship:

$$J(t) = J_0 + \sum_i J_i(1 - \exp(-t/\tau_i)) + t/\eta_0 \quad (2.1.2-13)$$

The use of a single Voigt-Kelvin element can be viewed as an average element of the distribution of all elements. Consequently, the retardation time, τ_1 , is a mean retardation time of the entire distribution.

The four parameter Voigt-Kelvin model can be used to model the creep of many polymers (Nielsen, 1974). It applies, at least, for the creep at shorter times until a more complicated creep behavior (i.e. yielding, plastic flow) takes place. Nonlinear viscoelastic models must then be used to represent the creep behavior.

2.1.3 NONLINEAR VISCOELASTIC MODELS

If Boltzmann superposition holds, the strain is directly proportional to the stress. This is usually a very good assumption for the creep at low strain levels below the linear elastic limit of the polymer. At higher stresses which induce large strains beyond the elastic limit, the strain takes on a nonlinear dependence on the stress. For epoxy resins, the brittle nature of the tightly crosslinked network induces nonlinearity in the creep behavior at very low stress levels (10% of the ultimate tensile strength). A number of equations have been proposed to model nonlinear viscoelasticity (Nielsen, 1974), but most do not have a theoretical basis. In the simplest empirical form, nonlinear viscoelasticity can be modeled by a power law form such as the Nutting equation (Nutting, 1921; Nielsen, 1974),

$$\epsilon(t) = k\sigma^\beta t^n + \epsilon_0 \quad (2.1.3-1)$$

The stress and time are related to the strain through the temperature dependent parameters, β and n respectively. The constant k is also a function of temperature. The equation is simplified by grouping the term, $k\sigma^\beta$, into one constant for the material, D_1 . The constant is still a function of temperature.

$$J(t) = J_0 + D_1 t^n \quad (2.1.3-2)$$

where

$$D_1(T) = k(T) \sigma_0^{\beta}(T) / \sigma_0 \quad (2.1.3-3)$$

The final expression of the power law model in equation 2.1.3-2 is expressed in terms of compliance. The initial creep compliance is the term J_0 . The use of one constant, D_1 , avoids the problem of determining the power law dependence of stress on strain so that the number of parameters required to fit the creep data has been reduced to three rather than the four parameters used in the Voigt-Kelvin model. An attempt has been made by Schapery (1969) to give theoretical significance to the model. In the current work, the power law model will be used as an empirical equation for fitting the creep data. Since it has only three parameters, the model will not fit more complicated systems which exhibit yielding phenomena (i.e. semi-crystalline polymers) in their creep behavior.

2.2 DYNAMIC MECHANICAL MODELS

The dynamic mechanical testing performed on an instrument such as the Rheovibron DDV-II-B imposes an oscillating sinusoidal strain on a test specimen. The measured amplitude of the applied strain and stress yield the value of the complex dynamic modulus, $|E|$, calculated directly from the machine. The oscillation occurs at a constant frequency while temperature is varied. In actuality, the dynamic functions such as the dynamic modulus are dependent upon frequency and temperature. These functions defined in this section assume that frequency is constant (11 Hz); therefore, they are a function of temperature only.

A viscoelastic material will dissipate some of the energy provided by the oscillation of the test machine. Viscoelastic behavior of the polymer during cycling causes the strain to lag behind the stress by a phase angle, δ . A measure of the angle δ is given by the "loss tangent" or $\tan\delta$. If part of the stress is in phase with the strain and the rest of the stress is out of phase with the strain, the complex dynamic modulus has two vectorial components. The storage modulus, E_1 , is in phase with the applied strain and the loss modulus, E_2 , is out of phase with the applied strain. They are the real and imaginary components of the complex modulus,

$$E^* = E_1 + iE_2 . \quad (2.2-1)$$

The value of the complex dynamic modulus obtained from the Rheovibron is the magnitude of the vector:

$$|E| = ((E_1)^2 + (E_2)^2)^{1/2} \quad (2.2-2)$$

The values of the modulus can be computed from the knowledge of $|E|$ and $\tan\delta$, the measured variables; viz,

$$E_1 = |E| \cos\delta \quad (2.2-3a)$$

$$E_2 = |E| \sin\delta \quad (2.2-3b)$$

The ratio of loss and storage modulus (or compliance) gives the value of the loss tangent,

$$\tan\delta = E_2/E_1 = J_2/J_1 \quad (2.2-4)$$

For an elastic material where the phase angle or loss tangent is very small ($\tan\delta \approx \delta$), the storage modulus (or compliance) is approximately the same value as the complex dynamic modulus, $|E|$. This approximation is true for epoxy resins near room temperature well below their glass transition temperature (200° - 220°C).

Similarly, the complex compliance contains two components, the storage compliance, J_1 , and the loss compliance, J_2 ,

$$J^* = J_1 + iJ_2 \quad (2.2-5)$$

The compliance functions can be computed directly from the dynamic modulus and loss tangent data because the magnitude of the complex modulus is the reciprocal of the magnitude of the complex compliance. Equation 2.2-6b and equation 2.2-6c were used in the calculation of the storage and loss compliances from the loss tangent and dynamic modulus data.

$$|J| = 1/|E| \quad (2.2-6a)$$

$$J_1 = (1/|E|) \cos \delta \quad (2.2-6b)$$

$$J_2 = (1/|E|) \sin \delta \quad (2.2-6c)$$

Comparison of equations 2.2-3 through 2.2-5 shows that the storage or loss moduli are not the simple reciprocals of the storage or loss compliance. Consequently, the shapes of the plots of the dynamic spectra are quite different from each other. For very stiff materials where the loss tangent is very small ($\tan \delta < 10^{-2}$), the following approximation can be made:

$$J_1 \approx 1/E_1 \approx 1/|E| \quad (2.2-7)$$

This means that the loss compliance and the loss and storage modulus have the approximate relationship:

$$J_2 \approx E_2/(E_1)^2 \quad (2.2-8)$$

The approximation of small values of $\tan\delta$ is true for epoxy resins at temperatures below the glass transition. Since the loss compliance is dependent on the inverse square of the storage modulus, it will exhibit the greatest change over a similar temperature range. Since the loss compliance was the most sensitive to any changes in the resin, it was used primarily for comparing the plasticized and unplasticized dynamic mechanical behavior.

The dynamic viscoelastic functions provide a key to the understanding of the transitions occurring in a polymer with changing temperature at a constant frequency. As temperature is raised, the increased kinetic energy of the molecular segments enables them at one point to free themselves of steric entanglements by rotation or translation. The increased freedom of movement is recorded as a transitional peak in the loss tangent (Schultz, 1974). The most

common transitions are the glass transition and melting, but glassy polymers such as epoxy resins can exhibit other transitional peaks in the loss tangent at temperatures far below the glass temperature. These transitions correspond to an "unlocking" of certain portions of the molecular chain (Schultz, 1974; Bell and Murayama, 1969; Kenyon and Nielsen, 1967). The peak heights vary from half an order of magnitude in the loss tangent at lower temperatures to a few orders of magnitude at the glass transition. The loss compliance and loss modulus will also exhibit such peaks, but at different temperatures.

The loss peaks are related to the ability of the polymer to dissipate energy. The extra mobility of the chain segments obtained at a certain temperature and frequency generally indicates a greater viscous dampening of the material. The rate of energy dissipation can be calculated by the following relationship (Schultz, 1974),

$$\dot{W} = (\omega/2) f_0^2 (J_2) = (\omega/2) (f_0^2 / |E|) \sin \delta \quad (2.2-9)$$

where

ω = the frequency in radians, and

f_0 = the maximum amplitude of sinusoidal force.

Both the loss compliance and the sine of the phase angle are directly proportional to the rate of energy dissipation.

2.3 THE PREDICTION OF CREEP FROM DYNAMIC MECHANICAL MEASUREMENTS

Creep and stress relaxation behavior can be predicted if one of the dynamic mechanical functions is known. Creep and dynamic mechanical behavior are related through the retardation time spectrum for creep, $L(\tau)$, and the relaxation time spectrum for stress relaxation, $H(\tau)$, where

$$J(t) = \int_0^{\infty} L(\tau) (1 - \exp(-t/\tau)) d \ln \tau \quad (2.3-1a)$$

$$E(t) = \int_0^{\infty} H(\tau) (1 - \exp(-t/\tau)) d \ln \tau \quad (2.3-1b)$$

Many approximations and methods of computing the time spectra from raw data have been proposed, and they are summarized in Ferry (1961). To a first order approximation,

$$L(\tau) = [dJ(t)/d(\ln t)]_{t=\tau} \quad (2.3-2a)$$

$$H(\tau) = [dE(t)/d(\ln t)]_{t=\tau} \quad (2.3-2b)$$

Under this simplification, the distributions can be calculated directly from the creep and stress relaxation data by numerically determining the slope of the data plotted on a log time axis. Once one of the distributions is

known, the other can be calculated by using well known relationships (Schultz, 1974; Ferry, 1961).

The dynamic mechanical behavior of a polymer can also be used to determine the distribution time functions provided data over a wide range of frequencies is available. In this case, the data must be presented in terms of a frequency distribution, the only time related variable. Any of the functions described in section 2.2 can be used to construct $H(\tau)$ or $L(\tau)$ by using the first order approximations compiled by Ferry (1961). A few are given below (Schultz, 1974):

$$L(\tau) = -\frac{d(J_1)}{d(\ln\omega)} = J_2 + \frac{d(J_2)}{d(\ln\omega)} \quad (2.3-3a)$$

$$H(\tau) = \frac{d(E_1)}{d(\ln\omega)} = E_2 - \frac{d(E_2)}{d(\ln\omega)} \quad (2.3-3b)$$

The fact that these time distributions can be extracted from the dynamic mechanical data means that the creep and stress relaxation can be computed using equation 2.3-1. A complete creep curve can be predicted from a few short sinusoidal experiments; therefore, dynamic mechanical testing is preferred over creep testing from this point of view. Since strain levels are within the linear elastic

limit on the Rheovibron, the creep or stress relaxation holds for low values of stress only.

The above calculations hold for one temperature and the procedure would have to be repeated for every different temperature. Fortunately, an empirical tool known as time-temperature superposition mitigates this problem. For creep data, time-temperature superposition states that the creep of a polymer at one time and temperature is equal to the creep at a shorter time and higher temperature. By reduction of the compliance and time variables, a master curve for the polymer can be created which can predict the creep at any other time and temperature. The method does not presuppose a particular analytical form to the creep. It provides a way to extrapolate short term creep tests performed over a range of temperatures to longer times. The method is outlined more fully in section 4.2.3 and appendix D. A creep master curve can simply be transformed using equations 2.3-1 and 2.3-2 to give a stress relaxation master curve.

For the dynamic mechanical data, time-temperature superposition is applied to create a master curve of the reduced dynamic modulus, dynamic compliance, or any of its loss or storage functions plotted against a reduced

frequency. Using equations 2.3-3 and 2.3-1, creep and stress relaxation master curves can be predicted. Shifting to a higher temperature is equivalent to shifting to a lower frequency. A few experiments on the Rheovibron at different frequencies can give sufficient data to create a dynamic property master curve.

CHAPTER 3

EXPERIMENTAL PROCEDURES AND RESULTS

3.1 SAMPLE PREPARATION AND CHARACTERIZATION

The high performance 3501-6 epoxy resin used in the AS/3501-6 carbon fiber composite contains 0.25 pound of diaminodiphenyl sulfone (DDS) crosslinking agent per pound of the uncured resin. This mixture is the standard formulation of the resin as received from the supplier, Hercules, Inc., of Magna, Utah. The uncured resin is a tetraglycidyl amine epoxide which is crosslinked at the epoxide sites upon cure. A boron trifluoride (BF_3) type catalyst thermally initiates the crosslinking reaction near 135°C (275°F) (Carpenter, 1978). The approximate structure of the 3501-6 resin is shown in figure 3.1-1. The "R" group is confidential to the supplier. The structure shown in figure 3.1-1 is typical of all epoxy resins used by the Armed Forces in their carbon fiber composites. The choice of the "R" group and the crosslinking chemistry are the major differences between resins that are used in the epoxy matrix composites.

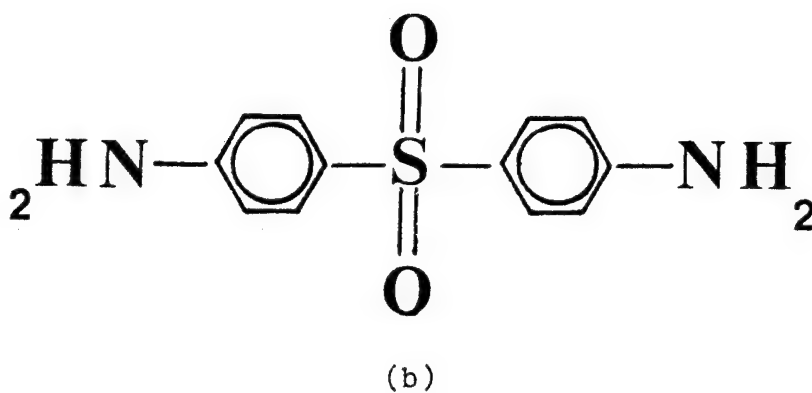
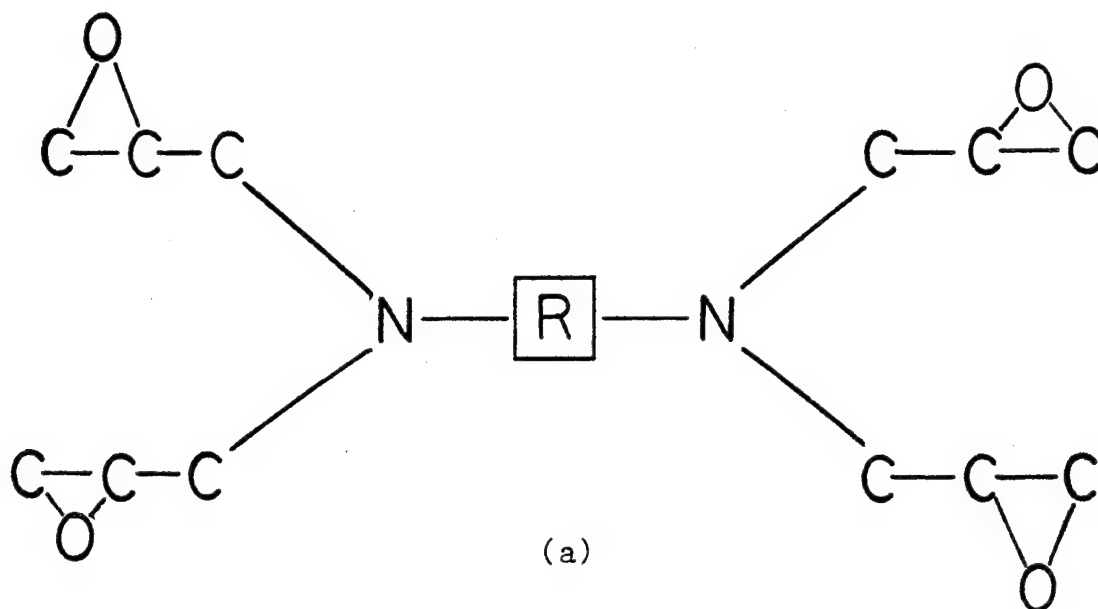


Figure 3.1-1 The approximate chemical structure of the 3501-6 epoxy resin:
 (a) tetraglycidyl amine linear polymer
 (b) DDS crosslinking agent

These epoxy resins will be referred to as tetraglycidyl amine resins. They are a clear choice for aircraft applications over the weaker and less thermally resistant diglycidyl ether of bis-phenol A epoxy resins (DGEBA). The structure of these resins is shown in figure 3.1-2. The origin of the higher performance properties of the tetraglycidyl amine epoxies stems from the tetra-functional amine groups which can form a tighter network than the di-functional DGEBA epoxy resin.

One half gallon of the 3501-6 resin was premixed by Hercules, packed in dry ice, and shipped to the University of Delaware. The resin was stored below -18°C in a refrigerator until portions of it were used for making test specimens. The resin is a one part system containing the uncured amine linear polymer, DDS crosslinking agent, catalyst, and diluents. At room temperature, the uncured resin is a dark, amber colored, brittle paste of extremely high viscosity. In order to process the resin, higher temperatures are needed to reduce the viscosity. Carpenter (1978) has measured the viscosity-temperature profile for the 3501-6 resin and he has found that the optimum temperature for processing occurs at a viscosity of a few hundred poise near 115°C (240°F). This was the temperature chosen for molding the resin. Only moderate pressures (500-2000 psi) were needed to force the resin into the mold.



Figure 3.1-2 The chemical structure of the diglycidyl ether of bis-phenol A epoxy resins (DGEBA)

Based on a personal communication with Dr. J. Augl (1979), Naval Surface Weapons Center, Silver Springs, Maryland, a curing procedure for the resin was devised in order to make creep and dynamic mechanical test specimens. These curing procedures are quite similar to those used by other investigators who have tested the mechanical properties of the 3501-6 resin. Minor differences in the curing procedures between various sources in the literature occur in the choice of the post-cure temperature. All investigations agree on initially curing the resin at 350°F for four hours. The procedures used to cure the resin and to make tensile creep and dynamic mechanical test specimens are listed below:

1. The resin was degassed of entrapped air in a bell jar under a vacuum of one torr (133 N/m^2).
2. The resin was poured into the settling chamber of the mold and allowed to sit for one half hour at 115°C in an oven at ambient pressure. The mold had been coated with a wax-like lubricating agent to prevent adhesion.
3. The resin was injected molded between parallel stainless steel plates using a brass piston to

force the resin from the settling chamber into the mold (see below). A hydraulic press which was preheated to 115°C provided the necessary force. The parallel plates were separated to the desired thickness by stainless steel shimstock. The thicknesses were 3.8×10^{-4} m (0.015 in) for creep specimens and 1.27×10^{-4} m (0.005 in) for dynamic mechanical test specimens.

4. The mold was placed in a forced convection oven and the resin was cured for four hours at $177 \pm 6^\circ\text{C}$ (350°F). Post-curing followed for eight hours at 191°C (375°F). The mold was oven cooled to room temperature afterwards.
5. The resulting square sheet (7 in (17.8 cm)) was cut on a water cooled diamond saw to the final specimen dimensions. The creep specimens were cut to 5.0×0.75 in ($0.13 \times 1.91 \times 10^{-2}$ m) and the dynamic mechanical test specimens were cut to 0.20×2.5 in ($5.0 \times 10^{-3} \times 0.064$ m). The cut specimens were given a five minute acetone bath to remove sawdust particles.

6. In the final step, the specimens were heated for 24 hr at 100°C removing any water or acetone that might have absorbed into the resin during the sawing procedure. The specimens were stored at room temperature and humidity until use.

The injection molding device was manufactured in the mechanical shop at the University of Delaware and it is shown in figure 3.1-3. The degassed resin was poured into channel A. A brass piston fitted with an O-ring squeezed the resin through the rectangular channel created by the separated stainless steel plates into channel B. The pressure was applied by a Wabash hydraulic press electrically preheated to 115°C. The mold was then removed from the press and placed in the oven for curing. Since both channels are open to the air, shrinking stresses occurring during the cure were alleviated through the channels A and B and not in the mold. The thickness of the uniform sheets were accurate to within one-thousandth of an inch (2.54×10^{-5} m) across the entire sheet leaving only a maximum variation in the thickness in any one specimen to less than 5×10^{-4} in (1.27×10^{-5} m). All measurements were made with a micrometer accurate to within 1×10^{-4} in.

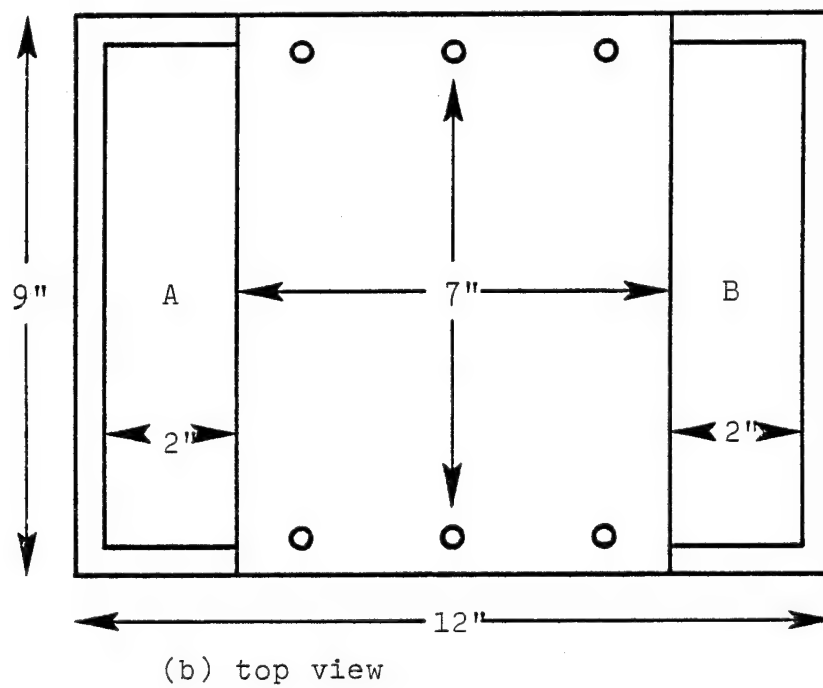
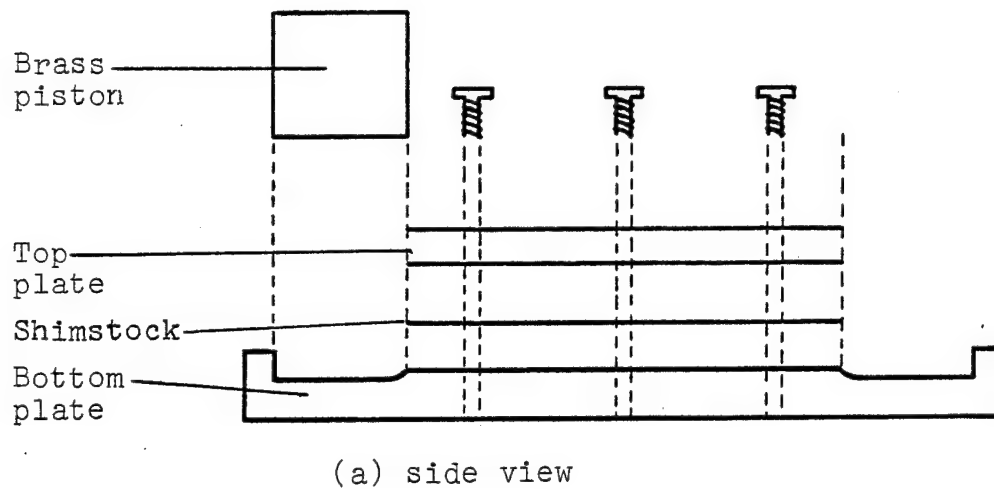


Figure 3.1-3 Diagram of the injection molding device

The test specimens were stored at room humidity in order to simulate the humid environment the resin in the composite would experience if stored for a long period of time at ambient conditions. Therefore, sufficient background moisture had a chance to absorb into the resin. The term "plasticization" refers to the absorption beyond the background moisture already present in the specimen at testing. Specimens were stored between one and six months before testing (see appendix F).

Direct chemical analysis of the resin was not permitted by a non-disclosure agreement between the author and Hercules, Inc. Since that agreement was signed, some information has been published by Carpenter (1978) and that source should be consulted for further details. The physical properties of the resin have been determined partly by the author and Dr. Augl (1978). Other published sources were not available. A summary of the properties of the 3501-6 resin appears in Table 3.1-1. The resin being an amorphous network solid, is isotropic and requires only two mechanical property descriptors to characterize it, viz., E and ν .

TABLE 3.1-1
PHYSICAL PROPERTIES OF THE 3501-6 RESIN AT 25°C

Property		Value
Tensile modulus, E	psi (GN/m ²)	6.5±0.3 × 10 ⁵ (4.48)
Shear modulus, G*	psi (GN/m ²)	2.25 × 10 ⁵ (1.55)
Poisson's ratio, ν*		0.38
Linear expansion coefficient, α	in/in-C ⁻¹	2.3±0.2 × 10 ⁻⁵
Density, ρ	g/cm ³	1.28±0.01
Ultimate tensile strength, σ _{max} *	psi (GN/m ²)	7.2 × 10 ³ (5.0 × 10 ⁻²)
Ultimate tensile strain, ε _{max} *		1.3%

*Source: Augl, J. M., 1978

3.2 CREEP TESTING PROCEDURES

Epoxy resin samples cut to the dimensions mentioned earlier were tested in tensile creep by applying a constant stress on the specimen and measuring the strain as a function of time. The test specimen was inserted into the creep grips designed by the author. These grips have a double tightening mechanism to prevent slippage during testing. A schematic diagram of the grips is shown in appendix B. A self-tightening pair of MTS grips were also used in a few experiments. The grips were fastened to a deadweight steel frame. Weights made of brass or steel were applied to the loading pan in order to provide a constant stress to the specimen. A schematic diagram of the apparatus is shown in figure 3.2-1. The small frame fit inside the forced convection oven where the temperature could be controlled to $\pm 1^\circ\text{C}$. The circulation of air was sufficient enough to keep the temperature near the specimen constant, but not enough to sway the grip-specimen-weight assembly. Room temperature testing was performed inside a closed oven, but the temperature was controlled by the room thermostat at $22.5 \pm 1^\circ\text{C}$. Humidity varied as the ambient conditions. Temperatures were measured by calibrated thermometers and iron-constantan thermocouples.

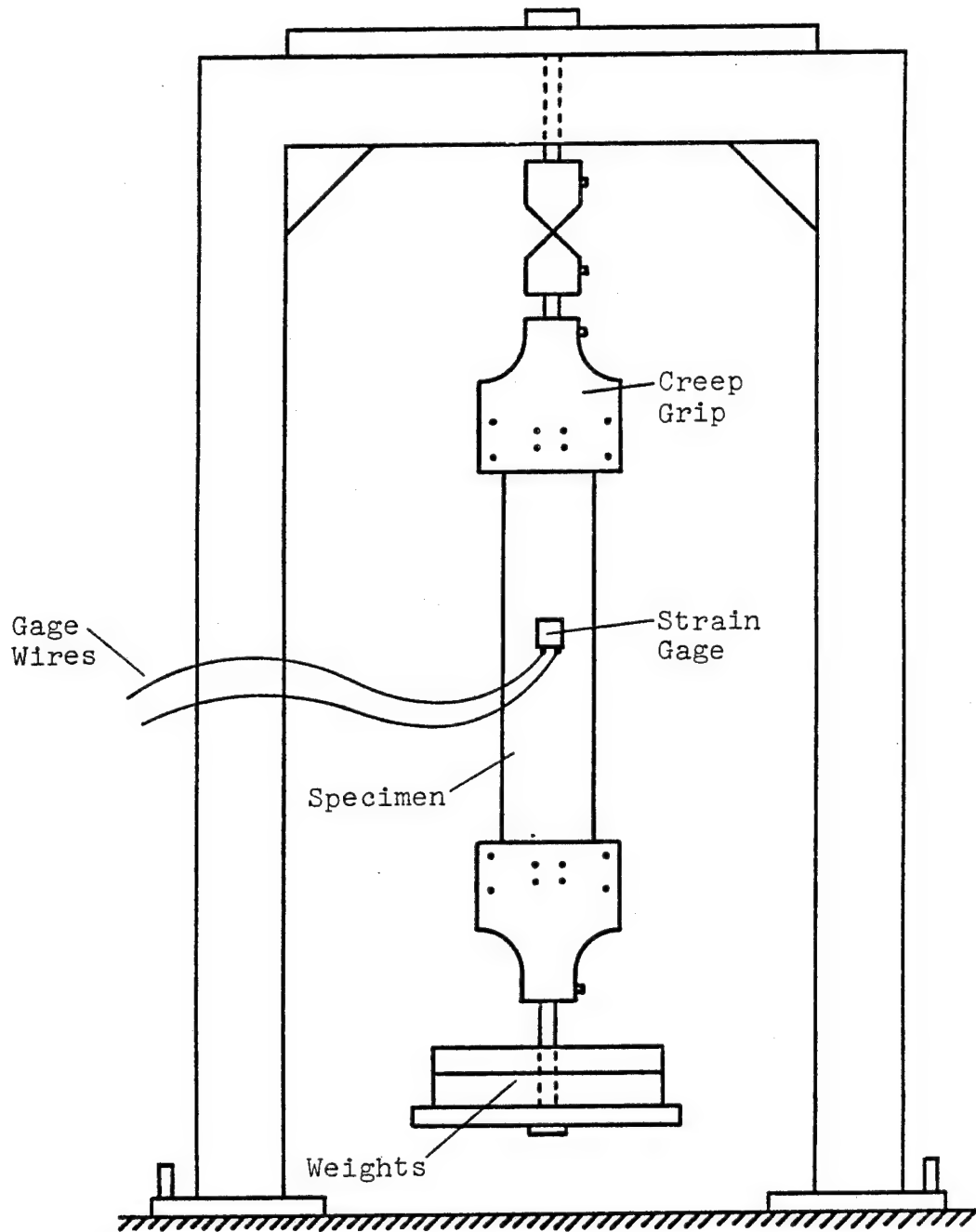


Figure 3.2-1 Diagram of creep apparatus

Strain was measured using series EA linear resistance (350 ohm) strain gages acquired from Micro-Measurements, Inc. These gages are capable of being used in a wide range of temperatures (-120°F to 350°F) for extended periods of time.

The gages were mounted onto the 3501-6 creep specimens using standard techniques developed by Micro-Measurements (1977). A high temperature epoxy adhesive, M-Bond[®] 600 was used to bond the gage directly to the specimen. To prevent oxidation, a polyimide coating, M-Coat[®] A, was applied to the gage and the wiring. The strain was measured on a portable P-350A Strain Indicator with an accompanying switch and balance unit, both marketed by Vishay Technology. Strain could be recorded to the nearest microstrain ($1 \mu\epsilon = 1 \times 10^{-6}$ in/in).

At the start of each experiment, the specimen was aligned in the grips and allowed to stabilize for 24 hours at the test conditions as suggested by the standard procedure, ASTM D674-56. To start the creep experiment (after calibrating and balancing the P-350A), weights were applied within a five second period. To let the sway from loading dampen out, the first measurement was taken at one minute. At higher temperatures, the first measurement was taken after two minutes. Thermocouple readings showed that the temperature in the oven rose back to its initial level within two minutes after the door had been opened. Since the epoxy resin is a

thermal insulator, it is doubtful that the short cooling "spike" would have altered the specimen temperature. Measurements were taken on the P-350A for every minute for the first five minutes, every five minutes for the first one-half hour, every ten or fifteen minutes up to two hours, every hour up to twelve hours, every six hours up to two days, and twice a day thereafter.

Eleven creep tests were run between room temperature ($22.5 \pm 1^\circ\text{C}$) and 116°C . The particulars on each test are compiled in table 3.2-1. The temperature, stress, and duration of each test is given. Reasons for choosing such a schedule are presented in section 4.2 along with the analysis of the data.

The test specimens were numbered according to the date the batch was cured. Different dates indicate different batches of resin. An example is given below:

7 - 10 - 79 - 04
month - day - year - specimen number

The numbering sequence is not to be confused with the dynamic mechanical test specimens which begin their sequence with letters "RH". That numbering sequence is described in section 3.3.

TABLE 3.2-1

LIST OF CREEP TESTS PERFORMED ON THE 3501-6 RESIN

Test No.	Description	Temp. (C)	Initial Stress σ_0 (GN/m ² $\times 10^2$)	Duration (sec. $\times 10^{-3}$)
7-5-79-01	Long term, RT	23.8	0.775	272.4
7-5-79-02	Figure 4.2.1-3	23.5	0.395	15.4
12-11-79-01	Figure 3.2-4	22.5	0.735	29.1
12-11-79-05	Figure 3.2-4	21.2	0.782	25.3
12-11-79-06	Soaked to 6.65% in water-phenol (50/50)	21.2	0.633	496.8
6-29-79-01	Figure 3.2-3	79.0	0.755	286.7
6-29-79-02	Figure 3.2-3	23.8	0.762	8.4
6-29-79-03	Figure 3.2-3	103.	0.425	264.0
7-10-79-04	Long term, RT	22.8	0.914	589.2
4-6-79-02	Figure 4.2.1-3	23.5	1.02	23.0
11-3-79-01	Appendix D	116.	0.492	130.5

Before presenting a few examples of the results of the creep tests, some interesting problems that were encountered are discussed first. It is the hope that the effort spent in solving these problems will save other investigators time and effort. Each of the problems mentioned either completely nullified the results or shortened the length of the creep test in which they were encountered. For example, five creep tests at room temperature were conducted for only 8 hours because of the problems encountered. The longer tests were run with most of the problems having been solved. Since creep testing epoxy resins is difficult, the information contained below should be useful for future investigations.

The first problem encountered concerned the brittleness of the resin at room temperature. Working with thin films was necessitated by the small space available in the ovens. Ten kilograms was the maximum load the ovens could support; therefore, thin specimens were used to achieve the necessary observable strains (greater than $1000 \mu\epsilon$). Consequently, a number of films cracked during loading wasting gages and time. Standardized test machines such as the Instron which use thicker tensile coupons were not available

for this work. Separate frames had to be built for each oven.

In the second problem, the length of the creep test was shortened because the glue line relaxed after a certain period of time. The glue line failure was caused by the excitation voltage of the P-350A Strain Indicator (Micro-Measurements, 1968). The 3501-6 resin acts as an insulator which causes a localized heat build-up under the gage. The heat increases until the epoxy adhesive starts to relax thereby causing the observed strain output to decrease from the true value. Earlier creep tests showed an increase in the strain as expected on the first day, but when the glue line started to relax, the strain would go through a maximum. The problem was solved by:

1. Using a higher temperature gage adhesive, M-Bond[®] 600.
2. Using a compensation gage glued to another creep test specimen except no load was placed on it. The compensation gage splits the excitation voltage in two thereby delaying heating effects until longer times.
3. Conducting creep tests for short periods of time.

The use of a compensation gage also dampens any shifts in the strain due to temperature changes. The strain can shift as much as 24 $\mu\epsilon$ for every degree Centigrade. Using strain gages with linear expansion coefficients similar to those of the resin also helps to reduce heating effects.

In the third problem, the injection molding device was incapable of making large amounts of creep specimens. Only four to six specimens could be prepared at any one time. Heating effects and cracking when loading the grips reduced the number of effective samples from each batch to one or two. Therefore, a number of different batches were used to acquire the creep data on the resin. The effect of batch-to-batch variation on the creep results is discussed in section 4.2.1.

Finally, the lone creep test performed on a sample of resin soaked to 6.65% weight gain in water-phenol (50/50) was achieved only after a few additional problems were solved. Strain gages had to be put on the specimen before it was immersed into any solvent because the solvent would have appreciably desorbed if the strain gages were mounted after immersion (see section 3.4). Since the gage adhesive is an epoxy resin also, it swells like the immersed specimen. Only moderate levels of absorption could be

sustained because a high level of absorption made the glue line more susceptible to heating effects. Dynamic mechanical testing on the Rheovibron does not require strain gages; therefore, specimens can be soaked to all desired levels. Since the length of the creep tests make repeated testing unfeasible, dynamic mechanical testing is preferred for examining the effects of plasticization.

Typical creep curves from data collected at room temperature are shown in figure 3.2-2. The creep of two long term tests from different batches are plotted against log time. The log time axis allows all the data to fit on one curve. The ordinate of the figure is creep compliance, $J(t)$, the time dependent strain divided by the constant stress. Compliance has units of reciprocal giga-newtons per meter-squared (or giga pascals, GPa). Compliance is also the reciprocal of the modulus, but since the strain is measured and not the stress, the compliance is the more appropriate variable. In terms of the actual strain, specimen 7-5-79-01 extended from 0.1844% at zero time to 0.2457% and specimen 7-10-79-04 extended from 0.1590% to 0.2179% in the time tested. These extensions were typical of all specimens. The initial stresses used were between 0.0040 and 0.010 GN/m² (580-1450 psi). All recorded strains were between 0.10% and 0.30%.

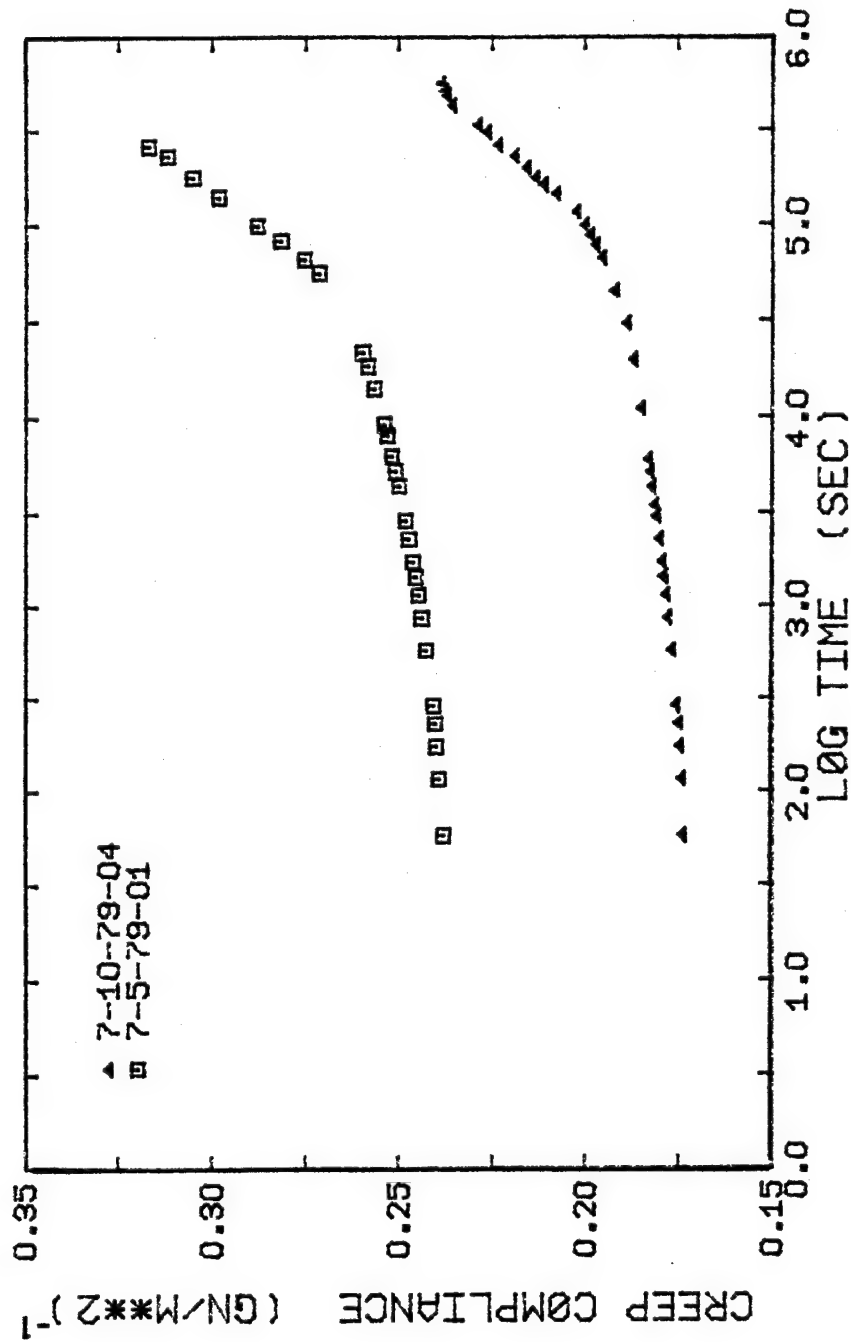


Figure 3.2-2 The room temperature creep of the 3501-6 resin

The value of the creep compliance at 60 seconds differs by 0.6 (GN/m²) in figure 3.2-2. This difference is indicative of the batch-to-batch variation seen in the mechanical properties of the 3501-6 resin. The causes of this large range in property values is discussed in section 4.2.1. The curves presented here represent the maximum and the minimum in the range of batch-to-batch variation of the compliance. Notice, however, that the two curves are parallel which indicates that their creep behavior is identical.

The creep at higher temperatures is shown in figure 3.2-3. All three specimens were produced from the same batch of resin and they were tested at 23.8°, 79.0°, and 103°C respectively. The compliance is plotted against normal time for the first 30,000 seconds. The shortened time scale (data is available beyond 21,000 seconds for specimens 6-29-79-01 and 6-29-79-03) was chosen to show the actual form of the creep at shorter times in what is called the viscoelastic creep zone (see section 4.2.1). Note that the exponential pattern to the creep data is indicative of linear viscoelasticity. The effect of temperature on the creep compliance (J_0 of the Voigt-Kelvin model, see section 2.1) increases with increasing temperature (corresponding to a decrease in the modulus with increasing temperature). The creep rate or the amount of creep in an equivalent period of time is also greatly enhanced.

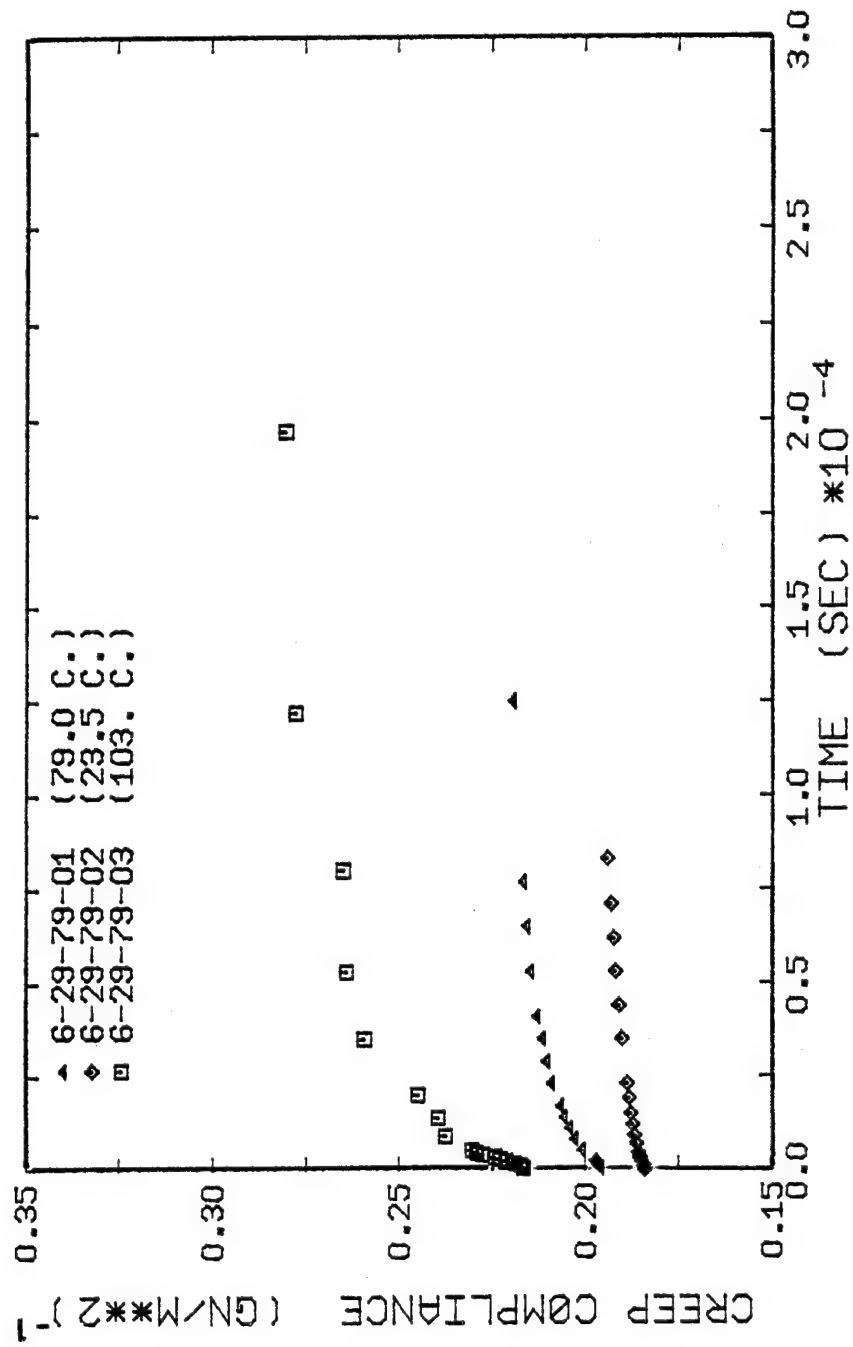


Figure 3.2-3 The creep of batch no. 6-29-79-00 at different temperatures

The example of the creep of a plasticized specimen, 12-11-79-06, is plotted in figure 3.2-4 along with the creep of two virgin resin specimens from the same batch. The two virgin resin tests were conducted for a shorter time to show two results. First, the two creep curves are within experimental error of each other (as shown by the error bars). The difference in the creep curves of figure 3.2-2 is much larger than the experimental error; therefore, the difference between the creep of the resin from different batches must be attributed to the batch-to-batch variation and not experimental anomalies. Secondly, the creep of the plasticized resin, though slightly greater than the virgin resin, is still within experimental error of the virgin resin up to 25,000 seconds. Plasticization by water-phenol (50/50) solution (50% by weight of each component) does not have a deleterious effect on the creep of the resin at shorter times. There is a marked increase in the creep at longer times. This effect is discussed in detail in section 4.3.

The creep data for all the specimens listed in table 3.2-1 are compiled in appendix A. Further graphs of the compliance data can be found in section 4.2. The calculation of the experimental error is contained in appendix D.

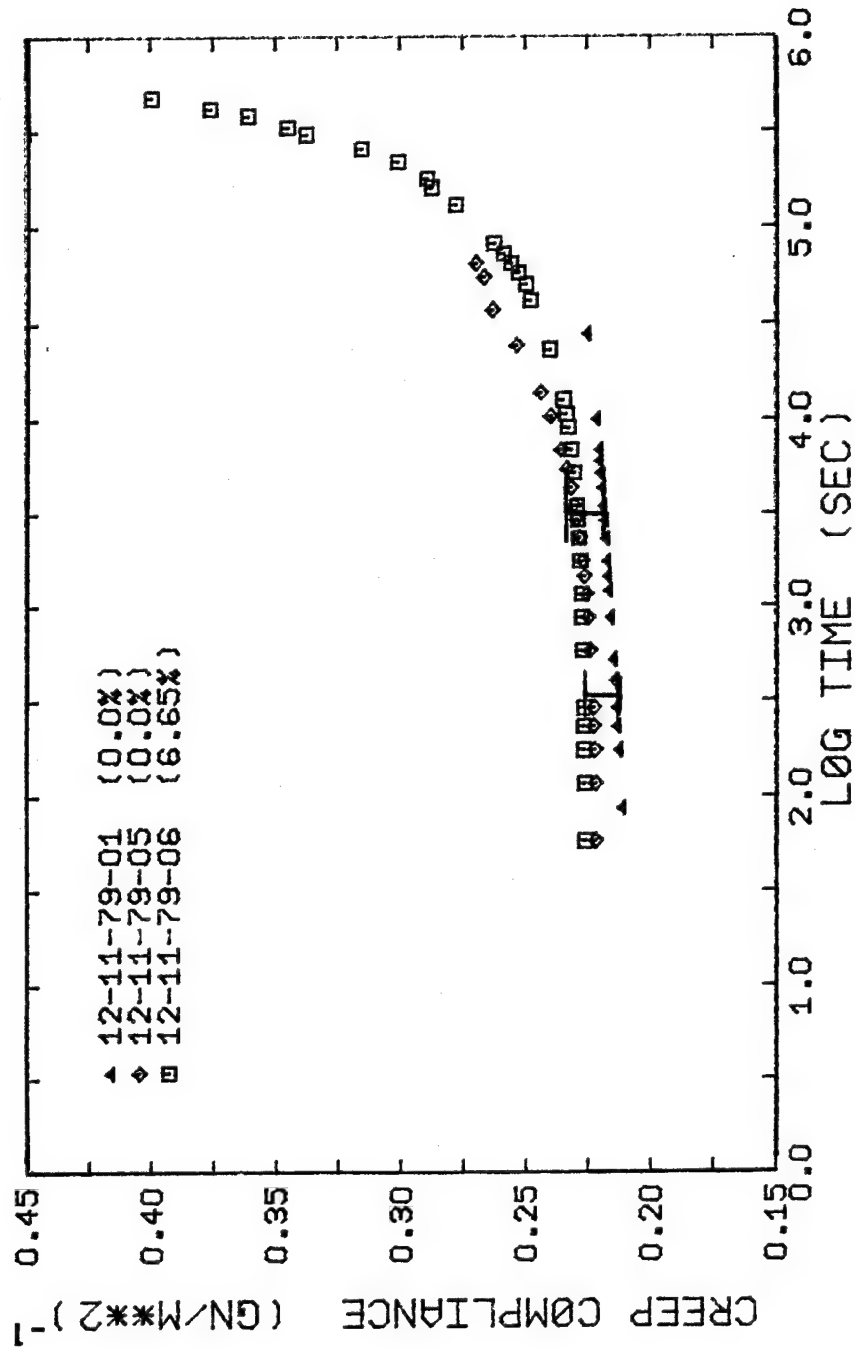


Figure 3.2-4 The creep of the 3501-6 resin plasticized with water-phenol (50/50) vs. the virgin resin (same batch) at room temperature

3.3 DYNAMIC MECHANICAL TESTING PROCEDURES

The dynamic tensile properties of the plasticized and virgin resin were determined by using a commercially available dynamic viscoelastometer, the Rheovibron model DDV-II-B manufactured by Toyo Measuring Instruments, Inc. of Japan. A schematic diagram of the apparatus is presented in figure 3.3-1. The general operating instructions are given in the instruction manual (Toyo Measuring Instruments, 1969), but several improvements in the operating procedure used here have been outlined by other investigators (Guenther, 1978; Joshi, 1975; Seferis, 1977; Bomberger, 1975). Only a brief review will be given here.

Thin films of the 3501-6 resin (cross-sectional area of 1×10^{-2} cm) were placed in the grips of the Rheovibron. The holding arms of the grips on one side is attached to a driver which when activated provides a constant oscillation at a chosen frequency and amplitude. A frequency of 11 hz was used for all tests. The sinusoidal strain imposed by the driver produces a sinusoidal stress in the test specimen. The amplitude of the strain is measured from the output voltage of the strain transducer, T-7, and the amplitude of the stress is

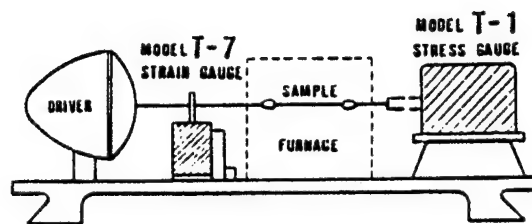


Figure 3.3-1 Schematic diagram of the Rheovibron DDV-II-B

measured by the T-1 transducer. The ratio of the maximum amplitudes computes the value of the complex dynamic modulus of the material, $|E|$. Since polymeric materials are not perfectly elastic, the stress produced by the applied strain lags behind it by a phase angle, δ (i.e. $\delta = 0$ for a perfect elastic solid and $\delta = \pi/2$ for a perfectly viscous fluid). The discriminating circuitry of the Rheovibron gives a direct reading of the tangent of the phase angle, $\tan \delta$, called the "loss tangent." The measurement is taken at a particular temperature by tightening the specimen until there is no slack produced by the oscillation. This precise length is very crucial to the $\tan \delta$ reading and this length is referred to as the "nodal length." Temperature is varied at a constant frequency by an electrically heated furnace. For these experiments, temperatures ranged from 25°C to 260°C, the design limit of the furnace. Two iron-constant thermocouples placed equidistantly above and below the specimen measured the temperature, and an average was used for the final value. The heating rate was $1.0 \pm 0.2^\circ\text{C}/\text{min}$ which was controlled by two variable transformers.

The constant frequency of 11 hz was chosen for two reasons. First, this frequency is the most common one used by other investigators who report dynamic mechanical data on polymers from tests on the Rheovibron. Secondly, the other available frequencies all have certain instabilities: harmonic resonance of the grips (35 hz), noise (0.35 hz), and inertial errors (110 hz) (Joshi, 1975).

The grip system that came with the Rheovibron was not used because grip slippage occurs with higher modulus materials such as epoxy resins. A different grip system was employed which prevents slippage. A description of the grips and the proper loading sequence is described elsewhere (Guenther, 1978). The new grips; however, can cause sideways vibration during testing. It became necessary during the middle of the experimental program to replace the holding arms and stress transducer. These changes required some retesting of the virgin resin in order to determine if the changes would give a different dynamic mechanical response than before. Two sets of data are reported: those prior to the improvements and those taken afterwards. The tests conducted after the improvements were instituted also used nitrogen

gas flow in the heater of the chamber where it had not been used earlier. This practice was instituted upon the advice of Dr. Seferis (personal communication, 1979) of the University of Washington. The flow of an inert gas supposedly reduces the temperature gradients in the chamber. The application of nitrogen gas did not alter the quality of the data taken before the new improvements were made, however. The temperature readings before the new improvements showed a maximum difference in the top and bottom thermocouple of 8°C. The difference was reduced to less than this value with the nitrogen gas addition, but the batch-to-batch variation in the dynamic mechanical behavior proved to be greater than either of these differences. The process of averaging the two temperatures was sufficient in either case. This point is more thoroughly discussed in section 5.2. Horizontally shifting the data two degrees centigrade in either direction does not change the final outcome.

The data generated off the Rheovibron requires some correction for sample length and for elasticity of the grips and transducers (Toyo Measuring Instruments, Inc., 1969; Seferis, 1977; Bomberger, 1975). The complex

dynamic modulus with a length correction term, K , is computed by the following equation:

$$|E| = 0.2 L / (S(AxD - K)) \quad (3.2-1)$$

where

$|E|$ = complex modulus, GN/m^2

A = a machine constant

D = force parameter of the Rheovibron

L = specimen gage length, cm

S = specimen cross-sectional area, cm^2

K = length correction constant

0.2 = proportionality constant

The constant, K , is dependent upon the type of material and temperature. It is the residual value of the force constant, D , at zero specimen length. The value of K , computed before and after the new improvements were instituted, was 25 ± 2 . The calculation of K is explained in appendix E. The value of K does change slightly at higher temperatures, but the recomputation of K at each higher temperature was not warranted. The value of D increases significantly near the glass transition, enough to make the value of K negligible in comparison.

The $\tan \delta$ reading is dependent upon sample length until a critical length is reached. For polypropylene,

the critical length was found to be 4.6 cm (Joshi, 1975). Taking this value as being representative of a typical structural plastic, the epoxy resin test specimens were cut longer than this value. The effects of the length of the sample are usually minor. It was assumed by the author that any dynamic test specimen greater than 5 cm had negligible length effects. No corrections were made.

The sideways vibration of the test specimen affected the data in two ways. Sideways vibration creates a range of output voltages from the strain and stress transducers (where only one voltage would exist if a single amplitude were measured without vibration). The measured modulus has a range of values, but the scatter is on the order of the experimental error. Secondly, the correct nodal length is very hard to find. Overtightening of the specimen usually decreases the value of $\tan \delta$ (Heinrich, 1979). Overtightening decreases sideways vibration which causes the observed nodal length to be much longer than the true nodal length. The complex dynamic modulus is also decreased if the overtightening exceeds the linear elastic limit of the resin (0.1% strain at 25°C). The life of the experiment can be cut short if overtightening causes failure in the specimen.

Near the glass transition ($170^{\circ} - 220^{\circ}\text{C}$), this problem was encountered in a few cases. The specimen can break at the temperature where the modulus begins to decrease dramatically. The data collected until that time was kept because most of the test had been run; especially for the plasticized specimens which desorb at the glass transition. These effects are discussed in more detail in section 5.3.

The experimental problems such as sideways vibration of the grips is the source of the experimental scatter in the loss tangent and dynamic modulus. The scatter in the data is prevalent at the lower temperatures because they tend to disappear as the glass transition is approached. In effect, the experimental problems observed on the Rheovibron enlarge the scatter around the data of what might be a "perfect" test if everything was conditioned properly. Qualitative differences between the virgin and plasticized resin are not affected by these problems because they are both affected equally when tested on the same machine.

A typical example of the dynamic mechanical behavior of the 3501-6 virgin resin is plotted in figures 3.3-2 and 3.3-3. In figure 3.3-2, the complex dynamic modulus of two specimens, RH-1-2-80-12 and RH-23

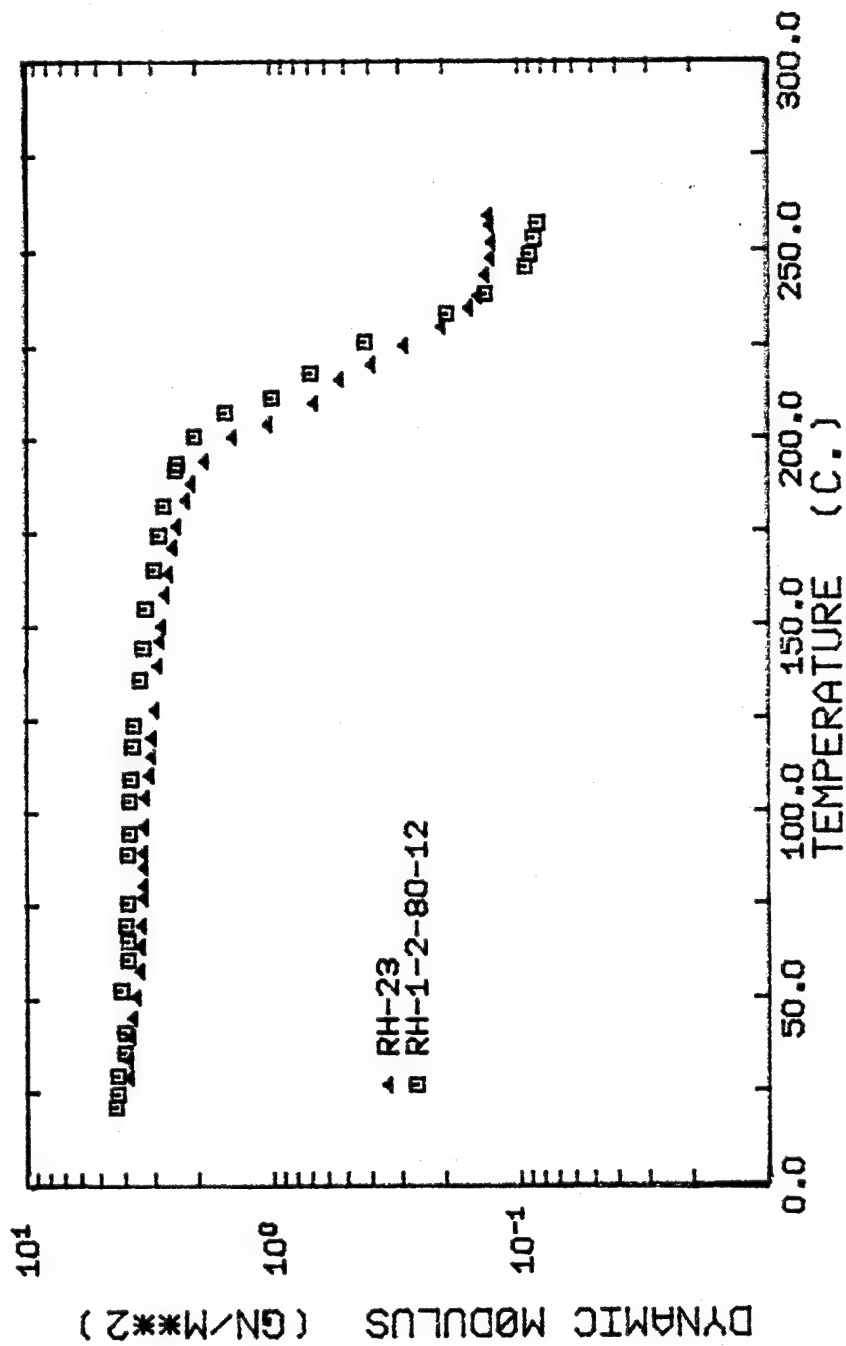


Figure 3.3-2 Complex dynamic modulus of the 3501-6 virgin resin for two different specimens

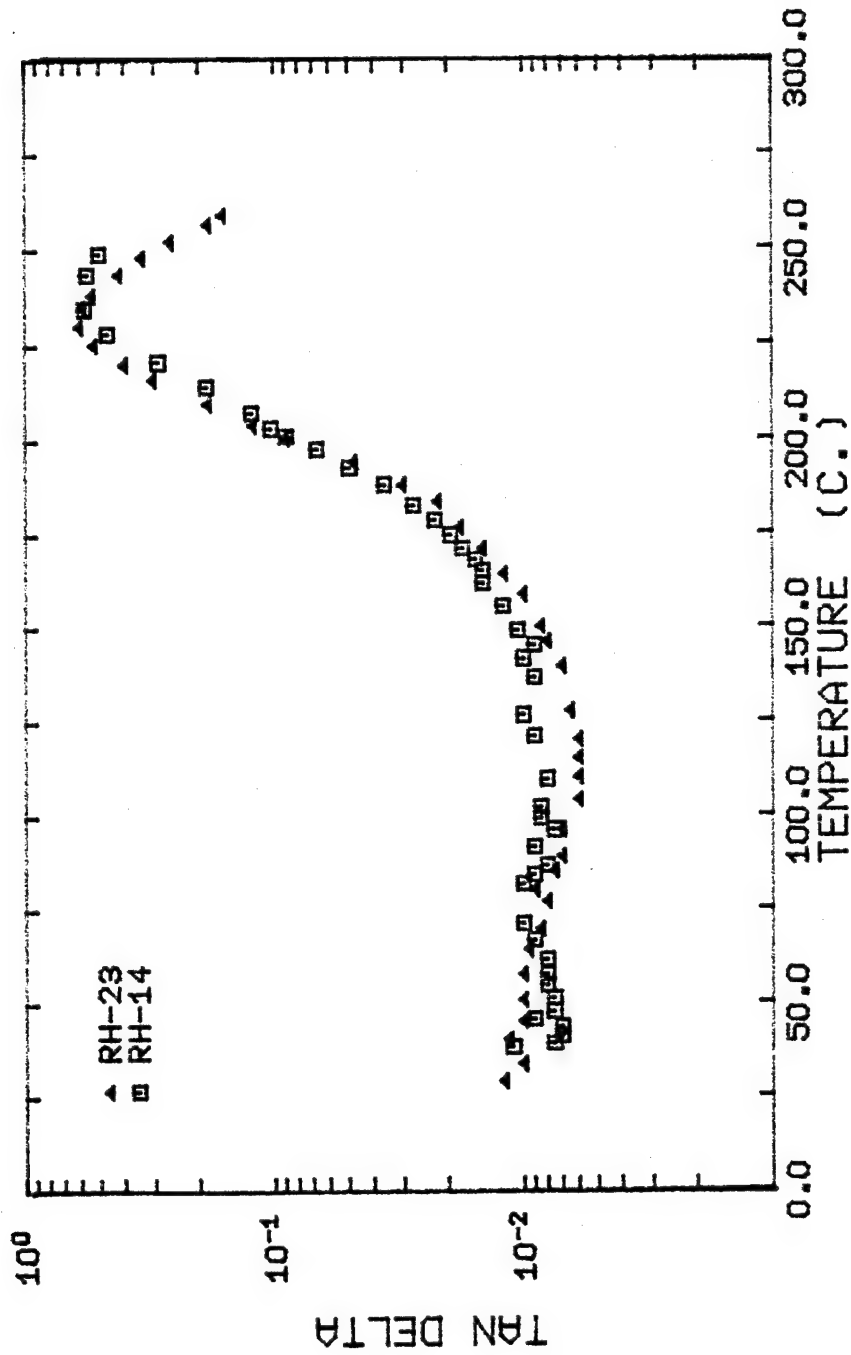


Figure 3.3-3 The loss tangent of the 3501-6 virgin resin for two different specimens

is shown. Specimen RH-23 represents the dynamic mechanical behavior before improvements were made and specimen RH-1-2-80-12 represents the dynamic mechanical behavior after improvements were made. The test with the new improvements shows a higher modulus, a value closer to the value of the tensile modulus. This reflects the fact that the new improvements reduced sideways vibration. In section 5.2, the comparison between the tensile and dynamic modulus is presented. The dynamic modulus at 25°C of specimen RH-1-2-80-12 is still within two standard deviations of the batch-to-batch variation of the average modulus (without improvements). One could state that the better and more realistic data of specimen RH-1-2-80-12 might be caused by batch-to-batch variation.

In figure 3.3-3, the loss tangent data of specimen RH-23 and RH-14 are plotted together. The former represents a test with little sideways vibration. The curve is very smooth and it exhibits a definite minimum and maximum. The latter is a test with some sideways vibration problems. The data is rather flat and scattered as expected from overtightening, but the loss tangent goes through the same maximum when the higher temperatures are reached.

Examples of the dynamic behavior of the plasticized resin are contained in section 5.3 along with the discussion on the differences between the dynamic behavior of the plasticized and virgin resin. The list of all dynamic mechanical tests performed on the Rheovibron is presented in table 3.3-1. A brief description of each test (i.e. the solvent used for plasticization) and the cross-sectional area of each specimen are given. The experimental data for all dynamic mechanical tests are compiled in appendix A along with the creep data.

The numbering system of the dynamic mechanical test specimens is shown in an example below:

RH	-	MIL	-	10
Rheovibron		Plasticization solvent		Number

This designation was used for all tests performed on the grips without the improvements. No distinction is made between different batches of resin because the experimental error is nearly equal to the batch-to-batch variation in the dynamic behavior. The solvent code system for each solvent is:

MIL	-	paint stripper, MIL-81294
H	-	water

TABLE 3.3-1
LIST OF DYNAMIC MECHANICAL EXPERIMENTS

Test no.	Description	S (cm ²) × 10 ²
RH-12	Virgin resin, no imp.	0.980
RH-13		.684
RH-14		.896
RH-20		.957
RH-21		.694
RH-22		.672
RH-23		.901
RH-24		.905
RH-1-2-80-07	Virgin resin, new imp.	1.05
RH-1-2-80-12		0.907
RH-HMPH-10	Water-methylene chloride- phenol (12.2%)	1.03
RH-II-10	Water (2.65%)	0.801
RH-M-10	Methylene chloride (0.0%)	0.621
RH-1-2-80-14	Water-phenol (10.2%)	1.13
	(8.81%)	1.19
RH-MIL-10	MIL-81294 (12.2%)	1.02
RH-MIL-11	(12.5%)	1.22
RH-MIL-12	(1.68%)	1.02
RH-MIL-13	(4.52%)	0.780
RH-MIL-14	(11.8%)	0.762
RH-MIL-15	(7.89%)	0.761

M - methylene chloride
 HMPH - water-methylene chloride-phenol
 None - virgin resin (no plasticization)

Only four tests were run on the Rheovibron with the new improvements. To distinguish these tests from the others, a different numbering system was employed. Since all specimens were from the same batch (both virgin resin and resin plasticized with water-phenol (50/50)), the date of the cure is used after the letters "RH." An example is shown below.

RH - 1 - 2 - 80 - 12

Date of cure

Specimen number

The two virgin resin tests were numbers 07 and 12.

The two plasticized resin test numbers were 14 (10.2%) and 15 (8.81%). They are listed in table 3.3-1 also.

3.4 THE ABSORPTION OF PAINT STRIPPER SOLVENTS

The major points on the effects that the paint stripper and its individual components have on the 3501-6 resin are discussed in appendix C. The purpose of this section is to present the procedures used in swelling the resin to a desired percentage weight gain before testing for its creep or dynamic mechanical behavior. Some of the procedures and results

used to determine the times and temperatures necessary to swell a specimen to a desired weight gain are also presented. The determination of which solvent (or solvents) plasticize the resin and to what extent was determined, but the role of diffusion in the absorption process was not characterized. However, diffusion coefficients and other characterizations may be calculated from the data, so it is presented in appendix C along with a few observations that were written down during the immersion tests.

The level of plasticization is commonly measured by the percentage weight gained by the polymer, M (Springer, 1979), defined by equation 3.4-1.

$$M = \frac{(\text{Weight of resin and absorbed plasticizer}) - (\text{Weight of dry resin})}{(\text{weight of dry resin})} \times 100 \quad (3.4-1)$$

The weight of dry resin in this case refers to the weight of the virgin resin including any background moisture. Absorption curves shown here and appendix C both have the variable M plotted against the time of immersion.

The solvents used to plasticize the resin were the paint stripper MIL-81294, and its individual components. The components of the paint stripper in decreasing weight fraction are:

1. methylene chloride (halogenated hydrocarbon)
2. water (small protic solvent)
3. phenol (aromatic-protic solvent)
4. surfactants (anionic and nonionic)
5. waxes and stabilizers (long chain aliphatics)

Of all the solvents listed above, only the effect of water on the mechanical properties of the 3501-6 resin has been investigated (DeIasi and Whiteside, 1978; Browning, et al., 1977; Augl, 1978).

The results of the series tests shown in appendix C yielded the following conclusions:

1. Water and phenol are the only components that swell the 3501-6 resin to any extent.
2. Phenol is the major swelling agent. MIL-81294, water, water-phenol (50/50), and phenol alone will swell the resin until it fractures while water will only reach an equilibrium absorption level.

3. The paint stripper, MIL-81294, is a better swelling agent than any combination of its components. Synergism between all the components is probably due to the surfactants or methylene chloride with water and phenol.

One example of the absorption testing is shown in figure 3.4-1 (absorption and plasticization are used synonymously throughout the thesis). Two tests were performed on two specimens from different batches that were immersed in distilled water at 92°C. Equilibrium was reached in 100 hr in both cases, but at different levels of plasticization. The difference in the final equilibrium values is due to the amount of background moisture that absorbed into the samples before immersion. Specimen 5-28-79-03 is 44 days older; therefore, it absorbed atmospheric moisture for that amount of time longer than specimen 7-11-79-01. Since specimen 5-28-79-03 had a greater level of background moisture, it absorbed less water during the immersion test resulting in a lower equilibrium concentration. The equilibrium level of water in the resin near 100°C is about 6-6.5% (DeIasi and Whiteside, 1978). The amount of background moisture in the resin can vary between 2% and 4%.

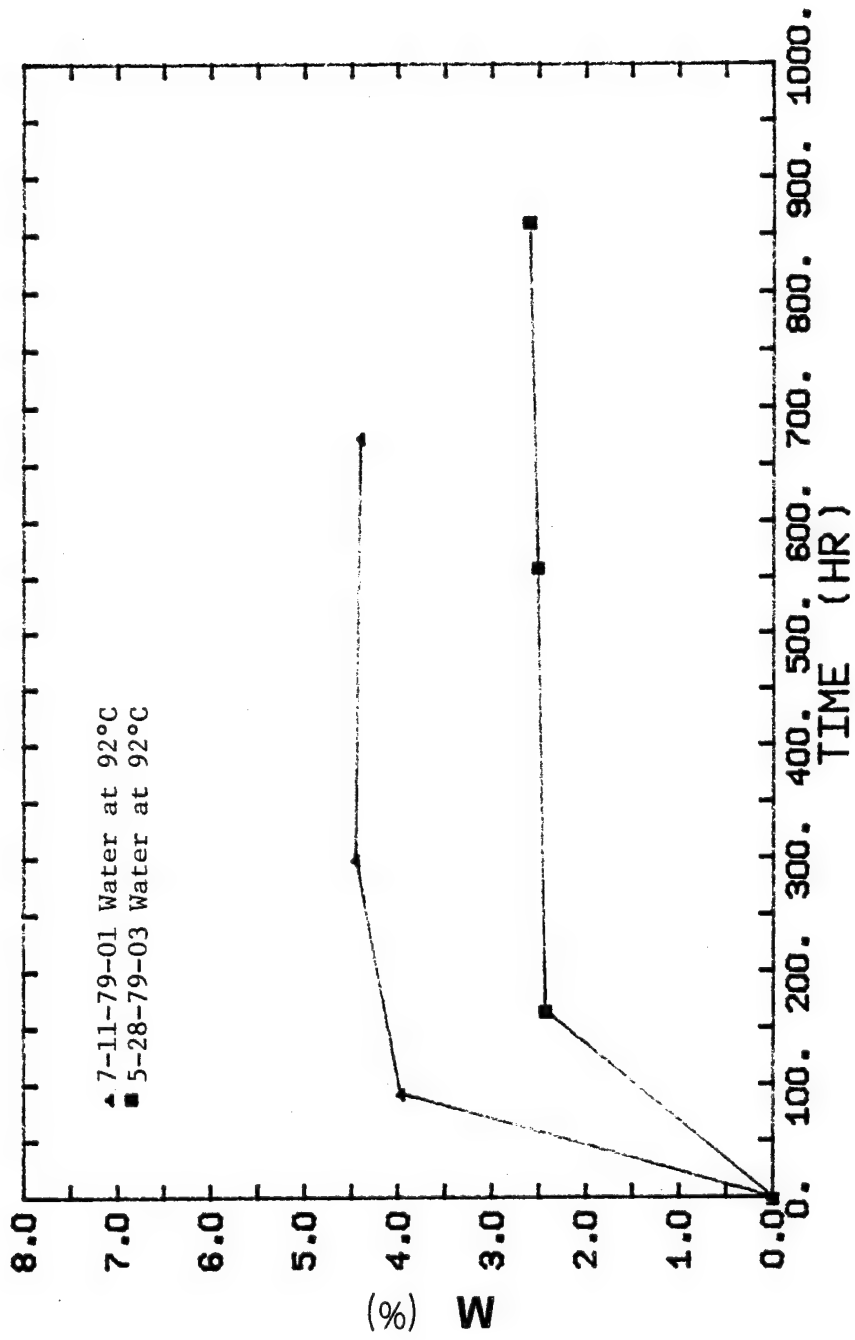


Figure 3.4-1 Water absorption into the 3501-6 resin

As a consequence of these tests, the time and temperature needed to soak different dynamic test specimens to a desired level of M was determined. The specimens that were soaked and tested on the Rheovibron are listed in table 3.3-1. Six tests were run on the paint stripper. The absorption levels ranged from 1.68% to 12.5%. An equal weight ratio of water-phenol solution was used to plasticize the resin for two tests (8.81% and 10.2%). Since the swelling behavior of water-phenol (50/50) and MIL-81294 are similar, only two tests were run on the water-phenol plasticized specimens. The weight ratio of water to phenol in MIL-81294 and in the water-phenol solution is the same. Single tests were run on water, methylene chloride, and water-methylene chloride-phenol plasticized specimens. The results of each test are presented in section 5.3.

The samples used for the absorption study were all similar in size with the creep or the dynamic mechanical test specimens. The actual test specimens and the ones used for the absorption study were subjected to the identical plasticization procedure. Each was immersed in a long test tube made from 1.25 in inside diameter Pyrex[®] glass containing the solvent. Specimens

were not suspended inside the solvent, but they were long and narrow enough to lean against the side of the glass tube without having any appreciable surface area in contact with the glass. The soaking apparatus is shown in figure 3.4-2. The test tube was sealed by a rubber stopper secured at the top. Either an oil or water bath controlled the temperature of the apparatus. A Sargent-Welch thermocontroller was accurate to within 0.1°C and a Blue M oil bath was accurate to within 1.0°C . Agitation kept the temperature in the baths fairly uniform.

The weight of the specimen was measured before and after immersion on a Mettler H80 analytical balance accurate to within 1×10^{-4} g. The specimen was carefully removed from the solvent and washed in acetone or water for five minutes, then patted dry. Air drying ensued for the next half hour. This was the time necessary for left-over solvent on the surface to evaporate (as monitored on the analytical balance). Since the weight decrease in one half hour was on the order of a few ten-thousandths of a gram, desorption was probably not taking place. The specimen was reimmersed depending on whether it was to be tested

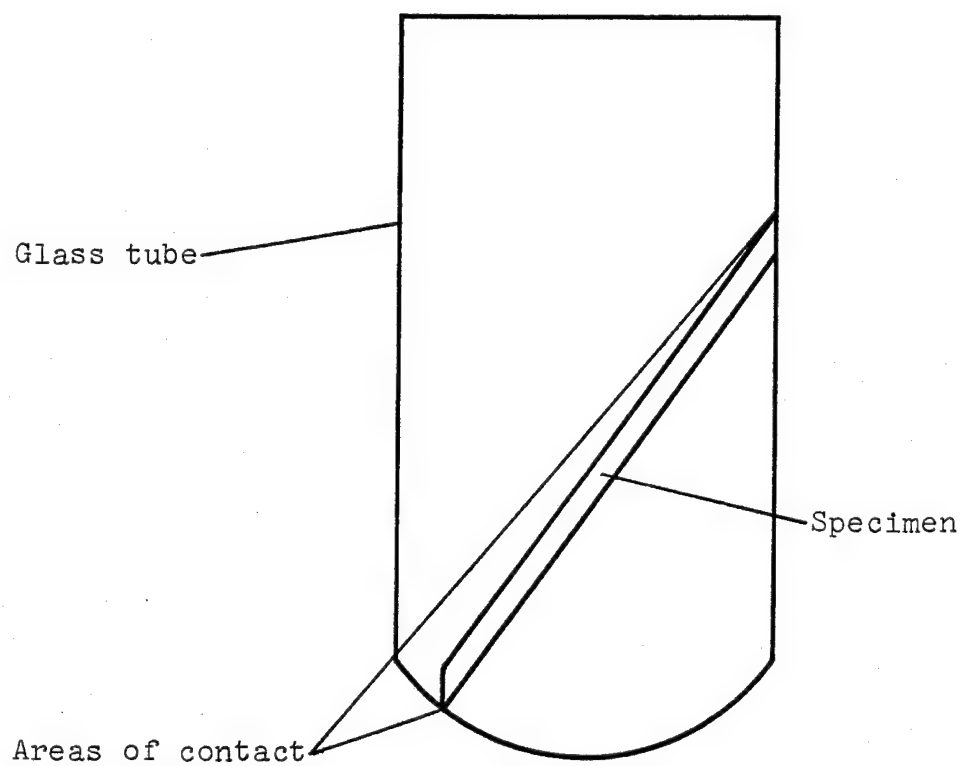


Figure 3.4-2 Diagram of the immersion apparatus used to swell the 3501-6 resin

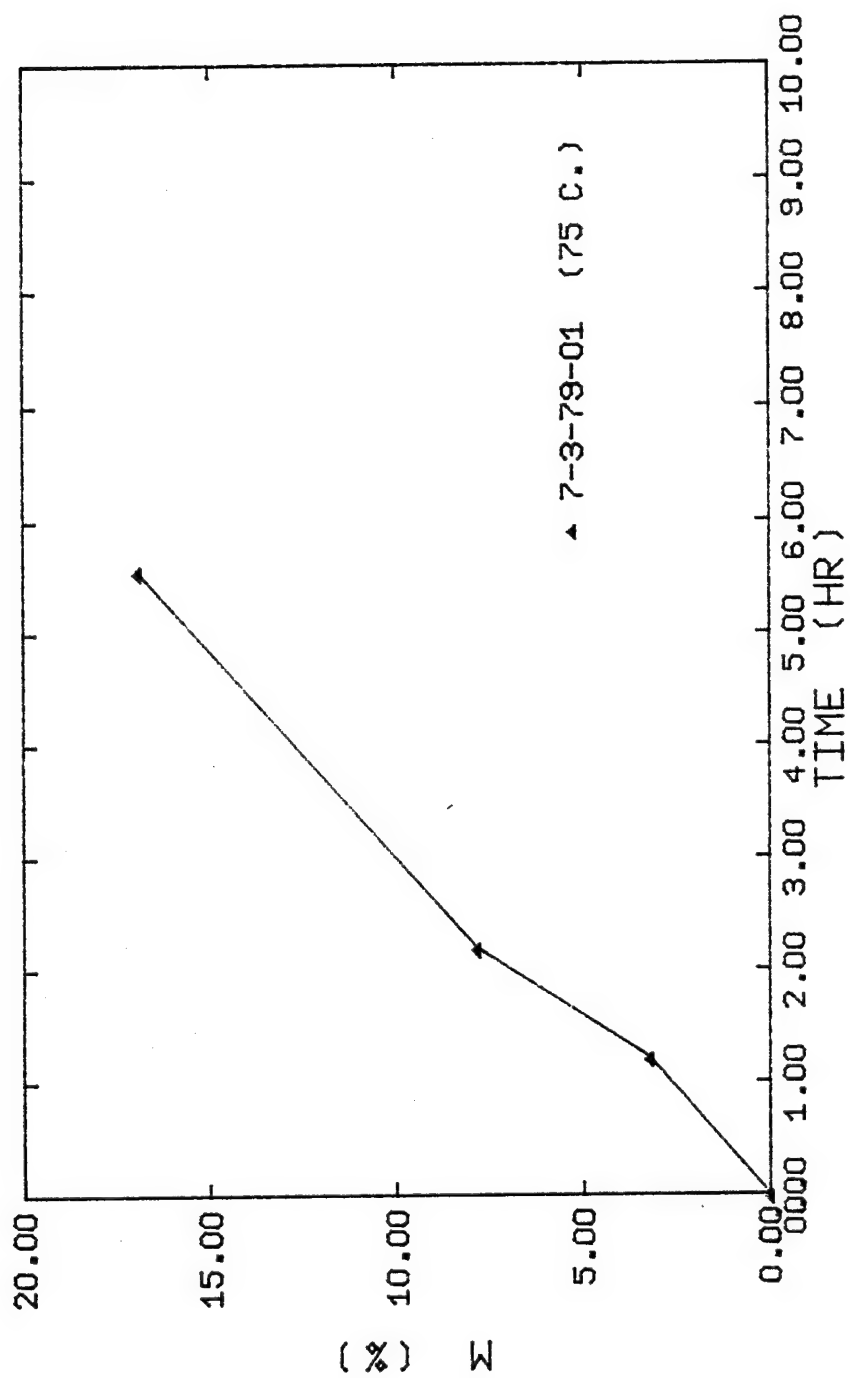


Figure 3.4-3 Water-phenol (50/50) absorption into the 3501-6 resin at 75°C

in the Rheovibron or used in an absorption study.

The dynamic test specimens plasticized by the paint stripper, methylene chloride, or water-methylene chloride-phenol solutions were soaked at 25°C. Methylene chloride boils at 41°C; therefore, heating these solutions above that temperature would drive it out of solution. Specimens immersed in water-phenol solution (50/50) were soaked at 75°C, slightly above the upper consolute temperature at 66°C. The absorption curve for water-phenol (50/50) is plotted in figure 3.4-3. The plasticization levels used in testing could be attained in three hours. The specimen soaked in water was immersed at 92°C ensuring that an equilibrium moisture level was maintained.

The concentration profile across the specimen was not measured, so it cannot be stated that it is uniform across the specimen. Since the samples were so thin, it was assumed that the concentration profiles were fairly uniform.

3.5 CHARACTERISTICS OF DESORPTION

A few desorption tests were conducted in order to determine how much of the plasticizer desorbed from a

test specimen during a creep or dynamic test. Two types of experiments were conducted. First, a plasticized resin specimen was subjected to the same thermal environment another test specimen would experience except that no load was applied. For the creep simulation, the plasticized specimen was suspended in the grips for one week at the desired temperature. For the dynamic mechanical test simulation, the specimen was placed in the Rheovibron grips and heated at $1^{\circ}\text{C}/\text{min}$ with nitrogen gas flow. The second type of test was a straight desorption experiment in a forced convection oven. The two experiments run in this fashion are plotted in figure 3.5-1. Both samples were initially plasticized with water-phenol (50/50) at 75°C . Higher temperature causes a greater rate of diffusion out of the specimen. The other experimental simulation tests are compiled in table 3.5-1. The initial plasticization level is M_0 and the final level is M_f . The percentage difference from M_0 is also listed in table 3.5-1.

Desorption at room temperature is significant over a one week period, but not enough to alter the interpretation of the results of the creep test. In the one creep test performed on a water-phenol plasticized

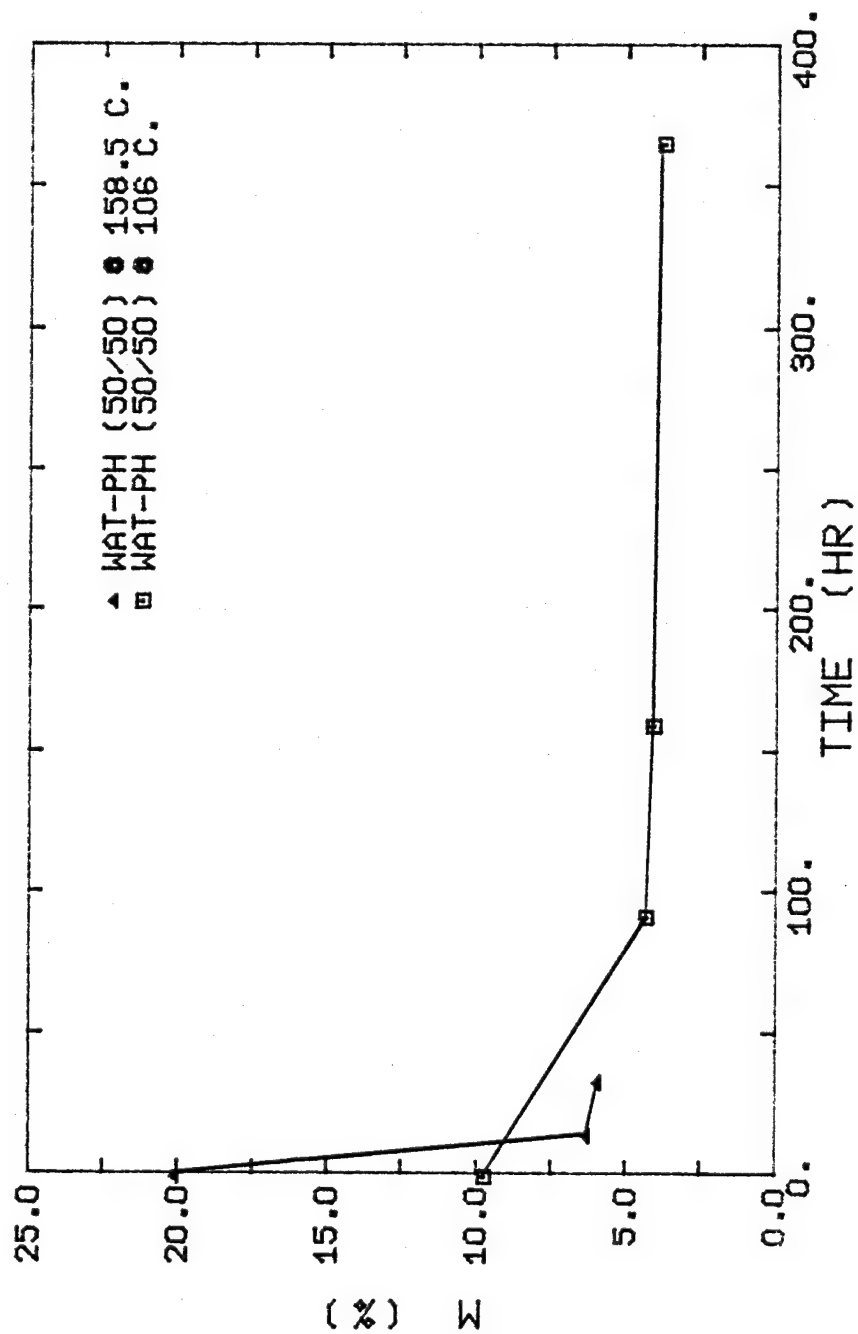


Figure 3.5-1 The desorption of water-phenol (50/50) from the 3501-6 resin above room temperature

TABLE 3.5-1
RESULTS OF THE EXPERIMENTAL SIMULATION DESORPTION TESTS

Number	Test simulation	M_o (%)	M_f (%)	ΔM (%)
4-6-79-01	Creep at 21°C, 225 hr, water-phenol (50/50)	7.15	6.09	-14.8
7-3-79-02	Creep at 22°C, 180 hr, water-phenol (50/50)	12.01	9.72	-19.1
7-3-79-02	Creep at 106°C, 160 hr, from 180 hr test	9.72	4.07	-58.1
RH-1-2-80-16	Creep at 158.5°C, 145 hr, water-phenol (50/50)	20.1	6.43	-68.6
RH-1-2-80-17	Dynamic mech. with new improvements	18.8	-1.62	-109.0

specimen immersed to an absorption level of $M_o = 6.65\%$ (12-11-79-06), the desorption during the test mimicked the desorption of specimen 4-6-79-01 (table 3.5-1). The initial levels of M were about the same. Assuming that the relative decrease in the initial weight, ΔM , was the same for both specimens (-14.8%), the average level of plasticization in specimen 12-11-79-06 was near 6.0%. The actual desorption could not be measured because soldering the strain gage wires on the gage after immersion changed the weight of the specimen. The average of M_o and M_f should suffice as the plasticization level for creep tests at room temperature.

The desorption of specimen 7-3-79-02 took place in two stages; a creep test simulation at 22°C for 180 hr, then a creep simulation at 106°C for 160 hr. The desorption at room temperature, when compared with the desorption of specimen 4-6-79-01 shows that the rate of desorption depends on the initial concentration level. Specimen 7-3-79-02 desorbed to a lower percentage level (-19% vs. -15%) in a shorter period of time (180 hr vs 225 hr). At higher temperatures, the desorption of specimen 7-3-79-02 at 106°C (plotted in figure 3.5-1) shows that the rate of desorption is greater at 106°C

than at 22°C. Specimen RH-1-2-80-16 desorbed at 158.5°C even shows a greater rate of desorption. The desorption of specimen RH-1-2-80-16 is also plotted in figure 3.5-1.

Specimen RH-1-2-80-17 was the only dynamic mechanical desorption simulation test. With nitrogen gas flow (new improvements) the specimen completely desorbed from $M = 18.8\%$ to $M = -1.62\%$. The extra desorption past the initial virgin resin weight was caused by the expulsion of the background moisture as well as the water-phenol (50/50) solvent. It is unknown whether or not total desorption would occur without nitrogen gas flow because that test was not run. This point is discussed further in section 5.3.2.

The desorption at higher temperatures also leads to a conclusion about desorption near the glass transition temperature of the resin. It is well established that the glass transition temperature is dramatically lowered when a polymer is plasticized by an external solvent. Water, for example, will cause the glass temperature of the 3501-6 resin to decrease from 220°C to 120°C (DeIasi and Whiteside, 1978). As mentioned in section 5.3, water-phenol (50/50) can

cause a decrease in the glass temperature to 150°C for M greater than 10%. In figure 3.5-1, specimen 7-3-79-02 at 106°C is an example of desorption below the glass temperature. The value of M decreases slowly until it seems to level out at longer periods of time. The desorption of specimen RH-1-2-80-16 shows a similar behavior; however, the temperature of 158.5°C is above the glass temperature for a value of M near 20%. Desorption is very quick, but as the solvent is desorbed, the glass temperature starts to rise back to its virgin resin level. The final plateau near 6% shows that the glass temperature is above 158.5°C. Furthermore, total desorption appears to occur only above the glass transition temperature of the resin. Desorption below the glass transition temperature is very slow in comparison.

The conclusions that can be drawn from the results are:

1. Creep testing of the 3501-6 resin plasticized by these solvents is possible at temperatures below the glass transition temperature (depressed glass temperatures occur due to the plasticization effect). The amount of

desorption will be noticeable over a week's time, but shorter tests can be conducted without losing large amounts of the solvent.

2. Dynamic mechanical testing of the plasticized resin is not recommended above the glass transition temperature because total desorption can occur. Since only the fast desorption rates occur above the glass transition temperature, acquiring meaningful data from room temperature to just below the glass transition temperature should be possible. The Rheovibron test only lasts for 4 hr at the most.
3. The fact that the specimens experience total desorption shows that solvent absorption is reversible. Whether or not the changes in the mechanical properties are reversible is discussed in section 5.3.2.

CHAPTER 4

ANALYSIS OF THE CREEP RESULTS

4.1 INTRODUCTION

In this chapter, the creep behavior of the virgin and plasticized 3501-6 resin is discussed and compared. The observations noted here apply to the creep between room temperature and 116°C. Both temperatures are well below the glass transition temperature of the resin. The creep of the virgin resin is especially discussed in detail because the creep behavior not only serves as a control which is compared to the plasticized creep behavior, but it is also representative of the creep of other tetraglycidyl amine epoxy resins. Both of these themes are emphasized throughout the chapter.

In section 4.2, the creep of the virgin resin is analyzed. The general trends in the creep behavior are outlined (section 4.2.1.A) and compared with the creep behavior of other epoxy resins. Consequently, the literature on the creep of tetraglycidyl amine and some

DGEBA epoxy resins is reviewed. Inherent to the resin is the batch-to-batch variation in its mechanical properties (e.g. tensile modulus and compliance). Several reasons for the causes of batch-to-batch variation are discussed in section 4.2.1.A. In section 4.2.1.B, the creep of two other tetraglycidyl amine resins used in carbon fiber composites are compared directly to the creep of the 3501-6 epoxy resin. This section provides a quantitative comparison between the creep of the 3501-6 resin and other resins rather than the more qualitative comparison discussed in section 4.2.1.A. In section 4.2.2, the results of the application of the viscoelastic creep models discussed in sections 2.1.2 and 2.1.3 are presented. Examples of each of the curve fits are shown. Statistical methods are used to compare both models at room temperature and at higher temperatures below the glass transition. In section 4.2.3, the applicability of time-temperature superposition is discussed. A master creep curve for the resin is presented and its prediction of the creep at long periods of time is compared to the creep data and the prediction of the viscoelastic models. It is shown that time-temperature superposition only provides a lower bound to the creep behavior of the neat resin.

In section 4.3, the creep of the 3501-6 resin plasticized in water-phenol (50/50) is discussed and compared with the virgin resin creep data. The changes in the creep behavior are related to the changes in the physical structure of the crosslinked network caused by the presence of an absorbed solvent.

4.2 CREEP OF THE VIRGIN RESIN

4.2.1.A GENERAL TRENDS

Three distinct zones of creep are observable in epoxy resins (Ishai, 1967; Ferry, 1961; Hancox and Minty, 1978) at moderate stress levels. The first zone is called the primary creep zone in which the creep behavior is governed by simple viscoelastic models (the first zone is also referred to as the viscoelastic creep zone). The strain rate is a decreasing function of time and both linear and nonlinear viscoelastic laws have been applied to this region (see section 4.2.3). The second zone is called secondary creep or linear creep. The strain is constant with time; therefore, the creep curve is a straight line in this region (giving it its name). A linear deformation with time is characteristic of the flow of a viscous liquid. The last zone, tertiary

creep, can have either the strain rate increase or decrease with time depending upon the stress level experienced by the polymer. Generally an increase in the strain rate is noticed as failure becomes imminent, but the moderate stress levels employed in this study ($0.30 - 1.1 \times 10^{-2}$ GN/m²) showed a decrease in the strain rate with increasing time indicating an approach to an equilibrium creep compliance. The three creep zones are illustrated in figure 4.2.1-1 for two long term creep tests at room temperature. The specimens are from different batches of resin and they bracket the batch-to-batch variation inherent in the epoxy resin. The curves are the same as the specimens plotted in figure 3.2-2 except that a normal time abscissa has been used to reveal the three creep zones. A decreasing rate of creep occurs in the first 25 to 50 thousand seconds which is indicative of the creep of a network solid as shown by Ferry (1961). Between 50 and 150 thousand seconds, the creep rate is constant with time which results in a linear relationship. Beyond 150 thousand seconds, tertiary creep sets in with a decreasing rate of strain. The tests conducted here were not long enough to establish the existence of an equilibrium compliance.

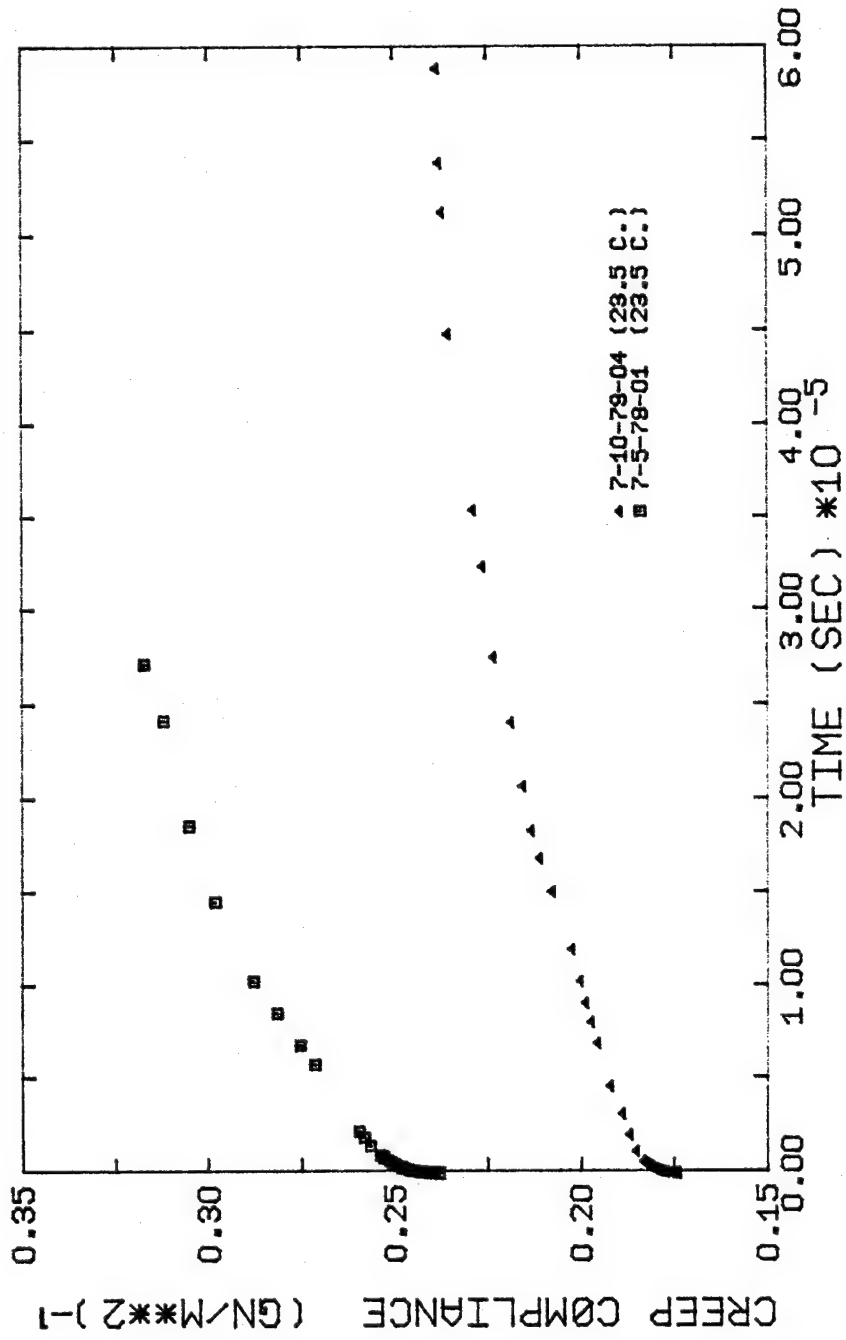


Figure 4.2.1-1 The creep of 3501-6 epoxy resin at room temperature vs. time

In other articles found in the literature for the creep at higher stress levels (0.018 to 0.035 GN/m^2), Ishai (1967) showed that an increasing strain rate in the tertiary creep zone was caused by a post-yielding process. Yielding, or irrevocable damage due to viscous flow, starts in the secondary creep zone, then it gradually increases during tertiary creep. The transition occurs when the linear creep region breaks off into an increasing rate of creep towards an eventual failure. In the case of an increasing rate of creep, scission of the crosslinked network must be involved (Nielsen, 1962). Identical results to these observations were also found for the creep of epoxy resins in compression (Ishai, 1967) and torsion (Hancox and Minty, 1978). The decreasing rate of creep observed in the 3501-6 resin indicates that the scission of the crosslinked network is not taking place at these stress levels. The post-yielding noticed by Ishai is not applicable here. The yielding exhibited by the data in the secondary creep zone is really a brittle-viscous flow transition rather than the brittle-ductile transition observed at higher stress levels. Therefore, the creep behavior of the 3501-6 resin indicates that yielding of some form takes place without damaging the crosslinked network.

The possibility of such a form of yielding can be envisioned if a heterogeneous crosslinked density is present in the network. Morgan and O'Neal (1978) have shown this to be the case for other tetraglycidyl amine resins used in carbon fiber composites. A detailed discussion of the situation is given later.

The exact stress level required to cause an increasing tertiary creep rate (post-yielding) can be bounded. Using a value of 7,200 psi for the ultimate tensile strength of the 3501-6 resin (see table 3.1-1), stresses up to 19% of the ultimate tensile strength did not incur post-yielding. This value obtained from the creep tests on the 3501-6 resin serves as a lower bound. The work of Ishai (1967), Koeneman and Kicher (1972), and Molenpah, et al. (1969) on the creep of DGEBA resins did not exhibit post-yielding until a stress equal to 33.5% of the ultimate tensile strength was reached at room temperature. The upper limit of tertiary creep obtained from the same tests on the DGEBA resins was 75% of the ultimate tensile strength. Above 75%, the creep behavior tends to approach failure without going through the first two zones of creep. For epoxy resins in general, the onset of post-yielding

should occur between 19% and 75% of the ultimate tensile strength. The ratio of the initial stress to the ultimate tensile strength of the resin is a dimensionless variable which should serve as an independent measure of the onset of post-yielding.

Though the 3501-6 resin does not exhibit post-yielding, the other form of yielding shown in the secondary zone is definitely a nonlinear viscoelastic creep response that cannot be fit to simple linear viscoelastic models. One would also presume that the change from secondary to tertiary creep at longer times as shown in figure 4.2.1-1 would also make it difficult to fit simple nonlinear viscoelastic models. These points are discussed in detail later, but these models should apply nicely in the primary creep zone. For this reason, the bulk of the room temperature testing did focus on shorter tests within this zone.

At higher temperatures, the experimental creep data exhibited the first two zones of creep while the tertiary zone was absent. The higher temperature tests were not performed for as long a period of time as the room temperatures tests, but it was clear that the first two zones were extended to longer times. Much longer

tests would be needed to establish whether tertiary creep still existed at higher temperatures. Problems with the strain gage glue line mentioned in section 3.3 prevented these longer tests from taking place.

Two creep tests from the same batch of resin at 79°C and 103°C are plotted in figure 4.2.1-2. Both tests were voluntarily stopped and they did not exhibit the glue line problems. Both tests show that the primary creep zone is lengthened well beyond the 25 to 50 thousand second limit at room temperature. For the test at 79°C, linear creep (secondary) appears to start at 150 thousand seconds. Linear creep may not appear at all for the test at 103°C. A better comparison can be obtained if the data is plotted on a log time axis like figure 4.2.1-7. The effects of increased temperature will be discussed later.

The seven creep tests at room temperature exhibited a wide range in the initial creep behavior of the 3501-6 resin. The first data point in most cases was measured at a time of 60 sec. The range in the creep compliance is indicative of the variety of values in the mechanical properties caused by batch-to-batch variation in the resin. The seven creep tests are plotted in figure 4.2.1-3 for times less than 25 thousand seconds. Five different

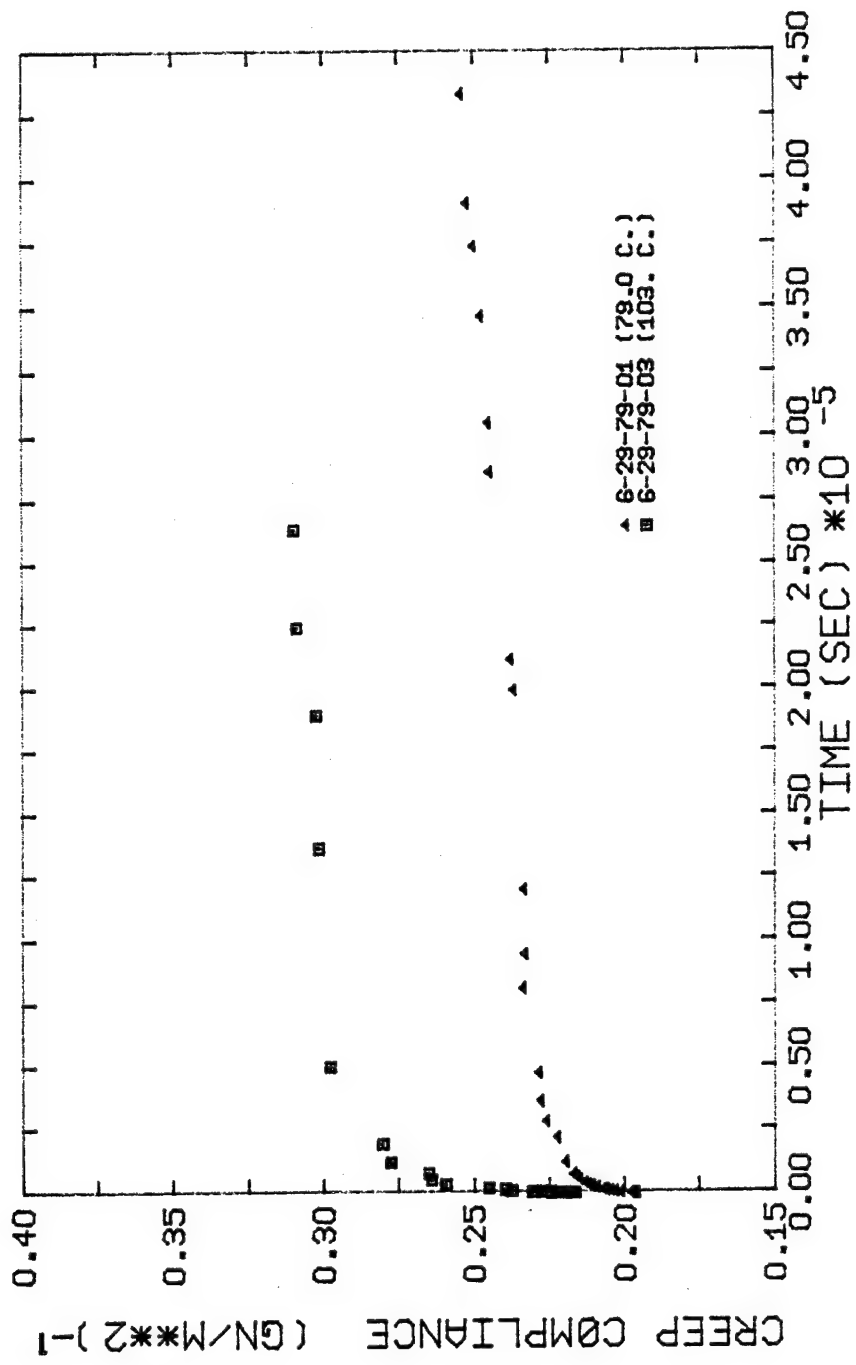


Figure 4.2.1-2 Creep of 3501-6 epoxy resin at higher temperatures

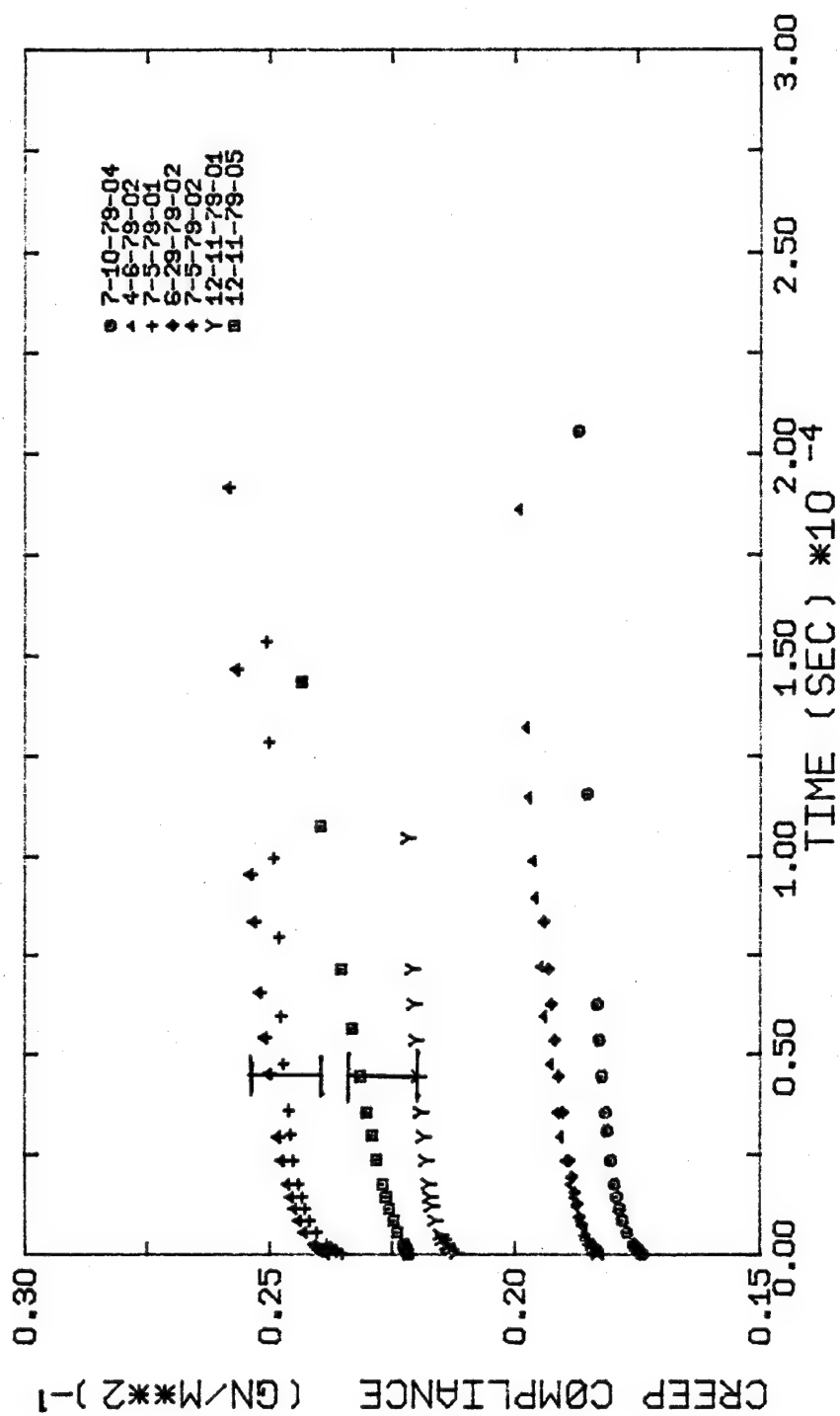


Figure 4.2.1-3 The room temperature creep of 3501-6 resin in the viscoelastic zone

batches are represented in the figure. The initial compliance (the value of the creep compliance at zero time extrapolated by the Voigt-Kelvin model) varied between 0.174 and 0.238 reciprocal giga-newtons per meter squared ($[\text{GN/m}^2]^{-1}$). The mean compliance at room temperature ($22.5 \pm 1^\circ\text{C}$) is $0.207 (\text{GN/m}^2)^{-1}$ with a standard deviation of $0.026 (\text{GN/m}^2)^{-1}$ forming an envelope of 12.6% variation about the mean. In terms of a creep modulus, the mean tensile creep modulus is 4.84 GN/m^2 ($7.01 \times 10^5 \text{ psi}$) with a standard deviation of 0.61 GN/m^2 ($8.8 \times 10^4 \text{ psi}$). Assuming that the reciprocal initial creep modulus is comparable to the Young's modulus, the mean creep modulus is slightly higher, yet still within one standard deviation of some of the reported values of the Young's modulus of the 3501-6 resin. A single tensile coupon of the 3501-6 resin was supplied to this investigation by R. Blake of the Center of Composite Materials, University of Delaware. This sample was pulled in tension on an Instron test machine. A Young's modulus of 4.48 GN/m^2 ($6.50 \times 10^5 \text{ psi}$) was obtained. The stress-strain diagram for the 3501-6 resin is plotted in appendix A. One additional note on this test; the sample (referred to in the future as the Blake sample) was post-cured at 210°C , a higher temperature

than the 191°C post-cure temperature used in this investigation. Augl (1978) also measured the Young's modulus of the 3501-6 resin. His value was 4.27 GN/m^2 ($6.20 \times 10^5 \text{ psi}$). This value was within the five percent experimental error of the modulus of the Blake sample. Augl's tests were run on creep specimens which were cured in an identical manner to this investigation, but his samples were dessicated for a few months. Both the moduli of the Blake sample and Augl are within two standard deviations of the mean creep modulus.

While the creep behavior varied from batch to batch, creep of the resin made from the same batch was within normal experimental error. Tests from the same batch, batches 7-10-79-00 and 12-11-79-00, are plotted in figure 4.2.1-3 with error bars denoting the experimental error. The negative error limit is larger than the positive error limit because the misalignment of the strain gage only reduces the observed strain value. This peculiarity is discussed in appendix E in detail. It is clear that the differences in the creep results were caused by material variation instead of characterization errors in the experiment. For this reason, the master curve of section 4.2.3 was constructed from creep data measured from the same batch of resin.

The batch-to-batch variation was not explored at higher temperatures, but the variation should be present up to the glass transition temperature because the molecular motions of the molecular segments are "locked" into place below that temperature.

The causes of batch-to-batch variation in the creep behavior can be traced to either chemical or environmental phenomena. The chemical phenomena occur during the cure. The complex kinetics of the catalyzed crosslinking reaction may cause the variation in the properties observed in the results. The environmental phenomena occur later during storage and during the test itself. Aging and the absorption of moisture from the air are the major environmental effects. Before exploring those effects further, one case in the literature where the batch-to-batch variation was also observed is discussed below.

Most studies of epoxy resins do not comment on the batch-to-batch variation in the mechanical properties because most of the resin samples are made from the same batch of resin. The one source where data is given is in a paper by J. P. Bell (1970). Bell gave data on the tensile modulus of a DGEBA resin crosslinked with various

amounts of methylene dianiline. No dependence between the tensile modulus and the effective molecular weight between crosslinks could be proven (each sample was from a different batch). Assuming that the modulus does not vary with the effective molecular weight between crosslinks, the scatter in Bell's data can be used to compute the average variance in the tensile modulus due to batch-to-batch variation. The calculated standard estimate of error was (square root of the variance) 0.194 GN/m^2 which in terms of compliance is $0.012 (\text{GN/m}^2)^{-1}$. This value is slightly smaller than the standard deviation in the creep compliance of the 3501-6 resin (0.026 reciprocal GN/m^2). Two different types of epoxy resins are represented so some differences in their batch-to-batch variations can be expected. The values are close enough to each other to indicate that batch-to-batch variation is significant.

The work of Bell (1970) and Morgan and O'Neal (1978) both clearly show that the curing reaction goes nearly to completion for DGEBA resins. The resulting homogeneous network structure indicates that variations in the mechanical properties should be small, at least smaller than the variation in the

tetraglycidyl amine epoxies which have the inhomogeneous network structure. The inhomogeneous structure is caused by an incomplete curing reaction which leaves areas of high and low crosslink density (Morgan and O'Neal, 1978; Cuttrell, 1967; Nielsen, 1969). It is reasonable to assume that the heterogeneous crosslink density in the network is not reproducible from cure to cure; therefore, the heterogeneous crosslink density is the source of the batch-to-batch variation in the mechanical properties of tetraglycidyl amine epoxies.

Morgan and O'Neal proposed that the inhomogeneity in the crosslink density exists because the glass transition temperature, when plotted against the amount of DDS crosslinking agent, goes through a maximum. The maximum occurs at a concentration of DDS that cannot occupy all the epoxide sites theoretically. Excess crosslinking agent must then be present in the resin and such aggregates have been found by electron diffraction and X-ray emission spectroscopy (Morgan and O'Neal, 1978). In effect, the presence of unreacted crosslinking agent means:

1. The crosslinking reaction is indeed incomplete.
2. The excess DDS plasticizes the resin.

3. Further weakening of resin could occur if the unreacted DDS is expelled during the cure (microvoids are created).

A few theories have been put forth which attempt to describe the network. Cuttrell (1967) suggested that a highly crosslinked microgel phase was evenly distributed in a homogeneous, less highly crosslinked matrix. Further suggestions have been given by Solomon, et al. (1967); Erath and Robinson (1963); Wohnsiedler (1963); and Kenyon and Nielsen (1969).

The presence of microvoids and areas of different crosslink density can also aggravate environmental effects on the resin by serving as a site for stress concentration as well as a sink for absorbed moisture or aging effects. Humidity and aging were not controlled during the creep experiments or cure of the specimens; therefore, environmental factors are present also. To test for aging effects, a plot of the initial creep compliance, J_0 , vs. the aging time was constructed and it is shown in figure F-1 of appendix F. For times of storage as long as six months, no dependence between the two variables could be established. Humidity effects are also not observed because the longer a sample

is stored at room temperature and room humidity, the more background moisture is absorbed into the resin specimen. The lack of a dependence on aging time does not mean that these effects are not present. If aging effects were present, the creep of the 3501-6 resin would horizontally shift to longer times (see appendix F). The creep compliance at a fixed time like 60 sec would decrease slightly as the aging time increased. Humidity has the opposite and possibly cancelling effect of increasing the compliance at a fixed time because moisture plasticization weakens the resin resulting in an accelerated creep behavior. In addition, the batch-to-batch variation may be large enough to mask any net changes caused by either of the environmental effects.

In summary, many possibilities have been explored which might have caused the variation in the creep compliance of the resin. Two general phenomena that can cause the variation, chemical and environmental phenomena, have been outlined, but the extent to which each contributes to the variation is unknown. The tests conducted here indicate that the chemical phenomena may be dominant because of the heterogeneous crosslinked density found in tetraglycidyl amine resins. Since the batch-to-batch variation is larger than the experimental error, the

variation is inherent to the material.

Problems in analyzing the creep of the 3501-6 resin arising from batch-to-batch variation can be mitigated by plotting the quotient of the creep compliance and the initial creep compliance, $J(t)/J_0$, vs. time. By forming this reduced variable, the effects of temperature and plasticization should dominate over batch-to-batch variation. The initial creep compliance, J_0 , is the compliance extrapolated back to zero time by the Voigt-Kelvin model. The seven room temperature tests of figure 4.2.1-3 are plotted this way in figure 4.2.1-4. With this normalization, all five batches represented in this curve fall within the error bar denoting the experimental error of the variable $J(t)/J_0$ (see appendix E). The two tests at room temperature plotted in figure 4.2.1-1 have been replotted in the normalized fashion in figure 4.2.1-5 vs. a log time scale. Since the two curves superimpose over the entire time scale, the normalization scheme holds at longer times. Secondary and tertiary creep fall within the same experimental error indicating that the creep behavior at the same temperature for different batches of resin is identical.

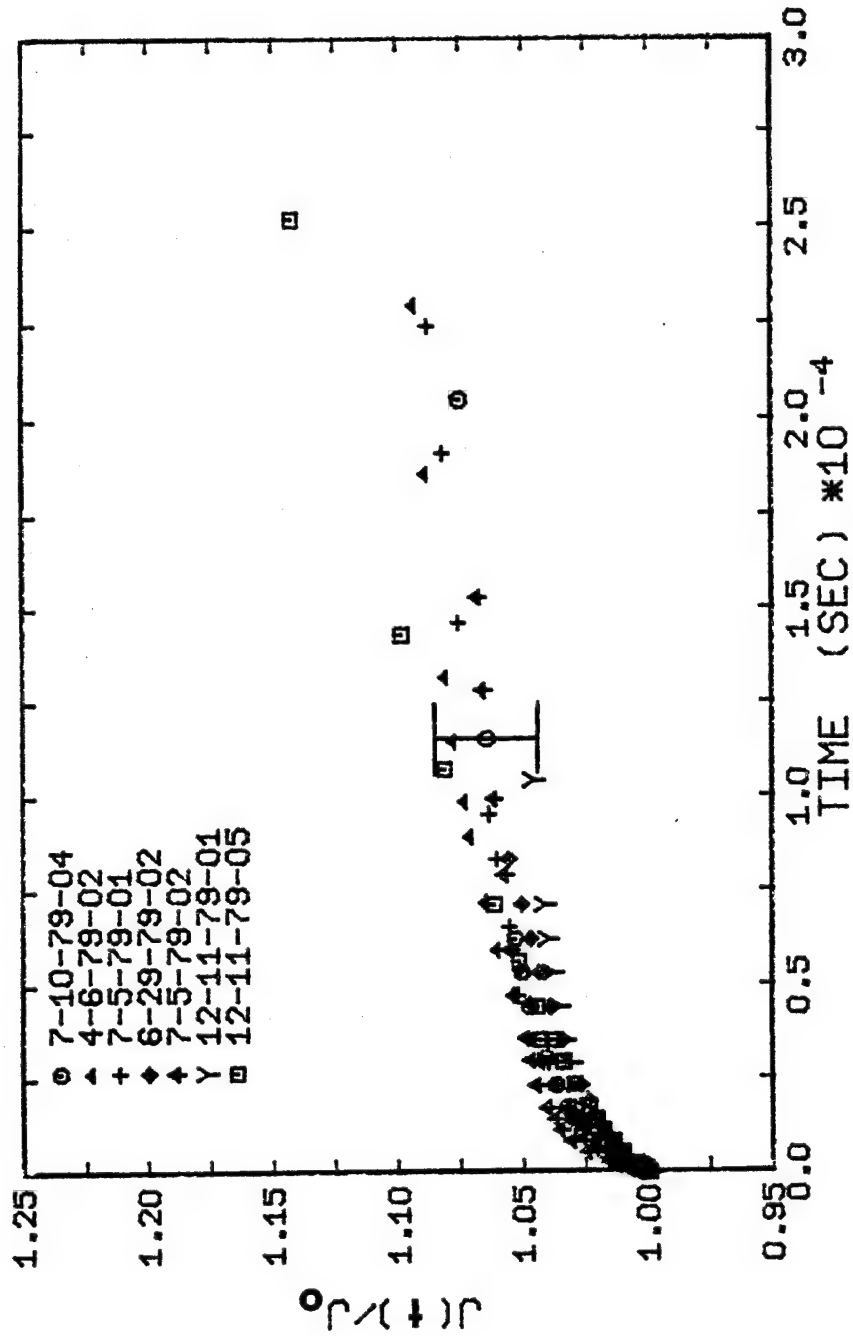


Figure 4.2.1-4 Reduced creep compliance of 3501-6 resin at room temperature in the viscoelastic zone

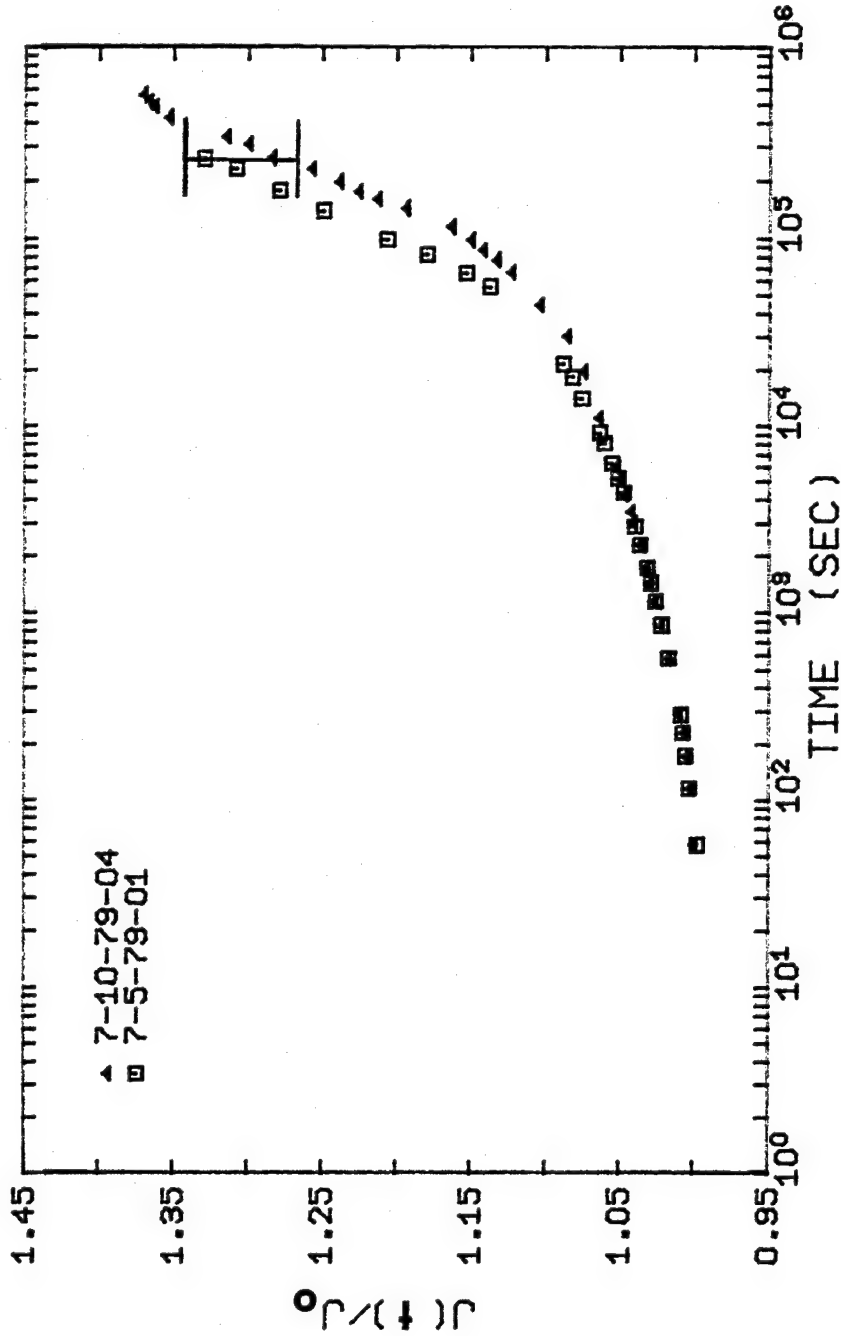


Figure 4.2.1-5 Long term reduced creep compliance of the 3501-6 resin at room temperature (different batches)

Using reduced compliance data also provides a means for comparing creep data at different temperatures. In figure 4.2.1-6, the creep curves of batch 6-29-79-00 at three different temperatures are presented for the viscoelastic creep zone (primary creep). The effect of temperature can be identified more easily this way. The scatter at higher temperatures reflects some oven instabilities ($\pm 0.5^\circ\text{C}$ could vary the strain reading by as much as 20 microstrain). An increase in temperature causes an increase in the rate of creep resulting in a higher increase in the compliance over an identical period of time. This simply reflects the increased mobility of the molecular chains and the enhanced ability of the polymer to "flow" at a higher temperature. An analysis of the shapes of the creep curves is given in section 4.2.2.

At longer times and higher temperatures, the onset of linear creep (secondary creep) is delayed and tertiary creep is not found at all. In figure 4.2.1-7, the reduced creep compliance is plotted at three different temperatures. Specimen 7-10-79-04 at 25°C exhibits all three zones of creep. On a log time axis the viscoelastic zone is almost linear for the first

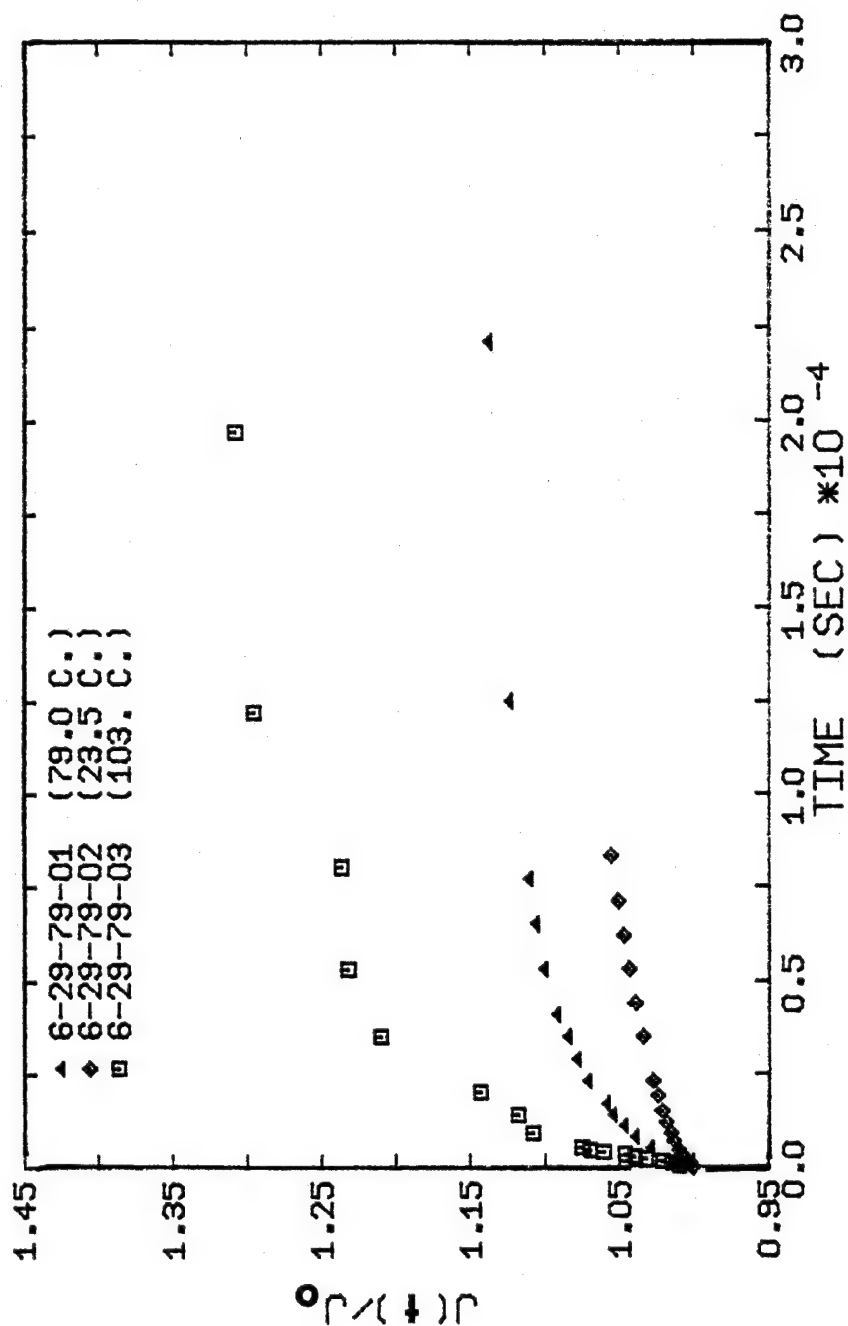


Figure 4.2.1-6 Reduced compliance vs. time for batch no. 6-29-79-00 at three different temperatures in the viscoelastic zone

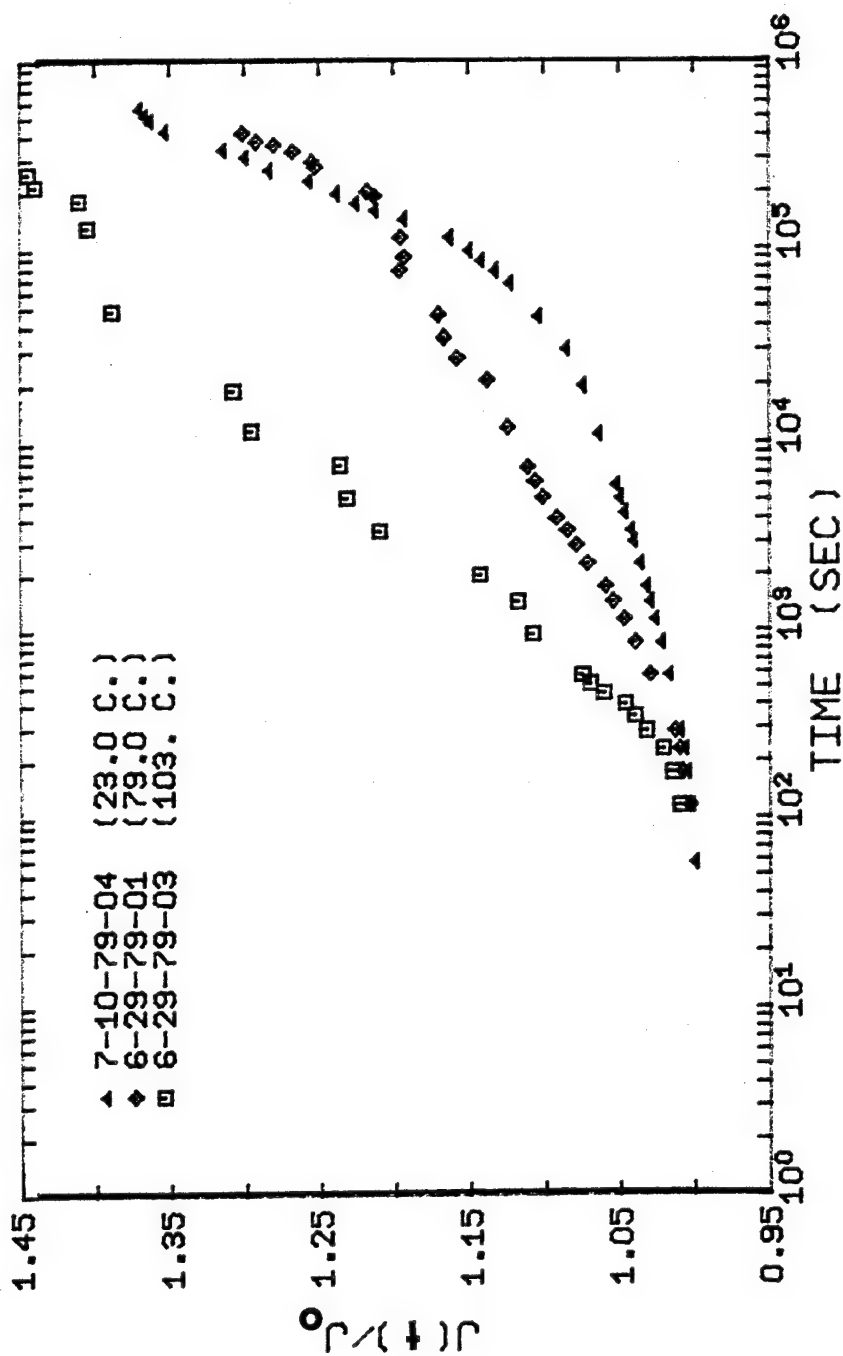


Figure 4.2.1-7 Reduced creep of the virgin resin at other temperatures

30 thousand seconds. Secondary or linear creep occurs between 30 and 100 thousand seconds. The creep behavior has nonlinear curvature on a log time axis ($f(x) = a + bx$ takes on the appearance of an exponential curve when plotted on a log time axis). Beyond 100 thousand seconds, the tertiary creep zone appears to be linear on a log time axis. Specimen 6-29-79-01 does not show linear creep until after 100 thousand seconds, thereby showing the delay at higher temperatures. The crossover of curves 7-10-79-04 and 6-29-79-01 is inconsequential because the reduced compliance is being plotted here (J_0 is different for each curve). The actual creep curves themselves never intersect. Specimen 6-29-79-03 at 103°C shows the primary zone for the entire length of the test. Its greater slope than specimen 6-29-79-01 shows the greater rate of creep at a higher temperature.

4.2.1.B COMPARISON OF THE CREEP OF THE 3501-6 WITH OTHER EPOXY RESINS

Since no previous creep data on the 3501-6 resin could be found in the literature, the creep of other tetraglycidyl amine resins were used for a comparison.

The end-use of these resins in carbon fiber composites is the same and their creep behavior will be reviewed here. Unfortunately, very few tests on the creep of the neat resin have been reported. Generally, only a few short creep tests are run to verify the predicted or measured creep in the transverse direction of the composite ($J_{22}(t)$). Therefore, only two sources of creep data conducted below the glass transition temperature were found, one for the 5208 neat resin and one other for the 3502 neat resin.

The first data source was taken from Schapery, et al. (1979) for the work performed on the virgin 3502 resin. Five data points were read off a creep curve to within an estimated accuracy of five percent. The original data source was Knauss, et al. (1979). The second source of data for the creep of the 5208 resin was taken from Kibler and Carter (1979). Five, 300 min creep tests at various temperatures were performed on the resin and all resin specimens were prepared from the same batch.

The room temperature creep curves of the 5208, 3502, and 3501-6 resin are plotted in figure 4.2.1-8. The two creep curves representing the 3501-6 resin in figure 4.2.1-1 have been replotted in figure 4.2.1-8

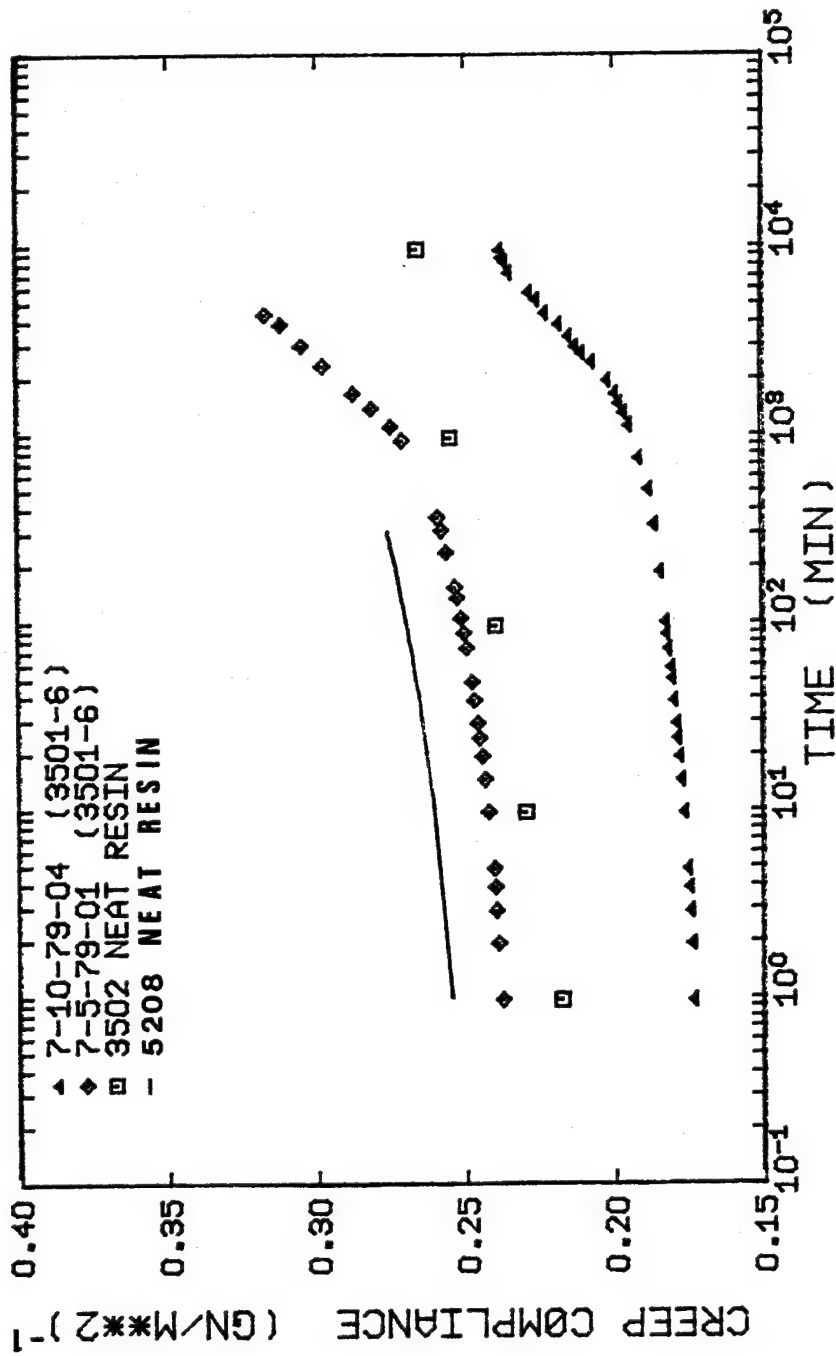


Figure 4.2.1-8 The creep of tetraglycidyl amine epoxy resins at room temperature

to show the boundaries of batch-to-batch variation. The experimental creep curve for the 5208 resin is represented by a power law function derived by Kibler and Carter (1979).

$$J(t) = 0.245 + 0.010t^{0.20} \quad (4.2.1-1)$$

The time is in minutes and the creep compliance is in reciprocal giga-newtons per meter squared (or giga-pascals).

Both the creep curves of the 5208 and 3502 resin are within ten percent of the upper limit of the creep behavior of the 3501-6 resin. The shapes of the curves are similar in the primary creep zone (less than 300 min). The 5208 and 3502 resins appear to be more compliant materials, but it is difficult to ascertain this without knowing the batch-to-batch variation of the resins. The most important factor of figure 4.2.1-8 is the deviation in the creep at longer times. The 5208 and 3501-6 resins exhibit a definite curvature on the compliance-log time plot. As mentioned in part A, this curvature is caused by the presence of secondary and tertiary creep. Data beyond 300 min was not available for the 5208 resin. On the other hand, the 3502 resin exhibits linearity at longer times on the log

time axis. The difference can be explained by investigating the conditions under which the test was run. Aging effects may have affected the creep data of Schapery, et al. According to Struik (1978), aging shifts the creep horizontally to longer times. An old specimen can show a linear creep range if the curvature has been shifted to longer times. The 3502 specimens were over a year old when tested. Schapery, et al. did investigate the aging phenomena. The transverse creep of a $(90)_{15}$ AS/3502 laminate was measured for 7,000 min before and after heating the composite above the glass transition temperature of the matrix resin. The creep curve of the one year old specimen was linear with time. The creep curve of the one year old specimen heated for fifteen minutes above the glass temperature showed a definite curvature with time. Therefore, aging effects were present in the old specimens and the creep curve of the 3502 resin should show some curvature. Heating the composite above the glass temperature effectively annealed the resin and removed the aging previously present in the specimen. In addition, the curvature in the creep of tetraglycidyl amine resins can only be present if the stress level is high enough to induce nonlinear behavior (like the yielding

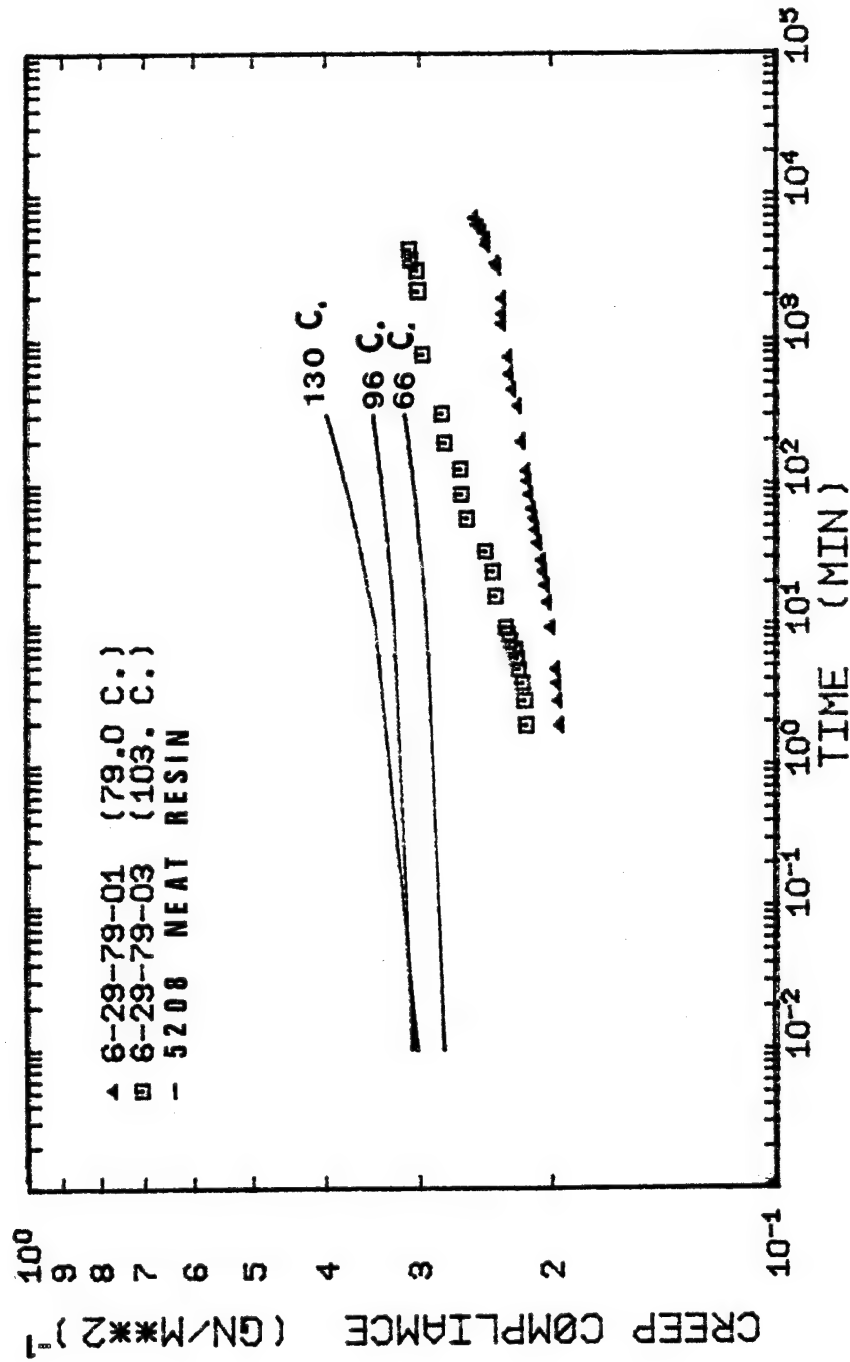


Figure 4.2.1-9 The creep of the 3501-6 resin vs. the 5208 resin above room temperature

observed in secondary creep). The initial stresses used on the 3502 resin were not given, but the stresses used on the 5208 resin were between 1.1×10^{-2} and 1.8×10^{-2} GN/m². These stresses fall within the same range of the stresses used on the 3501-6 resin.

The creep of the 5208 and 3501-6 resins at higher temperatures is shown in figure 4.2.1-9. No two temperatures of the investigations matched exactly, but it is clear that the 5208 resin is a more compliant resin at higher temperatures. Both show a slight curvature on a log time axis, but the creep is still fairly linear since all the curves shown here fall within the primary creep zone. The power law representation of the 5208 data does not show the original scatter in the data. The creep of the 5208 data resembles the 3501-6 data except that the creep compliance of the 5208 curves is higher. The power law fit used to represent the data was chosen by Kibler and Carter as a matter of convenience.

4.2.2 THE APPLICATION OF VISCOELASTIC MODELS

For this investigation, the viscoelastic models apply only in the primary creep zone (time less than

30 thousand seconds at room temperature). Pure viscous flow associated with the linear or secondary creep is a different mode of deformation requiring more complex models with more extravagant semi-theoretical equations. Modelling the secondary and tertiary creep is not the purpose here. The objective is to simply determine if the short term creep can be modelled by simple viscoelastic laws. A secondary objective is to use these models to predict the creep at longer times beyond the primary creep zone. In particular, these models are compared with the master curve of the resin computed using time-temperature superposition. In many investigations, the master curves are generated from a few short tests in the primary creep zone.

The model chosen to represent linear viscoelasticity was the four parameter Voigt-Kelvin model. The nonlinear viscoelastic model was the empirical power law model. The development of each model is presented in chapter 2. The results of the curve fitting of each of these models to the 3501-6 data is presented below. Both models fit the data equally well as determined by statistical methods (see the

discussion about the F-score test in appendix G).

In this case, the power law model would be preferred because it has one less parameter than the Voigt-Kelvin model, and the power law model does predict the creep better at longer times. However, the power law model has difficulty predicting the initial creep compliance at the higher temperatures, and its parameters at the same temperature also vary quite a bit. The Voigt-Kelvin model has none of these problems and it gives an excellent prediction of the initial creep compliance. The parameters of the Voigt-Kelvin model also give a more realistic interpretation of the events going on inside the structure of the crosslinked network. For this reason, the parameters of the Voigt-Kelvin model were used in an extensive analysis of the creep data at various temperatures.

4.2.2.A THE VOIGT-KELVIN MODEL

The applicability of linear viscoelasticity to the creep of DGEBA resins has been well documented. Both the work on the virgin resin and the transverse creep of the composite has been shown to agree with linear viscoelastic models (Ishai, 1967; DiBenedetto and Gauchel, 1974; Molenpah, et al.; 1969, Schapery, et

al., 1979). Generally the strain limit at the yield stress (linear elastic limit) is the limit of the applicability of linear viscoelasticity. The work presented here contains one of the few analyses of the viscoelastic creep behavior of tetraglycidyl amine resins, but the analogies previously presented for DGEBA resins are expected to apply.

The Voigt-Kelvin model discussed in section 2.1.2 is represented by the following equation:

$$J(t) = J_0 + J_1(1 - \exp(-t/\tau_1)) + t/\eta_0 \quad (2.1.2-12)$$

where

$J(t)$ = creep compliance, a function of time

J_0 = initial creep compliance at zero time

J_1 = the difference between the equilibrium compliance, J_E , and J_0 at infinite time
 $(J_1 = J_E - J_0)$

τ_1 = retardation time, the product of J_1 and the viscoelastic dashpot viscosity, η_1

η_0 = long term pure viscous flow viscosity

These descriptions of the parameters are the interpretations which define certain features of the creep behavior of a linear viscoelastic material. The definitions of the parameters in terms of the spring and dashpot

definitions are discussed in section 2.1.2.

The graphical depiction of equation 2.1.2-12 on time and log time axes along with an indication of the role of the parameters is shown in figure 4.2.2-1. In figure 4.2.2-1a, the initial creep compliance, J_0 , is the compliance at zero time. The exponential rise in the compliance (the form of linear viscoelastic creep behavior) then dominates the creep behavior until the linear creep behavior of pure viscous flow takes over at longer times. The point where linear creep becomes dominant is the value of the equilibrium compliance ($J_E = J_0 + J_1$). The slope of the linear creep region is the reciprocal of the long term viscosity, η_0 . Normally, crosslinked materials omit the pure viscous flow term from the model resulting in the leveling out of the creep to the equilibrium compliance (i.e. no linear creep region). The pure viscous flow term has been retained because the four parameter model matches the secondary creep region much better than the three parameter form of the Voigt-Kelvin model. A better fit to the creep data can be obtained by retaining the " t/η_0 " term of equation 2.1.2-12. In figure 4.2.2-1b, the exponential

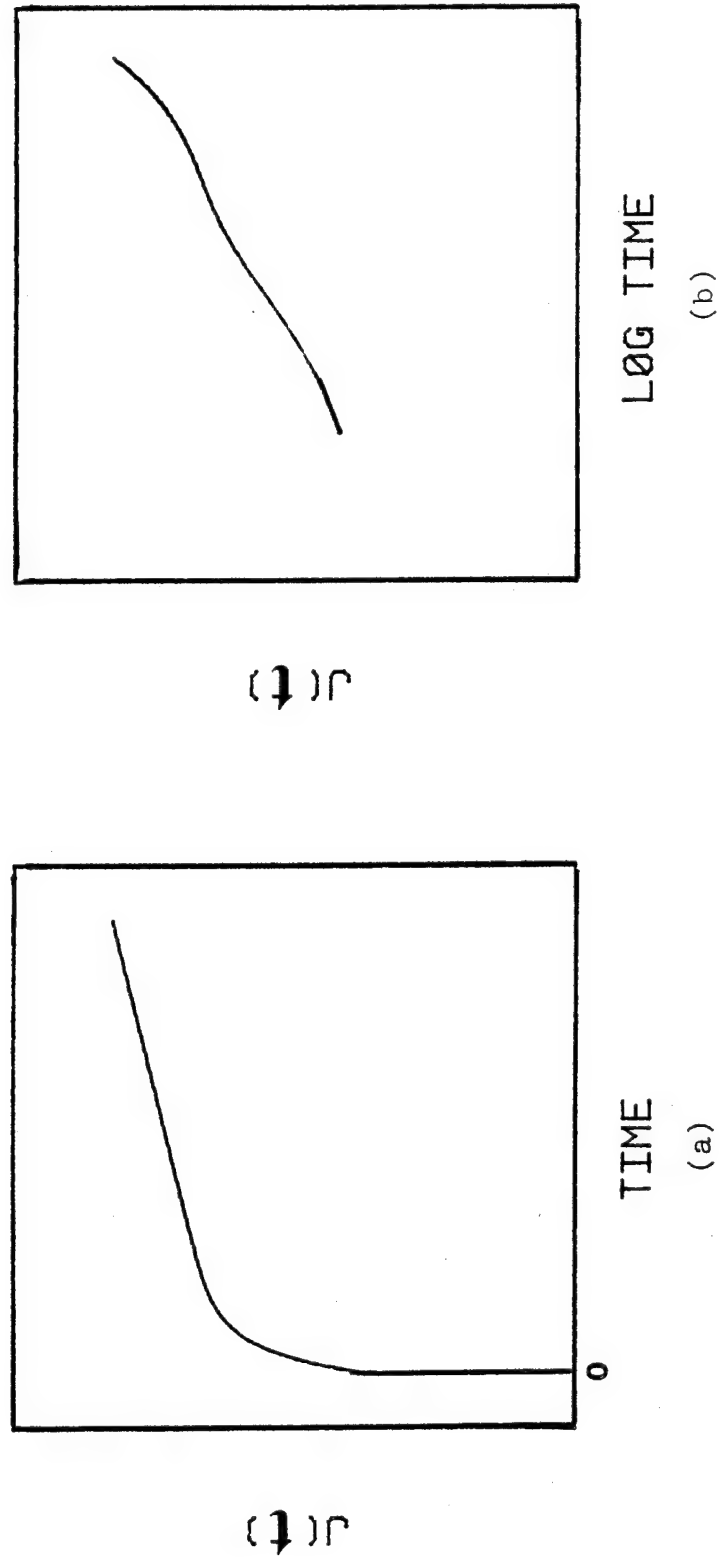


Figure 4.2.2-1 Representation of the Voigt-Kelvin model on different time coordinates

part of the curve takes on a sigmoidal shape on a log time axis. Linear creep at longer times exhibits a sharp increase in the creep behavior in what appears to be an exponential rise. If the onset of a linear creep region occurs early enough, the equilibrium "plateau" is never realized and the whole creep curve can appear to be linear in the beginning, then increasing like a power law model as shown in figure 4.2.2-7b. This form of the creep behavior is seen in the creep curves of figures 4.2.1-5 and 4.2.1-7 through 4.2.1-9. The real linear viscoelastic shape of the creep curves is depicted on normal time coordinates in figures 4.2.1-1, 4.2.1-2, 4.2.1-6, and 3.2-3.

The data for all eleven creep tests was fitted to equation 2.1.2-12 using a nonlinear least squares (NLLS) curve fitting routine available from the library of programs of the University of Delaware Computing Center. The values of each of the four parameters and the viscoelastic standard estimate of error of the fit is listed in table 4.2.2-1. The standard estimate of error is an indication of the average error (predicted compliance minus the measured compliance) between the data and the Voigt-Kelvin model. In each case, the fit is good to at

TABLE 4.2.2-1
PARAMETERS OF THE VOIGT-KELVIN MODEL

Specimen no.	J_O (GN/m ²) ⁻¹	J_1 (GN/m ²) ⁻¹ × 10 ²	τ_1 (sec)	η_O (GN/m ² -sec) × 10 ⁻⁶	s (GN/m ²) ⁻¹ × 10 ⁴
7-5-79-01	0.239	0.987	1524	1.95	4.34
7-5-79-02	.235	1.011	896	2.55	2.75
12-11-79-01	.212	.671	1168	4.20	3.63
12-11-79-05	.222	.785	3312	1.06	2.80
12-11-79-06	.226	.168	3059	2.00	1.14
7-10-79-04	.174	.724	1418	3.41	2.78
4-6-79-02	.183	1.074	2598	3.37	2.90
6-29-79-02	.184	.354	1120	1.23	1.02
6-29-79-01	.195	1.909	2060	2.74	4.19
6-29-79-03	.214	4.519	1750	0.889	24.1
11-3-79-01	.222	2.663	1180	1.60	12.9
RT Mean ± (σ)	.207 (0.026)	.787 (0.33)	1720 (970)	2.54 (1.1)

least three significant figures in the creep compliance. At room temperature the standard estimate of error, s , is less than $5 \times 10^{-4} \text{ (GN/m}^2\text{)}^{-1}$, which is much better than the experimental error. Also listed in table 4.2.2-1 are the room temperature average parameters plus or minus one standard deviation. Since the plasticized specimen, 12-11-79-06, did not show any changes in the primary creep zone where the fit was made, its parameters were averaged in also. A visual comparison between the creep data and the model is shown for specimens 7-10-79-04 and 6-29-79-03 in figure 4.2.2-2. Example calculations for the standard estimate of error are shown in appendix G.

At higher temperatures, the model does not fit the creep data as well as it did at lower temperatures because the scatter in the data was greater. At least two significant figures in the creep compliance could be predicted. This is comparable to the experimental error. The creep data at longer times was fit to the Voigt-Kelvin model for only a few cases. Examples of these results are shown in appendix G. The overall result was poor because the model could not fit the nonlinear elements of secondary and tertiary creep. For example, the value of J_0 was much higher than the

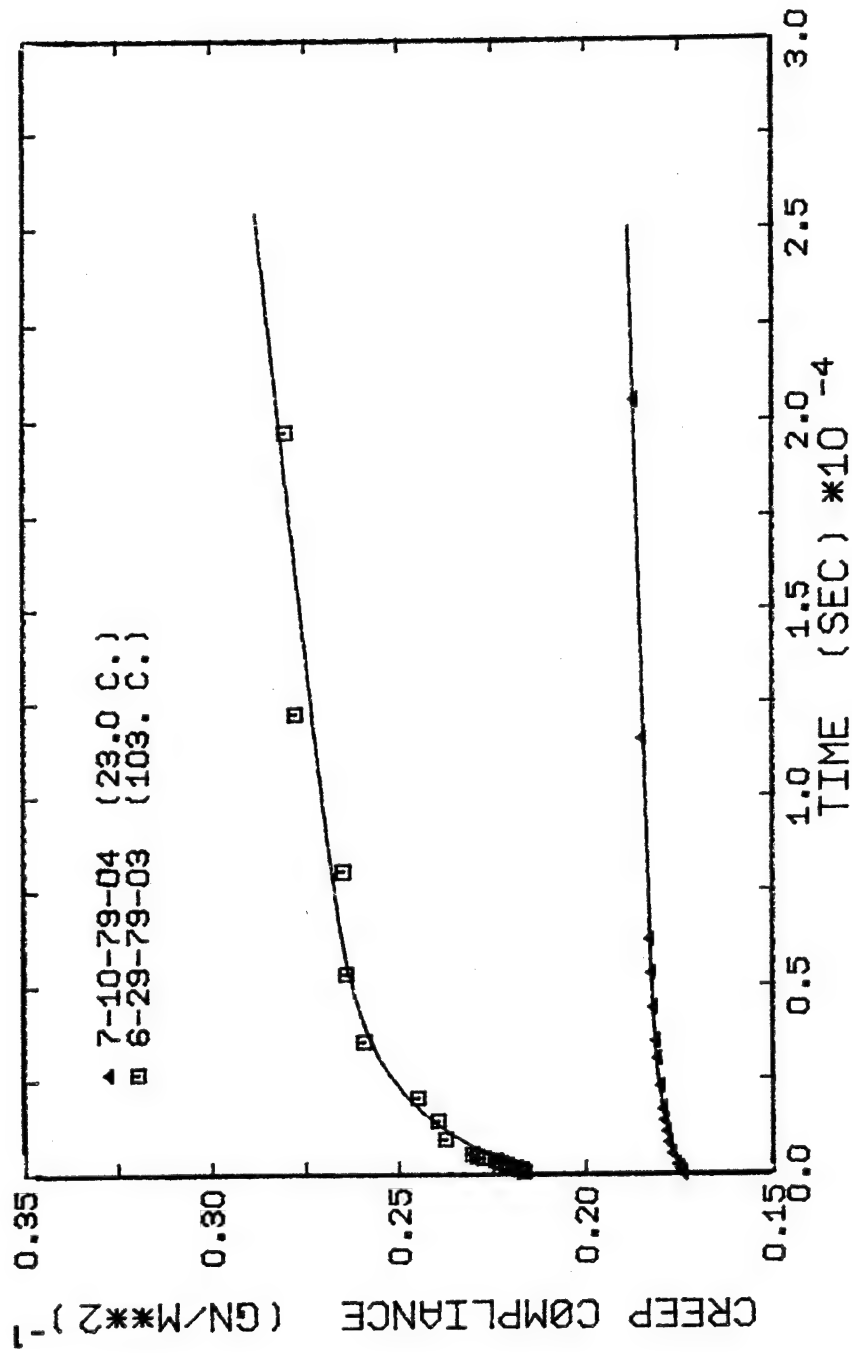


Figure 4.2.2-2 The Voigt-Kelvin model vs. the creep data of the 3501-6 resin in the viscoelastic zone

creep data in the entire viscoelastic creep zone.

A more complicated combination of springs and dashpots would be needed to fit the creep data at longer times and higher temperatures, but for the creep in the viscoelastic zone, the Voigt-Kelvin model fits the data very nicely.

The parametric values in table 4.2.2-1 provide a very useful method for examining the effect of temperature on the creep in the viscoelastic zone. The variations of each of the parameters with temperature are plotted in figures 4.2.2-3 through 4.2.2-6 and in appendix G. All results from room temperature testing have been averaged into a mean value for the parameter. That value is plotted in the figures with a one standard deviation error bar. This error bar represents 65% of the batch-to-batch variation in the parameters about the mean value. For instance, the initial creep compliance, J_0 , in figure 4.2.2-3 has an error bar width equal to $0.026 \text{ (GN/m}^2\text{)}^{-1}$ around the mean of $0.207 \text{ (GN/m}^2\text{)}^{-1}$. The other single tests at higher temperatures have error bars representing the 95% confidence limit of the parameters as calculated by the NLLS program. In figures 4.2.2-3 and 4.2.2-4, the variation in parameters J_0

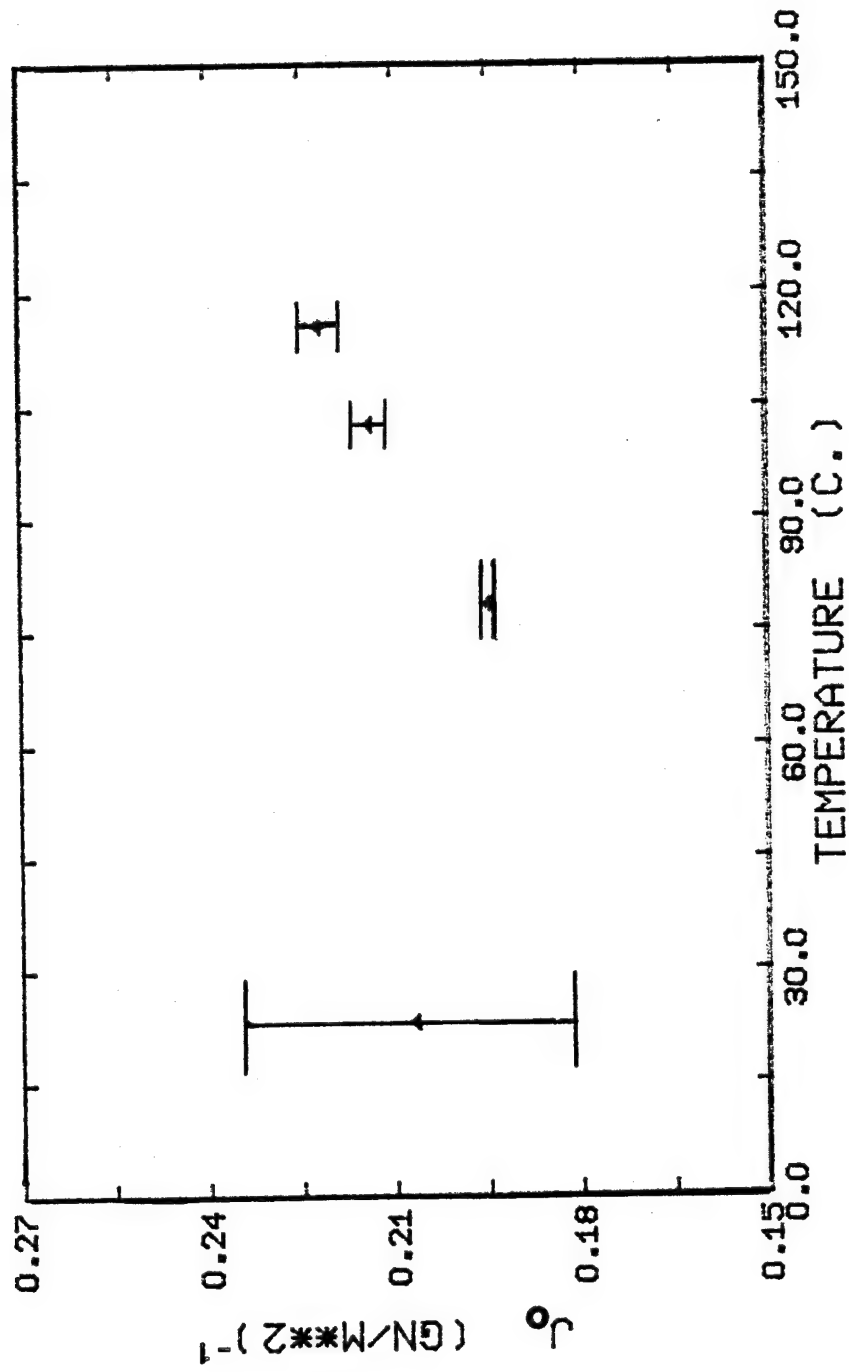


Figure 4.2.2-3 J_O vs. temperature for all batches

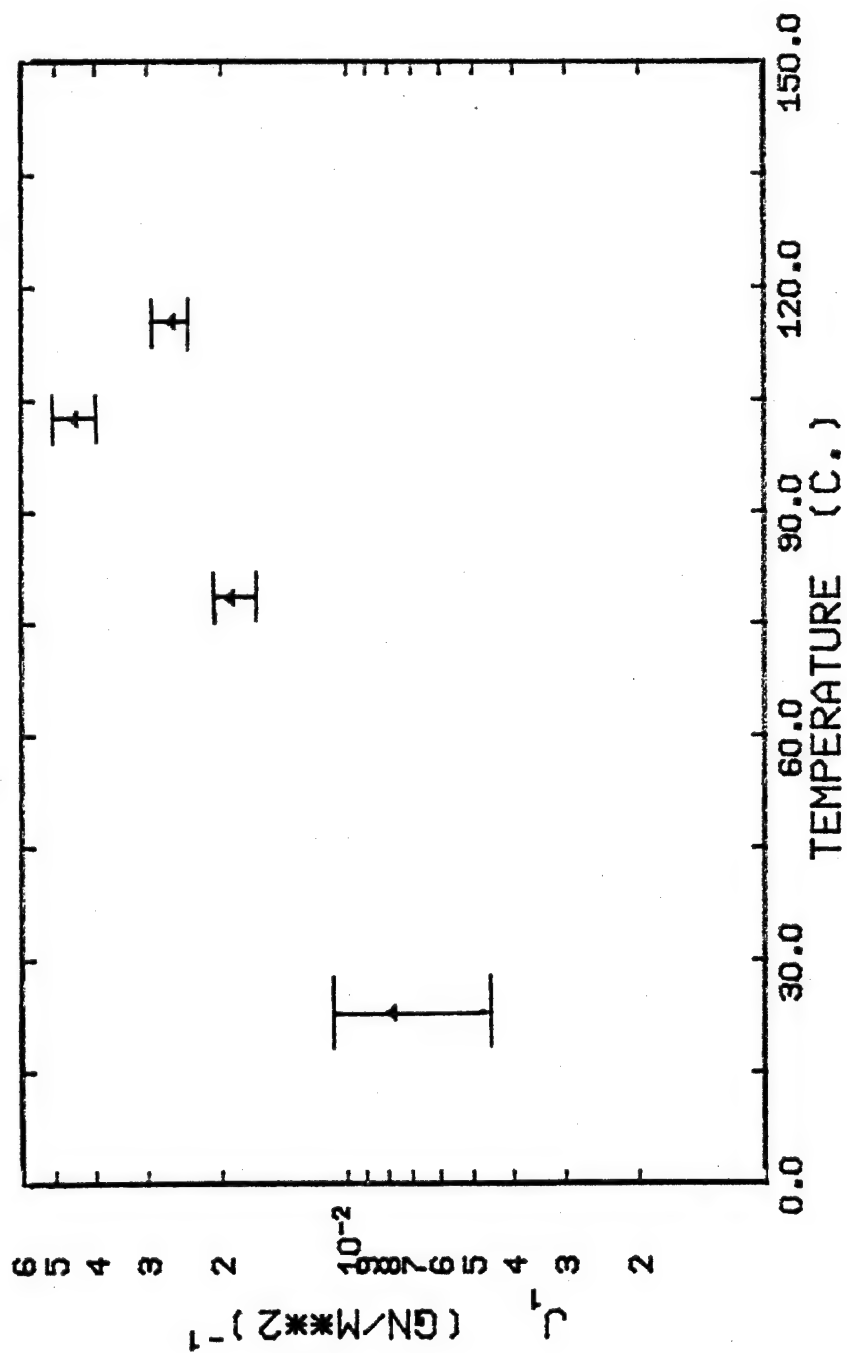


Figure 4.2.2-4 J_1 vs. temperature for all batches

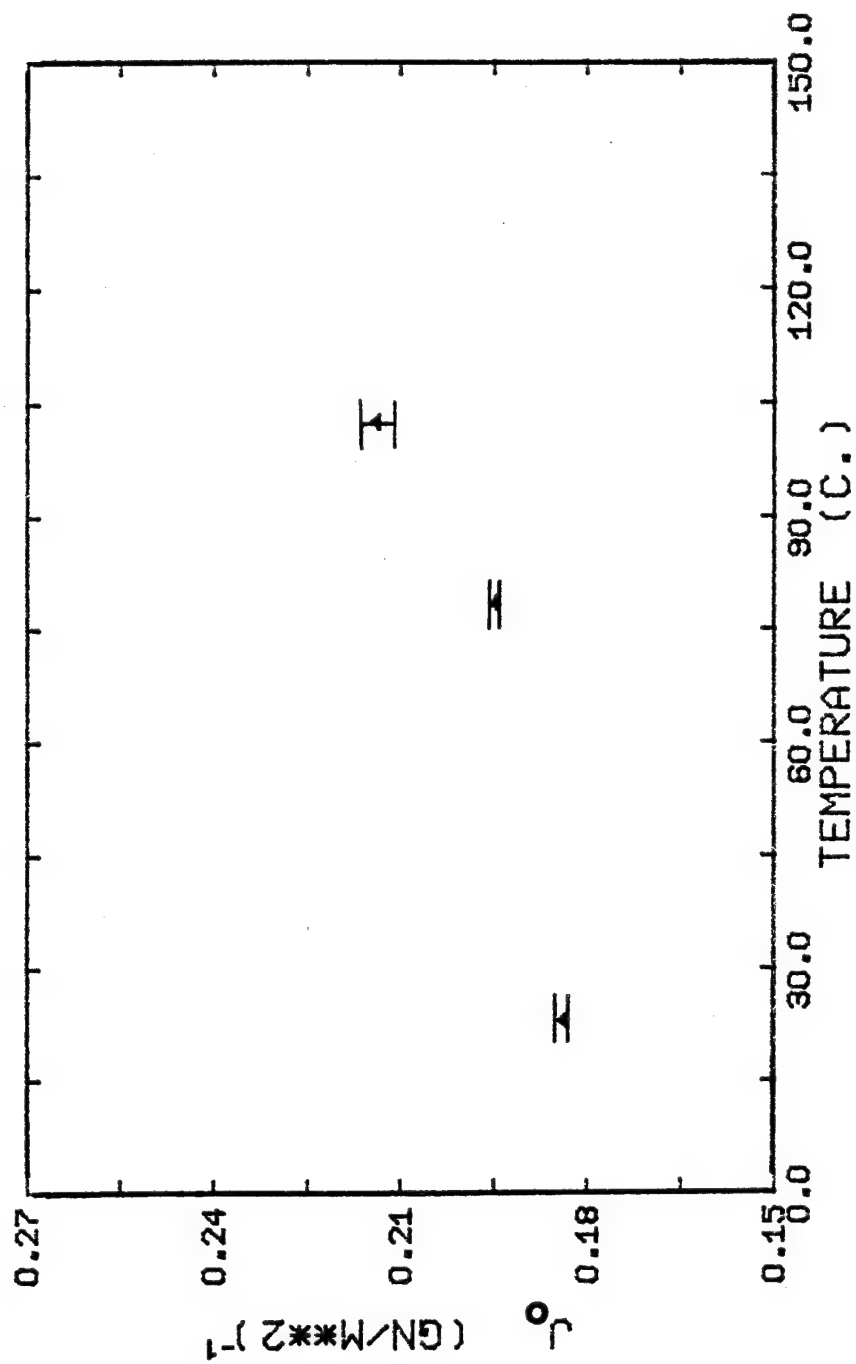


Figure 4.2.2-5 J_O vs. temperature for batch 6-29-79-00

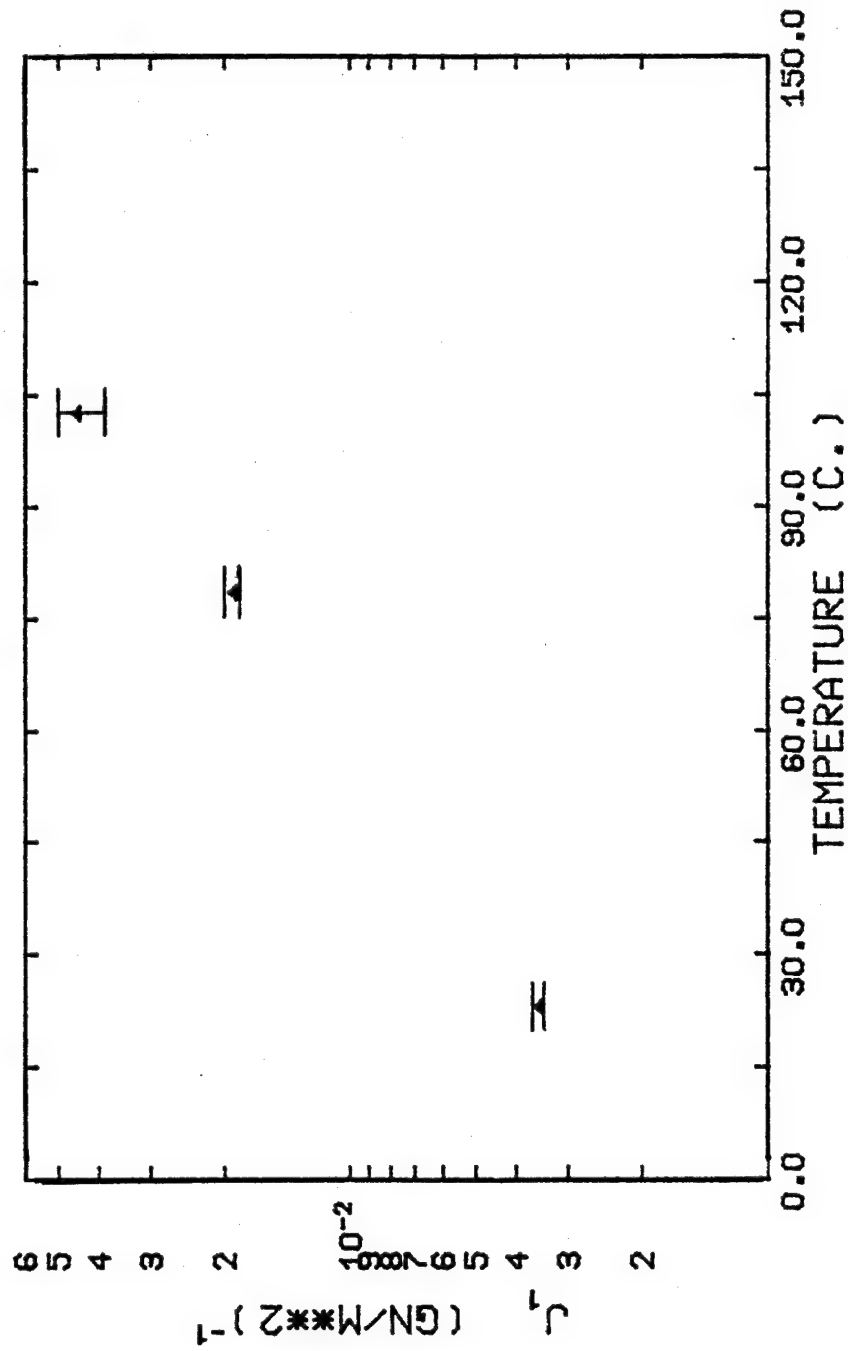


Figure 4.2.2-6 J_1 vs. temperature for batch 6-29-79-00

and J_1 with temperature are shown for various batches of the resin in order to establish the effect of batch-to-batch variation on the parameters. In figures 4.2.2-5 and 4.2.2-6, the variation of the parameters J_0 and J_1 determined from tests on the same batch is shown. The variation in the parameters τ_1 , η_1 , and η_0 with temperature for the batch-to-batch and single batch cases is plotted in appendix G.

The initial creep compliance does not vary with temperature if figure 4.2.2-3 is used as the only basis for that decision. The range in the parametric values at room temperature; however, encompasses the entire range of values at all temperatures (between 21° and 116°C). The batch-to-batch variation in the parameters is just too great to justify any statement on whether or not J_0 increases, decreases, or remains the same with increasing temperature. An increase in J_0 should be present because the reciprocal of J_0 is the instantaneous creep modulus. It is a well known fact that the modulus of a material decreases with increasing temperature. The expected is observed in figure 4.2.2-5 where J_0 has been plotted for tests from the same batch. The creep compliance increases

by 16.5% from the value at 22.5° to the value at 103°C. More tests would be needed to establish the proper analytical dependence of J_0 on temperature. For these few tests, the functional relationship appears to be nonlinear below the glass transition temperature of the resin (200°C).

Assuming that the tensile modulus and the reciprocal of the initial creep compliance are equal, the value of $1/J_0$ can be compared to the tensile modulus of the 3501-6 resin as measured at several temperatures. A decrease in the Young's modulus for dessicated specimens with increasing temperature has been measured by Augl (1978). The modulus decreased from 6.2×10^5 to 5.5×10^5 psi (4.27 to 3.79 GN/m²) as temperature was raised from 20° to 100°C. This corresponds to an increase in the creep compliance from 0.234 to 0.264 reciprocal GN/m² (an increase of 12.8%) over the same temperature range. The percentage increase of 16.5% observed in the increase in the creep compliance of the current study agrees quite nicely. The difference between the two is probably due to the level of background moisture existing in the present study's specimens. In the current work, background

moisture plasticization would cause a greater increase in the initial creep compliance when compared to a dessicated specimen. Augl's data support this conclusion. The Young's modulus decreased faster over the same temperature range with increasing amounts of sorbed moisture.

Unlike J_0 , parameter J_1 does exhibit an increase with increasing temperature outside of batch-to-batch variation. In figures 4.2.2-4 and 4.2.2-6, J_1 increases by almost an order of magnitude. The parameter J_1 is a direct measure of the creep between the viscoelastic equilibrium compliance and the initial creep compliance (assuming that there is no pure viscous flow characterized by a later linear creep). The increasing value of J_1 with temperature reflects the gradual "loosening up" of the network structure caused by enhanced thermal vibrations. The overall free volume of the network has not appreciably increased as indicated by the moderate increase in the values of J_0 . However, the mobility of the segments of the chains within that free volume has increased considerably. The greater vibrations in the network increases the probability that steric hindrances can be overcome. One segment of a chain

can "jump" more easily over another chain while under the influence of an external stress (Schultz, 1974; Bueche, 1956; Meares, 1965).

The increased segmental mobility will decrease the viscosity of the dashpot parameter, η_1 . From figures G-2 and G-5, the viscosity, η_1 , decreases with increasing temperature, even outside of batch-to-batch variation. According to Schultz (1974), the most agreed upon equation which models the relationship between viscosity and temperature of a network polymer below the glass transition temperature is an Arrhenian relationship of the form,

$$\log \eta_i = (\log E_i) / (2.303R) (1/T - 1/T_g) \quad (4.2.2-1)$$

where

T = absolute temperature in $^{\circ}\text{K}$

T_g = glass transition temperature

The product of η_1 and J_1 defines the retardation time, τ_1 . For one simple spring and dashpot in parallel (see figure 2.1.2-1), only one retardation time exists which is a mean retardation time for an entire distribution of retardation times. The parameter, τ_1 , should be weakly dependent upon temperature because η_1 and J_1 are dependent upon temperature in opposite ways. Since η_1

and J_1 each change by an order of magnitude between 22° and 103°C, their product should be a constant. In figures G-1 and G-4, neither batch-to-batch variation nor the same batch results show a dependency between τ_1 and temperature. The variations shown by the error bars are too great to draw any conclusion except that the retardation time is relatively constant at temperatures well below the glass transition temperature.

The pure viscous flow parameter, η_0 , is strongly dependent upon the curve fitting routine. As temperature increases, a slight decrease in η_0 should occur, but as shown in figures G-3 and G-6, a decrease is difficult to substantiate. The problem lies in the fact that the pure viscous flow term attempts to match the visco-elastic creep zone with the secondary creep zone. Therefore, the pure viscous flow term is really being used to fit the model to the creep data instead of being used in its proper analytical form. In this curve fitting application, the parameter η_0 loses the identity of viscosity so that no physical significance can be attributed to its temperature dependence.

4.2.2.B POWER LAW MODEL

The power law model was originally developed as an empirical approach in representing nonlinear visco-elastic creep behavior. The model is shown in equation 2.1.3-2 with an initial compliance term, J_0 . A discussion of the model is given in section 2.1.3.

$$J(t) = J_0 + D_1 t^n \quad (2.1.3-2)$$

The model differs from the Voigt-Kelvin model in two respects. First, an equilibrium compliance term (J_E) is not inferred from the power law model. Secondly, a pure viscous flow term is absent. For exponent "n" less than one, the creep rate is a decreasing function of time. The representation of the power model in time and log time coordinates is shown in figure 4.2.2-7.

The eleven creep tests were fitted by the NLLS program to the power law model. The values of the parameters, the room temperature mean of the parameters with the standard deviation, and the standard estimate of error are listed in table 4.2.2-2. A qualitative assessment of the fit can be seen in figure 4.2.2-8 where the same two creep curves of figure 4.2.2-2

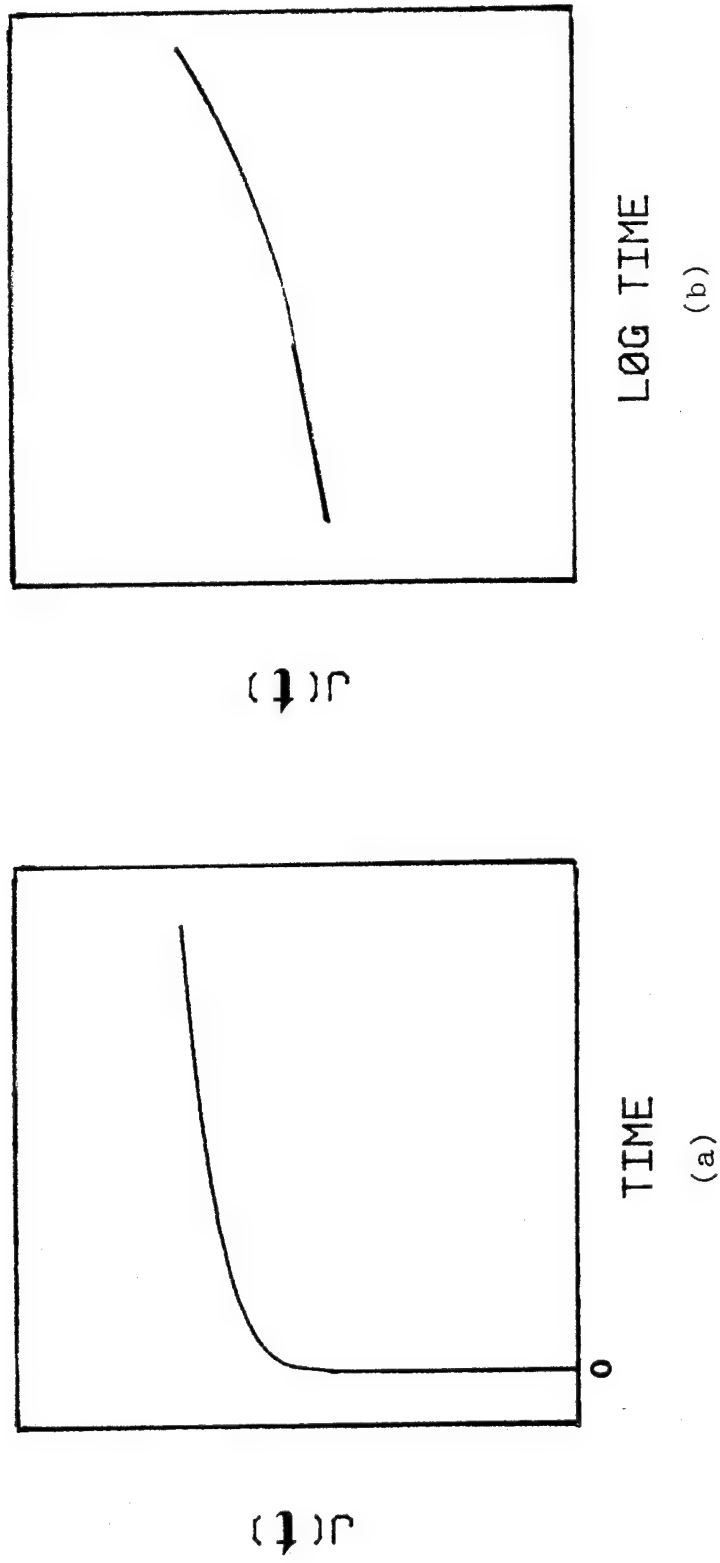


Figure 4.2.2-7 The representation of the power law model on different time coordinates

TABLE 4.2.2-2
PARAMETERS OF THE POWER LAW MODEL

Specimen no.	J_O $(GN/m^2)^{-1}$	D_1 $(GN/m^2)^{-1} \times 10^3$	n	s $(GN/m^2)^{-1} \times 10^4$
7-5-79-01	0.233	1.66	0.28	1.03
7-5-79-02	.193	32.3	.060	3.71
12-11-79-01	.202	5.34	.14	1.67
12-11-79-05	.221	0.050	.64	1.25
12-11-79-06	.225	0.032	.61	5.31
7-10-79-04	.167	2.80	.20	1.89
4-6-79-02	.181	0.55	.36	6.94
6-29-79-02	.183	0.118	.50	6.81
6-29-79-01	.161	19.2	.12	8.24
6-29-79-03	.136	42.0	.13	25.2
11-3-79-01	0.0	190.	.033	5.38
RT Mean \pm (σ)	.201 (0.024)	5.4 (11.)	.35 (.21)

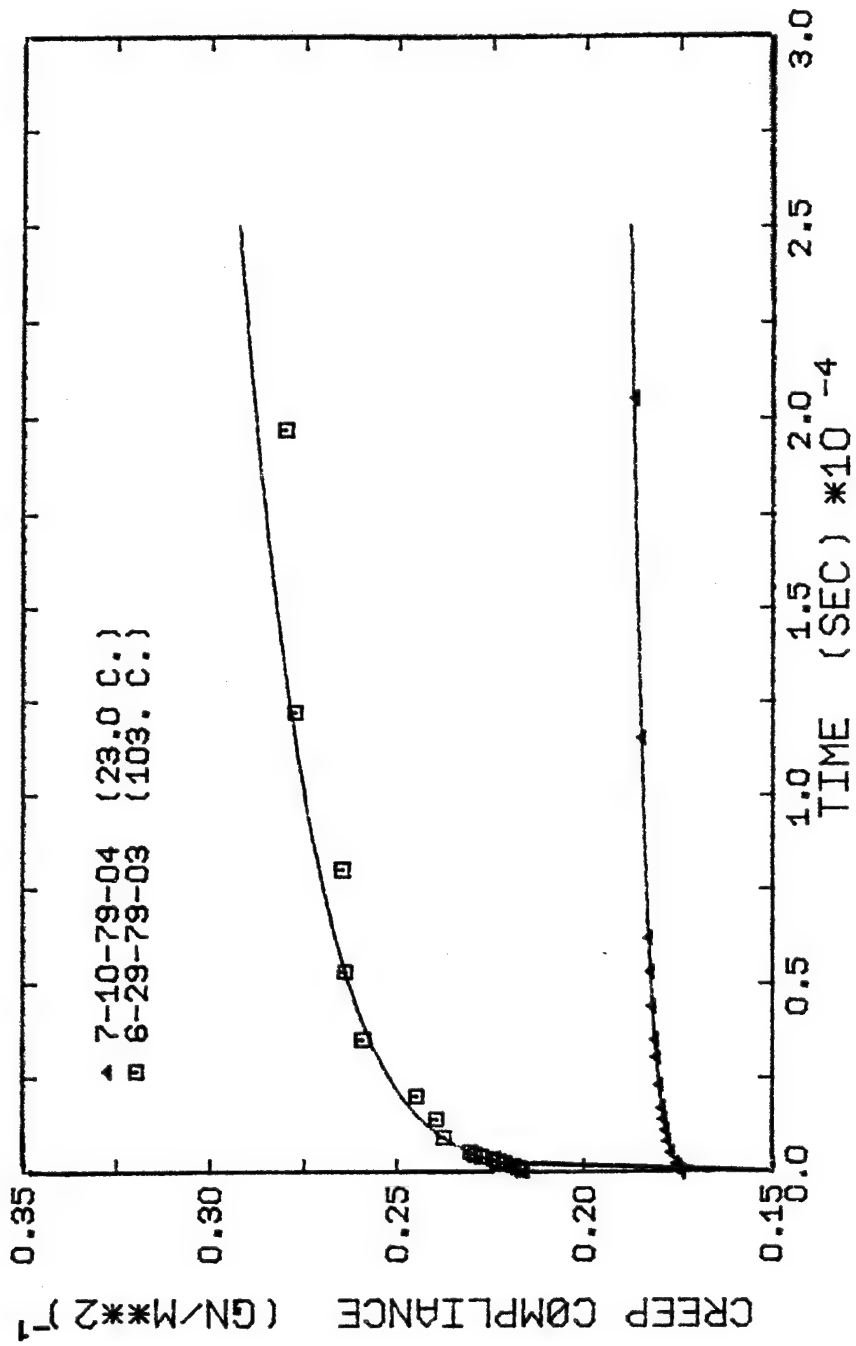


Figure 4.2.2-8 The power law model vs. the creep data of the 3501-6 resin in the viscoelastic zone

have been replotted against the power law model. The curve fitting procedure only applies to the visco-elastic creep zone. The statistical comparison between the two models using the F-score test is given in appendix G.

The prediction of the initial creep compliance at room temperature is consistent with the mean value of J_0 computed from the Voigt-Kelvin model (0.201 vs. 0.207 reciprocal GN/m² from the V-K model). The standard deviations are also fairly close (0.024 vs. 0.026 for the V-K model). In contrast, the stability of the parameters D_1 and n was lacking. The batch-to-batch variation in the parameters was quite large as shown by the large standard deviations in D_1 and n . The variation in the parameters for the Voigt-Kelvin model is much less; therefore, those parameters were used to show the effect of temperature on the resin. The standard estimate of error for the power law model is equal to if not less than the standard estimate of error of the Voigt-Kelvin model. Both can predict the creep compliance to within three significant figures. Both models also fit the data equally well according to the F-score test (appendix G).

At higher temperatures, the fit becomes increasingly poorer. The initial creep compliance decreases as the temperature increases which is an absurd result. The model fails to fit the data properly for two reasons: (i) the primary creep zone is extended to longer times at higher temperatures so the curve fitting procedure should be redone over the whole length of the test, (ii) and the viscoelastic creep behavior at higher temperatures may require more complex models to fit the data (i.e. a model with more than three parameters). At longer times, the power law model does do a better job of fitting the data than the Voigt-Kelvin model. This situation is discussed in section 4.2.3.

Kibler and Carter (1979) stated that they successfully applied the power law model to the 5208 neat resin creep data at a variety of temperatures. A constant value of $n = 0.20 \pm 0.04$ was chosen as a constant. Usually the exponent n is a function of temperature (Nielsen, 1974). It is unclear what assumptions they used to determine that n was constant. The values of n in table 4.2.2-2 clearly show that n is not a constant for the 3501-6 resin. Their method of determining the power law parameters was different from the NLLS method used

in the present work and no statistical analysis was mentioned in their paper (the testing of the viscoelastic nature of the creep behavior of the 5208 resin was not the principal aim of their investigation); therefore, the quality of their curve fitting remains unknown. Future use of the power law model in modelling the creep behavior of these epoxy resins should keep all the parameters temperature dependent.

4.2.3 TIME-TEMPERATURE SUPERPOSITION

All previous work on time-temperature superposition concerning the creep or stress relaxation of epoxy resins or their composites has been performed more as an exercise to create the master curve rather than to gain insight into its applicability. Most authors have conducted a few tests at various temperatures and "pasted" curves together on reduced variable axes without performing any long term testing to establish if the master curve really predicts the creep or stress relaxation beyond the length of the tests originally used to construct the master curve. Without further testing, a master curve can give a false sense of security concerning the long term behavior of the material. It was found that time-temperature superposition does not predict the

long term creep very well for the 3501-6 resin, but instead it only provides a lower bound to the creep behavior. The ramifications of the failure of time-temperature are discussed below.

Time-temperature superposition was originally developed as an empirical tool by which the data at shorter times could be extrapolated to longer times at any temperature. Some theoretical justification has been developed in support of time-temperature superposition (Ferry, 1961) for polymers above their glass temperatures, but it remains an empirical tool below the glass temperature. Since it is an empirical tool, neither linear nor nonlinear viscoelastic models are implied. Ferry (1961) has laid out certain criterion for its applicability, but these criterion are restricted to an "apply it and see if it works" approach. This criterion is still the only method of adequately testing the applicability of time-temperature superposition. In this study, the results of applying time-temperature superposition towards constructing the master creep curve for the 3501-6 resin indicated that:

1. Superposition applied to short term creep experiments underestimates the long term

creep of the virgin resin.

2. It is applicable only up to 30 thousand seconds, the length of the original tests.

Therefore, creep data reported in master curves should be viewed with some caution. The detailed analysis of the failure of time-temperature superposition for the 3501-6 resin is discussed below, but the conclusions made here apply to the resin at temperatures between 22° and 103°C.

In essence, the time-temperature superposition scheme asserts that a compliance (or modulus) measured at a time, t , and temperature, T , is equal to the compliance (or modulus) measured at time, t/a_T , and a reference temperature, T_0 . The horizontal time shift factor, a_T , is a function of temperature only. Ferry has suggested the need for vertical shift factor to correct for density changes. Employing both of these corrections, the principle can be represented by the equation below.

$$\rho_T J(t, T) = J(t/a_T, T_0) \rho_{T_0} \quad (4.2.3-1)$$

The choice of a reference temperature, T_0 , is arbitrary so it was chosen to be 23°C. For other creep tests above

or just below the glass transition temperature, the temperature parameter T_0 is taken as the glass temperature, T_g .

Rearrangement of equation 4.2.3-1 leads to a method by which a shifted compliance can be plotted against shifted time in order to derive the master curve.

$$J_p = J(t, T) \rho T / (\rho_0 T_0) = J(t/a_T, T_0) \quad (4.2.3-2)$$

By plotting the creep data multiplied by the density-temperature ratio vs. log time, the shift factor can be graphically computed. The creep data of batch 6-29-79-00 (three tests) has been plotted in this fashion in figure 4.2.3-1. The density ratio was determined from the linear thermal expansion coefficient at each temperature. The detailed description of determining the thermal linear expansion coefficient and the calculations of the shift factors is contained in appendix D. In figure 4.2.3-1, only the data of the primary creep zone has been used to determine the master curve (time less than 30 thousand seconds) for two reasons. First, one of the tests was of short duration and secondly, the restriction of the creep data to less than 30 thousand seconds concurs with the length of creep tests

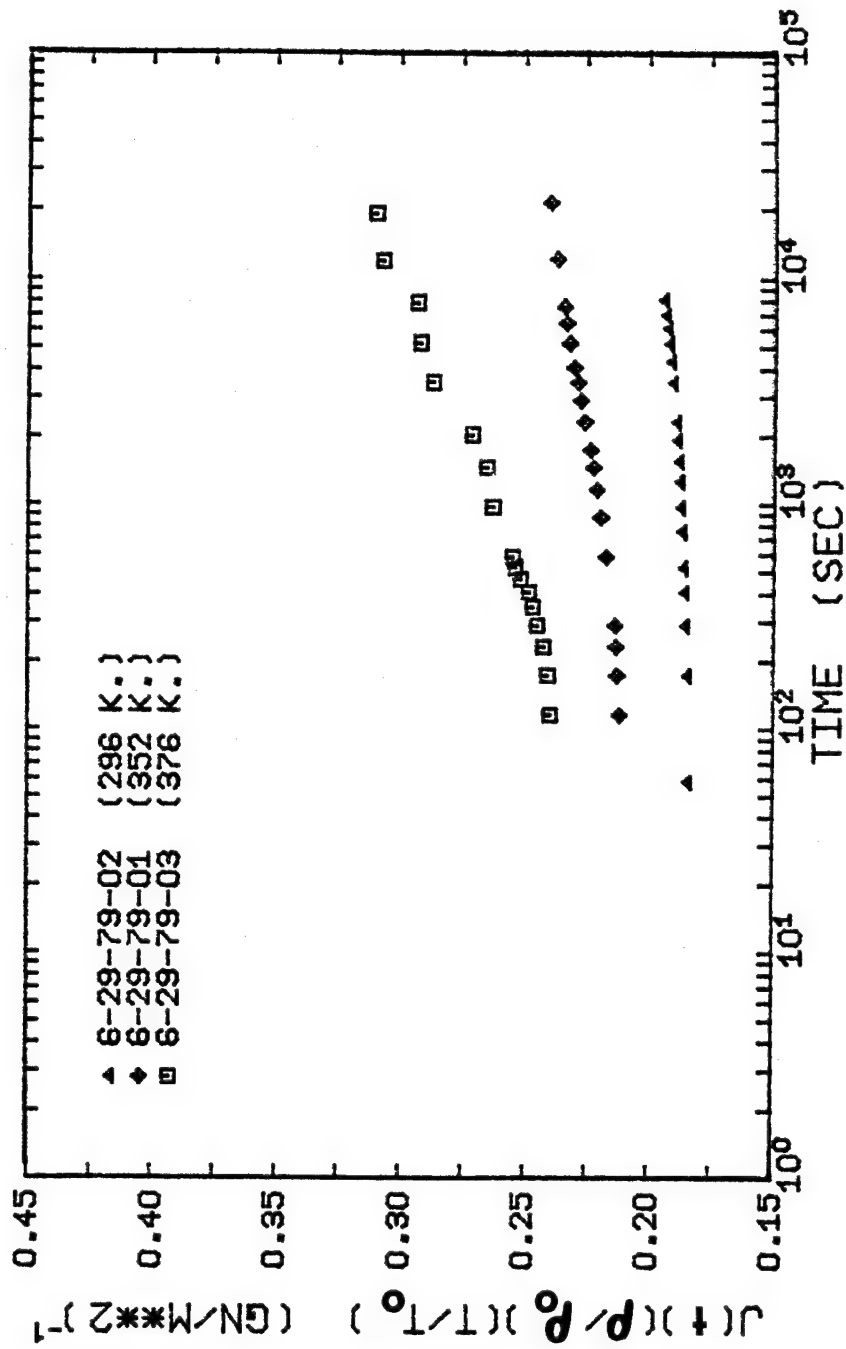


Figure 4.2.3-1 The creep curves of batch 6-29-79-00 shifted vertically for temperature. The reference temperature is 23°C.

used by other investigators to create their master curves (Kibler and Carter, 1979; Schapery, et al., 1979; Kim, et al., 1978; Yeow, et al., 1979). The lowest curve in figure 4.2.3-1 is not shifted because it is at the reference temperature. To form the master curve, the creep curves at higher temperatures are shifted to longer times as defined in equation 4.2.3-3.

$$\log (t/a_T) = \log t - \log a_T \quad (4.2.3-3)$$

The curves were shifted by using a computer graphics technique until the best smooth curve through the data was obtained. This is the "pasting" method referred to earlier. The master curve for the 3501-6 resin appears in figure 4.2.3-2. The shift factors are plotted in figure 4.2.3-3.

The master curve and its shift factors for the 3501-6 resin compare well with the master curves of other epoxy resins determined by other investigators. In figure 4.2.3-2, the master curve for the 5208 resin ($T_0 = 57^\circ\text{C}$) and the transverse creep of T300/934 and AS/3502 carbon fiber composites ($T_0 = 25^\circ\text{C}$) are plotted along with the master curve of the 3501-6 resin. On a

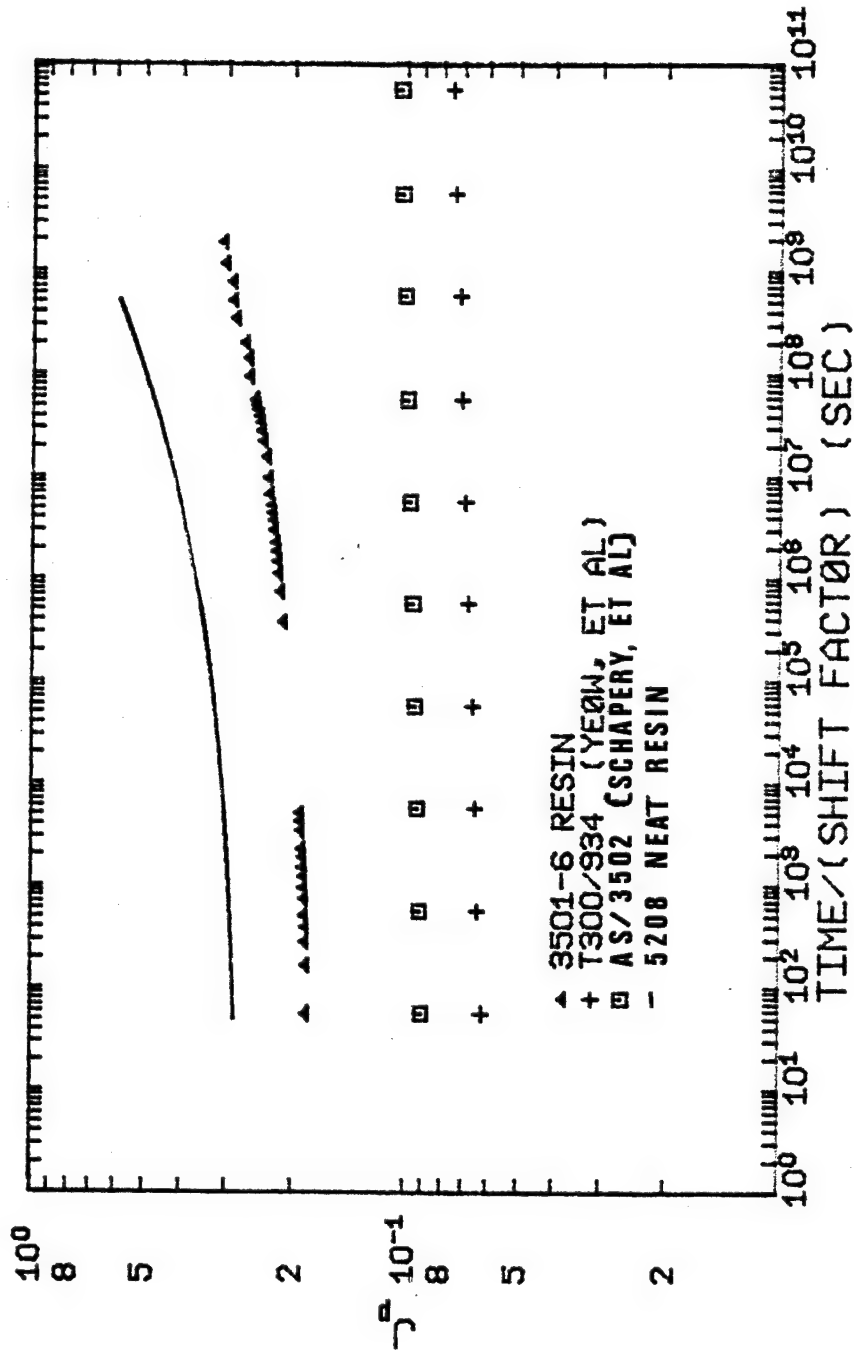


Figure 4.2.3-2 The room temperature master creep curves for some tetraglycidyl amine epoxy resins and their composites

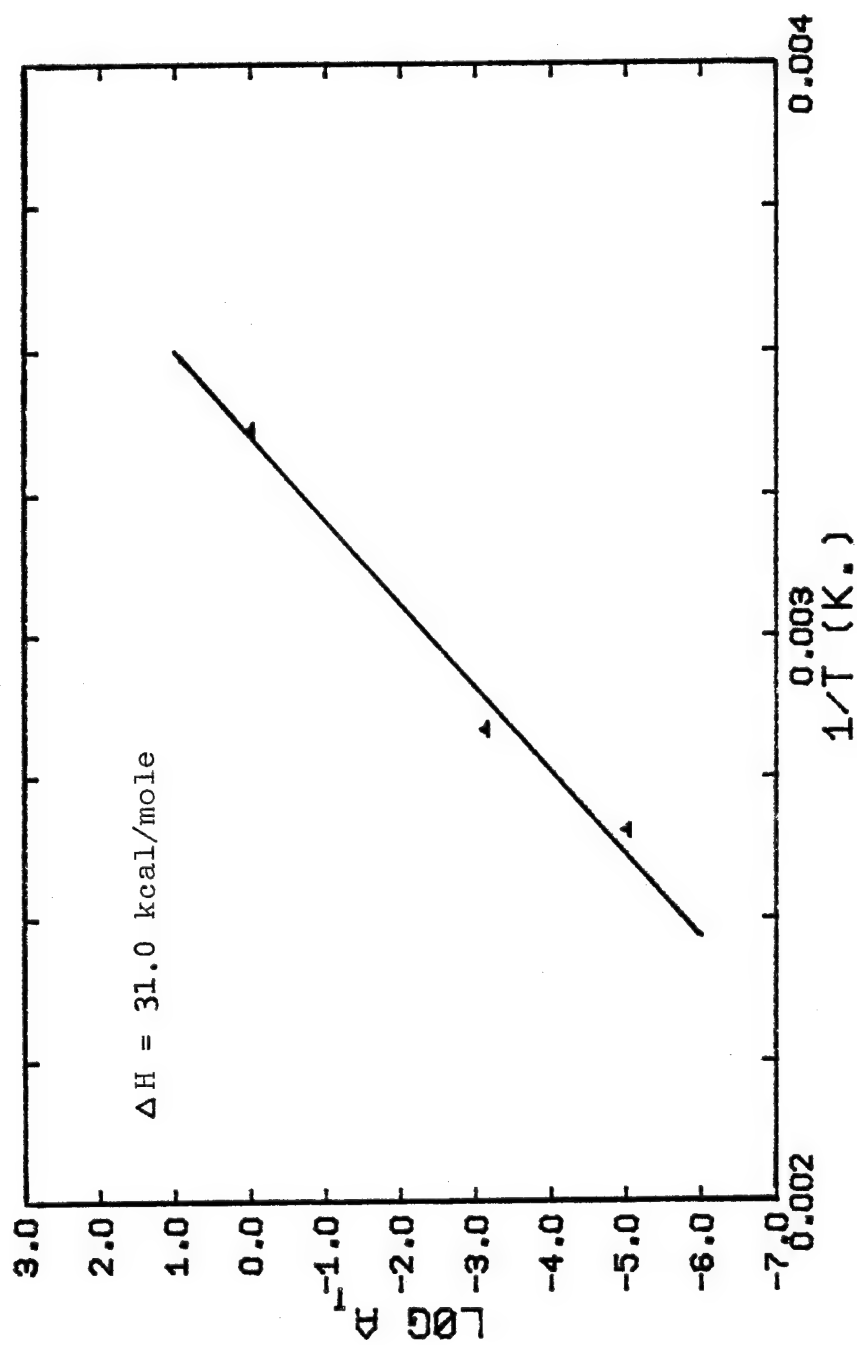


Figure 4.2.3-3 The Arrhenian type dependence of the shift factor, a_T , on temperature

log time axis, the resins show a curvature while the composite master curves are fairly linear. The transverse creep of the composites is resin dominated, but the lack of curvature is probably caused by the stiffening effect of the fibers. The curvature of the neat resin master curves has been recorded in the literature for DGEBA resins. Since these resins are more compliant than the tetraglycidyl amine resins, their master curves exhibit a rubbery plateau at longer times not seen in the tetraglycidyl amine master curves (DiBenedetto and Gauchel, 1974; Kim, et al., 1978).

The shift factor, a_T , is believed to follow an Arrhenian type equation for its dependence on absolute temperature below the glass transition:

$$\log a_T = \Delta H / (2.303R) \times (1/T - 1/T_0) \quad (4.2.3-4)$$

Other equations have been developed in order to determine the temperature dependence of the shift factor, but these empirical equations (such as the well known WLF equation) are generally used above the glass temperature of the polymer (Ferry, 1961). The simplicity of the Arrhenian type equation offers a means of comparing the "pasting" technique used to

determine the master curves of other epoxy resins.

The activation energy, ΔH , can be compared from data in the literature by plotting $\log a_T$ vs. reciprocal absolute temperature. The slope of the best straight line through the data is directly proportional to ΔH . The value of the activation energy for the 3501-6 resin is 31.0 kcal/g-mole (see figure 4.2.3-3). The activation energies of several other investigations determined by this method are given in table 4.2.3-1. All the activation energies were either calculated from creep data below the glass transition temperature or else the activation energy was given. A least squares straight line was fit to the $\log a_T$ vs. $1/T$ data. An example calculation is given in appendix D.

Three tendencies can be observed in table 4.2.3-1. First, the tetraglycidyl amine epoxy resins have similar activation energies regardless of whether fibers are present or not (15 to 65 kcal/g-mole). The fibers do not appear to interfere with the overall kinetic interactions of the resin. Secondly, some credence is given to the "pasting" technique. The similarity between the activation energies from study to study shows that the "best curve" criterion is adequate for developing the

TABLE 4.2.3-1

ACTIVATION ENERGIES OF THE ARRHENIAN TYPE EQUATION

Authors	Description	ΔH (kcal/mole)
May (present work)*	3501-6 resin	31.0
Kibler and Carter, (1979)*	5208 resin	15.2
Schapery, et al., (1979)*	AS/3502 (90°) ₁₅	36.3
	T300/5208 (90°) ₁₅	39.0
Yeow, et al., (1979)*	T300/934 (90°) ₁₅	65.4
Crowson and Arridge (1979)	Ciba-Geigy MY720/ Nadic melanhydride (torsion creep)	58.0
Kim, et al., (1978)	EPON 828 (DGEBA)	85.
Kitoh and Suzuki, (1976)	a DGEBA resin	91.
DiBenedetto and Gauchel (1974)*	EPON 815 (DGEBA)	113.

* A linear least squares fit was applied to the shift factor-temperature data.

master curves for the creep of tetraglycidyl amine resins. Thirdly, the DGEBA resins, which are more compliant and have lower glass transition temperatures than the tetraglycidyl amine resins, have higher activation energies for the more compliant resins. The value of ΔH varies inversely with the mobility of the segments of the polymer chains. This conclusion is contrary to the general conception of an activation energy, but no theoretical significance has been attributed to ΔH . It should perhaps be referred to as an energy of mobility.

The master curve for the 3501-6 resin predicts the creep behavior at any higher temperature up to 30 thousand seconds (the length of the creep curves originally used to determine the master curve). The creep test at 116°C did superimpose over predicted creep determined by the master curve when batch-to-batch variation was mitigated by the use of $(J(t)/J_0)$. However, at longer times the time-temperature superposition scheme does not predict the creep behavior. Figure 4.2.3-4 shows the room temperature creep behavior as predicted from the master curve (straight line through consecutive data points). Also plotted in figure 4.2.3-4 are the creep of specimen 7-10-79-04 and the power law and Voigt-Kelvin fits to the master curve. The 3501-6 resin creep behavior

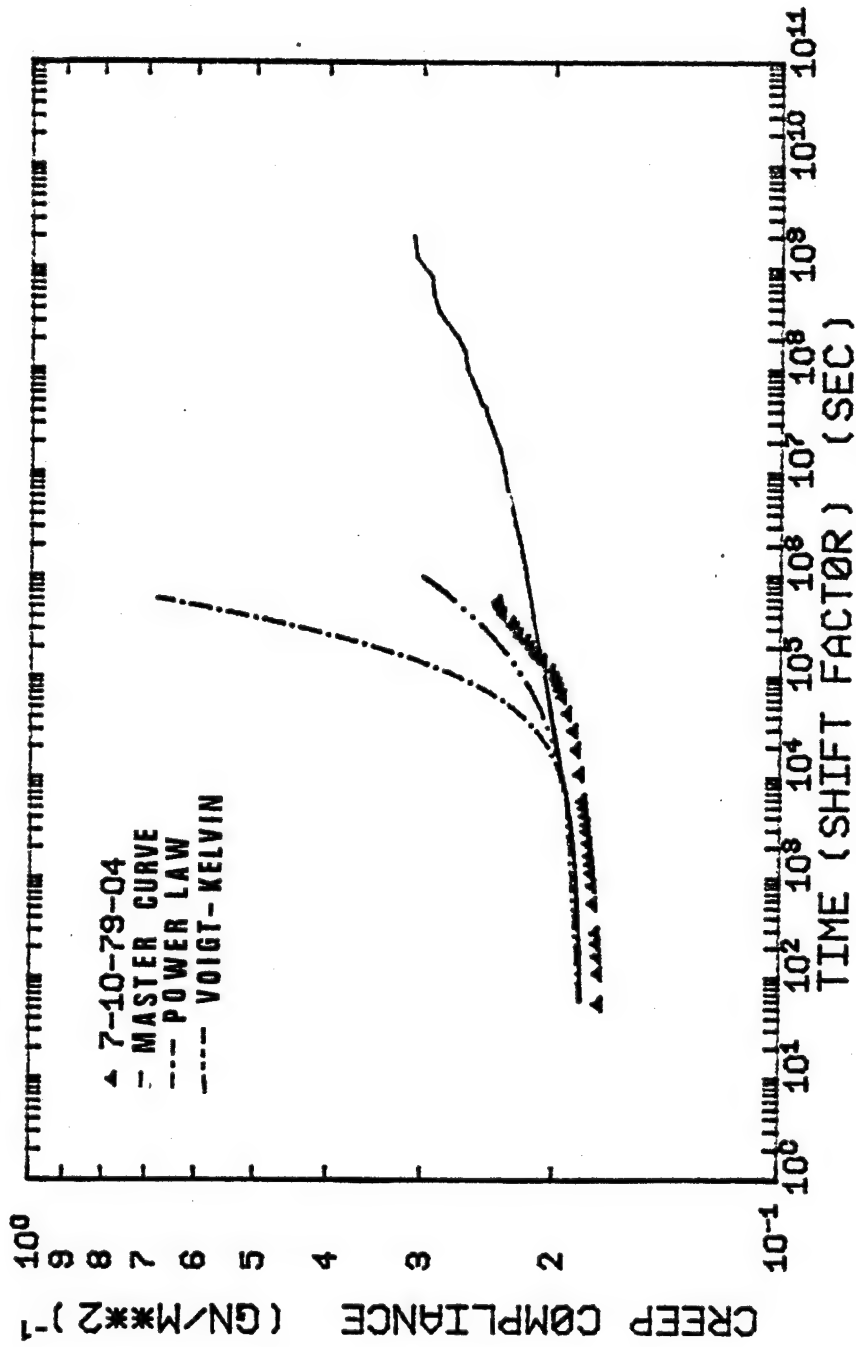


Figure 4.2.3-4 Comparison of various analytical models and the actual creep data vs. the master creep at room temperature

shown at longer times indicates a greater creep rate than the master curve predicts. Secondary creep is not predicted by the master curve; therefore, the prediction underestimates the actual creep of sample 7-10-79-04. The viscoelastic models (using the room temperature parameters determined from the NLLS fit to 6-29-79-02 for time less than 30 thousand seconds) also fail to predict the creep of the resin at longer times. The power law model provides a better estimate than the Voigt-Kelvin model, but it still overestimates the creep behavior of specimen 7-10-79-04. Evidently, the power law model provides an upper bound for the creep behavior while the master curve provides a lower bound. Other investigations which have calculated master curves from creep data in the viscoelastic zone may only have produced a lower bound to the creep behavior at longer times. Unless the master curve has been checked out by running a few long term creep tests, the master curve may suffer from this problem. In one case in the literature, a 24 hour creep test was compared with its master curve. Agreement between the master curve and the creep curve only occurred because the creep test was run at the glass transition temperature (Yeow, et al. 1979). Viscoelastic behavior at all times is usually expected at the glass transition

temperature. The nonlinear viscoelasticity observed at lower temperatures seems to be the cause of the failure of time-temperature superposition.

The reinforcing effect of the fibers may make the time-temperature superposition applicable for the transverse creep of the composite. Other investigations would have to be run to determine that possibility. If the master curves of the neat resin are used to determine the master curve of the composite (e.g. using the Tsai-Halpin equation), the creep of the composite will be slightly underestimated. The amount of error was not investigated here, but caution should surely be used when the master curve of the neat resin is used to predict the properties of the composite.

4.3 THE CREEP OF PLASTICIZED 3501-6 RESIN

Due to the problems in conducting creep tests on plasticized specimens mentioned in chapter 3, only one creep test was performed. The dynamic mechanical testing showed the effects of plasticization much better than the creep testing and more tests could be run with the dynamic test machine. The dynamic mechanical testing of plasticized specimens is discussed in detail

in section 5.3. The results of the one plasticized creep test, specimen 12-11-79-06, are mentioned and compared qualitatively with the effect of water on composites reported in the literature.

Specimen 12-11-79-06 was immersed in an equal weight ratio solution of water-phenol at 65°C until its weight had increased by 6.65% ($M = 6.65\%$). A solution of water and phenol was chosen for reasons determined in section 3.4. The specimen was tested for tensile creep one day later at room temperature. The length of the test was one week. The results are plotted in figures 3.2-4 and 4.3-1. In figure 4.3-1, the reduced compliance of specimen 12-11-79-06 is plotted along with the reduced compliance of specimen 7-10-79-04 in order to compare the creep of plasticized resin vs. virgin resin (different batches necessitate a reduced compliance). Desorption during testing was considered minimal and several comments on this situation are mentioned in section 3.5. The average plasticization level in specimen 12-11-79-06 can be considered to be 6%, very near the equilibrium absorption level of moisture in the 3501-6 resin (Augl, 1978; Browning, 1978; Delasi and Whiteside, 1978).

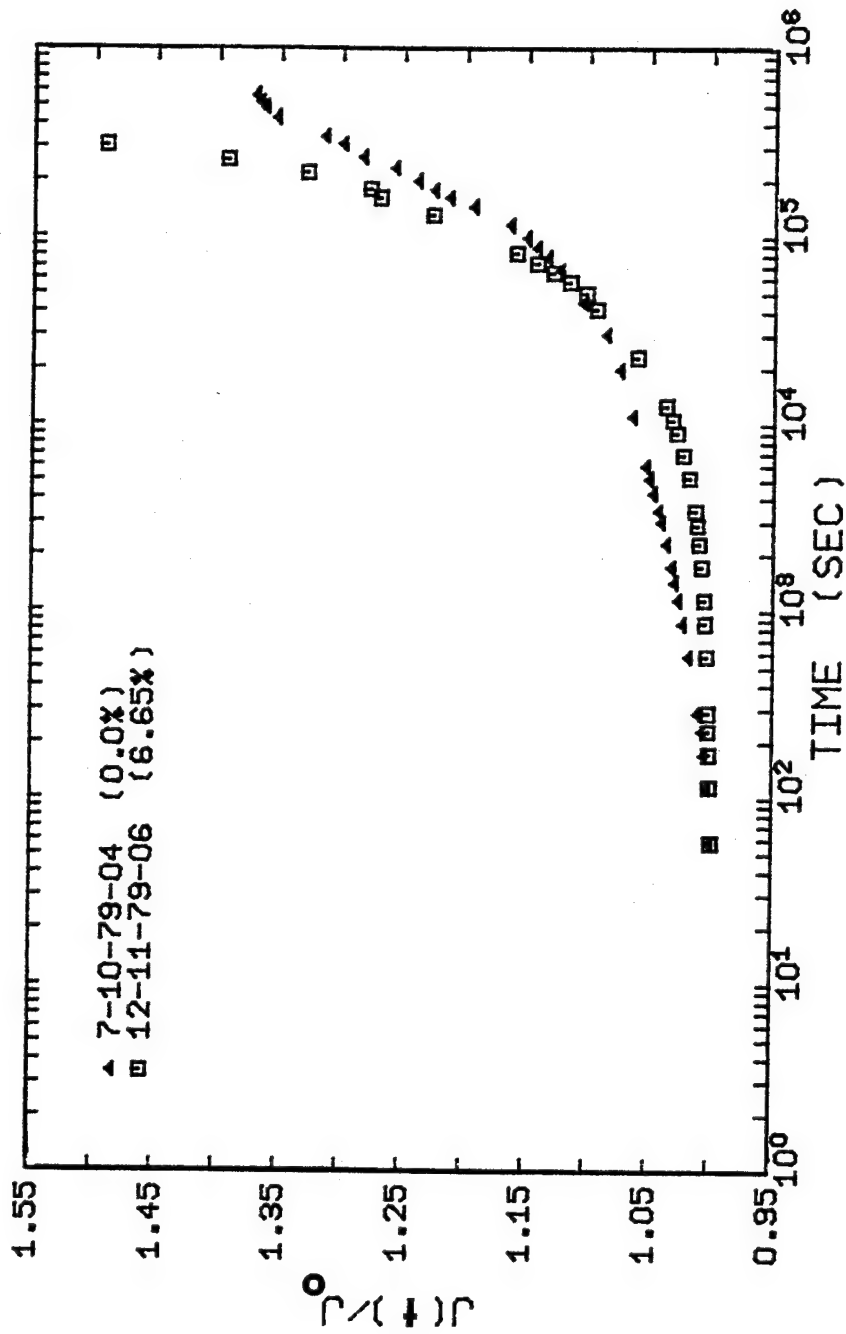


Figure 4.3-1 The effect of water-phenol (50/50) plasticization on the long term creep of the 3501-6 resin

The creep of the plasticized specimen clearly shows that its creep is greater than the virgin resin specimen, especially for time greater than 100 thousand seconds. At 350 thousand seconds, the plasticized specimen has crept almost twice as much as the virgin resin. Below 100 thousand seconds, the curves are within each other's experimental error. This indicated that the initial creep compliance (or modulus) does not significantly change at this level of plasticization. The identical creep between the plasticized resin and the virgin resin in the viscoelastic creep zone can be seen more clearly in figure 3.2-4.

These results indicate that the network structure is maintained because the relative instantaneous elastic properties of the resin are not altered. The swelling effect of the water-phenol solution allows a greater creep rate at longer times. Chain scission is not present otherwise the instantaneous creep compliance would have shown an increase beyond experimental error (see table 4.2.2-1). This same conclusion was reached by Browning (1978) who performed creep tests on a tetraglycidyl amine resin soaked to saturation in water above its glass transition temperature (300°F). His creep curves show a definite rubbery plateau region before rupture occurs.

The rubbery plateau in the creep behavior of a crosslinked polymer indicates that the maximum strain limit of the network structure has been reached. The strain is constant with time and any further deformation must be accompanied by scissioning of the crosslinks. At the equilibrium moisture levels of 6% tested by Browning, the network structure was maintained; therefore, the network structure is probably maintained in the tests performed for the current study.

Since the 3501-6 resin will swell to fracture in water-phenol (50/50) somewhere between M equal to 20% and 23%, significant crosslink scissioning must be prevalent above some critical absorption level.

The effect of moisture absorption on room temperature creep has been documented for tetraglycidyl amine resins in only one known source, the work of Schapery, et al. (1979) on the transverse creep of AS/3502 and T300/5208 carbon fiber composites. This source provided creep data on the effect of water absorption on the composite below the glass transition temperature. That creep data is duplicated in figure 4.3-2. The data was read off of graphs to within five percent. The creep master curves shown in figure 4.3-2 may not

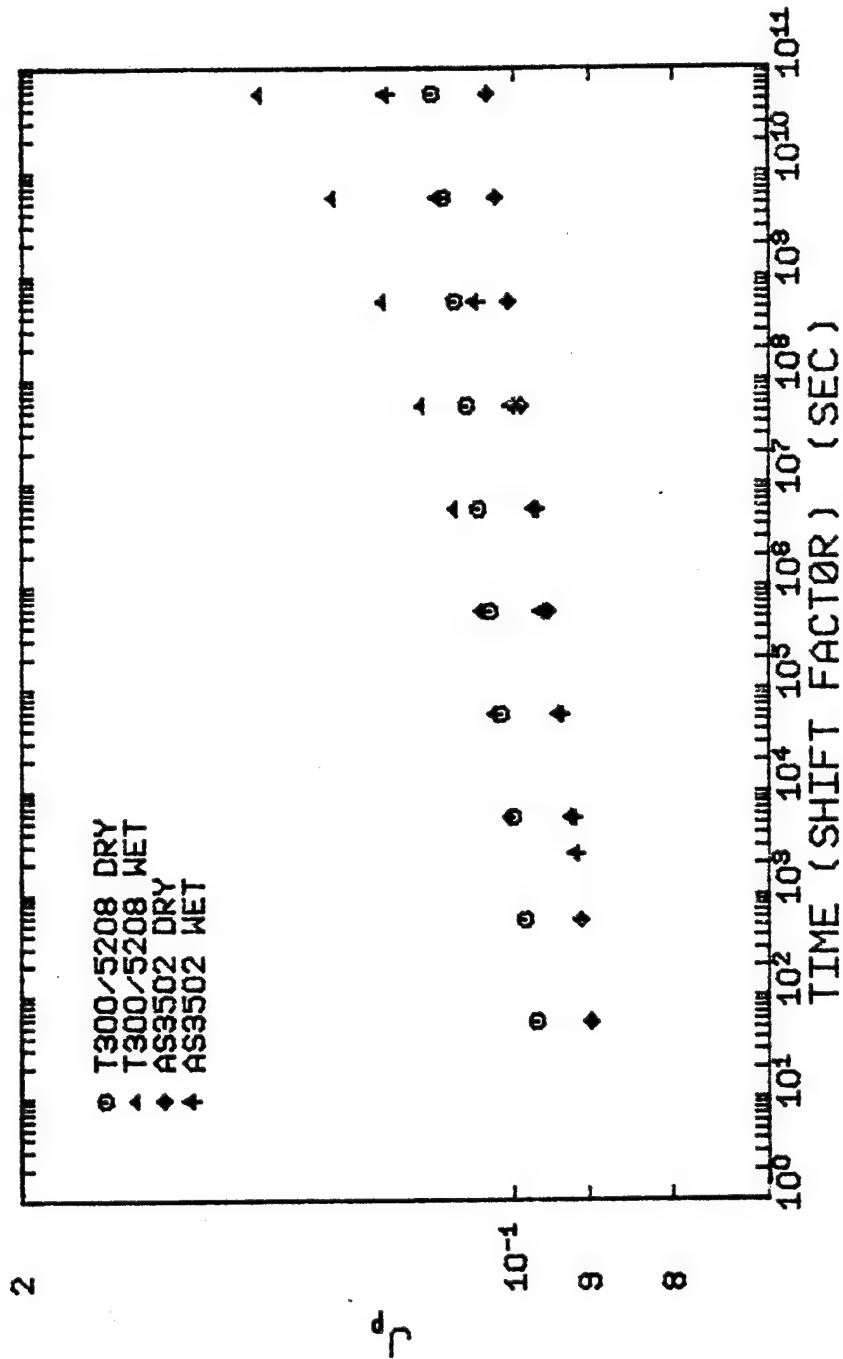


Figure 4.3-2 The transverse master creep curves of carbon fiber composites plasticized by water at room temperature

represent the long term creep data accurately (see section 4.2.3), but it is sufficient to compare qualitatively the wet and dry creep behavior of the composites. Each sample was dessicated before being immersed in a humid atmosphere at 95% relative humidity. The composite was saturated with moisture so the transverse creep of the composite should represent the creep of the saturated neat resin (in a qualitative sense).

The same effect of plasticization that appeared in the water-phenol soaked specimen is present in figure 4.3-2. For both composites, the initial creep compliance is unaffected by the presence of the solvent, but the creep at longer times is enhanced for the wet composite samples. Water and phenol are both protic solvents which can hydrogen bond within the network structure. Their effects on the resin at low levels of plasticization should be similar. The difference lies in the fact that phenol absorbs into the resin at a much faster rate and to a much higher loading. In fact, the resin can swell to fracture. This extra swelling ability is probably due to the aromatic character of the phenol which can foster secondary interactions with the resin through dispersion forces. The enhanced creep behavior

at longer times means that the network structure is being "loosened" up by the solvent. One can expect a decrease in the glass transition temperature which is discussed in the next chapter.

CHAPTER 5

ANALYSIS OF THE DYNAMIC MECHANICAL TEST RESULTS

5.1 INTRODUCTION

It has generally been recognized that the mechanical properties of polymeric materials are strongly dependent on temperature and the rate or frequency of the applied load of deformation. Changes in the mechanical properties can be attributed to the transitions in the structure of the polymer. Dynamic mechanical testing is well suited for measuring those mechanical property changes which give insight into the structural changes on a molecular scale. In the case of epoxy resins, the crosslinked network is the structure of particular interest. Dynamic mechanical testing provides a fruitful method of analyzing the virgin resin (section 5.2); in addition, dynamic mechanical testing is much more sensitive than static tests to changes in the polymer structure caused by the plasticization of external solvents (Keenan, et al. 1978; Kenyon and Nielsen, 1969; Kaebler, 1965; Murayama and Bell, 1970). The effect of plasticization of MIL-81294 and its components on the dynamic mechanical properties of the 3501-6 resin is discussed in section 5.3.

The definition of the dynamic mechanical property descriptors (complex dynamic modulus, loss tangent, etc.) and the experimental methods used to measure them have been previously discussed. The reader is referred to chapter 3 for a description of the operating procedures of the Rheovibron DDV-II-B and for the definition of the dynamic mechanical property descriptors.

In section 5.2, the dynamic mechanical test data on the virgin resin is presented and analyzed. The test results from one other investigation on the dynamic mechanical properties of the 3501-6 resin is also compared with the current work. This analysis emphasizes the thermal transitions of the resin (e.g. the glass transition) which indicate the type of changes occurring in the network structure. The test data also provide a control which is compared to the results of the plasticized dynamic tests. The influence of plasticizers is examined in section 5.3.

The plasticized resin results exhibit a definite change in the dynamic behavior when compared to the test results of the virgin resin. Both a shift in the glass transition temperature to lower temperatures and a degradation of the properties of the resin were observed. A qualitative comparison between the creep and dynamic

mechanical behavior is also given.

5.2 DYNAMIC MECHANICAL BEHAVIOR OF THE VIRGIN RESIN

Ten dynamic mechanical tests were run on virgin resin specimens from a variety of different batches. The description of each of these tests is given in table 3.3-1. The raw data for each of the tests is presented in tabular form in appendix A. An example of one test, specimen RH-23, is presented in section 3.3 where the loss tangent and complex dynamic modulus are plotted as a function of temperature. In figure 5.2-1, the complex dynamic modulus for the virgin resin is represented by a mean curve for eight of the tests. The complex dynamic moduli of each of the individual tests was averaged into a single mean curve by the following method. The data of each test was interpolated logarithmically to a value for every five degree Centigrade increment. All the interpolated values at the same temperature were averaged and a standard deviation about the mean was computed. The width of the error bars in figure 5.2-1 is one standard deviation about the mean. This is a direct indication of the batch-to-batch variation in the complex dynamic modulus of the resin. A typical value of the standard deviation below the glass transition temperature (200°C) is 0.20 GN/m^2 , or 5% about the mean.

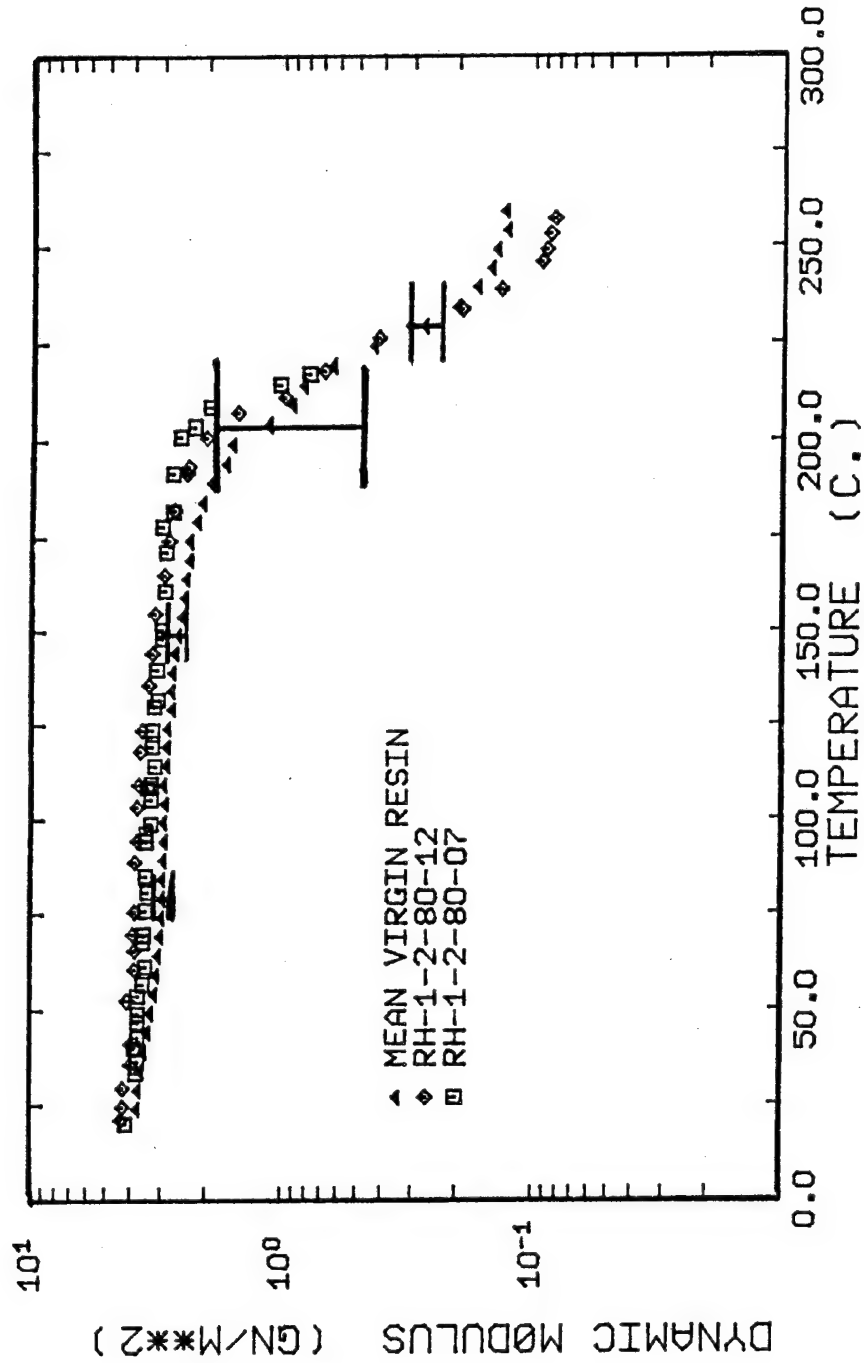


Figure 5.2-1 The complex dynamic modulus of the virgin resin at 11 hz: the mean virgin resin data was taken without any instrument improvements and batch no. 1-2-80-00 data was taken with improvements.

This variation is less than the experimental error at room temperature, 0.27 GN/m^2 (7% about the mean). The experimental error decreases with increasing temperature until the batch-to-batch variation becomes greater than the experimental error at 150°C . The experimental error decreases because the uncertainty in the length correction constant, K , (the residual force parameter at zero specimen length) becomes negligible at the higher temperatures. The uncertainty in K dominates the experimental error at the lower temperatures.

The mean dynamic modulus curve in figure 5.2-1 was calculated from the results of the dynamic tests performed on the Rheovibron which did not utilize the new improvements (see section 3.3). Eight of the ten virgin resin tests were used to determine the mean modulus curve. The other two tests with the new improvements are also plotted in figure 5.2-1. Both of the specimens were from the same batch of resin. As pointed out in section 3.3, the corrections in a malfunction of the Rheovibron during the middle of the testing program required the retesting of the virgin resin. The new series of tests with the improvements used nitrogen gas flow in the heater chamber and a new pair of specimen grips which improved the alignment. As a

consequence of these improvements, the measured value of the complex dynamic modulus increased. The higher modulus values agree more closely to the results of the creep tests and the values of the static Young's modulus reported earlier. The partial elimination of sideways vibration provided the more reliable results.

While the new improvements gave better results, the interpretation of the results may not be significantly different from the results of the tests without improvements. The two curves, RH-1-2-80-07 and RH-1-2-80-12, are within two standard deviations of the mean dynamic modulus curve. The general shape of the curves are quite similar and the value of the length correction constant, K , is the same in each case. The calculation of the constant K for each case is shown in appendix E ($K = 25 \pm 2$). The close agreement between the two sets of data indicates that both adequately represent the dynamic mechanical behavior of the resin. To insure consistency; however, the dynamic mechanical behavior of the plasticized resin measured on the Rheovibron with the new improvements was compared to the dynamic behavior of the virgin resin which was tested in a similar fashion. The dynamic mechanical behavior of the plasticized resin which was

tested without the new improvements were compared to the mean dynamic modulus curves.

Since the experimental error is not significantly different from the standard deviation of the batch-to-batch variation, batch-to-batch variation does not affect the results of the dynamic mechanical testing. Therefore, no effort was made to note the batch number of the dynamic mechanical specimens. The one exception was the series of tests performed on the Rheovibron with the new improvements. All the virgin and plasticized resin tests for this set of data were from batch 1-2-80-00.

The loss tangent or $\tan \delta$ exhibited a greater scatter in the data than the complex dynamic modulus. The results for five virgin resin tests are plotted in figure 5.2-2. Below 150°C, the scatter was too great to construct a mean curve which could represent the loss tangent, but the general shape of the curve is represented by specimen RH-23 (the squares in figure 5.2-2). A better plot of specimen RH-23 is shown in figure 3.3-3. Sideways vibration was kept to a minimum during this test (the problems of sideways vibration are discussed in section 3.3). Above 150°C, the resin becomes more compliant as the glass transition is approached and sideways vibration becomes

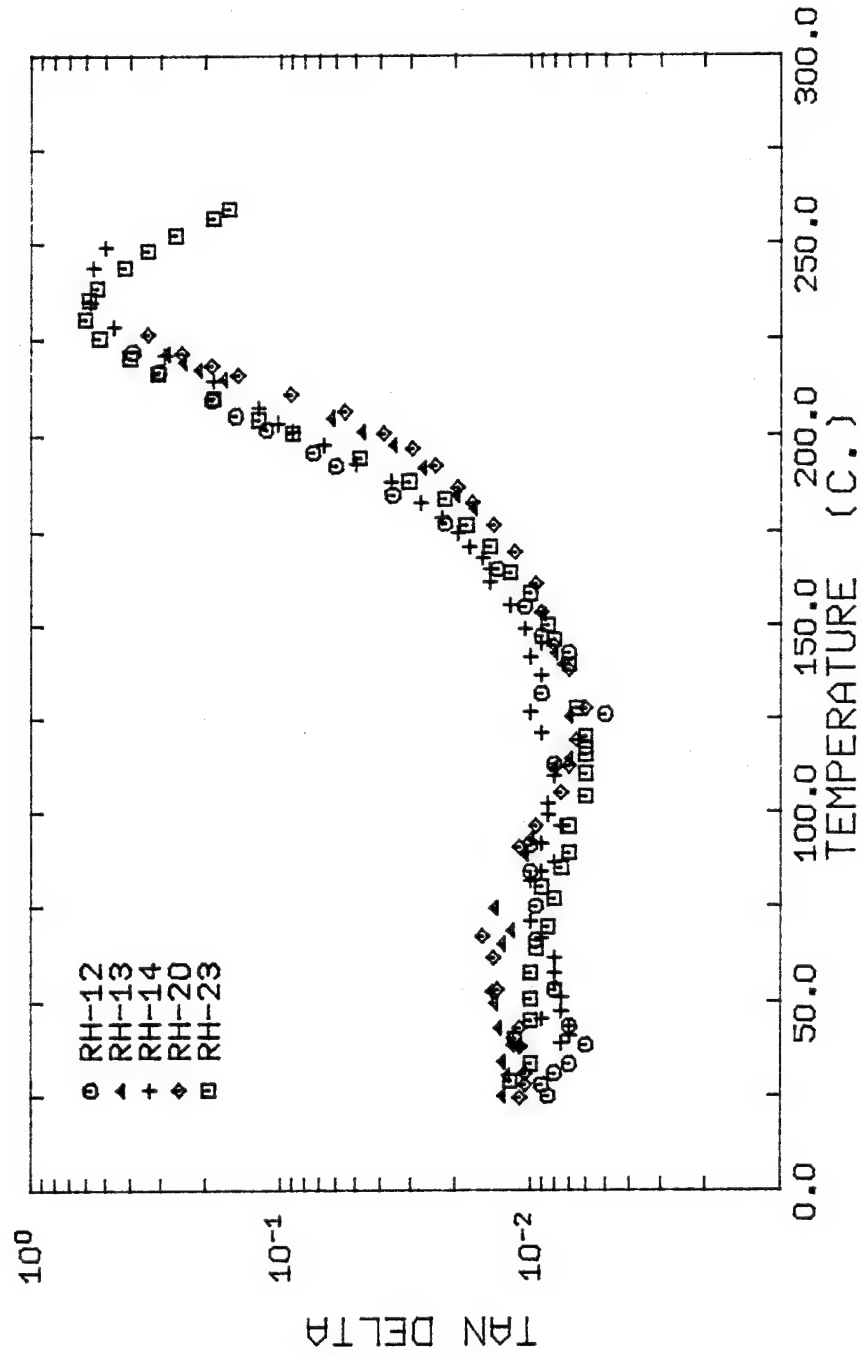


Figure 5.2-2 The loss tangent of the 3501-6 resin at 11 hz without improvements

less of a problem.

Any two dynamic functions completely characterize the dynamic mechanical behavior of a material. The loss and storage functions of the dynamic compliance and modulus can be computed from the loss tangent and the complex dynamic modulus using the equations of section 2.2. Therefore, the dynamic mechanical data in appendix A was used to generate the loss and storage modulus and the loss and storage compliance as a function of temperature. Before presenting these curves, the dynamic behavior shown in the complex modulus and loss tangent are discussed further below.

The complex dynamic modulus is a vector quantity which contains two components, one component in phase with the oscillating strain and the imaginary component out of phase with the strain. The static Young's modulus and the complex dynamic modulus are equal in the limit of zero frequency, but when a small oscillation is present, the values of the moduli are expected to differ. At low values of the phase angle, δ , (the angle between the two vectorial components) the imaginary component of the modulus is essentially negligible. The complex dynamic modulus can be considered to be the approximate static

modulus of the material. The 3501-6 resin near room temperature behaves in this manner.

The methods used to determine the moduli (Rheovibron and an Instron machine) develop different stress fields on the material being tested. In the case of the Rheovibron, part of the oscillating strain energy is lost to energy dissipation and sideways vibration so that the value of the dynamic modulus should be lower than the Young's modulus. Jenness and Kline (1974) have reported this conclusion based on their work on DGEBA resins. The data of Kaebble (1959) also corroborate these results. In table 5.2-1 below, the room temperature Young's modulus of the 3501-6 resin is compared against the room temperature mean dynamic modulus. The results of the comparison show that $|E|$ measured with the improvements was in closer agreement with the static Young's modulus.

At higher temperatures, the complex modulus decreases linearly on the semi-log plot. Near 200°C, the glass transition begins as the glass-like behavior of the crosslinked network converts to a rubbery-like behavior. The transition ends at 240°C as the modulus levels out at a rubbery plateau. The "rubber" modulus above 240°C is about 0.1 GN/m². The epoxy resin starts to degrade above

TABLE 5.2-1

ROOM TEMPERATURE TENSILE MODULI FOR THE 3501-6 RESIN

Type	Description	Modulus (GN/m ²)
Static	R. Blake sample	4.48±0.22
Static	Aug1 (1978)	4.27
Creep Modulus	Mean of RT tests	4.83±0.61
E at 11 hz	8 test mean (no imp.)	3.76±0.27
	2 test mean (with imp.)	4.26

260°C so all tests were halted at that temperature.

The glass temperature of the 3501-6 resin can be measured from the dynamic mechanical data, but the change from a glassy to a rubbery behavior does not occur at one particular temperature. Instead the transition occurs over a range of temperatures (190° - 240°C). It would be convenient if a single convention were adopted specifying one temperature as the glass temperature, T_g , since its measurement varies with the experimental procedure used. For dynamic mechanical testing, two such conventions are used. The onset of the glass transition has been arbitrarily selected by Morgan and O'Neal to be the glass temperature. For epoxy resins, half the dynamic modulus at 25°C has been selected as the point where the glass transition begins. This convention, though arbitrary, has worked well with other epoxy resins (Morgan and O'Neal, 1978; Keenan, et al. 1978). For the 3501-6 resin, an average Morgan and O'Neal glass temperature of $200^{\circ} \pm 8^{\circ}\text{C}$ was calculated. This result is independent of any change of the experimental procedure. The end of the glass transition has also been used to measure the glass temperature. For this convention, the peak of the α -transition of the loss tangent curve defines the glass temperature,

T_{α} . As seen in figure 5.2-2, the peak occurs at roughly $235^{\circ} \pm 5^{\circ}\text{C}$. Many other test methods (volume expansion, differential scanning calorimetry, etc.) usually approximate the glass temperature of the 3501-6 resin in the middle of the transition. For example, Carpenter (1978) measured a glass temperature of 219°C by differential scanning calorimetry. DeIasi and Whiteside (1978) measured T_g at 220°C by utilizing thermal expansion measurements.

The loss tangent curve is believed to have peaks at temperatures where certain functional groups on the polymer chain become "unlocked" from the steric hindrances which restrict their movement. The extra mobility in the polymer chain registers as an increase in the phase angle or $\tan \delta$. In epoxy resins, at least two loss tangent transitions have been found (May and Weir, 1962). The high temperature α -peak is associated with the glass transition. All the polymer chains experience the transition from a glassy state to a rubbery one. At lower temperatures near -50°C , the β -peak is attributed to the crankshaft rotation of the glycidyl portion of the linear chain of the 3501-6 resin (Muryama and Bell, 1970; Kaebler, 1959). In figure 5.2-2, the α -peak can be clearly seen. Since room temperature was the lowest test temperature, the β -peak is not present,

but the minimum at 120°C indicates that a maximum should occur at some lower temperature. A third transitional peak was observed by Keenan, et al. (1978) near 100°C for a dry tetraglycidyl amine epoxy resin used in carbon fiber composites. This " ω -peak" as defined by Keenan, et al. was not observed in the 3501-6 resin. The peak was fairly small and it is conceivable that the background moisture present in the specimens of the current study could have obscured the ω -peak. However, it will be noted that only the α -peak was observed between 25° and 260°C.

In the other investigation of the dynamic mechanical behavior of the 3501-6 resin, Carpenter (1978) measured the complex dynamic modulus and the loss tangent over the same temperature range and at the same frequency (11 hz). A newer model of the Rheovibron was used and the results of his measurements are plotted in figures 5.2-3 and 5.2-4. A standard formulation of the resin (25% DDS) was used in his tests. The amount of background moisture present in his samples was not discussed.

In figure 5.2-3, the general shape of the loss tangent curves is the same. Only the α -peak is observable and the ω -peak is not present at all. For Carpenter's data, the α -peak occurs at 252°C which is slightly higher

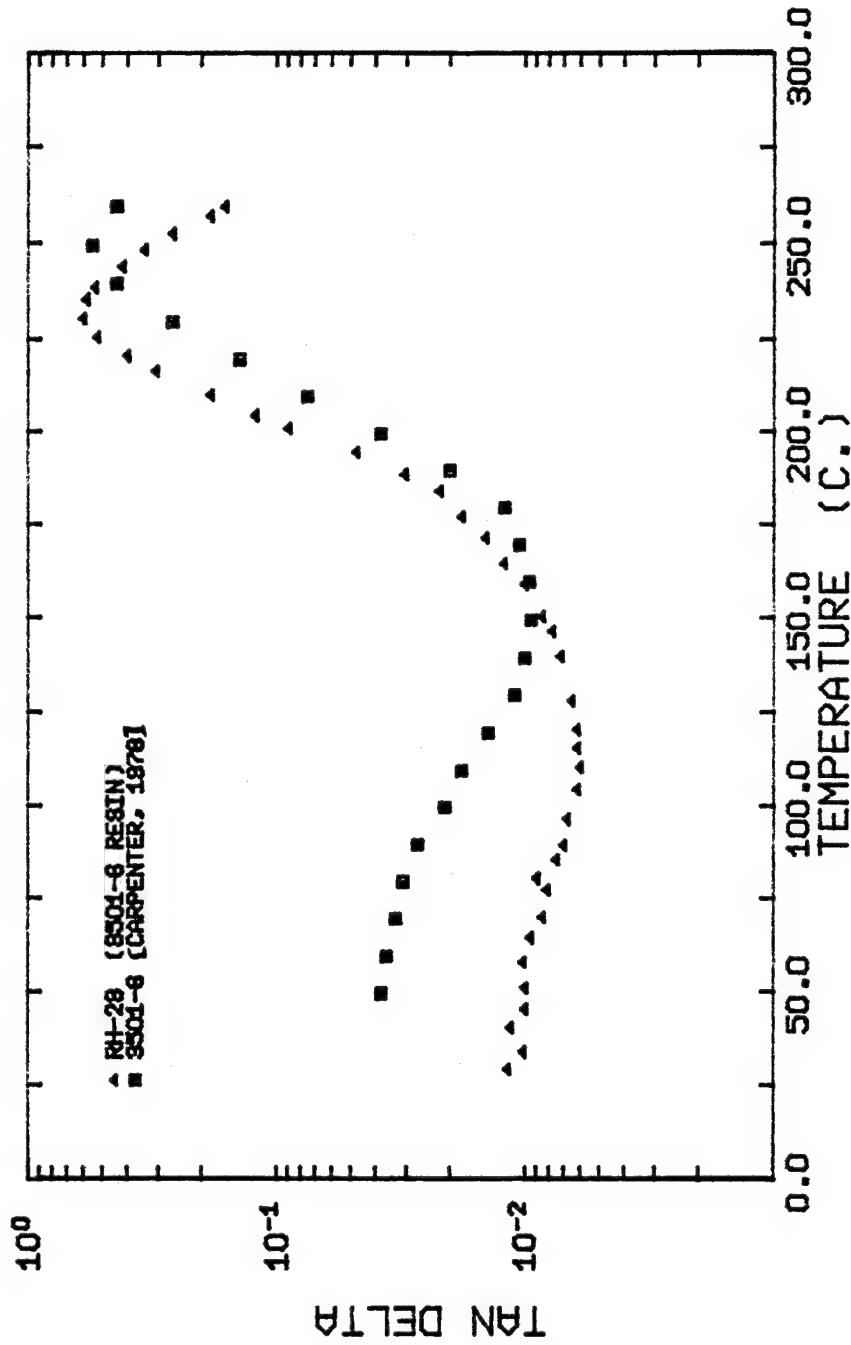


Figure 5.2-3 Tan Delta as a function of temperature for two independent tests on the 3501-6 resin

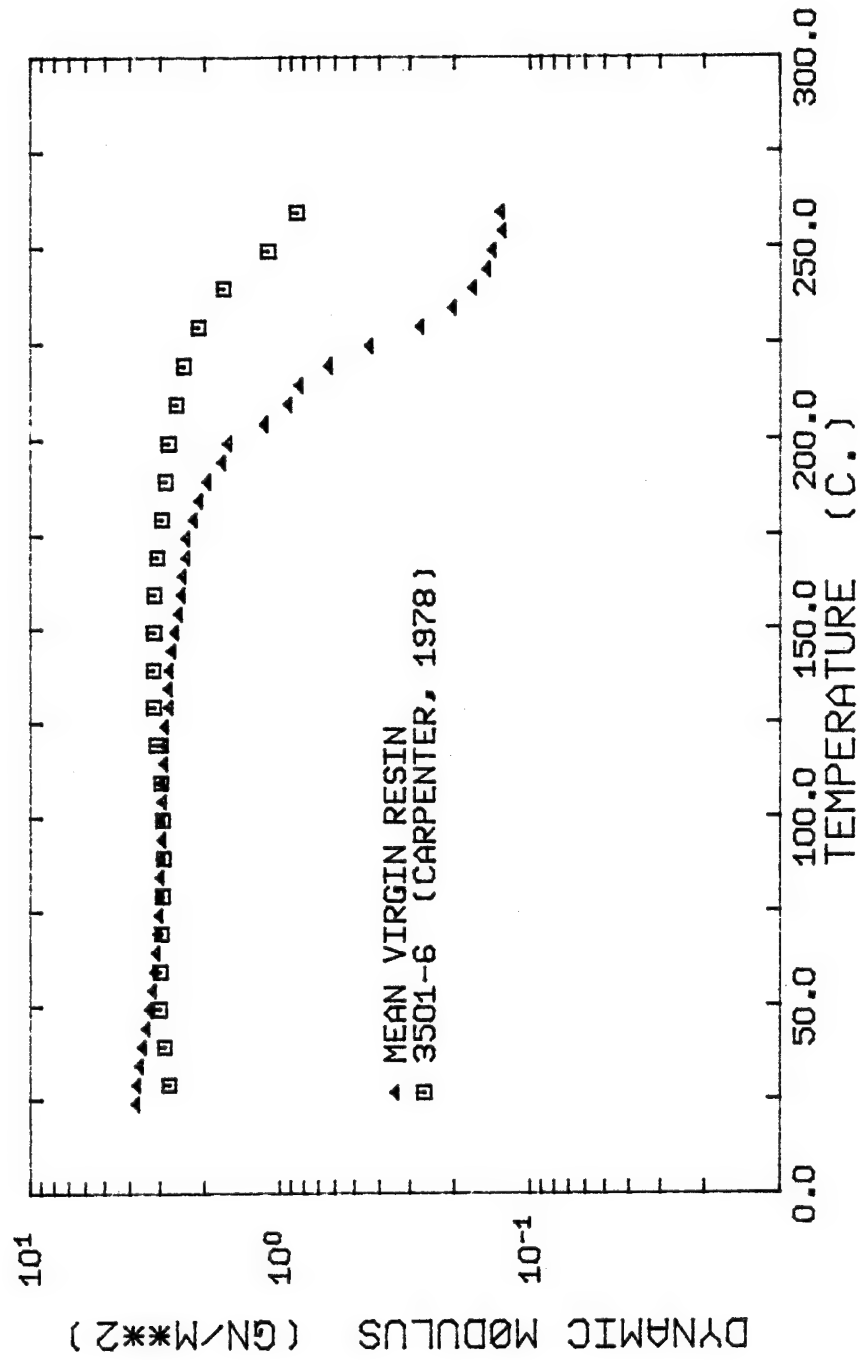


Figure 5.2-4 The complex dynamic modulus vs. temperature for two independent tests on the 3501-6 resin

than the 235°C peak observed from this investigation (specimens RH-23 and RH-1-2-80-12). Since the curing procedures and test procedures used by Carpenter were very similar to the present investigation, the difference between the two sets of tests must be attributed to the use of a newer, better calibrated model of the Rheovibron. The test results of specimen RH-1-2-80-12 (with the improvements in the grip system) were in better agreement with Carpenter's data than test results without improvements (RH-23). Carpenter's results are probably a better representation of the loss tangent of the virgin resin, but for consistency the present study will be used to determine the changes in the loss tangent caused by plasticization (section 5.3).

In figure 5.2-4, the complex modulus measured by Carpenter shows some unusual behavior. First, the Morgan and O'Neal glass temperature occurs at 240°C, well above the value of 200°C observed in the present study. Secondly, the complex modulus actually increases with increasing temperature between 30° and 150°C. An increasing modulus with increasing temperature has only been observed if post-curing of the resin is occurring (Keenan, et al. 1978). Post-curing is not likely to occur at these

low temperatures; therefore, the cause of the increasing modulus is unknown. The data from the current study is more representative of the complex dynamic modulus of the resin.

The storage and loss functions were calculated from the dynamic modulus and loss tangent data using the definitions supplied in section 2.2. From the data, mean curves for the loss modulus (or compliance) and storage modulus (or compliance) were calculated in the same manner as the mean dynamic modulus. The mean component moduli, E_1 and E_2 , are plotted in figure 5.2-5. The component compliances, J_1 and J_2 , are plotted in figure 5.2-6. Error bars denote a single standard deviation about the mean at every five degree increment. The mean curves were created from the eight virgin resin tests without the improvements. The two tests with improvements show basically the same dynamic behavior, so their inclusion is not necessary.

The storage modulus, E_1 , in figure 5.2-5 is essentially identical to the complex dynamic modulus, $|E|$. Since E_1 is the part of the complex modulus which is in phase with the applied strain, the difference between $|E|$ and E_1 will only occur at large enough values of the phase

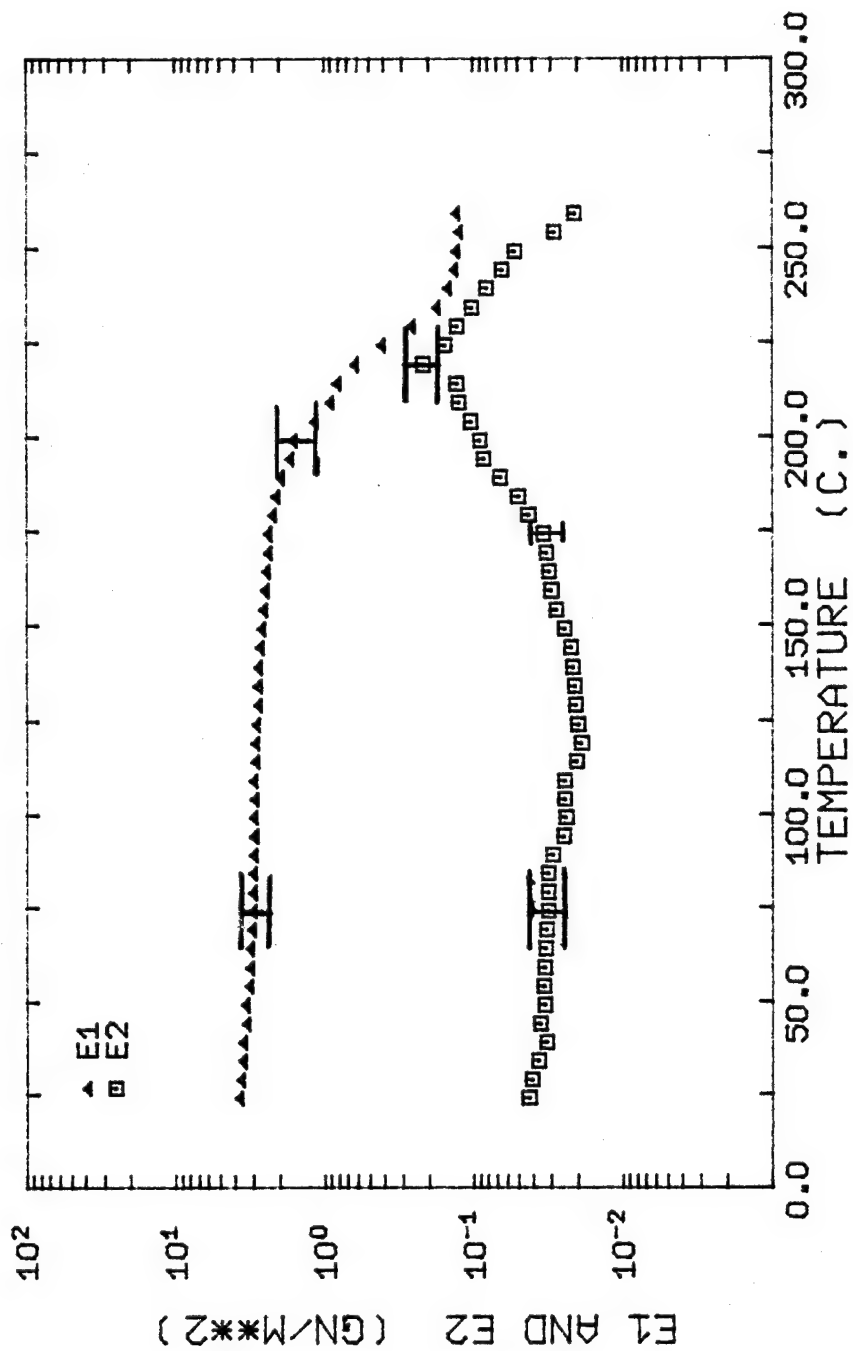


Figure 5.2-5 The mean loss and storage modulus for the virgin 3501-6 resin

angle, δ . Below the glass transition, the difference is less than 1% ($\delta \approx \tan \delta$). Even at the α -peak where the $\tan \delta$ has a maximum of 0.55 ($\delta = 29^\circ$), E_1 is still 87% of the value of $|E|$ ($E_1 = |E|\cos\delta$).

The loss modulus, E_2 , is directly affected by the phase angle (see equation 2.2-3b) and its shape will be very similar to the shape of the loss tangent curve. As would be expected, the values of E_2 are approximately two orders of magnitude less than the values of E_1 below the glass transition. The loss modulus peaks at 220°C , slightly below the temperature of the α -peak of the loss tangent. The loss modulus gives the magnitude of the complex modulus that is out of phase with the storage modulus. The two components can be combined by vector addition into the dynamic modulus as defined in equation 2.2-2.

These same comments also apply to the storage compliance, J_1 , and the loss compliance, J_2 , plotted in figure 5.2-6. In section 2.2, it is shown that for a small phase angle, δ , the storage compliance is essentially the reciprocal of the storage modulus. Since E_1 does not

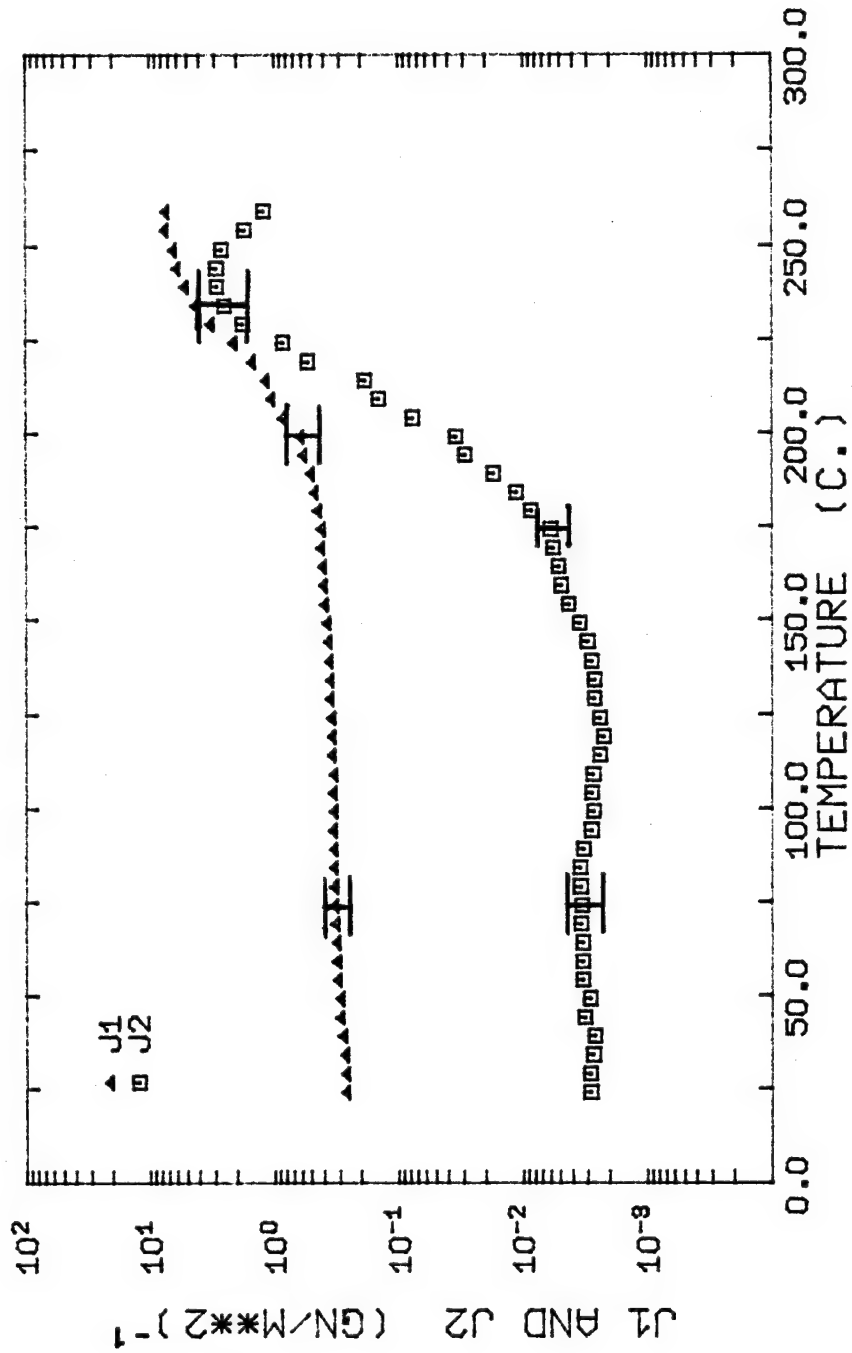


Figure 5.2-6 The mean loss and storage compliances for the 3501-6 virgin resin

differ dramatically from $|E|$ (to within 13%), the approximation of equation 2.2-7 holds over most temperatures:

$$J_1 \approx 1/|E| \quad (2.2-7)$$

The reciprocal of the complex modulus is the creep compliance at zero frequency; therefore, the shape of the storage compliance curve is similar to the shape of the long term creep compliance curves of chapter 4. Though the two curves are functions of different variables (time and frequency), the similarity in the shape points out the existence of a frequency-temperature superposition. If more data were available for a sufficient range of frequencies, a master curve could have been constructed. Basically, higher temperatures shift the retardation times of the polymer observed at lower temperatures to shorter times, or in the case of dynamic mechanical behavior, to higher frequencies. The superposition principle states that the dynamic behavior observed at one frequency and temperature can be observed at a higher temperature and higher frequency. The master curve so constructed could be used to predict the creep and stress relaxation of the epoxy resin using methods previously discussed in section 2.3. In a word of caution, the maximum strain the

Rheovibron exerts on a specimen is less than the linear elastic limit where linear viscoelastic laws are still applicable. A creep or stress relaxation master curve predicted from the dynamic mechanical data would only be useful in those cases where the constant stress (or strain) was less than the elastic limit. The nonlinearities observed in the creep curves of section 4.2 would not be predicted by such a transformation.

The loss compliance shows the largest change. Accordingly, the error bar widths are larger indicating that the scatter in the data is slightly greater than the other dynamic functions (the scatter originates from the scatter in the loss tangent). The large change in magnitude provides an excellent method for comparing the dynamic behavior of the plasticized resin versus the virgin resin.

The test results give insight into the microstructural changes occurring within the crosslinked network of the resin. At specific temperatures, certain portions of the segmental chains attain enough kinetic energy to "unlock" themselves from their steric hindrances. These transitions are identical to those found in other resins, namely the α and β loss peaks. Reproducible results were

obtained which were within the batch-to-batch variation of the resin. The improvements on the Rheovibron did yield closer agreement between the dynamic mechanical data and the static properties of the resin. Closer agreement with the results of one other investigation (Carpenter) were also obtained. The use of the Rheovibron should not be a substitute for the static measurements, however. The machine provides a useful qualitative insight into the dynamic behavior of polymers. A summary of the dynamic mechanical test results is listed in table 5.2-2.

TABLE 5.2-2

SUMMARY OF THE DYNAMIC MECHANICAL TESTING RESULTS

Property	Value
E at 25°C (GN/m ²)	3.76±0.27
E at 25°C with imp. (GN/m ²)	4.26
J at 25°C (GN/m ²) ⁻¹	0.266±0.037
T _{MO} (C)	200±8°
T _α	235±5°
T _g (Carpenter, 1978) (C)	219°
T _g (DeIasi and Whiteside, 1978)	220°

5.3 DYNAMIC MECHANICAL BEHAVIOR OF THE PLASTICIZED RESIN

5.3.1 INTRODUCTION

The plasticizing solvents used to swell the 3501-6 resin were paint stripper MIL-81294 and its components. The components of the paint stripper and their individual absorption and desorption curves are presented in sections 3.4 and 3.5 and appendix C. The effects of plasticization by these solvents are discussed in this section. The solvents used were: a chlorinated hydrocarbon (methylene chloride), an aromatic-protic solvent (phenol), a protic solvent (water), and large aliphatics (waxes and surfactants).

From the results of the absorption study described in section 3.4, the following test schedule was developed and the results were compared to the dynamic behavior of the virgin resin.

1. The 3501-6 resin immersed in MIL-81294; six tests with $M = 1.7\%$ to $M = 12.5\%$.
2. The 3501-6 resin immersed in a 50/50 by weight percent solution of water-phenol. Two tests were conducted at $M = 8.81\%$ and $M = 10.2\%$.

3. The 3501-6 resin immersed in other swelling agents; methylene chloride, water, and a combination of water, methylene chloride, and phenol in weight ratios that were identical to those in MIL-81294.

For the most part, the comparison of the virgin and plasticized resin is shown with the loss compliance curves. The changes in the complex dynamic mechanical modulus and the loss tangent are also presented. The dynamic mechanical experimental data is compiled in appendix A. Section 5.3.2 discusses the comparison between the plasticized resin and the virgin resin. The results are briefly summarized in section 5.3.3.

5.3.2 COMPARISON OF THE PLASTICIZED AND VIRGIN RESIN

5.3.2.A PAINT STRIPPER MIL-81294

The dynamic mechanical properties of the plasticized resin were determined at the same frequency and over the same temperature range as the virgin resin. The Rheovibron without the new improvements was used to measure the dynamic behavior of the plasticized resin (no nitrogen gas flow, old grip-transducer system, etc.). The changes in the complex modulus, loss tangent, and the

loss compliance were determined by comparing the plasticized resin behavior against the mean virgin resin curves. The mean curves appear as a straight line through consecutive data points in figures 5.3.2-1 and 5.3.2-3. In figure 5.3.2-2, the loss tangent of the virgin resin is represented by the test results of specimen RH-23. Samples of the 3501-6 resin were immersed in the paint stripper at 25°C until the absorption levels of $M = 1.68\%$, 4.52% , 7.89% , 11.8% , 12.2% , and 12.5% were obtained. For clarity, only the test results of $M = 1.68\%$, 4.52% , 7.89% , and 11.8% are plotted in figures 5.3.2-1 through 5.3.2-3; the complex modulus, loss tangent, and loss compliance curves respectively.

The four plasticized resin test results show the effect of an increasing amount of MIL-81294 in the resin. The lowest level at $M = 1.68\%$ exhibits very little change from the dynamic behavior of the virgin resin in any of the three figures. The plasticized test results fall within the variation shown by the error bars in figure 5.3.2-2. The width of the error bar shows the maximum and minimum values of the loss tangent of the virgin resin. The complex modulus and the loss compliance virgin resin curves are also very similar to the dynamic behavior of

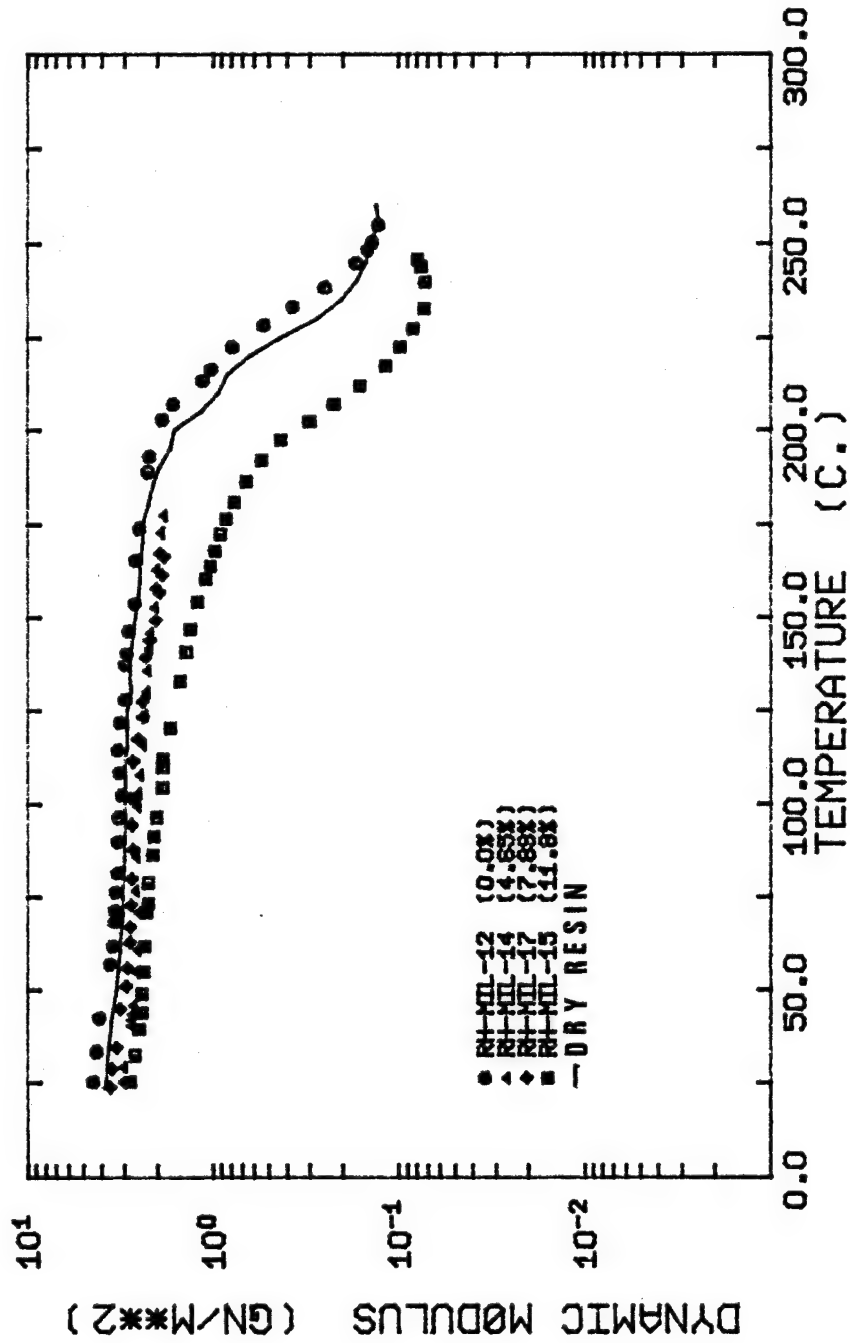


Figure 5.3.2-1 The effect of paint stripper, MIL-81294, on the complex dynamic modulus of the 3501-6 resin

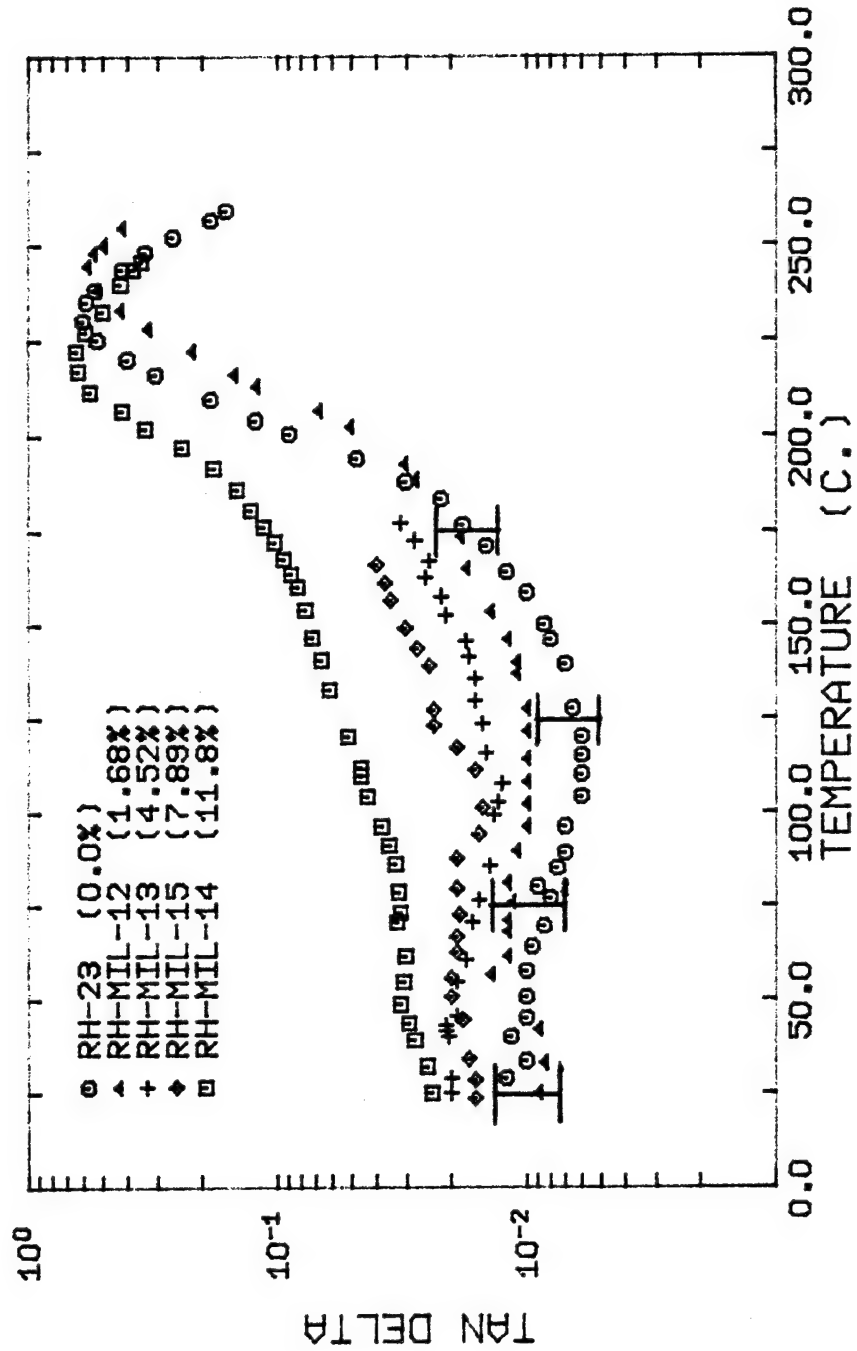


Figure 5.3.2-2 The effect of the paint stripper, MIL-81294, on the loss tangent of the 3501-6 resin

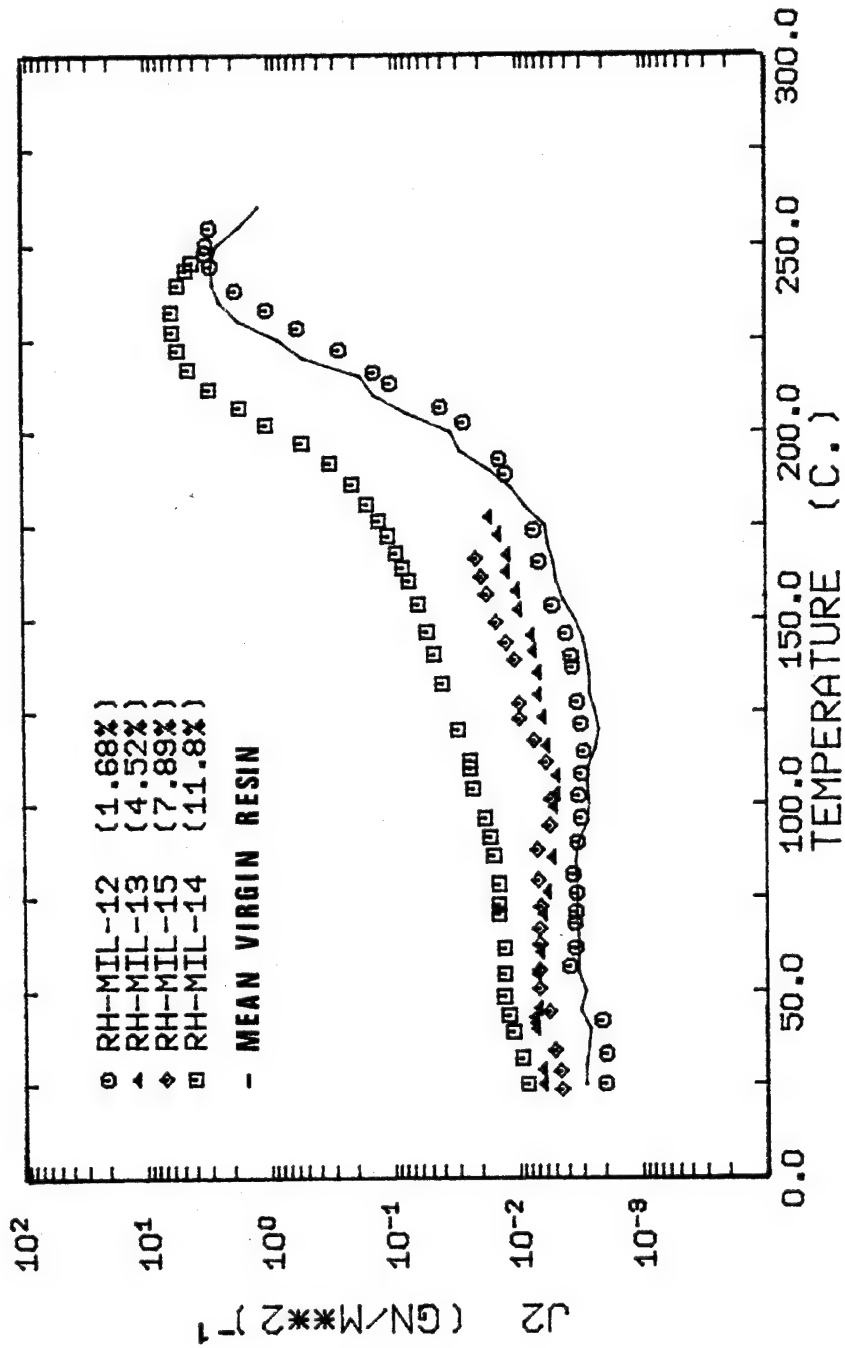


Figure 5.3.2-3 The effect of the paint stripper, MIL-81294, on the loss compliance of the 3501-6 resin

the plasticized resin at $M = 1.68\%$. In fact, the plasticized resin specimen results fall within one standard deviation of the mean resin curves.

At $M = 4.52\%$, the presence of the paint stripper begins to show its effect on the dynamic behavior of the resin. The loss tangent and the loss compliance curves show increases outside of experimental error or batch-to-batch variation. The values of the loss tangent and loss compliance are now two or three times that of the virgin resin below the glass transition. In contrast, the complex dynamic modulus shows no change outside of one standard deviation below the mean. A decrease in the modulus is expected, but the magnitude of the decrease is not sufficient to declare that any change has taken place. The test was stopped at 190°C because the specimen broke in the grips of the Rheovibron due to sideways vibration (see section 3.3). However, the loss of data above 190°C is not crucial because the solvent in the specimen desorbs at temperatures near and above the glass transition. Minimal desorption occurs at the lower temperatures where the effects of plasticization can be seen. The effects of desorption on the test results are discussed in detail in section 3.5.

At the higher absorption levels of $M = 7.89\%$ and 11.8% , the same trends are observed, but the differences between the plasticized and virgin resin are greater. The decrease in the complex modulus at 7.89% is still within the batch-to-batch variation of the virgin resin, but the decrease in the modulus at 11.8% is significant. The resin has softened enough to record a 25% decrease in the complex modulus at room temperature (compared with the 15% decrease found by Augl at a $M = 6.5\%$ water absorption level). The complex modulus decreases from 3.76 to 2.82 GN/m^2 . The loss tangent and loss compliance curves show an increase by nearly an order of magnitude. Accordingly, the ability of the resin to dissipate energy through viscous dampening has also increased by an order of magnitude. In addition, the α -peak at 11.8% has doubled in height and it has shifted 20°C downward. The precise amount of the paint stripper in the resin at this temperature is unknown, but the glass temperature as determined by the α -peak has decreased. It cannot be established whether the decrease in the glass temperature has been caused by the lubrication of the plasticizer or by some permanent damage, but the resin has become more compliant nonetheless.

The glass temperature as defined by Morgan and

O'Neal, T_{mo} , has also decreased with increasing amounts of MIL-81294. The data is recorded in figure 5.3.2-4 along with the decrease in the α -peak glass temperature, T_{α} . The original percentage weight gain, M_o , is used as the abscissa (M_o = the values of M quoted earlier). The decrease in T_{mo} is nonlinear with increasing amounts of M , but it is interesting to note that the shape of the curve is opposite to the expected curvature found in other studies (Browning, et al. 1977). From the work on moisture absorption, the decrease in the glass temperature usually follows a Bueche-Kelley relationship (Bueche and Kelley, 1960). The model is based on an increase in the free volume of the material which absorbs a solvent. The unusual behavior of the absorption of MIL-81294 by the 3501-6 resin can be expected for two reasons. First, the actual level of absorption at the glass temperature, T_{mo} , is not known because some minor desorption has already occurred. Secondly, if permanent damage has occurred (such as crazing and minor cracking), the Bueche-Kelley relationship does not apply. It is important to note that the glass temperature does decrease with increasing amounts of plasticizer.

The shifting of the α -peak and the lowering of the

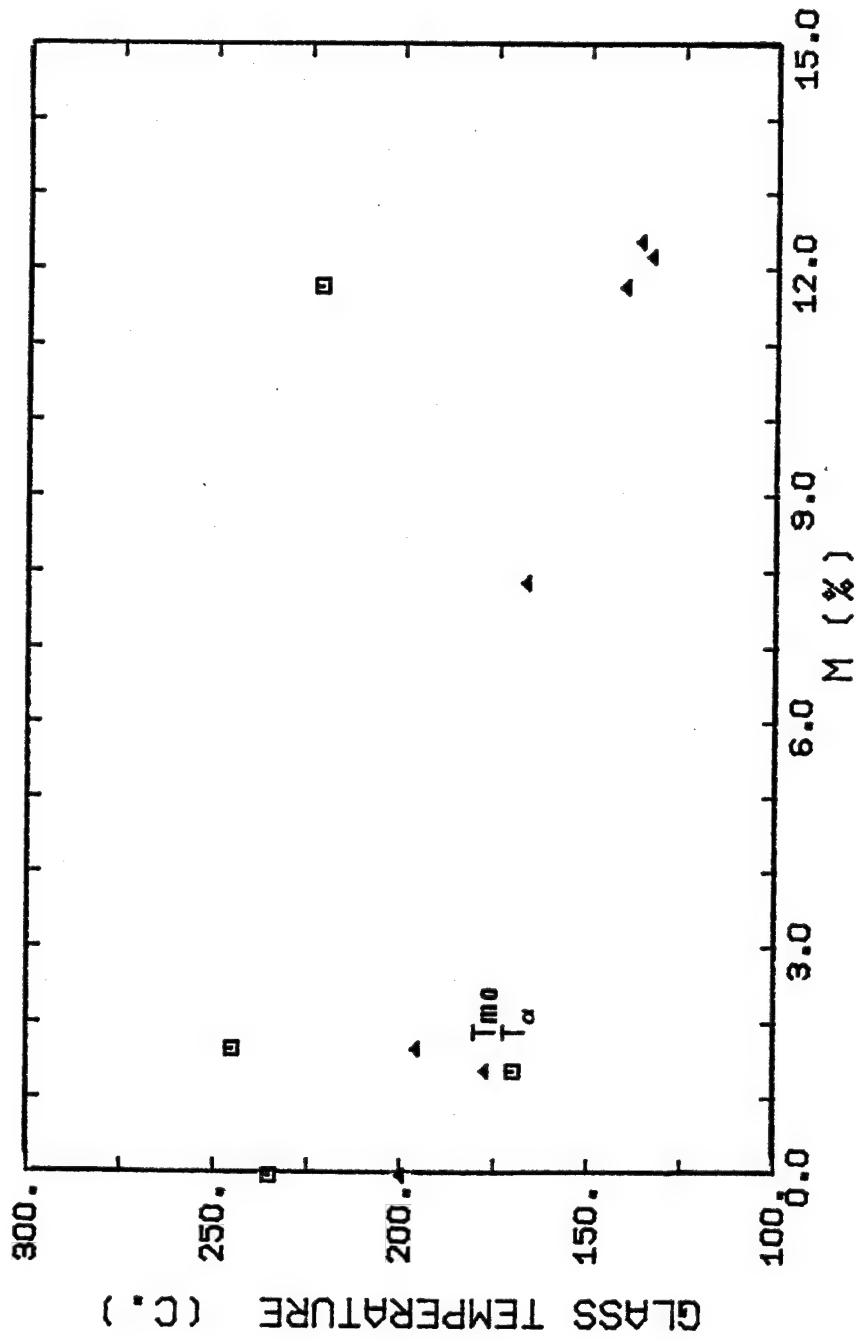


Figure 5.3.2-4 The glass transition temperature as a function of the percentage weight gain, M, for MIL-81294 plasticization

complex modulus are both evidence that permanent damage to resin may have occurred at $M = 11.8\%$. The scissioning of the crosslinks of the network may be involved. From the results of the swelling tests reported in section 3.4 and appendix C, crosslink scissioning must be occurring at levels of plasticization near $M = 20\%$. The resin fractures in the paint stripper at that level of absorption. At levels near 12%, it is not inconceivable that some microcracks could be forming. This localized destruction of the network would be detectable by electron microscopy, but further experimentation is needed to test the idea.

The reduction in the glass transition is consistent with the results presented in section 4.3. The presence of the plasticizer increases the free volume of the network. The increased free volume means that the network is better able to "loosen up" at lower temperatures than the virgin resin (Bueche, 1962). Creep is enhanced because the segments of the network can "flow" more easily. It can be expected that the creep rate would increase along with the ability of the polymer to dissipate energy through viscous dampening. The remarkable increases in the loss tangent and the loss compliance illustrate this last point nicely. As long as the network is undamaged, the dynamic modulus

should remain unchanged. The creep curve of specimen 12-11-70-06 in section 4.3 showed little change in the creep modulus. This specimen had an absorption level of $M = 6.65\%$ in water-phenol, the main plasticizing agents of MIL-81294. Some damage may exist at 11.8% plasticization since a 25% decrease in the complex modulus was observed. A critical level of adsorption probably exists between 7.89% and 11.8%.

5.3.2.B WATER-PHENOL SOLUTION

The results of the absorption study conducted in section 3.4 indicated that water and phenol were the only solvents of the paint stripper that had swollen the resin to any appreciable extent. Water reached an absorption equilibrium level dependent upon the amount of background moisture existant before immersion. Phenol swelled the resin the most fracturing the test specimens between $M = 20\%$ and 23% . Both solvents were used together because their swelling ability mimicked the swelling ability of the paint stripper. All samples tested on the Rheovibron (including creep specimen 12-11-79-06) were immersed at 75°C in a 50% by 50% weight ratio solution of water-phenol. Further details on the immersion procedures are given in section 3.4.

The plasticized specimens were made from the same batch of resin and they were tested on the Rheovibron fitted with the new improvements. The two plasticized resin specimens were soaked to levels of $M = 8.81\%$ and 10.2% . The comparison with the dynamic behavior of the virgin resin is shown in figures 5.3.2-5 through 5.3.2-7. The virgin resin specimens were also made from the same batch of resin and were tested on the Rheovibron fitted with the new improvements. The virgin resin behavior is represented by specimen RH-1-2-80-12.

The two plasticized specimens represent the higher end of absorption. Consequently, the results of the plasticization by water-phenol are quite similar to the results of section 5.3.2.A. The major differences between the dynamic behavior of the two solvents is due to the change in experimental procedure (MIL-81294 immersion used no improvements while water-phenol immersion used the new improvements). The difference can be seen in the loss tangent and the loss compliance of figures 5.3.2-6 and 5.3.2-7 respectively. The dynamic behavior of the water-phenol plasticized resin has increased by an order of magnitude. This result was also observed in the MIL-81294 plasticized dynamic behavior. The difference at

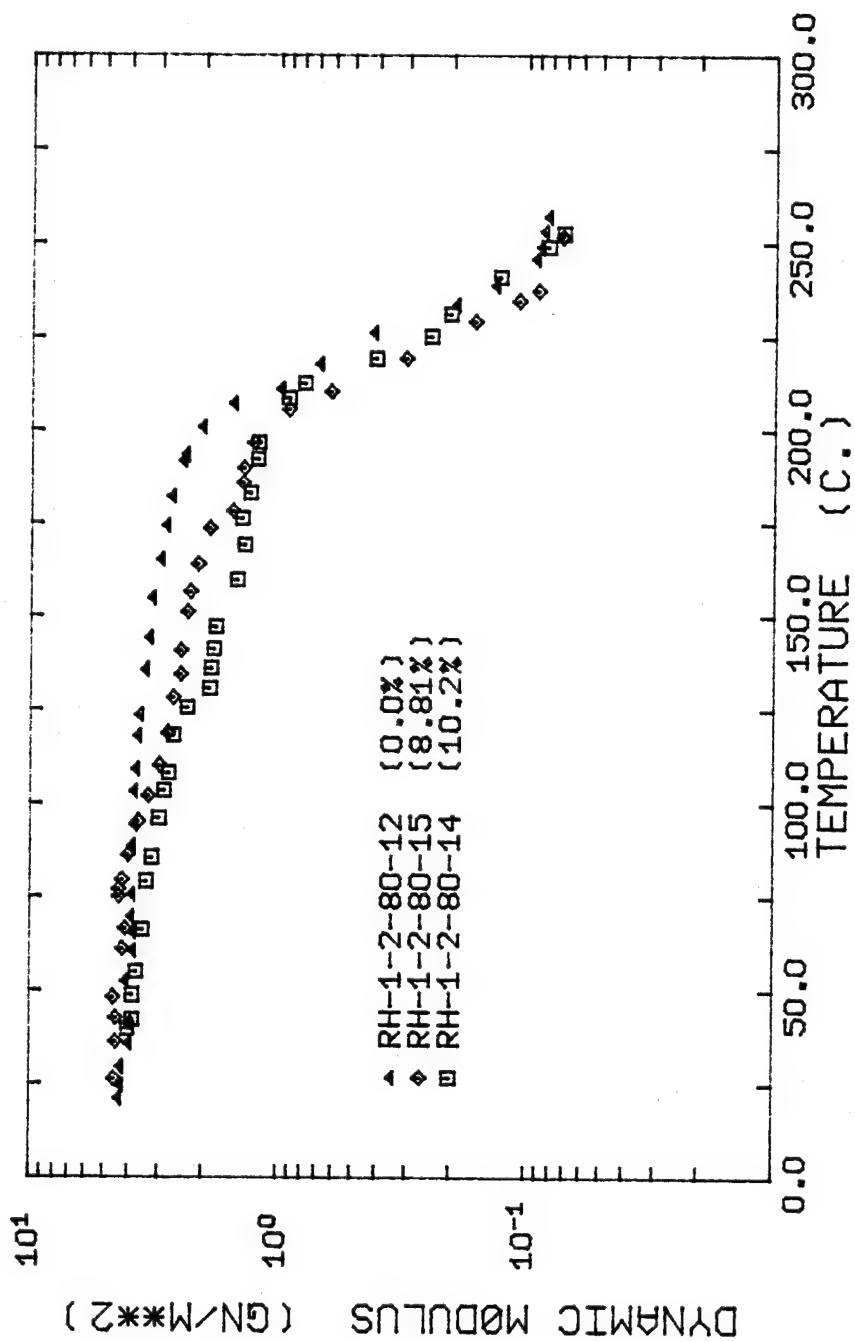


Figure 5.3.2-5 The effect of water-phenol (50/50) on the complex dynamic modulus of the 3501-6 resin

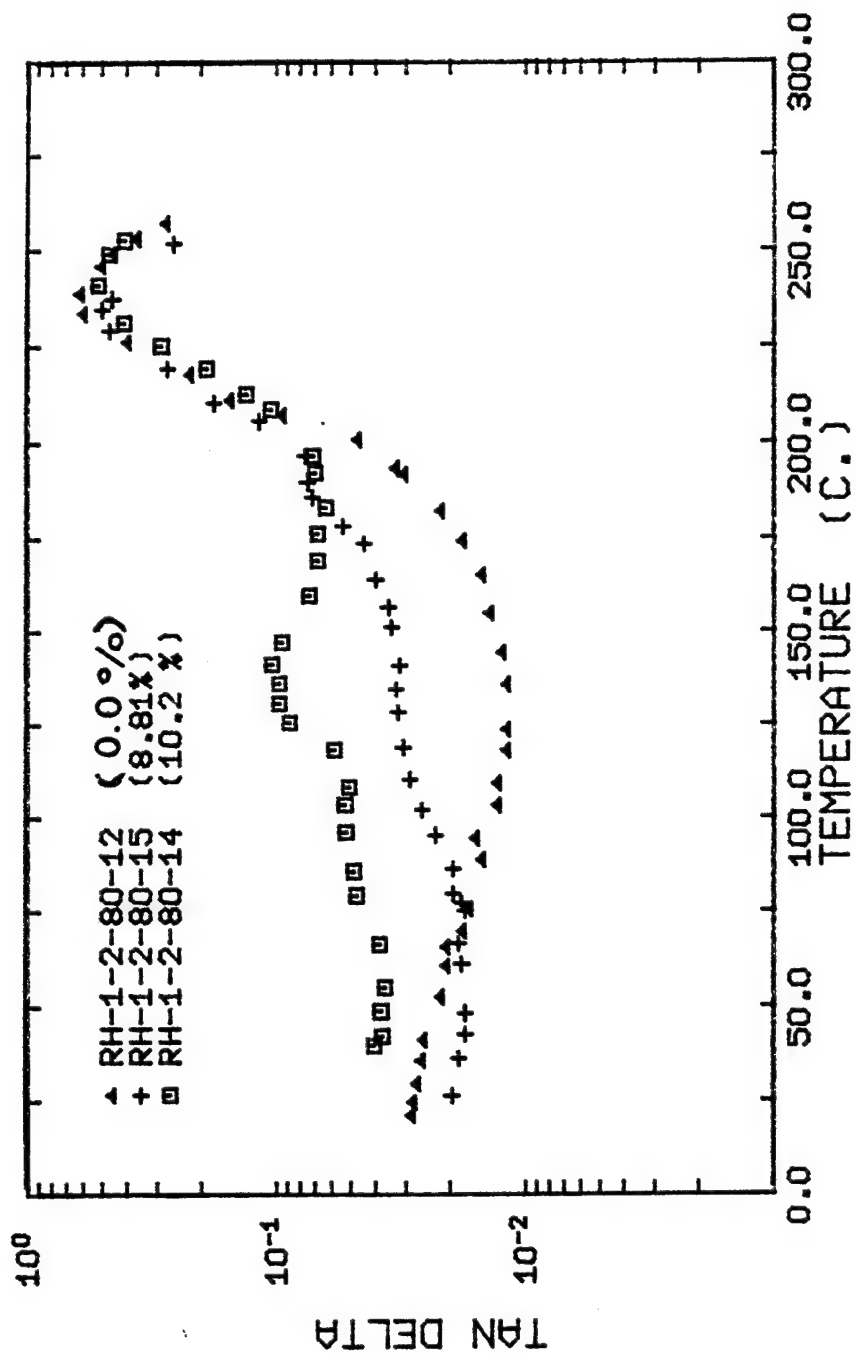


Figure 5.3.2-6 The effect of water-phenol (50/50) on the loss tangent of the 3501-6 resin

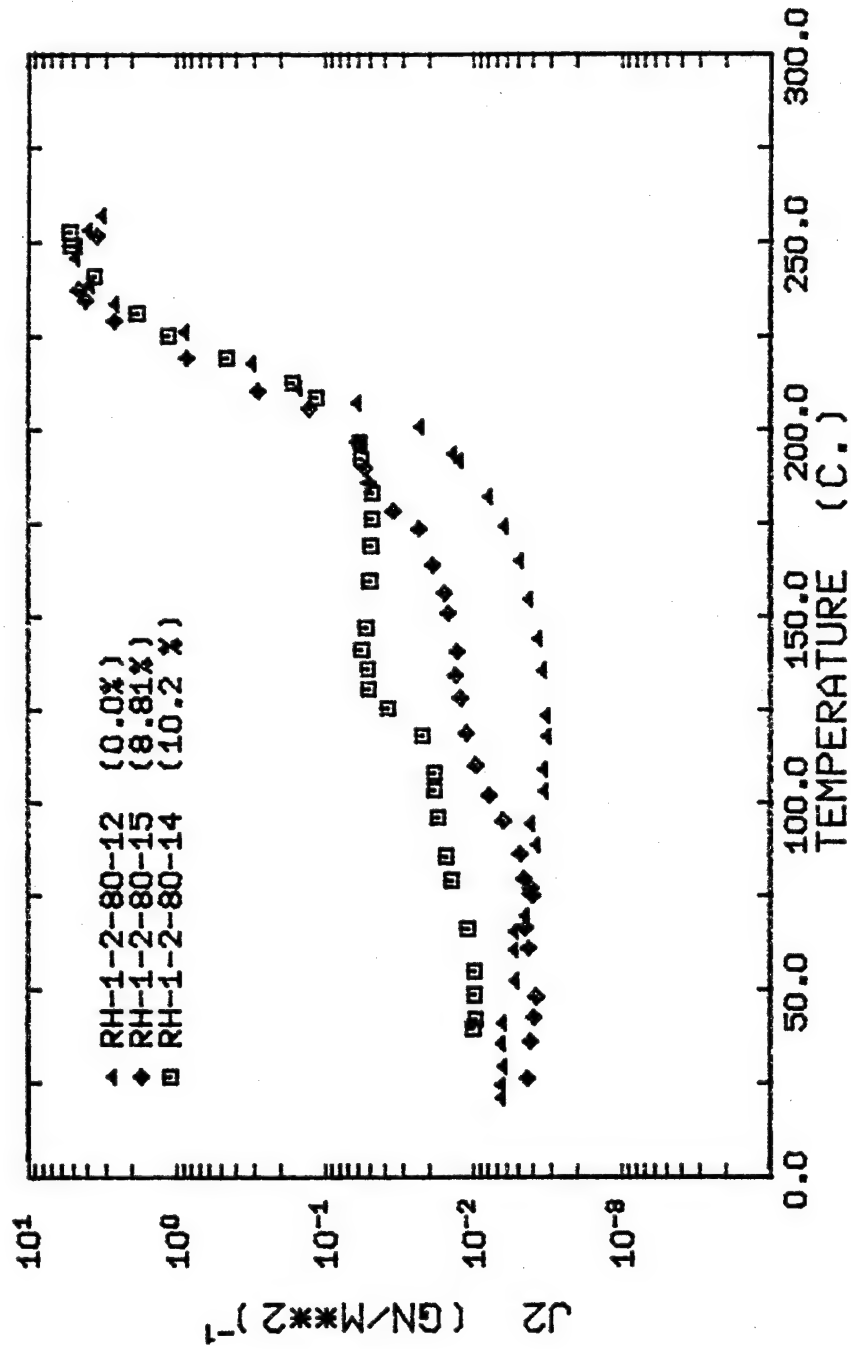


Figure 5.3.2-7 The effect of water-phenol (50/50) on the loss compliance of the 3501-6 resin

the higher absorption levels occurs at the α -peak. The water-phenol specimens converge with the dynamic behavior of the virgin resin where a 20°C shift was observed in the MIL-81294 plasticized specimens. The difference is caused by the use of nitrogen gas in the heater chamber of the Rheovibron with the water-phenol plasticized specimens. Convective diffusion causes the complete desorption of the specimen during the test. Before, only partial desorption was realized without any nitrogen gas flow. As discussed in section 3.5, a specimen soaked to $M = 17\%$ desorbed completely when tested in the Rheovibron with nitrogen gas flow. In fact, the weight of the specimen was less at the end of the simulation test than before the specimen was immersed in the water-phenol. Even the background moisture was desorbed out of the resin. Extensive desorption starts at the glass transition which is depressed below the temperature of the virgin resin glass transition temperature. Therefore, desorption aids in defining where the depressed glass transition temperature occurs. For instance, specimen RH-1-2-80-14 has a false peak in figure 5.3.2-7 at 130°C. The sudden loss of solvent when the glass transition temperature is passed reduces the amount of solvent in the specimen. The dynamic behavior observed is the behavior of a specimen with a slightly lower loading; therefore,

the loss compliance decreases until the α -peak temperature of the virgin resin is approached. The same phenomena occurs in the loss tangent and in the complex modulus. The complex modulus in this case only slows its descent with increasing temperature momentarily.

Desorption below the depressed glass transition temperature is minor (see section 3.5). A Morgan and O'Neal glass temperature can still be calculated. It is plotted in figure 5.3.2-8 for the two tests conducted. The decrease in the glass temperature is very similar to the results of MIL-81294 plasticization though perhaps slightly more pronounced. The α -peak glass temperature is also plotted in figure 5.3.2-8. There is no change between the plasticized glass temperature and the virgin resin temperature due to the effect of complete desorption.

The dynamic behavior of the plasticized resin in figure 5.3.2-5 shows the expected decrease in the complex modulus with increasing amounts of water-phenol. Oddly, the room temperature complex modulus at M = 10.2% does not show a decrease outside the range of the experimental error. Therefore, the swelling of the resin by water-phenol (50/50) has not caused permanent damage to the

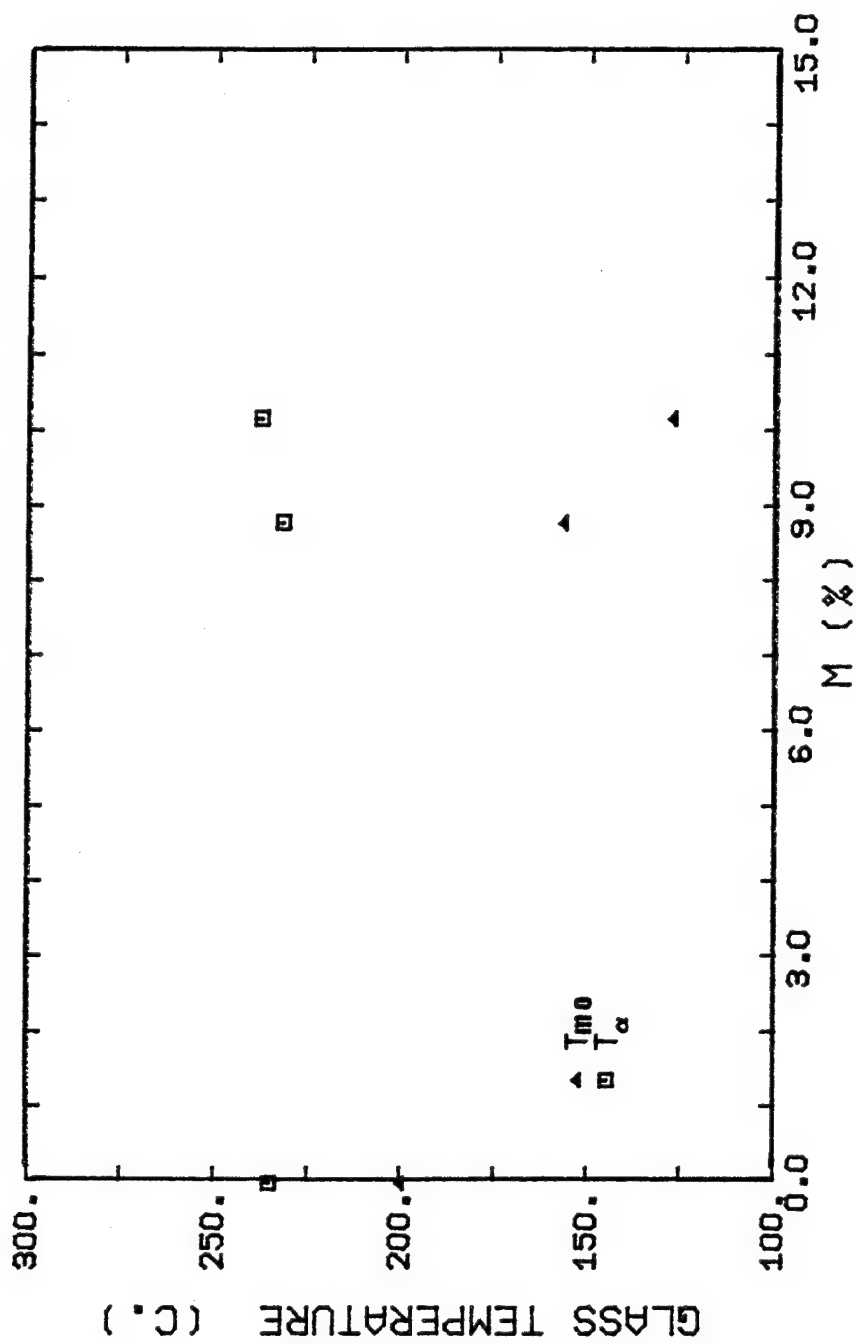


Figure 5.3.2-8 The glass transition temperature as a function of the percentage weight gain, M, for water-phenol plasticization

network. The specimen plasticized to 11.8% weight gain in MIL-81294 did show a decrease in the complex modulus outside of experimental error. Though the two solvents are not exactly alike (MIL-81294 contains waxes and surfactants which could have a synergistic effect with the other components), the critical absorption level probably occurs between $M = 10.2\%$ and 11.8% . The effect at higher temperatures is obvious though because the glass temperature, T_{mo} , has been shifted to lower temperatures.

5.3.2.C ABSORPTION OF OTHER SOLVENTS

To test the effect of the other paint stripper components on the resin, a single dynamic mechanical test was performed on specimens immersed in the three following solutions: water, methylene chloride, and a mixture of water, phenol, and methylene chloride with the same weight proportions as found in MIL-81294. The last solvent is the paint stripper without surfactants and waxes. The difference between the dynamic mechanical behavior of MIL-81294 and this solution would be caused by these components. The dynamic behavior of methylene chloride and water represent the dynamic behavior of two classes of solvents, a halogenated hydrocarbon and a protic solvent respectively.

All tests discussed in this section were performed on the Rheovibron without using any new improvements. Therefore, the plasticized results are compared against the mean virgin resin curves. The loss compliance is used as the basis for comparison.

Specimen RH-M-10 was immersed for two weeks in methylene chloride at 25°C. The weight of the specimen before and after immersion showed that the weight had not changed; however, earlier absorption tests (section 3.4) indicated that the weight of a resin specimen immersed in methylene chloride decreased during the first week and slowly increased thereafter. The yellowish color of the solvent meant that the 1% decrease in weight was caused by the leaching of DDS or other modifiers. The increase in weight during the second week was probably caused by the slow absorption of the methylene chloride. Some swelling of the resin is assumed. The dynamic mechanical behavior of the specimen exposed to methylene chloride is shown in figure 5.3.2-9. The increase in the loss compliance when compared against the mean virgin resin behavior is just outside the range of the error bars (one standard deviation from the mean). There is a reasonable chance that a plasticization effect is present. The softening of the

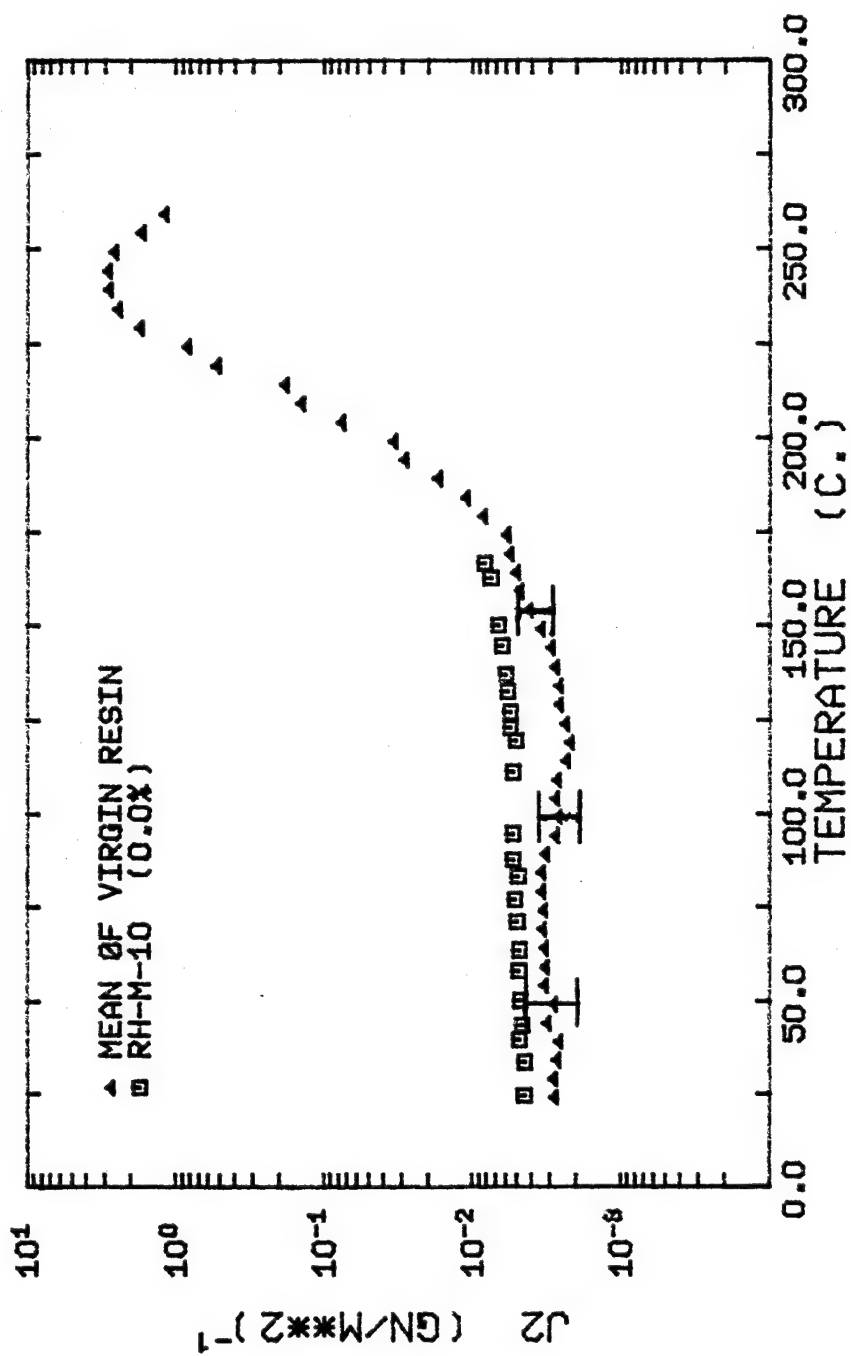


Figure 5.3.2-9 The effect of methylene chloride on the loss compliance of the 3501-6 resin

resin over a two week period is very slight. No change in the complex modulus was observed, so the network structure was unaffected by the solvent. A similar two week immersion in MIL-81294 or water-phenol would have devastated the specimen. It is reasonable to conclude that methylene chloride has a negligible effect on the resin in comparison with the absorption effects of water-phenol (50/50) or MIL-81294.

Other halogenated hydrocarbons can be assumed to have a similar effect on the 3501-6 resin. Long exposure times would be needed to show any increase in the compliant nature of the resin. The immediate elastic properties should be unaffected. Therefore, the creep behavior of the resin would probably be unaltered at room temperature. The only noticeable physiochemical attack was the elution of either unreacted DDS or other modifiers from the resin. Slow diffusional processes are probably involved. Unlike water and phenol, the methylene chloride molecule cannot hydrogen bond with the resin, but induced dipolar attractions can provide the associative forces necessary for some minimal absorption to take place.

Specimen RH-H-10 was immersed in distilled water at 92°C for one month. The high immersion temperature ensured

that an equilibrium absorption level would be attained. A level of $M = 2.65\%$ was established after 300 hours of immersion and the absorption level remained constant for the remainder of the immersion time. Background moisture accounts for the difference between the saturated level of 2.65% and the absorption level of a dessicated specimen (6.65% , DeIasi and Whiteside, 1978). The attainment of an equilibrium compliance is discussed in detail in appendix C. The loss compliance of the plasticized specimen is plotted against the mean virgin resin curve in figure 5.3.2-10.

The increase in the loss compliance in comparison with the mean virgin resin curve is similar to the plasticized behavior of the methylene chloride specimen. The value of the loss compliance has been doubled, just outside the range of the error bars (single standard deviation about the mean). As soon as desorption sets in near 170°C , the two curves merge together. Since the α -peak does not shift, the water either totally desorbs during the test or its absorption level is too small to render any effect. The α -peak height is doubled, however. Normally, this result would indicate that some permanent damage has resulted from the water absorption. Crazing

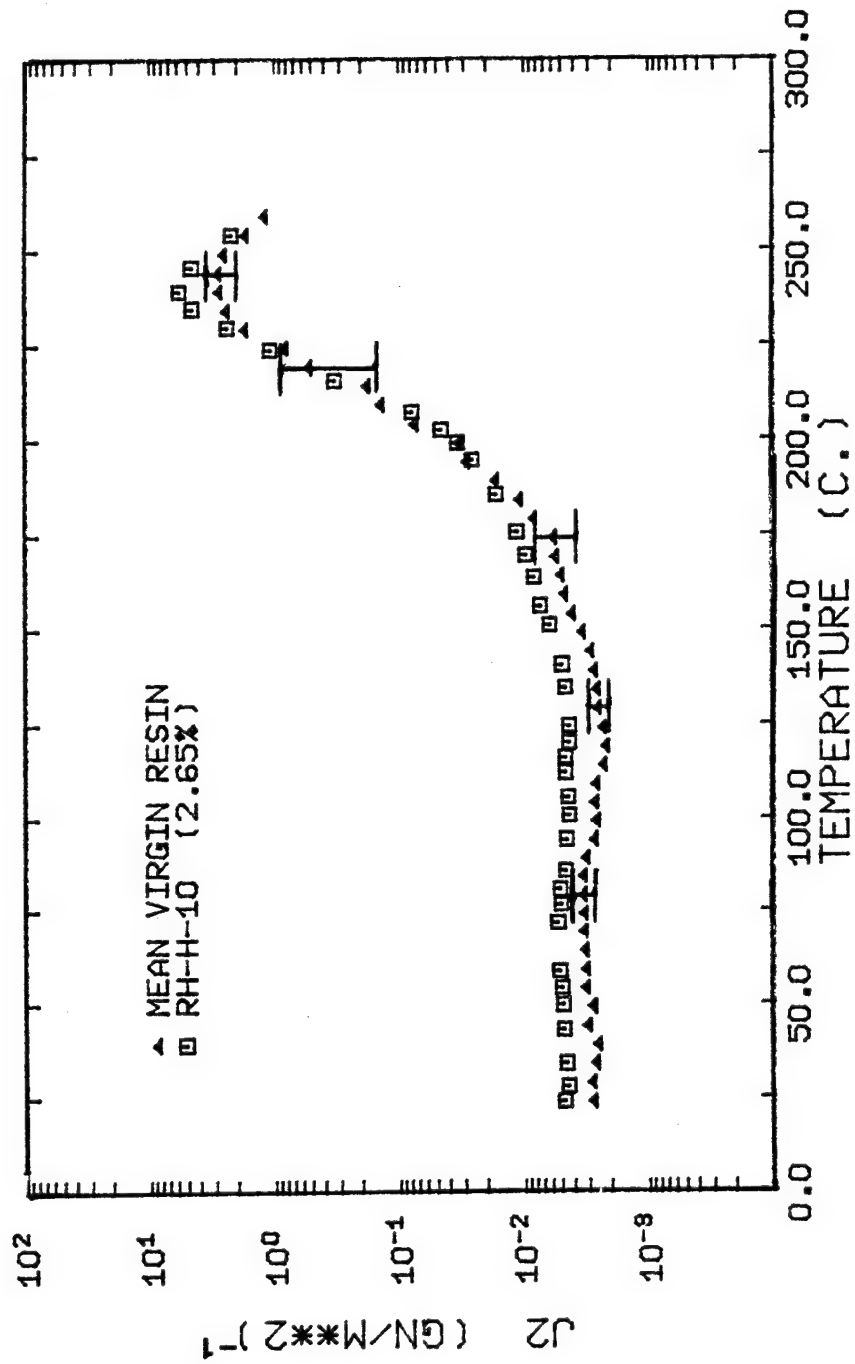


Figure 5.3.2-10 The effect of water on the loss compliance of the 3501-6 resin

can occur at the levels of absorption near saturation, but the results of one test are not conclusive enough to determine whether or not permanent damage has occurred. This would be an interesting point for further investigation. The effects of water absorption are known to be reversible (Augl, 1977; Browning, 1974), but the time the specimen spent above the glass temperature (in the Rheovibron) was very small.

The complex modulus of the water plasticized resin exhibited a decrease from 3.76 to 3.33 GN/m² at 25°C, a relative decrease of 11.4% which is greater than the experimental error of 0.27 GN/m² (7.2%). Since one mole of phenol weighs 5.2 times more than a mole of water, a specimen with a weight gain of 12% in MIL-81294 would have as many moles absorbed into the specimen as one immersed in water with a 2.5% weight gain. Recalling an earlier discussion, an absorption level of 11.8% in water-phenol (50/50) was required to notice any decrease in the complex modulus outside of experimental error. The decrease in the complex modulus exhibited by water can be expected if the number of moles present in the resin is the same as a like case for phenol absorption.

Keenan, Seferis, and Quinlivan (1978) have also

tested the effects of moisture on one other tetraglycidyl amine epoxy resin. Their resin samples were dessicated which allowed a greater amount of water absorption into their samples. Their results indicate that the resin softens at values of M between 3% and 5.5%. The β -peak of the loss tangent increased in value (the peak at -50°C) and it shifted to lower temperatures. The ω -peak (not observed in the 3501-6 resin) showed both those effects along with a more general broadening of the peak. Since the changes observed in the peaks of the loss tangent would also be observed in the loss compliance, it is reasonable to assume that the loss compliance would also show these changes in the β -peak of the 3501-6 resin.

Specimen RH-HMPH-10 was immersed in the water-phenol-methylene chloride solution at room temperature to an absorption level of $M = 12.2\%$. The loss compliance is plotted in figure 5.3.2-11. Plotted in the same figure are the mean virgin resin curve and the loss compliance of specimen RH-MIL-15 soaked to 7.89% in MIL-81294. Premature failure of the specimen terminated the water-phenol-methylene chloride test at 190°C . The water-phenol-methylene chloride solution has all the components of MIL-81294 except for the surfactants and waxes. The

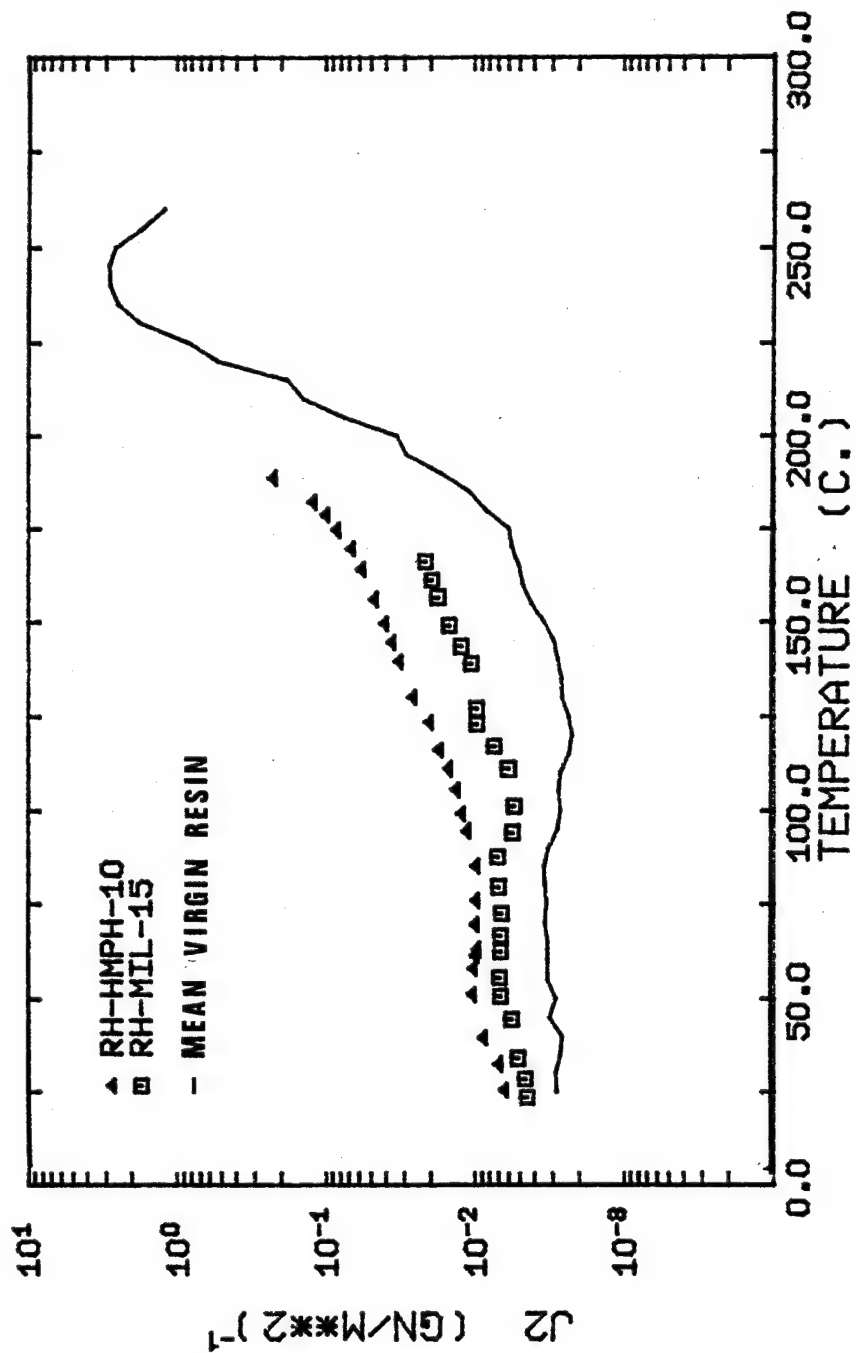


Figure 5.3.2-11 The effect of water-methylene chloride-phenol solution on the loss compliance of the 3501-6 resin

surfactants and waxes are assumed to have no effect on the dynamic mechanical behavior of the resin because these molecules are too large to compete with the absorption capabilities of water and phenol. The steric hindrances to diffusion are too great for these long chain aliphatic molecules. Consequently, the dynamic mechanical behavior of the pasticized resin should be the same for each solvent if the resin is immersed to the same absorption level. In fact, the dynamic mechanical behavior of specimen RH-MIL-14 (11.8% in MIL-81294, see figure 5.3.2-3) is nearly the same as specimen RH-HMPH-10 (12.2% water-phenol-methylene chloride). Specimen RH-MIL-15 (7.89% in MIL-81294) has been included in figure 5.3.2-11 in order to visually show the increase in the loss compliance with increasing amounts of absorbed water and phenol from solutions containing those two solvents. However, the surfactants may have had a role in increasing the swelling abilities of the paint stripper over its components. It is evident from the absorption study that the paint stripper swells the resin faster than the individual solvents at room temperature. Some synergistic phenomena may be involved (see appendix C).

5.3.3 SUMMARY

From the series of tests reported in this chapter, the following changes in the dynamic mechanical behavior of the 3501-6 resin have been observed:

1. The glass transition temperature is shifted to lower temperatures with increasing amounts of absorbed plasticizer.
2. The loss functions (e.g. $\tan \delta$ or J_2) exhibit a large increase when plasticized by water or phenol or combinations of the two solvents. The storage functions show only minor changes.
3. The complex modulus does not exhibit a decrease outside of experimental error unless a critical absorption level has been attained. Equilibrium water absorption and extremely high values of phenol absorption are the only two cases where the decrease has been observed.
4. The effects of absorption are reversible at low levels (M less than 10%) because total desorption occurs when the glass transition is surpassed.

The shifting of the glass transition temperature was

monitored by observing the shift at the beginning of the glass transition (T_{mo}). Shifts in the α -peak were not that noticeable because most of the solvent sufficiently desorbed from the specimen during the test on the Rheovibron. In one case, a decrease in the α -peak of 20°C was noted for a specimen tested without nitrogen gas flow.

The slight shift in the complex modulus and the storage functions indicates that the overall structural performance of the resin under short term loads is not affected by a significant amount of water or phenol. Large plasticization levels (12% for MIL-81294 and 2.5% for water) were required to show any reduction in the complex modulus outside of a 7% experimental error range. The network of the resin retains its integrity with only a slight amount of network damage at the higher plasticization levels. Absorbed solvents increase the ability of the resin to dissipate energy. Nearly an order of magnitude increase in the loss tangent and the loss compliance were observed.

The effects of absorption are self-healing though if heated above the glass transition temperature. If a swollen specimen is heated near or above its glass transition, water and phenol will desorb from the resin.

Tests in the Rheovibron with nitrogen gas flow indicated that a specimen would totally desorb when heated above its glass temperature. The glass temperature of the plasticized resin is less than the virgin resin glass temperature; therefore, when a specimen desorbs the dynamic behavior of the plasticized specimen "returns" to the dynamic behavior of the virgin resin.

Of all the components of MIL-81294, phenol is the most devastating. Water is the only other component which will swell the resin to any appreciable extent. The paint stripper swelled the resin at a faster rate than any combination of the other components.

The solvents containing phenol all had similar effects on the resin. Absorption levels of M = 10% to 12% showed an order of magnitude increase in the loss compliance and the complex modulus was decreased slightly beyond experimental error.

CHAPTER 6

CONCLUSIONS AND RECOMMENDATIONS

This investigation was undertaken with a two-fold purpose in mind. The first objective was to establish the time-dependent mechanical behavior of the virgin 3501-6 resin. This was accomplished by making creep and dynamic mechanical measurements to characterize the viscoelastic properties of the resin. The second objective sought was to characterize the effects of external plasticization by a paint stripping solvent and its components. The comparison of the results for the virgin and plastized resins led to several conclusions concerning the time-dependent mechanical behavior of the resin. The major points are reviewed in this chapter. Recommendations for further investigation are presented in order to extend the topics of research discussed in this thesis.

Dynamic mechanical testing was shown to serve as a sensitive means of detecting the effects of external plasticization. Furthermore, several dynamic mechanical tests can be conducted within the time it takes to run one creep or stress relaxation experiment. Using the Rheovibron model DDV-II-B to make dynamic mechanical

measurements eases the problems of loading and unloading of the specimen into the test machine. The problem of specimen damage in loading the creep grips is avoided by using the Rheovibron. Furthermore, the mathematical transformations in chapter 2 show the relationship of the creep and stress relaxation behavior to the dynamic mechanical spectra.

The Rheovibron, when properly calibrated, is effective in measuring the changes in the dynamic mechanical behavior caused by external plasticization. The largest changes are observed in the loss tangent ($\tan \delta$) and loss compliance (J_2) functions. The increase in either quantity can be directly related to the energy of dissipation. Smaller changes (but still greater than the experimental error) can be observed in the complex dynamic modulus, $|E|$. The reduction in the value of $|E|$ at a specific temperature can be qualitatively related to the expected decrease in the Young's modulus of the resin. For higher modulus materials, such as the 3501-6 resin, the value of $|E|$ is slightly lower than the Young's modulus. Monitoring the Morgan and O'Neal glass transition temperature (where the onset of the glass transition occurs, $T_{mo} = 1/2|E| (25^\circ\text{C})$) gives an indication of the

magnitude of the reduction in the glass transition temperature of the resin with increasing concentrations of the absorbed solvent.

There are a few disadvantages in using the Rheovibron and in dynamic mechanical testing in general. A plasticized specimen in a heated environment will lose some of its solvent to desorption. Fortunately, the desorption process is very slow until the glass transition temperature is approached. Therefore, plasticization studies on the Rheovibron are only valid if measured below the glass transition temperature. The presence of desorption also means that the creep experiments of plasticized resin specimens should be performed below the glass transition temperature. The correlation of the creep and stress relaxation behavior to dynamic mechanical test data has its limitations. The maximum strain exerted on a test specimen in the Rheovibron is less than the elastic limit of the resin. The predicted creep behavior would only be applicable at very low strain levels below this limit (i.e. for very low initial stress levels). For strains beyond the elastic limit, epoxy resins exhibit

nonlinear viscoelastic creep behavior; therefore, the predicted creep behavior would tend to underestimate the actual creep behavior. The elastic limit for the 3501-6 resin is approximately 0.1% strain.

The creep experiments on the virgin resin indicate that time-temperature superposition does not adequately predict the long term creep behavior of the resin between 22.5° and 103°C. Instead, the master creep curve serves as a lower bound for the long term creep of the resin. The failure of time-temperature superposition to adequately predict the long term creep behavior is caused by the nonlinear viscoelastic creep behavior exhibited at the longer times. A master curve was constructed from short term creep tests where linear viscoelastic models fit the data fairly well. Therefore, the master curve reflects the linear viscoelastic creep behavior over all periods of time. Long term creep tests can be successfully modelled only if nonlinear viscoelastic functions are used. In the current work, the power law model (nonlinear viscoelastic model) was found to be an upper bound to the long term creep behavior of the resin. The proper mathematical representation of the creep behavior of the resin would require more sophisticated nonlinear models. To accomplish

this, a clear understanding of the effect of stress level on the creep compliance would have to be fully understood. The dependence of the creep behavior on the initial stress level is recommended for further investigation.

An adequate method of predicting the long term creep behavior of the 3501-6 resin and other tetraglycidyl amine resins is necessary because the time-dependent properties of the carbon fiber composite are predicted from the creep and stress-relaxation data of the neat resin and the fiber. Many investigators have constructed master creep curves of epoxy resins without testing the validity of time-temperature superposition. The use of short term creep tests in the construction of master curves leaves the possibility that the nonlinear creep behavior observed at longer times may not be represented in the master curve. The predicted properties of the composite that might be affected are the transverse creep and stress relaxation ($J_{22}(t)$ and $E_{22}(t)$ respectively). The error in the prediction is proportional to the difference between the actual creep compliance (from a long term creep test) and the value of the compliance given by the master curve. Since the master curve is a lower bound to the actual creep, the predicted transverse creep

analyzing the effect of temperature on the creep compliance, this would mean preparing several test specimens for each batch of resin. This method would be impractical for creep testing because the number of tests involved would be too great. The second method proved more fruitful. For the creep compliance of the resin, a normalized variable can be used which eliminates the effects of batch-to-batch variation. By dividing the measured creep compliance, $J(t)$, by the initial creep compliance, J_0 ($J(t)$ at zero time as predicted by the Voigt-Kelvin model), the normalized creep compliance is formed. The effects of temperature and plasticization on the resin can be clearly exhibited by plotting $J(t)/J_0$ vs. time. Therefore, a few creep tests independent of the batch they were prepared from can adequately measure the effects of any independent variable on the creep compliance of the resin.

For dynamic mechanical testing the scatter in the complex dynamic modulus, $|E|$, and the loss tangent, $\tan \delta$, were caused by the experimental error (e.g. sideways vibration, misalignment of the stress and strain transducers). Batch-to-batch variation in these measured variables was equal to or less than the experimental error (7% about the mean).

is expected to be less than the actual transverse creep. The error would be dependent upon the stress level and the volume fraction of fiber in the composite.

Time-temperature superposition has been successfully applied to the transverse creep of the composite. The success is probably due to the stiffening effect of the carbon fibers which tends to limit the behavior to the linear region.

The scatter inherent in the creep and dynamic mechanical test data makes the analysis of the time-dependent mechanical behavior difficult. The scatter outside of experimental error is caused by the batch-to-batch variation in the mechanical properties of the resin. The value of the initial creep compliance, for instance, can randomly vary by as much as 15% about the calculated mean of the data. The choice of a particular value for any mechanical property at a specific time and constant temperature must be expressed as the mean value bounded by statistical limits. A single standard deviation was the statistical limit chosen for this work. The scatter in the data caused by batch-to-bath variation can be minimized in two ways. First, a great number of tests could be performed for a number of batches of resin. For

Batch-to-batch variation only affects the absolute value of the complex dynamic modulus or creep compliance. The changes in these time-dependent mechanical properties caused by external plasticization are not affected because the resulting scatter is the same for the virgin and plasticized resin test results. The qualitative interpretations of the effects of plasticization; therefore, can be directly determined from the differences in the creep and dynamic mechanical behavior.

Immersing the 3501-6 resin into paint stripper, MIL-81294, and several of its components enabled a qualitative assessment of the degree of aggressiveness of a variety of classes of solvents that plasticize (or absorb into) the 3501-6 resin. Of all the components, phenol (aromatic-protic solvent) was the most aggressive. A specimen immersed in phenol would swell until it fractured (at a 20% - 23% weight gain in the specimen), usually taking only a few hours. Solutions of phenol with water and water-methylene chloride also swelled the resin until it fractured. Distilled water (protic solvent) absorbed into the resin at a much slower rate reaching an equilibrium absorption level between 2.5% and 4.5% weight gain. The final equilibrium level varied

depending upon the amount of background moisture that had previously absorbed into the test specimen from the atmosphere. Immersion in methylene chloride (halogenated hydrocarbon solvent) produced only a slight effect on the resin. Some of the unreacted crosslinking agent (DDS) was leached out of the resin. The rate of absorption was negligible in comparison (less than 1% weight gain) to phenol or water. The surfactants and waxes (long chain aliphatic molecules) in the paint stripper were not tested directly. They may have had an affect on the aggressive swelling tendencies of the other components of the paint stripper. At 25°C, the paint stripper was the most aggressive swelling solvent and it fractured the resin in less time than any other component or combinations of components. One such combination was the paint stripper without surfactants (water-phenol-methylene chloride solution). The presence of the surfactant in the paint stripper appears to be the only difference between the two solvents. A synergistic effect between the surfactants and the other components may be occurring, but further experimentation is needed to adequately define the cause for the increased aggressive swelling tendency of the paint stripper.

The changes each solvent induces in the dynamic mechanical behavior of the virgin resin is indicative of the solvent's aggressive swelling ability. The more aggressive solvents decreased the magnitude of the complex dynamic modulus and increased the loss tangent much more than the less aggressive solvents. For instance, a water-phenol-methylene chloride solution, the paint stripper, and water-phenol (50/50) solution caused the following changes in the dynamic properties of the resin:

1. $|E|$ was decreased by 25% for absorption levels above 10% weight gain.
2. The loss tangent ($\tan \delta$) and loss compliance (J_2) increased by one order of magnitude for absorption levels above 10% weight gain.
3. The creep compliance at room temperature (0-50 thousand seconds) was unaltered in the short run, but the creep rate was greatly enhanced in the long run (greater than 50 thousand seconds).

Water made the resin more compliant as indicated by significantly decreasing $|E|$ beyond the limits of experimental error and by causing a two-fold increase in J_2 . Methylene chloride, on the other hand, had little

effect on the dynamic mechanical properties of the resin. The dynamic mechanical behavior of the resin plasticized with the paint stripper and water-phenol-methylene chloride solution (paint stripper without surfactants) was identical; therefore, the surfactants only aided the rate of absorption and they did not affect the dynamic mechanical properties.

A direct consequence of this investigation was the initiating of a data base for the 3501-6 resin. Many of the static and dynamic mechanical properties of the 3501-6 resin and other tetraglycidyl amine resins have either not been reported in the literature at all or else they have been scattered in several other sources. It is essential to have a good data base if the properties of the neat resin are being used in the design of composite materials. The creep and dynamic mechanical data measured on the virgin resin serve as a start towards acquiring this data base.

Finally, there are a few worthwhile efforts which can be undertaken and expand the scope of the work started by this investigation. The following suggested areas for further study not only apply to the effect of solvent plasticization on the 3501-6 resin, but these areas also

can be used to determine these effects on epoxy resins and other thermoset polymers as well. One of the additional areas for further study is the determination of the effect of solvent concentration on the viscoelastic properties of a polymer. Assuming time-temperature superposition can be applied to the polymer's viscoelastic behavior, the concentration might be used to determine either a time (horizontal) or temperature (vertical) shift factor. For a particular absorbed solvent, a master creep or stress relaxation curve could be constructed using the concentration dependent shift factors. Dynamic mechanical testing would be better suited to determine the concentration dependence of the shift factors which would be used to predict the long term creep or stress relaxation behavior from known transformations.

A further investigation could be aimed at finding a common link between various solvents. A parameter such as the diffusion coefficient or the solubility parameter might be useful in determining the overall shift factor for the thermoset polymer under consideration.

The modelling of the diffusion of water into epoxy resins and their composites has already been determined, but the diffusional characteristics of solvents other than

water have not been investigated (e.g. paint stripping solvents and aircraft fuels). The rate of absorption and desorption of these external solvents is useful information which can be used to determine certain design applications. There is need for further analysis. The more aggressive solvents which swell the resin to fracture absorb into the resin (above a certain concentration limit) via a non-Fickian diffusion process. The non-Fickian diffusion case has yet to be fully considered.

SYMBOLS

Alphanumeric Symbols

A	Rheovibron machine constant, equation 3.2-1
a,b,c	Dimensions of a rectangular solid test specimen
a_T	Horizontal time shift factor when applying time-temperature superposition, equation 4.2.3-4
C	Variable in F-distribution, equation G-2
D	Dynamic force parameter, equation 3.2-1
D_1	Parameter in power law model, equation 2.1.3-2
E	Young's modulus
E^*	Complex dynamic modulus, a vector
$ E $	Magnitude of complex dynamic modulus
E_0	Initial Hookian spring constant in Voigt-Kelvin model, the reciprocal is J_0
E_i	i^{th} Hookian spring modulus in Voigt-Kelvin model
$E(t)$	Stress relaxation or creep modulus
E_1	Real component of E^* , the storage modulus
E_2	Imaginary component of E^* , the loss modulus
exp	Exponential function, e^x
$f(x)$	dependent variable in regression analysis
f_0	Maximum sinusoidal force amplitude in dynamic mechanical testing
G	shear modulus

ΔH	Activation energy of Arrhenian rate equation (4.2.3-4)
$H(\tau)$	Relaxation time spectrum for stress relaxation
J	Compliance, the reciprocal of the modulus, E
$J(t)$	Creep compliance
J_0	Initial creep compliance at zero time, or the first parameter of the Voigt-Kelvin model (equation 2.1.2-12)
J^*	Complex dynamic compliance, the vector
$ J $	Magnitude of complex dynamic compliance
J_E	Equilibrium creep compliance
J_p	Master creep compliance of equation 4.2.3-2
J_r	Reduced creep compliance, the ratio of the creep compliance to the initial creep compliance
J_1	Real component of J^* , the storage compliance
J_2	Imaginary component of J^* , the loss compliance
$J_{22}(t)$	Transverse creep compliance of an anisotropic solid such as a continuous fiber composite
K	Length correction constant in equation 3.2-1
k	Constant in Nutting equation (2.1.3-1)
L	Gage length of creep or dynamic mechanical specimen
$L(\tau)$	Retardation time spectrum for creep
M	Percentage weight gained by test specimen after being immersed in a plasticizing solution (equation 3.4-1)
M_f	Percentage weight gained after some desorption has occurred
M_0	Percentage weight gained before desorption

ΔM	Percentage difference between M_f and M_0 with the percent calculation using M_0 as the basis
n	Exponent of power law model (equation 2.1.3-2), or the number of statistical observations for fitting regression models, or the strain correction offset (equation E-9)
p	Number of parameters in regression model
R	Universal gas constant
S	Cross-sectional area of test specimen
s	Standard estimate of error equal to the square root of the quantity, sum of the squares of the residual divided by the number of degrees of freedom (a residual is the difference between the dependent variable and the predicted value of the dependent variable as determined by the fitted regression model)
s^2	Square of the standard estimate of error, or the statistical variance
T	Temperature
T_g	Glass transition temperature
T_0	Reference temperature
T_{MO}	Morgan and O'Neal glass transition temperature
T_α	Glass transition temperature at the peak of the loss tangent curve (α -transition)
t, t'	Time variables
t_e	Aging time
V	Volume
\dot{W}	Rate of energy dissipation, equation 2.2-9
W	Weight of constant load in creep experiments
WLF	Williams-Landel-Ferry equation
x	Width of test specimen

x_i	Dummy variable denoting an independent measured variable
y	Thickness of test specimen

Greek Symbols

α	Linear thermal expansion coefficient
β	Exponent in Nutting equation (2.1.3-1), or angle of misalignment between the strain gage and the specimen axis
δ	The phase lag angle between the sinusoidal stress and strain in dynamic mechanical testing
ϵ	Mechanical strain
$\dot{\epsilon}$	Time rate of change of the strain ($d\epsilon/dt$)
ϵ_0	Initial deformation at zero time in a creep experiment
ϵ_p	Maximum strain in equation E-9
ϵ_q	Minimum strain in equation E-9
η	Viscosity
η_i	i^{th} dashpot viscosity
η_0	Long term pure viscous flow parameters in Voigt-Kelvin model (equation 2.1.2-12)
$\mu\epsilon$	Microstrain (1×10^{-6} in./in.)
ν	Poisson's ratio, or the number of degrees of freedom for a fitted regression model
π	Universal constant equal to 3.1459...
ρ	Density (kg/m^3)
σ	Mechanical stress, or standard deviation of a number of observations

σ_0	Constant stress for creep experiments
τ_i	Retardation time in spring and dashpot mechanical analogues (Voigt-Kelvin model is one example)
ϕ	Angle of misalignment between the specimen axis and the direction of gravity
ω	Frequency in radians

REFERENCES

- Alfrey, T. and Gurnee, E. F., Organic Polymers, Prentice-Hall, Englewood Cliffs, New Jersey, 1967.
- Augl, J. M., "The Effect of Moisture on Carbon Fiber Reinforced Composites -- II. Mechanical Property Changes," Technical Report NSWC/WOL/TR 76-149, Naval Surface Weapons Center, Silver Springs, Maryland, 1977.
- Augl, J. M., "Research on Composite Materials: Fourth Quarterly Report," Task No. A32000000/0123, Naval Air Systems Command, Silver Springs, Maryland, 1978.
- Augl, J. M., personal communication, March 1979.
- Bell, J. P., J. Polym. Sci., Part A-2, 8, 417 (1970).
- Bethea, R. M., Duran, B. S. and Boullion, T. L., Statistical Methods for Engineers and Scientists, Marcel Dekker, New York, 1975, 533.
- Beyer, W. H., Ed., CRC Handbook of Tables for Probability and Statistics, Chemical Rubber Company, Cleveland, 1966, 240.
- Billmeyer, F. W., Textbook of Polymer Science, Wiley and Sons, New York, 1962.
- Bird, R. B., Armstrong, R. C. and Hassager, O., Dynamics of Polymeric Liquids, Vol. 1: Fluid Mechanics, Wiley and Sons, New York, 1977, 280.
- Bomberger, T., B.Ch.E. thesis, Department of Chemical Eng'g, University of Delaware, Newark, Delaware, 1975.
- Browning, C. E., "Effects of Moisture on the Properties of High Performance Structural Resins and Composites," Composite Materials: Testing and Design (Third Conference), ASTM STP 546, American Society for Testing and Materials, 1974, 284.

- Browning, C. E., Husman, G. E. and Whitney, J. M., "Moisture Effects in Epoxy Matrix Composites," Composite Materials: Testing and Design (Fourth Conference), ASTM STP 617, American Society for Testing and Materials, 1977, 481-496.
- Browning, C. E., Polym. Eng. Sci., 18, 16 (1978).
- Bueche, F. J., Chem. Phys., 5, 271 (1956).
- Bueche, F. and Kelley, F. N., J. Polym. Sci., 45, 552 (1960).
- Beuche, F., Physical Properties of Polymers, Interscience, New York, 1962.
- Carpenter, J. F., "Test Program Evaluation of 3501-6 Resin," Contract No. N00019-77-C-0155-NASC, McDonnell Douglas Corporation, St. Louis, Missouri, 1978.
- Crowson, R. J. and Arridge, R. G. C., Polymer, 20 (6), 737 (1979).
- Cutthrell, R. E., J. Appl. Polym. Sci., 11, 949 (1967).
- DeIasi, R. and Whiteside, J. B., "Effect of Moisture on Epoxy Resins and Composites," Advanced Composite Materials Environmental Effects (J. R. Vinson, Ed.), ASTM STP 658, American Society for Testing and Materials, 1978, 2-20.
- DiBenedetto, A. J. and Gauchel, J. V., Proc. SPE 32nd Annual Technical Conference, Vol. 20, San Francisco, California, May 13-16, 1974, Society of Plastics Eng'rs, 487-491.
- Dick, W. A., personal communication, October 1979.
- Erath, E. H. and Robinson, M., J. Polym Sci., Part C, 3, 65 (1963).
- Ferry, J. D., Viscoelastic Properties of Polymers, Wiley and Sons, New York, 1961.
- Flügge, W., Viscoelasticity, Blaisdell, Waltham, Massachusetts, 1967.

- Guenther, C., B.Ch.E. thesis, Department of Chemical Eng'g, University of Delaware, Newark, Delaware, 1978.
- Hancox, N. L. and Minty, D. C. C., J. Mater. Sci., 13 (4), 797 (1978).
- Heinrich R., personal communication, June 1979.
- Ishai, O., J. Appl. Poly. Sci., 11, 1963 (1967).
- International Critical Tables, Vol. III, National Research Council, McGraw-Hill, New York, 1928, 383.
- Joshi, D. J., M.Ch.E. thesis, Department of Chemical Eng'g, University of Delaware, Newark, Delaware, 1975.
- Joshi, S., Ph.D. thesis, Department of Chemical Eng'g, University of Delaware, Newark, Delaware, 1980.
- Kaeble, D. H., SPE J., 15, 1071 (1959).
- Kaeble, D. H., J. Appl. Poly. Sci., 9, 1213 (1965).
- Keenan, J. D., Seferis, J. C., and Quinlivan, J. T., "Effects of Moisture and Stoichiometry on the Dynamic Mechanical Properties of Carbon Reinforced Epoxy Composites," Am. Chem. Soc.: Div. Org. Coat., Plast., Chem. Preprints, 40, (1979), 700-706.
- Kenyon, A. S. and Nielsen, L. E., J. Macromol. Sci.-Chem.: A, 3 (2), 275 (1969).
- Kibler, K. G. and Carter, H. G., "Viscoelastic Parameters of Epoxy Resin from Thermomechanical and Electrical Conductivity Measurements," Composite Materials: Testing and Design (Fifth Conference) (S. W. Tsai, Ed.), ASTM STP 674, American Society for Testing and Materials, 1979, 282-288.
- Kibler, K. G., Schapery, R. A., and Weitsman, Y., "Time-Dependent Environmental Behavior of Graphite Epoxy Composites: Quarterly Progress Report No. 9," Contract No. F33615-77-C-5109-AFML, General Dynamics, Fort Worth, Texas, 1979.

- Kim, S. L., Manson, J. A., and Misra, S. C., Am. Chem. Soc.: Div. Org. Coat., Plast., Chem. Preprints, 39, 158 (1978).
- Kitoh, M., and Suzuki, K., Kobunshi Ronbunshu, 33, 19 (1976).
- Koeneman, J. B. and Kicher, J. P., Creep Behavior of Elastic Fiber/Epoxy Matrix Composite Materials, ASTM STP 497, American Society for Testing and Materials, 1972, 503-515.
- Korn, G. A. and Korn, T. M., Mathematical Handbook for Scientists and Engineers, McGraw-Hill, New York, 1961, F-14.
- Liechti, K. M., Kenner, V. H. and Knauss, W. G., "Time-Dependent Fracture Processes Relating to Service Life Predicting of Adhesive Joints and Advanced Composites: Progress Report No.4," GALCIT SM 79-10, California Institute of Technology, Pasadena, California, 1979.
- May, C. A. and Weir, F. E., SPE Tech. Papers, 8, 2-2 (1962).
- McCullough, R. L., "Introduction to Statistical Analysis," Center for Composite Materials, University of Delaware, Newark, Delaware, 1979.
- Meares, P., Polymers: Structure and Bulk Properties, Van Nostrand Reinhold, New York, 1965.
- Micro-Measurements Tech Note TN-127, "Optimizing Strain Gage Excitation Levels," Micro-Measurements, Raleigh, North Carolina, 1968.
- Micro-Measurements Instruction Bulletin B-130, "Strain Gage Applications with M-Bond 600 and 610 Adhesives," Micro-Measurements, Raleigh, North Carolina, 1970.
- Micro-Measurements Tech Note TN-138, "Errors Due to Misalignment of Strain Gages," Micro-Measurements, Raleigh, North Carolina, 1977.
- Molenpah, A. E., Ishai, O., DiBenedetto, A. T., J. Appl. Polym. Sci., 13, 1231 (1969).

- Morgan, R. E. and O'Neal, J. E., Polym.-Plast. Technol. Eng., 10 (1), 49-116 (1978).
- Murayama, T. and Bell, J. P., J. Polym. Sci., Part A-2, 8, 437 (1970).
- Nielsen, L. E., Mechanical Properties of Polymers, Reinhold, New York, 1962.
- Nielsen, L. E., J. Macromol. Sci.-Revs. Macromol. Chem., C3 (1), 69-103 (1969).
- Nielsen, L. E., Mechanical Properties of Polymers and Composites, Vol. I, Marcel Dekker, New York, 1974, 1-235.
- Nutting, P. G., J. Frank. Inst. 191, 679 (1921).
- Schapery, R. A., Pol. Eng. Sci., 9 (7), 295 (1969).
- Schultz, J. M., Polymer Materials Science, Prentice-Hall, Englewood Cliffs, New Jersey, 1974, 293-379.
- Seferis, J. C., Ph.D. thesis, Department of Chemical Eng'g, University of Delaware, Newark, Delaware, 1977.
- Seferis, J. C., personal communication, June 1969.
- Salomon, D. H., Loft, B. C. and Swift, J. D., J. Appl. Polym. Sci., 11, 1593 (1967).
- Springer, G. S., "Environmental Effects on Epoxy Matrix Composites," Composite Materials: Testing and Design (Fifth Conference) (S. W. Tsai, Ed.), ASTM STP 674, American Society for Testing and Materials, 1979, 291-312.
- Struik, L. C. E., Physical Aging in Amorphous Polymers and Other Materials, Elsevier Scientific, Amsterdam, 1978.
- Takemori, M. T. and Yee, A. F., J. Appl. Polym. Sci., 21, 2597 (1977).
- Tobolsky, A. V., Properties and Structure of Polymers, Wiley and Sons, New York, 1960.

Toyo Measuring Instruments, "Rheovibron Direct Reading
Dynamic Viscoelastometer Instruction Manual,"
Tokyo, 1969.

Wohnseidler, H. P., J. Polym. Sci., Part C, 3, 77 (1963).

Yeow, Y. T., Morris, D. W., and Brinson, H. F., "Time-
Temperature Behavior of a Unidirectional Graphite/
Epoxy Composite," Composite Materials: Testing and
Design (Fifth Conference) (S. W. Tsai, Ed.), ASTM
STP 674, American Society for Testing and Materials,
1979, 263-281.

APPENDIX A

SUMMARY OF DATA

A.1 CREEP DATA

A.2 DYNAMIC MECHANICAL DATA

A.3 TENSILE DATA

A.1 CREEP DATA

The creep data for each of the eleven tests on the virgin and plasticized resin specimens is compiled in table A-2. Each specimen number is referenced by a run number. The list of run numbers is given in table A-1. In table A-2, the time in seconds is listed with the corresponding value of the strain. The strain is in units of microstrain ($1\mu\epsilon = 1 \times 10^{-6}$ in/in). The description of each test (e.g. initial stress level, test temperature, etc.) is given in table 3.2-1 of section 3.2.

TABLE A-1

RUN NUMBERS OF THE CREEP EXPERIMENTS

<u>Run number</u>	<u>Specimen number</u>
1	4-6-79-02
2	6-29-79-03
3	7-5-79-01
4	6-29-79-01
5	7-10-79-04
6	12-11-79-06
7	12-11-79-01
8	12-11-79-05
9	7-5-79-02
10	6-29-79-02
11	11-3-79-01

TABLE A-2
EXPERIMENTAL CREEP DATA

RUN 1		RUN 2	
TIME (SEC)	MICRO- STRAIN	TIME (SEC)	MICRO- STRAIN
.6000E+02	.1860E+04	.1200E+03	.9210E+03
.1200E+03	.1864E+04	.1800E+03	.9250E+03
.1800E+03	.1870E+04	.2400E+03	.9310E+03
.2400E+03	.1875E+04	.3000E+03	.9410E+03
.3000E+03	.1879E+04	.3600E+03	.9480E+03
.6000E+03	.1893E+04	.4200E+03	.9540E+03
.9000E+03	.1903E+04	.4800E+03	.9670E+03
.1260E+04	.1913E+04	.5400E+03	.9750E+03
.1500E+04	.1919E+04	.6000E+03	.9800E+03
.1800E+04	.1925E+04	.1000E+04	.1010E+04
.2400E+04	.1935E+04	.1500E+04	.1019E+04
.3000E+04	.1945E+04	.2100E+04	.1042E+04
.3600E+04	.1952E+04	.3600E+04	.1103E+04
.4800E+04	.1966E+04	.5400E+04	.1123E+04
.6000E+04	.1978E+04	.8100E+04	.1127E+04
.7260E+04	.1987E+04	.1230E+05	.1131E+04
.9000E+04	.1998E+04	.1980E+05	.1192E+04
.9940E+04	.2002E+04	.5040E+05	.1266E+04
.1152E+05	.2010E+04	.1370E+06	.1281E+04
.1326E+05	.2016E+04	.1900E+06	.1286E+04
.1866E+05	.2031E+04	.2251E+06	.1313E+04
.2304E+05	.2039E+04	.2640E+06	.1317E+04

TABLE A-2 (cont.)

RUN 3		RUN 4	
TIME (SEC)	MICRO- STRAIN	TIME (SEC)	MICRO- STRAIN
.6000E+02	.1844E+04	.1200E+03	.1493E+04
.1200E+03	.1854E+04	.1800E+03	.1500E+04
.1800E+03	.1859E+04	.2400E+03	.1503E+04
.2400E+03	.1862E+04	.3000E+03	.1507E+04
.3000E+03	.1865E+04	.6000E+03	.1532E+04
.6000E+03	.1880E+04	.9000E+03	.1547E+04
.9000E+03	.1889E+04	.1200E+04	.1558E+04
.1200E+04	.1896E+04	.1500E+04	.1569E+04
.1500E+04	.1902E+04	.1800E+04	.1576E+04
.1800E+04	.1907E+04	.2400E+04	.1594E+04
.2400E+04	.1916E+04	.3000E+04	.1605E+04
.3000E+04	.1922E+04	.3600E+04	.1614E+04
.4560E+04	.1936E+04	.4200E+04	.1625E+04
.5460E+04	.1943E+04	.5400E+04	.1638E+04
.6600E+04	.1951E+04	.6600E+04	.1646E+04
.8400E+04	.1960E+04	.7800E+04	.1653E+04
.9600E+04	.1966E+04	.1260E+05	.1673E+04
.1470E+05	.1988E+04	.2220E+05	.1693E+04
.1920E+05	.2000E+04	.2880E+05	.1723E+04
.2250E+05	.2011E+04	.3660E+05	.1736E+04
.5820E+05	.2102E+04	.4800E+05	.1742E+04
.6880E+05	.2132E+04	.8160E+05	.1780E+04
.8580E+05	.2181E+04	.9510E+05	.1776E+04
.1030E+06	.2230E+04	.1205E+06	.1779E+04
.1458E+06	.2309E+04	.2000E+06	.1805E+04
.1866E+06	.2364E+04	.2120E+06	.1812E+04
.2424E+06	.2417E+04	.2867E+06	.1864E+04
.2724E+06	.2457E+04		

TABLE A-2 (cont.)

RUN 5		RUN 6	
TIME (SEC)	MICRO- STRAIN	TIME (SEC)	MICRO- STRAIN
.6000E+02	.1590E+04	.6000E+02	.1430E+04
.1200E+03	.1594E+04	.1200E+03	.1432E+04
.1800E+03	.1598E+04	.1800E+03	.1433E+04
.2400E+03	.1601E+04	.2400E+03	.1434E+04
.3000E+03	.1606E+04	.3000E+03	.1434E+04
.6000E+03	.1618E+04	.6000E+03	.1436E+04
.9000E+03	.1626E+04	.9000E+03	.1438E+04
.1200E+04	.1632E+04	.1200E+04	.1439E+04
.1500E+04	.1637E+04	.1800E+04	.1442E+04
.1800E+04	.1641E+04	.2400E+04	.1445E+04
.2400E+04	.1648E+04	.3000E+04	.1447E+04
.3140E+04	.1655E+04	.3600E+04	.1450E+04
.3600E+04	.1658E+04	.5400E+04	.1457E+04
.4500E+04	.1665E+04	.7200E+04	.1464E+04
.5400E+04	.1670E+04	.9480E+04	.1472E+04
.6300E+04	.1674E+04	.1110E+05	.1477E+04
.1160E+05	.1692E+04	.1320E+05	.1484E+04
.2060E+05	.1709E+04	.2406E+05	.1518E+04
.3170E+05	.1726E+04	.4320E+05	.1566E+04
.4670E+05	.1756E+04	.5220E+05	.1578E+04
.6976E+05	.1786E+04	.6000E+05	.1597E+04
.8100E+05	.1802E+04	.6720E+05	.1616E+04
.9150E+05	.1816E+04	.7500E+05	.1635E+04
.1030E+06	.1829E+04	.8490E+05	.1659E+04
.1206E+06	.1850E+04	.1359E+06	.1756E+04
.1512E+06	.1898E+04	.1671E+06	.1817E+04
.1692E+06	.1929E+04	.1854E+06	.1829E+04
.1840E+06	.1949E+04	.2283E+06	.1902E+04
.2076E+06	.1970E+04	.2676E+06	.1994E+04
.2415E+06	.1999E+04	.3186E+06	.2134E+04
.2760E+06	.2041E+04	.3460E+06	.2182E+04
.3240E+06	.2067E+04	.3996E+06	.2282E+04
.3546E+06	.2090E+04	.4341E+06	.2377E+04
.4490E+06	.2152E+04	.4968E+06	.2527E+04
.5130E+06	.2167E+04		
.5390E+06	.2173E+04		
.5892E+06	.2179E+04		

TABLE A-2 (cont.)

RUN 7			RUN 8			RUN 9			RUN 10			RUN 11		
TIME (SEC)	MICRO- STRAIN		TIME (SEC)	MICRO- STRAIN		TIME (SEC)	MICRO- STRAIN		TIME (SEC)	MICRO- STRAIN		TIME (SEC)	MICRO- STRAIN	
.9000E+02	.1556E+04		.6000E+02	.1734E+04		.6000E+02	.9270E+03		.6000E+02	.1402E+04		.1200E+03	.1097E+04	
.1800E+03	.1565E+04		.1200E+03	.1735E+04		.1200E+03	.9330E+03		.1800E+03	.1403E+04		.1800E+03	.1110E+04	
.2400E+03	.1569E+04		.1800E+03	.1736E+04		.1800E+03	.9330E+03		.3000E+03	.1410E+04		.2400E+03	.1120E+04	
.3000E+03	.1571E+04		.2400E+03	.1737E+04		.2400E+03	.9330E+03		.4200E+03	.1413E+04		.3000E+03	.1127E+04	
.4200E+03	.1577E+04		.3000E+03	.1741E+04		.3000E+03	.9410E+03		.5400E+03	.1415E+04		.6000E+03	.1151E+04	
.5400E+03	.1580E+04		.6000E+03	.1751E+04		.6000E+03	.9470E+03		.7000E+03	.1420E+04		.9000E+03	.1170E+04	
.9000E+03	.1580E+04		.9000E+03	.1757E+04		.9000E+03	.9550E+03		.1000E+04	.1423E+04		.1200E+04	.1170E+04	
.1260E+04	.1593E+04		.1200E+04	.1764E+04		.1200E+04	.9590E+03		.1300E+04	.1427E+04		.1800E+04	.1200E+04	
.1500E+04	.1596E+04		.1500E+04	.1769E+04		.1500E+04	.9630E+03		.1600E+04	.1431E+04		.2400E+04	.1210E+04	
.1800E+04	.1598E+04		.1800E+04	.1774E+04		.1800E+04	.9630E+03		.2000E+04	.1435E+04		.3000E+04	.1217E+04	
.2400E+04	.1602E+04		.2400E+04	.1774E+04		.2400E+04	.9630E+03		.2400E+04	.1438E+04		.4200E+04	.1229E+04	
.3000E+04	.1606E+04		.3000E+04	.1779E+04		.3000E+04	.9700E+03		.3600E+04	.1439E+04		.7200E+04	.1257E+04	
.3600E+04	.1610E+04		.3600E+04	.1800E+04		.3600E+04	.9720E+03		.4200E+04	.1439E+04		.7200E+04	.1301E+04	
.4200E+04	.1613E+04		.4200E+04	.1810E+04		.4200E+04	.9720E+03		.4800E+04	.1439E+04		.7300E+04	.1343E+04	
.5400E+04	.1617E+04		.5700E+04	.1823E+04		.6000E+04	.9740E+03		.5400E+04	.1439E+04		.9100E+04	.1355E+04	
.6300E+04	.1620E+04		.7200E+04	.1840E+04		.8000E+04	.9800E+03		.6300E+04	.1439E+04		.9300E+04	.1355E+04	
.7200E+04	.1625E+04		.1000E+05	.1874E+04		.1000E+05	.9840E+03		.7200E+04	.1477E+04		.1305E+05	.1367E+04	
.1050E+05	.1629E+04		.1440E+05	.1904E+04		.1440E+05	.9850E+03		.8400E+04	.1477E+04				
.2910E+05	.1657E+04		.2530E+05	.1900E+04		.2530E+05	.9700E+03							

A.2 DYNAMIC MECHANICAL DATA

Run numbers are also used to identify each of the twenty-one dynamic mechanical tests on the virgin and plasticized resin. The listing of the specimen number with its corresponding run number is contained in table A-3. The actual test data is contained in three different tables: A-4, A-5, and A-6. In each table, the temperature ($^{\circ}\text{C}$), $\tan \delta$, and complex dynamic modulus (giga-newtons per meter-squared) is listed for each run. Specific information on each test is given in table 3.3-1 in the body of the text.

The data collected from the ten experiments on the virgin resin is listed in table A-4. The tests of primary importance are run numbers 3, 6, and 7. A few of the shorter tests (runs 8-10) were used to provide a greater statistical sampling when computing the mean dynamic modulus for the virgin resin. In table A-5, the dynamic mechanical data of the resin plasticized in paint stripper MIL-81294 are presented. Consult table 3.3-1 for the corresponding absorption level (value of M) for a particular specimen. In table A-6, the dynamic mechanical data for the resin plasticized by all other solvents besides MIL-81294 are presented. The resin plasticized by water,

water-phenol (50/50), methylene chloride, and water-phenol-methylene chloride solutions are represented in this table.

TABLE A-3

RUN NUMBERS OF THE DYNAMIC MECHANICAL EXPERIMENTS

Run Number	Specimen number
1	RH-12
2	RH-13
3	RH-1-2-80-12
4	RH-20
5	RH-14
6	RH-23
7	RH-1-2-80-07
8	RH-22
9	RH-24
10	RH-21
11	RH-MIL-13
12	RH-MIL-11
13	RH-MIL-15
14	RH-MIL-14
15	RH-MIL-12
16	RH-MIL-10
17	RH-1-2-80-15
18	RH-1-2-80-14
19	RH-H-10
20	RH-HMPH-10
21	RH-M-10

TABLE A-4

DYNAMIC MECHANICAL DATA OF THE VIRGIN RESIN

RUN 1			RUN 2		
T (C)	TAN DELTA	/E/ (GPA)	T (C)	TAN DELTA	/E/ (GPA)
26.0	.0130	.350E+01	26.0	.0085	.384E+01
31.5	.0125	.356E+01	29.0	.0090	.384E+01
35.0	.0130	.340E+01	32.0	.0080	.384E+01
39.5	.0120	.335E+01	34.5	.0070	.372E+01
41.5	.0120	.332E+01	39.5	.0060	.372E+01
44.0	.0135	.318E+01	44.5	.0070	.361E+01
50.5	.0140	.312E+01	54.0	.0080	.340E+01
53.5	.0145	.299E+01	67.0	.0095	.314E+01
66.0	.0130	.299E+01	76.0	.0095	.306E+01
69.5	.0120	.296E+01	85.0	.0100	.298E+01
75.5	.0140	.294E+01	92.0	.0100	.298E+01
89.5	.0105	.292E+01	113.5	.0080	.284E+01
94.0	.0100	.282E+01	118.0	.0060	.284E+01
112.5	.0080	.278E+01	127.0	.0050	.278E+01
115.0	.0070	.272E+01	132.5	.0090	.266E+01
126.5	.0070	.272E+01	143.5	.0070	.266E+01
140.5	.0075	.263E+01	148.0	.0090	.260E+01
143.5	.0080	.262E+01	156.0	.0105	.244E+01
154.0	.0090	.250E+01	166.0	.0135	.228E+01
182.0	.0170	.221E+01	178.0	.0220	.196E+01
185.5	.0200	.215E+01	185.5	.0355	.190E+01
192.5	.0270	.200E+01	193.0	.0600	.158E+01
198.5	.0355	.186E+01	196.5	.0740	.146E+01
202.0	.0475	.171E+01	202.5	.1140	.927E+00
205.5	.0630	.155E+01	206.0	.1510	.864E+00
215.5	.1700	.950E+00	210.0	.1880	.688E+00
218.0	.2130	.824E+00	217.5	.3060	.446E+00
220.0	.2470	.737E+00	222.5	.3900	.356E+00
222.0	.2870	.651E+00			

TABLE A-4 (cont.)

RUN 3			RUN 4		
T (C)	TAN DELTA	/E/ (GPA)	T (C)	TAN DELTA	/E/ (GPA)
22.0	.0290	.435E+01	25.5	.0110	.396E+01
25.6	.0285	.427E+01	29.0	.0105	.390E+01
30.5	.0275	.427E+01	32.0	.0105	.382E+01
36.6	.0265	.398E+01	39.0	.0110	.368E+01
42.0	.0260	.398E+01	44.0	.0110	.354E+01
53.2	.0220	.411E+01	54.0	.0135	.328E+01
61.5	.0210	.385E+01	62.5	.0140	.309E+01
66.3	.0210	.385E+01	68.0	.0155	.298E+01
70.6	.0180	.391E+01	91.5	.0110	.298E+01
76.5	.0170	.386E+01	97.0	.0095	.302E+01
89.5	.0150	.386E+01	106.0	.0075	.308E+01
95.2	.0160	.379E+01	113.0	.0070	.307E+01
104.0	.0130	.380E+01	120.0	.0065	.307E+01
110.0	.0130	.374E+01	128.5	.0060	.301E+01
118.8	.0120	.368E+01	139.0	.0070	.295E+01
124.4	.0120	.363E+01	145.5	.0080	.282E+01
136.6	.0120	.343E+01	154.5	.0090	.276E+01
145.0	.0125	.332E+01	162.0	.0095	.267E+01
155.6	.0140	.324E+01	170.5	.0115	.264E+01
166.0	.0150	.299E+01	177.5	.0140	.250E+01
175.2	.0180	.285E+01	183.5	.0170	.240E+01
183.0	.0220	.272E+01	187.5	.0195	.232E+01
192.5	.0310	.244E+01	193.0	.0240	.221E+01
194.2	.0335	.239E+01	197.5	.0295	.209E+01
201.7	.0475	.204E+01	201.5	.0385	.194E+01
208.0	.0950	.153E+01	207.0	.0550	.170E+01
212.0	.1540	.989E+00	211.5	.0905	.145E+01
218.6	.2240	.689E+00	216.5	.1480	.109E+01
227.0	.4000	.416E+00	219.0	.1880	.903E+00
234.5	.6000	.194E+00	222.0	.2480	.732E+00
239.5	.6200	.135E+00	227.0	.3400	.540E+00
246.7	.5100	.930E-01			
250.0	.4550	.890E-01			
254.0	.3650	.860E-01			
258.0	.2800	.830E-01			

TABLE A-4 (cont.)

RUN 5				RUN 6				RUN 7			
T (C)	TAN DELTA	/E/ (GPA)	T (C)	TAN DELTA	/E/ (GPA)	T (C)	TAN DELTA	/E/ (GPA)	T (C)	TAN DELTA	/E/ (GPA)
146.0	.0090	.261E+01	177.5	.0180	.242E+01	130.9	.0130	.326E+01			
150.0	.0105	.258E+01	184.4	.0220	.223E+01	132.6	.0280	.314E+01			
156.5	.0120	.257E+01	189.0	.0305	.212E+01	140.6	.0220	.318E+01			
162.5	.0145	.245E+01	195.0	.0480	.186E+01	149.0	.0310	.303E+01			
166.0	.0145	.236E+01	201.5	.0895	.143E+01	151.5	.0275	.303E+01			
169.0	.0155	.234E+01	205.0	.1220	.103E+01	161.8	.0330	.296E+01			
172.0	.0175	.229E+01	210.5	.1850	.671E+00	172.2	.0170	.293E+01			
175.5	.0195	.225E+01	217.0	.3080	.530E+00	178.8	.0260	.304E+01			
179.5	.0225	.218E+01	221.0	.4000	.394E+00	182.8	.0210	.277E+01			
183.5	.0275	.208E+01	226.0	.5300	.290E+00	192.6	.0370	.277E+01			
189.0	.0360	.193E+01	231.0	.6050	.204E+00	202.0	.0310	.258E+01			
193.5	.0495	.178E+01	236.0	.5950	.159E+00	204.5	.0395	.228E+01			
198.5	.0670	.158E+01	239.0	.5400	.145E+00	209.5	.0660	.196E+01			
202.0	.0890	.138E+01	244.5	.4200	.136E+00	215.3	.1350	.103E+01			
204.0	.1020	.127E+01	249.0	.3400	.129E+00	218.0	.1600	.789E+00			
208.0	.1220	.108E+01	253.0	.2620	.128E+00						
215.0	.1860	.745E+00	257.5	.1850	.130E+00						
221.5	.2900	.544E+00	260.0	.1610	.132E+00						
229.0	.4650	.360E+00									
235.5	.5750	.238E+00									
244.5	.5600	.265E+00									
250.0	.5000	.156E+00									

TABLE A-5

DYNAMIC MECHANICAL DATA OF THE MIL-81294 PLASTICIZED RESIN

RUN 11				RUN 12				RUN 13			
T (C)	TAN DELTA	/E/ (GPA)	T (C)	TAN DELTA	/E/ (GPA)	T (C)	TAN DELTA	/E/ (GPA)	T (C)	TAN DELTA	/E/ (GPA)
26.0	.0200	.308E+01	26.3	.0195	.351E+01	24.6	.0160	.359E+01			
30.0	.0200	.305E+01	33.5	.0190	.343E+01	29.5	.0160	.352E+01			
41.0	.0205	.279E+01	38.0	.0205	.329E+01	35.0	.0170	.334E+01			
42.5	.0210	.278E+01	43.5	.0240	.305E+01	45.5	.0180	.319E+01			
44.0	.0210	.277E+01	48.0	.0260	.289E+01	51.5	.0200	.294E+01			
46.5	.0190	.270E+01	53.0	.0275	.280E+01	56.5	.0200	.291E+01			
55.5	.0190	.260E+01	59.5	.0280	.275E+01	63.5	.0190	.280E+01			
61.5	.0175	.258E+01	63.0	.0275	.277E+01	67.5	.0190	.280E+01			
71.5	.0165	.256E+01	66.0	.0270	.279E+01	73.5	.0185	.278E+01			
77.5	.0155	.263E+01	73.5	.0280	.275E+01	80.5	.0190	.275E+01			
86.5	.0140	.261E+01	79.5	.0180	.261E+01	88.5	.0190	.270E+01			
100.0	.0135	.257E+01	83.0	.0280	.259E+01	95.0	.0155	.276E+01			
103.5	.0130	.254E+01	88.0	.0300	.253E+01	102.0	.0150	.277E+01			
108.5	.0125	.249E+01	93.0	.0320	.250E+01	112.0	.0160	.270E+01			
116.5	.0145	.242E+01	106.0	.0370	.230E+01	118.0	.0190	.255E+01			
124.5	.0150	.237E+01	110.0	.0385	.223E+01	124.0	.0235	.240E+01			
130.5	.0160	.230E+01	115.5	.0420	.212E+01	128.0	.0235	.239E+01			
136.5	.0160	.227E+01	120.0	.0450	.202E+01	140.0	.0245	.231E+01			
142.5	.0170	.223E+01	127.0	.0490	.100E+01	144.5	.0275	.220E+01			
146.5	.0175	.220E+01	130.0	.0480	.180E+01	150.0	.0305	.204E+01			
153.5	.0210	.209E+01	135.0	.0550	.173E+01	157.5	.0350	.196E+01			
158.5	.0220	.209E+01	138.0	.0555	.167E+01	162.0	.0370	.189E+01			
163.5	.0255	.203E+01	144.5	.0580	.156E+01	167.0	.0400	.185E+01			
168.0	.0245	.199E+01									
173.5	.0280	.193E+01									
178.0	.0320	.185E+01									

TABLE A-5 (cont.)

RUN 14				RUN 15				RUN 16			
T (C)	TAN DELTA	/E/ (GPA)	T (C)	TAN DELTA	/E/ (GPA)	T (C)	TAN DELTA	/E/ (GPA)	T (C)	TAN DELTA	/E/ (GPA)
26.0	.0240	.282E+01	26.0	.0090	.446E+01	25.5	.0170	.344E+01	25.5	.0170	.344E+01
33.0	.0250	.266E+01	34.0	.0085	.428E+01	34.0	.0165	.333E+01	34.0	.0165	.333E+01
40.0	.0280	.252E+01	43.0	.0090	.412E+01	37.5	.0165	.312E+01	37.5	.0165	.312E+01
44.5	.0295	.244E+01	57.5	.0140	.361E+01	41.0	.0180	.294E+01	41.0	.0180	.294E+01
49.5	.0320	.242E+01	62.5	.0120	.349E+01	46.0	.0205	.267E+01	46.0	.0205	.267E+01
55.5	.0310	.237E+01	69.0	.0120	.340E+01	49.5	.0215	.260E+01	49.5	.0215	.260E+01
62.5	.0305	.235E+01	72.0	.0120	.340E+01	57.5	.0220	.254E+01	57.5	.0220	.254E+01
71.5	.0330	.228E+01	77.0	.0115	.337E+01	64.5	.0240	.245E+01	64.5	.0240	.245E+01
74.0	.0320	.224E+01	82.0	.0120	.328E+01	71.0	.0240	.245E+01	71.0	.0240	.245E+01
79.5	.0325	.224E+01	90.5	.0110	.328E+01	76.5	.0210	.245E+01	76.5	.0210	.245E+01
87.0	.0335	.211E+01	97.0	.0100	.325E+01	83.5	.0150	.255E+01	83.5	.0150	.255E+01
92.0	.0355	.209E+01	103.0	.0100	.312E+01	86.5	.0220	.247E+01	86.5	.0220	.247E+01
97.0	.0380	.202E+01	109.0	.0100	.322E+01	91.5	.0165	.252E+01	91.5	.0165	.252E+01
105.0	.0435	.188E+01	115.0	.0100	.328E+01	97.5	.0245	.237E+01	97.5	.0245	.237E+01
110.5	.0460	.188E+01	122.5	.0100	.319E+01	99.5	.0260	.235E+01	99.5	.0260	.235E+01
112.5	.0460	.187E+01	128.5	.0100	.299E+01	101.5	.0255	.230E+01	101.5	.0255	.230E+01
121.0	.0520	.170E+01	138.0	.0110	.300E+01	105.0	.0285	.225E+01	105.0	.0285	.225E+01
133.5	.0615	.150E+01	141.0	.0110	.294E+01	108.5	.0235	.223E+01	108.5	.0235	.223E+01
141.5	.0665	.140E+01	147.0	.0120	.288E+01	110.5	.0240	.220E+01	110.5	.0240	.220E+01
147.5	.0720	.133E+01	154.5	.0140	.266E+01	115.0	.0300	.208E+01	115.0	.0300	.208E+01
155.0	.0770	.121E+01	166.0	.0175	.261E+01	120.5	.0355	.194E+01	120.5	.0355	.194E+01
161.0	.0830	.110E+01	174.5	.0185	.251E+01	125.0	.0335	.185E+01	125.0	.0335	.185E+01
164.5	.0880	.104E+01	189.5	.0280	.225E+01	129.5	.0410	.168E+01	129.5	.0410	.168E+01
168.5	.0940	.982E+00	193.5	.0310	.222E+01	136.5	.0440	.159E+01	136.5	.0440	.159E+01

TABLE A-6

DYNAMIC MECHANICAL DATA OF ALL OTHER PLASTICIZED RESINS

RUN 17			RUN 18		
T (C)	TAN DELTA	/E/ (GPA)	T (C)	TAN DELTA	/E/ (GPA)
27.2	.0197	.451E+01	40.5	.0405	.399E+01
37.0	.0185	.444E+01	43.0	.0375	.383E+01
43.4	.0175	.445E+01	49.5	.0380	.383E+01
49.0	.0175	.458E+01	55.8	.0365	.369E+01
62.0	.0180	.420E+01	67.0	.0385	.349E+01
67.4	.0185	.409E+01	80.0	.0475	.336E+01
76.0	.0175	.433E+01	86.4	.0490	.319E+01
77.8	.0180	.433E+01	96.8	.0525	.300E+01
80.3	.0195	.421E+01	104.2	.0530	.286E+01
87.0	.0195	.399E+01	109.0	.0510	.274E+01
96.0	.0230	.362E+01	119.0	.0585	.263E+01
102.8	.0260	.330E+01	126.4	.0885	.231E+01
111.0	.0290	.298E+01	131.5	.0970	.188E+01
119.6	.0310	.276E+01	137.0	.0970	.186E+01
129.0	.0325	.263E+01	142.2	.1040	.181E+01
135.2	.0330	.246E+01	148.0	.0950	.178E+01
141.7	.0320	.246E+01	160.6	.0735	.146E+01
152.0	.0345	.231E+01	170.0	.0680	.137E+01
157.3	.0355	.225E+01	177.0	.0680	.140E+01
164.7	.0400	.210E+01	184.0	.0630	.130E+01
174.3	.0445	.189E+01	193.0	.0700	.121E+01
179.0	.0540	.153E+01	197.5	.0710	.120E+01
186.7	.0715	.139E+01	209.5	.1050	.912E+00
190.5	.0750	.138E+01	213.5	.1320	.784E+00
197.5	.0765	.126E+01	220.2	.1900	.406E+00
206.5	.1170	.906E+00	226.0	.2900	.243E+00
211.2	.1780	.614E+00	232.0	.4100	.204E+00
220.2	.2750	.307E+00	241.8	.5200	.129E+00
230.0	.4700	.162E+00	250.0	.4700	.824E-01
235.5	.5000	.108E+00	253.5	.4050	.718E-01
238.2	.4550	.900E-01			
252.5	.2580	.720E-01			

TABLE A-6 (cont.)

RUN 19				RUN 20				RUN 21			
T (C)	TAN DELTA	/E/ (GPA)	T (C)	TAN DELTA	/E/ (GPA)	T (C)	TAN DELTA	T (C)	TAN DELTA	/E/ (GPA)	
25.0	.0160	.333E+01	26.5	.0205	.316E+01	25.5	.0160	25.5	.0160	.359E+01	
29.0	.0150	.335E+01	33.5	.0210	.303E+01	34.5	.0150	34.5	.0150	.339E+01	
35.0	.0150	.324E+01	40.5	.0245	.274E+01	40.5	.0160	40.5	.0160	.333E+01	
44.0	.0155	.317E+01	52.0	.0275	.260E+01	44.5	.0155	44.5	.0155	.336E+01	
50.5	.0155	.313E+01	59.0	.0270	.260E+01	51.0	.0155	51.0	.0155	.326E+01	
55.0	.0155	.307E+01	62.5	.0270	.267E+01	59.0	.0155	59.0	.0155	.319E+01	
59.5	.0160	.304E+01	64.0	.0260	.266E+01	64.5	.0150	64.5	.0150	.312E+01	
72.5	.0160	.294E+01	70.5	.0260	.256E+01	72.0	.0150	72.0	.0150	.300E+01	
77.5	.0150	.294E+01	77.0	.0260	.259E+01	78.0	.0150	78.0	.0150	.291E+01	
81.5	.0150	.288E+01	86.0	.0260	.258E+01	84.0	.0140	84.0	.0140	.284E+01	
86.5	.0140	.296E+01	95.5	.0280	.244E+01	88.5	.0150	88.5	.0150	.282E+01	
95.0	.0135	.293E+01	100.0	.0300	.237E+01	95.5	.0145	95.5	.0145	.273E+01	
101.5	.0128	.293E+01	106.5	.0315	.231E+01	112.0	.0140	112.0	.0140	.264E+01	
106.5	.0130	.292E+01	112.0	.0340	.221E+01	120.5	.0130	120.5	.0130	.255E+01	
113.0	.0135	.287E+01	117.0	.0385	.217E+01	124.0	.0140	124.0	.0140	.251E+01	
117.0	.0135	.285E+01	124.5	.0410	.199E+01	128.0	.0140	128.0	.0140	.251E+01	
121.0	.0125	.285E+01	131.0	.0490	.185E+01	133.5	.0145	133.5	.0145	.249E+01	
125.5	.0125	.283E+01	140.5	.0555	.169E+01	138.0	.0145	138.0	.0145	.244E+01	
135.5	.0130	.275E+01	145.5	.0585	.159E+01	145.5	.0150	145.5	.0150	.238E+01	
141.5	.0135	.270E+01	150.5	.0620	.150E+01	151.0	.0155	151.0	.0155	.233E+01	

A.3 RESULTS OF THE TENSILE TEST ON THE 3501-6 RESIN

A premade tensile test coupon of the 3501-6 resin was provided for this investigation by Robert Blake, Center for Composite Materials at the University of Delaware. The tensile specimen was prepared from a standard formulation of the 3501-6 resin (25% by weight DDS, the same as in the resin supplied from Hercules, Inc.). The resin in the "Blake" sample had been cured for four hours at 177°C, then postcured at 214°C. The dimensions measured 9.0×1.0×0.215 in inches. The sample was highly polished by sand blasting and it had been thermally treated to remove as many of the residual stresses as possible (a photograph of the specimen through crossed polarized lenses revealed that some minor stresses remained). The sample was stored at room temperature and room humidity until testing. In comparison with the creep and dynamic mechanical test specimens, the Blake sample was post-cured at a higher temperature and thermal residual stresses had been minimized.

The specimen was pulled in tension on an Instron test machine. The strain was measured by M-M strain gages mounted directly onto the sample. A calibrated Vishay P350-A strain recording device measured the strain

(in microstrain) directly. The tensile test was run at the following conditions:

1. Temperature = 22°C
2. Relative humidity = 55 ± 5%
3. Strain rate = 0.05 cm/min

The stress-strain plot is shown in figure A.3-1. The test was terminated at a stress of 250 kg-force (0.016 GN/m²) after the linear elastic limit of the resin (1000µε) had been surpassed. Past the linear elastic limit, a nonlinear decrease in the slope of the resin is observed as shown in figure A.3-1.

The first twelve data points inside the linear elastic limit of the resin (1000µε) were fitted to a least squares straight line. The slope of the straight line was taken as the Young's modulus of the 3501-6 resin ($E = 4.48 \text{ GN/m}^2$ or $6.50 \times 10^5 \text{ psi}$). Using the conventional statistical equations (McCullough, 1979), the variance, s^2 , in the Young's modulus for a linear fit to the data was calculated. Its value was less than one percent of the Young's modulus (5,000 psi or 0.035 GN/m^2). The straight line fits the data quite well because the experimental error is greater than the variance. The calculated

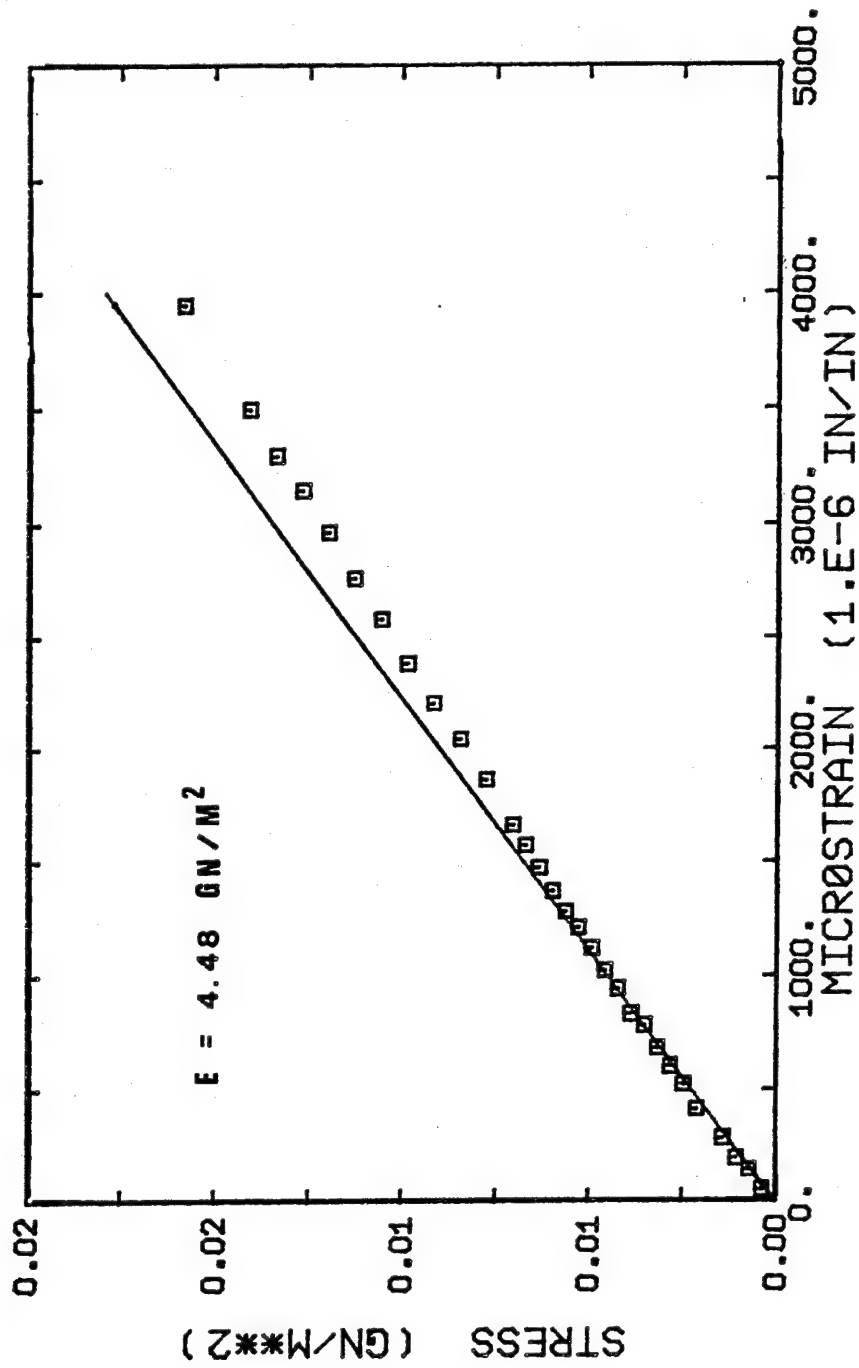


Figure A.3-1 Stress-strain data for the tensile test on the Blake sample of the 3501-6 resin

experimental error (see appendix E) was 3.2×10^4 psi (0.221 GN/m^2) or 5% about the value of the Young's modulus. The experimental error was used as the error limits of the Young's modulus reported in table 3.1-1, $E = 4.48 \pm 0.22 \text{ GN/m}^2$.

The equations used to calculate the experimental error of the Young's modulus appear below.

$$E = \sigma / \epsilon \quad (\text{A.3-1a})$$

$$\Delta E = \left| \frac{\partial E}{\partial \sigma} \right| \Delta \sigma + \left| \frac{\partial E}{\partial \epsilon} \right| \Delta \epsilon \quad (\text{A.3-1b})$$

$$\Delta E = \frac{\Delta \sigma}{\epsilon} + \frac{\sigma}{\epsilon^2} \Delta \epsilon \quad (\text{A.3-1c})$$

The fixed experimental errors in the stress and the strain are:

$$\Delta \sigma = 5.1 \text{ psi } (3.52 \times 10^{-5} \text{ GN/m}^2) \quad (\text{A.3-2a})$$

$$\Delta \epsilon = 1 \mu \epsilon (1 \times 10^{-6} \text{ in/in}) \quad (\text{A.3-2b})$$

APPENDIX B

DIAGRAMS OF EXPERIMENTAL APPARATUS

In figures B-1 and B-2 the top, front, and right end views of the creep grips designed by the author are presented. These grips were designed and built especially for this investigation. The grips can be used to test thin films of any resin up to 0.0625 inches thick. To load the specimen into the grips, it is first inserted between the bottom and top plates. After aligning the specimen in the grips, the grips are tightened in two stages. First, the four outside screws are tightened (see top view) which provide only slight pressure to the specimen. The final tightening is provided by the four inside screws (see right end view). These four screws apply pressure to a shimstock pressure plate. A tremendous torque can be applied to the second stage of tightening; therefore, caution has to be exercised with epoxy resins because they will shatter if tightened too much.

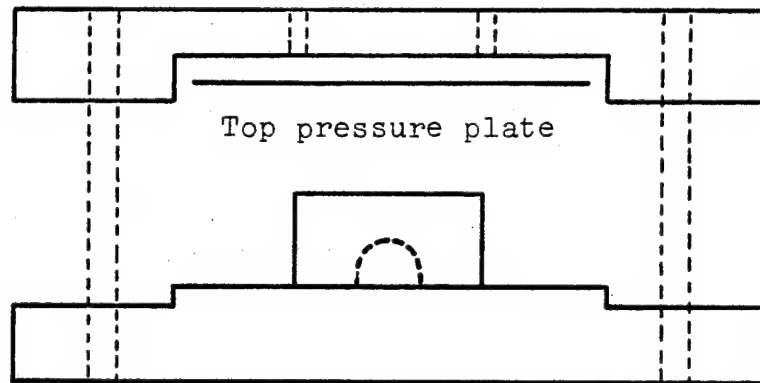
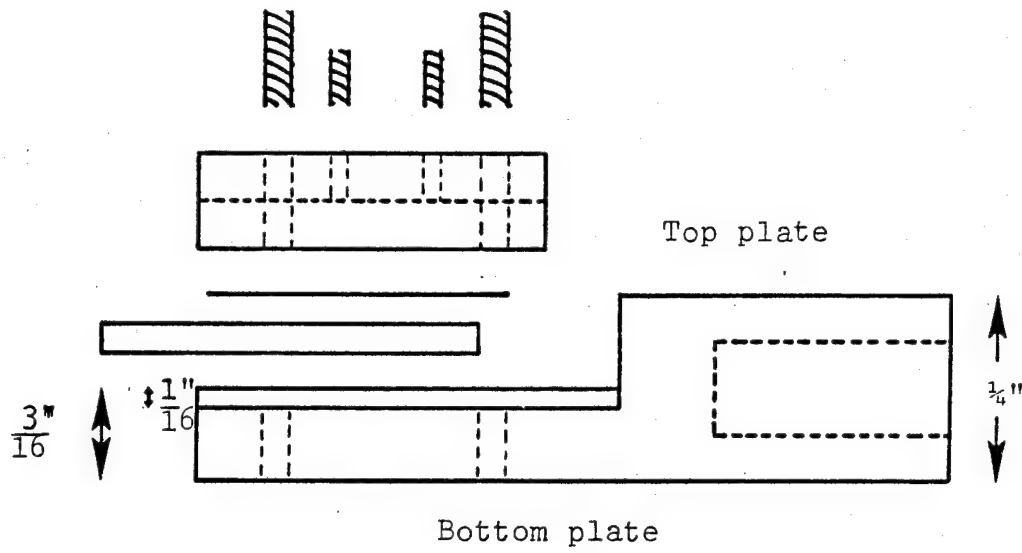


Figure B-1 Right end and front view of the creep grips

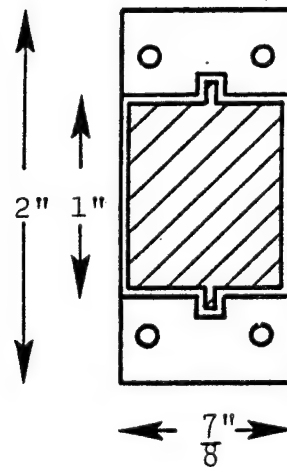
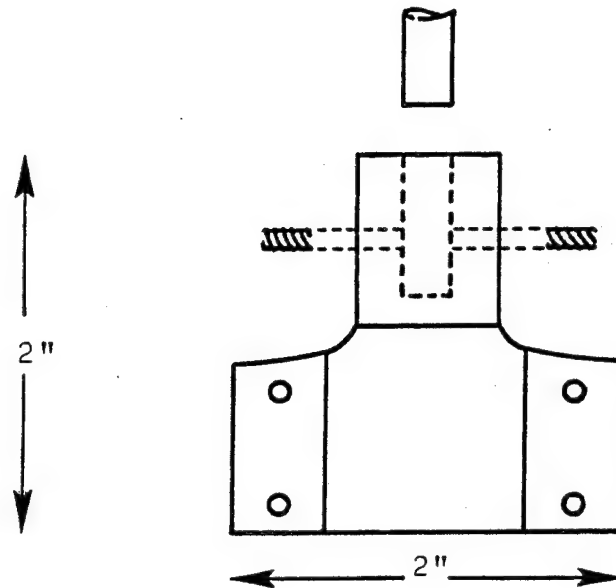


Figure B-2 Top view of the creep grips

APPENDIX C

SOLVENT ABSORPTION INTO THE 3501-6 RESIN

As stated in section 3.4, the purpose of the absorption tests was to determine the immersion times and temperatures necessary to plasticize a resin test specimen to a certain percentage weight gain, M. From these tests came information which might be useful in (1) calculating the diffusion coefficients of the solvents that swell the epoxy resin, or (2) in determining the degree of swelling of that solvent. Each of the solvents is representative of a particular class of solvents. In this appendix, only the absorption data not previously discussed in section 3.4 are given. The swelling behavior of the resin is discussed, but no direct analysis is presented.

Besides the absorption tests on paint stripper MIL-81294 and its components, a few tests were conducted on combinations of these components. These later tests revealed which components were aggressive or nonaggressive in swelling the resin. By making the combination solvents in the same proportions as exists in the paint stripper, any synergistic effect between the components could be examined. The results of these tests are plotted in

TABLE C-1
SUMMARY OF ABSORPTION TESTS

Solvent	Description	T (°C)
water	#7-11-79-01, 4.4% equil. value of M	92.
water	#5-28-79-03, 2.65% equil. value of M	92.
MIL-81294	#RH-10	25.
MIL-81294	#4-6-79-06, fractured in 195 hr	37.5
phenol	#4-6-79-04, fractured within 24 hr	92.
meth. chl.	#5-29-79-02, 450 hr test	40.
water-phenol	#6-29-79-04, (29%/71%) wt. fr. ratio	25.
water-phenol	#4-6-79-07, (33%/67%) wt. fr. ratio, 300 hr fract.	40.
water-phenol	#12-11-79-02, (50/50), 17 hr fracture	64.
water-phenol	#6-29-79-05, (50/50), 12 hr fracture	92.
water-phenol	#7-3-79-01, (50/50), a 6 hr test	75.

figures C-1 and C-2. The experimental procedures used to immerse the resin in the solvents has been previously discussed in section 3.4. A list of the absorption tests performed on the 3501-6 resin is given in table C-1 along with the specimen number, test solvent, immersion temperature, and other pertinent information.

In figure C-1, two different absorption curves have been plotted, one for the paint stripper at 25°C and one for methylene chloride at 40°C. The paint stripper is the most aggressive swelling agent at room temperature, even more aggressive than a saturated water-phenol solution at the same temperature (see figure C-2). The water-phenol (29/71) solution does not have the same water to phenol ratio as found in the paint stripper (50:50 by weight), but the water-phenol (29/71) solution does have a higher percentage of the more aggressive swelling agent, phenol.

Two different diffusional processes appear to be involved in paint stripper absorption. In the first 100 hr, normal Fickian-type diffusion is dominant. The other solutions shown in figures 3.4-1 and C-2 also show this type of pattern until a weight gain of 3% - 5% is realized. After 100 hr, the absorption of the paint stripper appears to be non-Fickian. The straight lines between consecutive

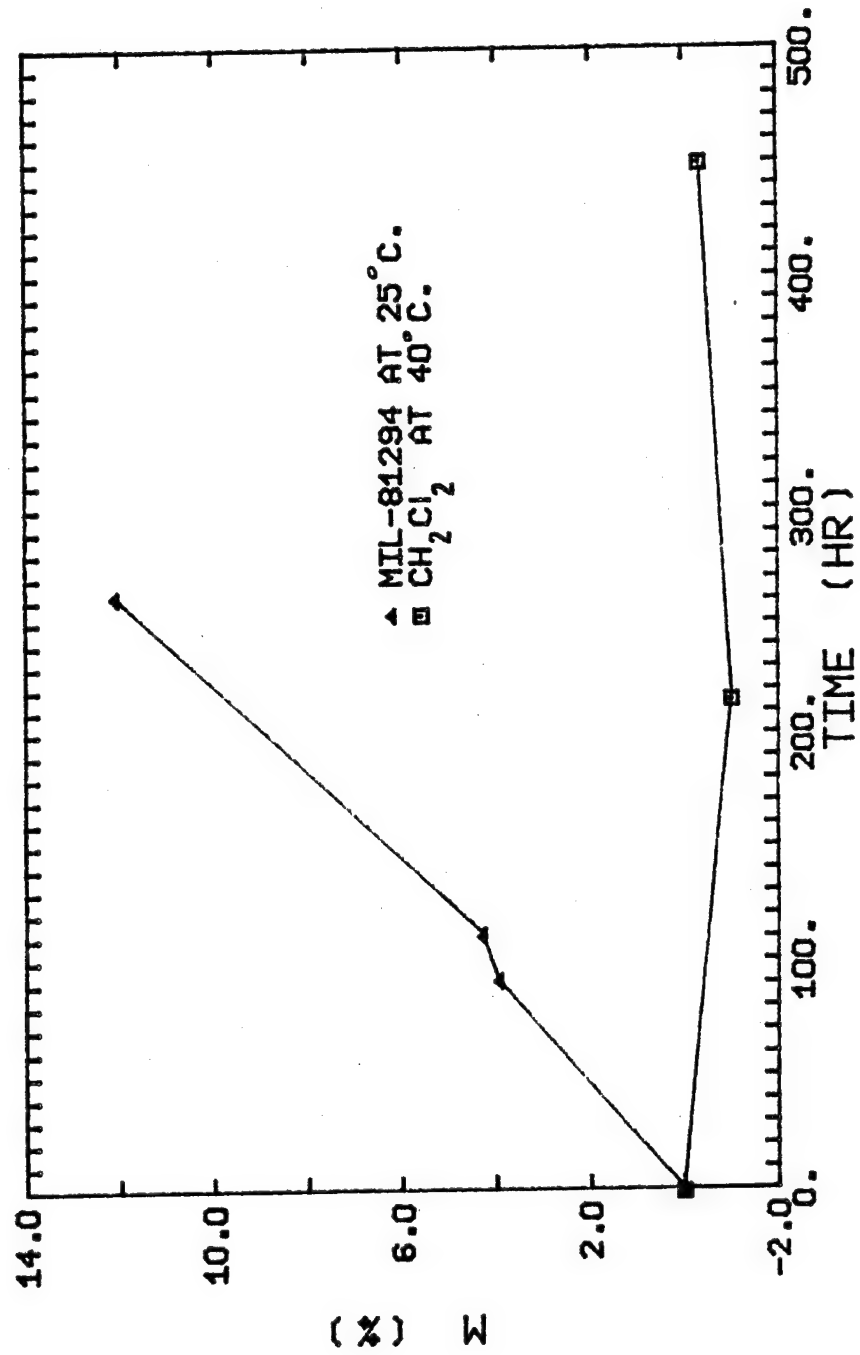


Figure C-1 The absorption curves for the paint stripper and methylene chloride for the 3501-6 resin

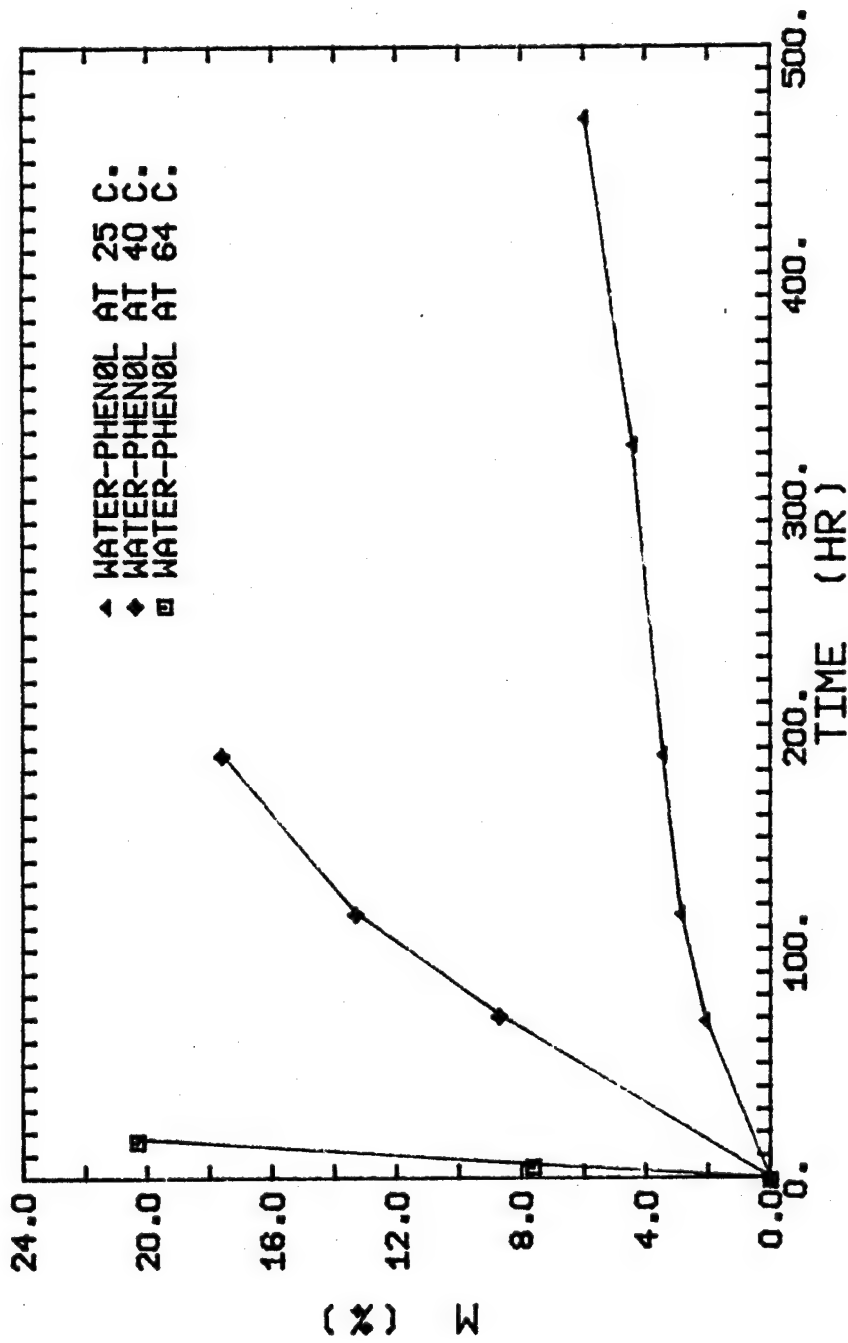


Figure C-2 The absorption curves for water-phenol at various temperatures. The saturation concentrations are: (29/71) at 25°C, (33/67) at 40°C, (50/50) at 64°C.

data points clearly shows that an inflection point has been passed. The 3501-6 resin will eventually fracture in the paint stripper. For example, specimen 4-6-79-06 tested at 37.5°C fractured in 195 hours for M=23%. The two zones of solvent absorption are typical of the diffusion of aggressive solvents into glassy polymers (Joshi, 1980).

Methylene chloride exhibited an unusual absorption behavior when plasticizing the 3501-6 resin. The weight of a resin specimen immersed in methylene chloride actually decreased during the first 200-300 hours of the absorption test. The solvent turned into a yellowish color indicating that the crosslinking agent, DDS, and any other modifiers had been leached out of the resin. The increase in the weight of the specimen after 200-300 hours was probably due to the absorption of methylene chloride into the resin. The rate of absorption is very slow and it is noticeable only after the rate of leaching is exceeded.

The absorption of the other components of the paint stripper, water and phenol, occurs at a much higher rate. The absorption of water into the 3501-6 resin is shown in figure 3.4-1. An equilibrium absorption level is established depending upon the amount of background

moisture already present in the specimen. The maximum equilibrium level is 6.5% (DeIasi and Whiteside, 1978) when a perfectly dry specimen is plasticized by water. Further details on water are contained in section 3.4-1. In one immersion test on phenol at 92°C, specimen 4-6-79-04 was fractured within 24 hours. Only a single experiment was performed because phenol is a very toxic chemical. Phenol absorption was primarily studied in combination with the other solvents such as water or methylene chloride. The evidence of specimen fracture in the combinations with phenol indicates that phenol is the major swelling agent of the paint stripper MIL-81294. Water and methylene chloride did not absorb into the resin at high enough levels to cause fracture.

To test the effect of water and phenol together, three different saturated solutions were prepared at 25°, 40° and 65°C. The absorption curves for the resin in these solutions is plotted in figure C-2. Below 66°C, water-phenol mixtures exist in two phases. The heavier phase contains more phenol by weight and that phase was used in the immersion tests. Using the heavier phase ensured that the weight ratio of water to phenol was greater than or equal to the weight ratio that exists in

the paint stripper (50% to 50%). The weight ratios at each temperature are: 29/71 at 25°C, 33/67 at 40°C, and 50/50 at 64°C (International Critical Tables, 1933). The test at 64°C has the same weight ratio as the paint stripper; therefore, the absorption behavior at 64°C should approximate the absorption behavior of the paint stripper at that temperature. The paint stripper cannot exist at 64°C because methylene chloride boils at 43°C. For preparing the creep and dynamic mechanical test specimens, an immersion temperature of 75°C was used which is above the upper critical solution temperature of 66°C. The absorption curve at 65°C is plotted in figure 3.4-3.

The resin also fractured in the water-phenol solutions. A few weeks were needed to accomplish the fracturing of the specimen below 40°C. The rate of diffusion appears to be greatly enhanced by increasing temperature. Even though the weight ratio decreases in the favor of more water, the rate of diffusion into the resin appears to increase with increasing temperature in figure C-2. In a separate test at 92°C, the resin fractured in less than 12 hours when immersed in water-phenol (50/50) (specimen 6-29-79-05). This is less time than the 24 hours needed to fracture the resin at 64°C.

APPENDIX D
MASTER CURVE CONSTRUCTION

The construction of the creep master curves from short term creep tests at a variety of temperatures requires the application of time-temperature superposition. Time-temperature superposition is described fully in section 4.2.3. It is represented in equation 4.2.3-2 below:

$$J_p = J(t, T) [\rho T / (\rho_o T_o)] = J(t/a_T, T_o) \quad (4.2.3-2)$$

The term in brackets on the left hand side of the equation is the vertical shift factor which corrects for temperature and density changes. The term, a_T , on the right hand side of the equation is the time or horizontal shift factor. It is a function of temperature only. The vertical shift factor can be calculated directly while the horizontal shift factor is determined by a graphical procedure referred to as the "pasting" method of section 4.2.3.

The creep master curve for the 3501-6 virgin resin was constructed from three short term creep tests from batch no. 6-29-79-00. The creep data for these tests is

contained in appendix A (and it is plotted in figure 3.2-3). The procedures used to make the master curve are listed below:

1. Choosing a reference temperature of 23°C (296°K), the creep compliance of specimens 6-29-79-01, 6-29-79-02, and 6-29-79-03 were multiplied by the value of the vertical shift factor, $\rho T / (\rho_o T_o)$. The results are plotted against log time in figure 4.2.3-1. An example calculation is given in section D.1.
2. The horizontal shift factor, a_T , was determined graphically from a plot like figure 4.2.3-1. The bottom curve, 6-29-79-02, is already at the reference temperature so it does not need to be shifted ($\log a_T = 0$). The other two curves were shifted to the right (longer times) until the best smooth curve was obtained as shown in figure D.1-1. The time coordinates were multiplied by the reciprocal of the shift factor (the actual shift factor is defined as $1/a_T$) and the data points were replotted until the best smooth curve was obtained. For the middle curve (6-29-79-01),

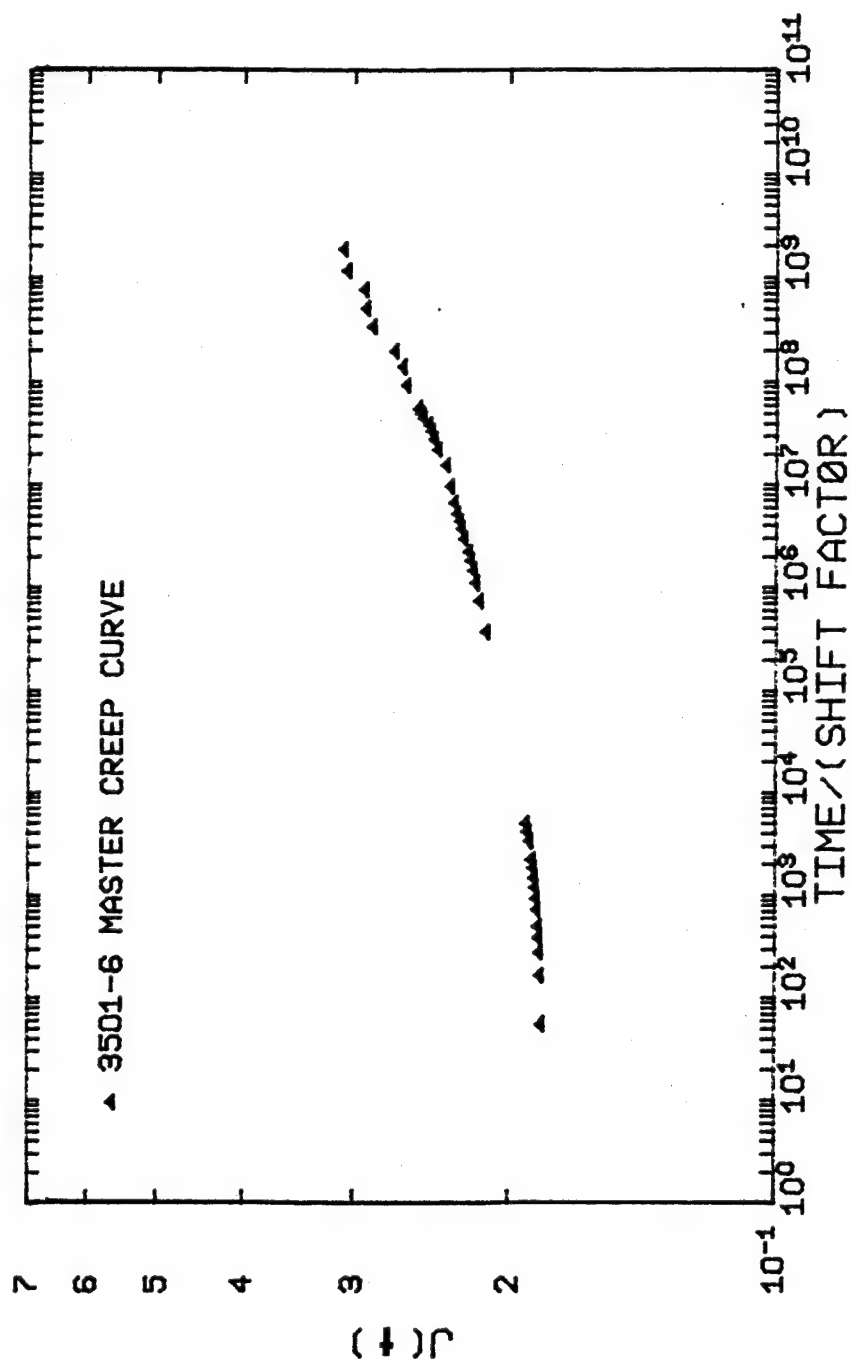


Figure D.1-1 Master creep curve for the 3501-6 resin ($T_0 = 23^\circ\text{C}$)

the shift factor was $\log a_T = -3.12$ and for the upper curve (6-29-79-03), $\log a_T = -5.00$. These values are plotted in figure 4.2.3-3.

3. To determine the effect of temperature on the horizontal shift factor, an Arrhenian rate equation was fit to the data (figure 4.2.3-3) and the activation energy, ΔH , was calculated. An example calculation is shown in section D.1.
4. To test the prediction of the creep from the master curve, the creep curve at 116°C was compared to the long term creep test at that temperature (11-3-79-01). That data is plotted in figure D.2-1. The creep at any temperature can be predicted from the master curve by multiplying J_p and t/a_T by their respective reciprocal shift factors.

D.1 EXAMPLE CALCULATIONS

D.1.1 VERTICAL SHIFT FACTOR

The bulk density of the 3501-6 resin was not measured at every temperature, but the density ratio at any temperature, T , to the density at temperature $T_0 = 23^\circ\text{C}$, was approximated from the linear thermal expansion coefficient, α . Assuming the creep test specimen was a rectangular

solid, average specific dimensions can be assigned to the specimen at the reference temperature. At a higher temperature, the length, width and thickness of the specimen can be determined from the linear thermal expansion coefficient. At the reference temperature, T_0 , a volume V_0 can be computed. At the higher temperature, T , a volume V can be computed. The ratio of V/V_0 is the same as the density ratio, ρ_0/ρ . An example calculation is given below.

Two sources were used to determine a value for the linear thermal expansion coefficient of the resin. The expansion coefficient is the same in all directions for the isotropic resin, but the transverse expansion coefficient, α_2 , for the AS-3501-6 composite should be very similar to the value of α for the neat resin. The value of α given by the Center for Composite Materials was 13.5×10^{-6} in/in-°F (24×10^{-6} in/in-°C) (Dick, 1979). A few thermal expansion tests were also run by the author. A value for α equal to $24 \pm 1 \times 10^{-6}$ in/in-°C was measured. Since the two values of the thermal expansion coefficient are very close, an average value of 24×10^{-6} in/in-°C was chosen for the calculation.

The following dimensions were chosen as the basis for the calculation. Items subscripted with a zero refer to the reference temperature. The letters a, b and c refer

to the width, thickness and length of the specimen, respectively.

$$\begin{aligned} a_o &= 0.75 \text{ in.} \\ b_o &= 0.0133 \text{ in.} \\ c_o &= 5.00 \text{ in.} \end{aligned} \quad (\text{D.1.1-1})$$

$$V_o = a_o b_o c_o = 0.0499 \text{ in.}^3 \quad (\text{D.1.1-2})$$

For computing the vertical shift factor at 79°C (352°K), the linear thermal expansion coefficient is used to compute the new dimensions at the new temperature, T. The value of α is assumed constant over the temperature range.

$$\begin{aligned} a &= 0.75 (1 + (24 \times 10^{-6}) (352 - 296)) = 0.7510 \text{ in.} \\ b &= 0.0133 (1 + (24 \times 10^{-6}) (352 - 296)) = 0.0133178 \text{ in.} \\ c &= 5.00 (1 + (24 \times 10^{-6}) (352 - 296)) = 5.00672 \text{ in.} \end{aligned} \quad (\text{D.1.1-3})$$

$$V = abc = 0.0549 \text{ in.}^3 \quad (\text{D.1.1-4})$$

The density ratio is simply related to the volume ratio defined in equation D.1.1-5,

$$\rho/\rho_0 = V_0/V = 0.909 \quad (\text{D.1.1-5})$$

The vertical shift factors can be directly computed after the density ratio is known. The vertical shift factors at each of the temperatures are:

$$\frac{\rho T}{\rho_0 T_0} (296^\circ\text{K}) = 1$$

$$\frac{\rho T}{\rho_0 T_0} (352^\circ\text{K}) = 1.08$$

$$\frac{\rho T}{\rho_0 T_0} (376^\circ\text{K}) = 1.11$$

D.1.2 ACTIVATION ENERGY, ΔH

The Arrhenian rate equation used to calculate the activation energy, ΔH (see section 4.2.3) is given by the equation below. Absolute temperature ($^\circ\text{K}$) is used.

$$\log a_T = \Delta H / (2.303R) [1/T - 1/T_0] \quad (4.2.3-4)$$

Plotting the shift factor against reciprocal temperature as shown in figure 4.2.3-3 will yield the value of ΔH , the slope of the best straight line through the data. A linear

least squares fit to the data gave the following result:

$$\log a_T = -22.73 + 6780(1/T) \quad (\text{D.1.2-1})$$

The activation energy calculated from the slope of the straight line is

$$\Delta H = (6780) \times R \times 2.303 = 31.0 \frac{\text{kcal}}{\text{mole}} \quad (\text{D.1.2-2})$$

Several sources in the literature also provided shift factor-temperature data. If the activation energy was not calculated in the source, the data was used to calculate ΔH in the same manner as shown here. These calculations only apply to the creep data below the glass transition temperature of the polymer being studied.

D.2 PREDICTING CREEP BEHAVIOR FROM MASTER CURVES

The data given by the master curve is expressed by equation 4.2.3-1. The master curve is already the predicted creep behavior of the resin at the reference temperature, but the prediction of the long term creep behavior at other temperatures requires some reshifting of the master curve. The reciprocal of the vertical and horizontal shift factors must be multiplied against J_p and t/a_T respectively. This

gives back the $J(t)$ versus time curve at temperature T .
 An example is shown in figure D.2-1. The equations used
 to predict the creep behavior at 116°C are presented below.

$$J(t, 116^{\circ}\text{C}) = \frac{\rho_o^T}{\rho^T} (J_p) = 0.891 J_p \quad (\text{D.2-1})$$

$$\begin{aligned} \log a_T(116^{\circ}\text{C}) &= -22.75 + 6780/389 \\ &= -5.32 \end{aligned} \quad (\text{D.2-2})$$

$$t(116^{\circ}\text{C}) = 10^{-5.32} (t/a_T) \quad (\text{D.2-3})$$

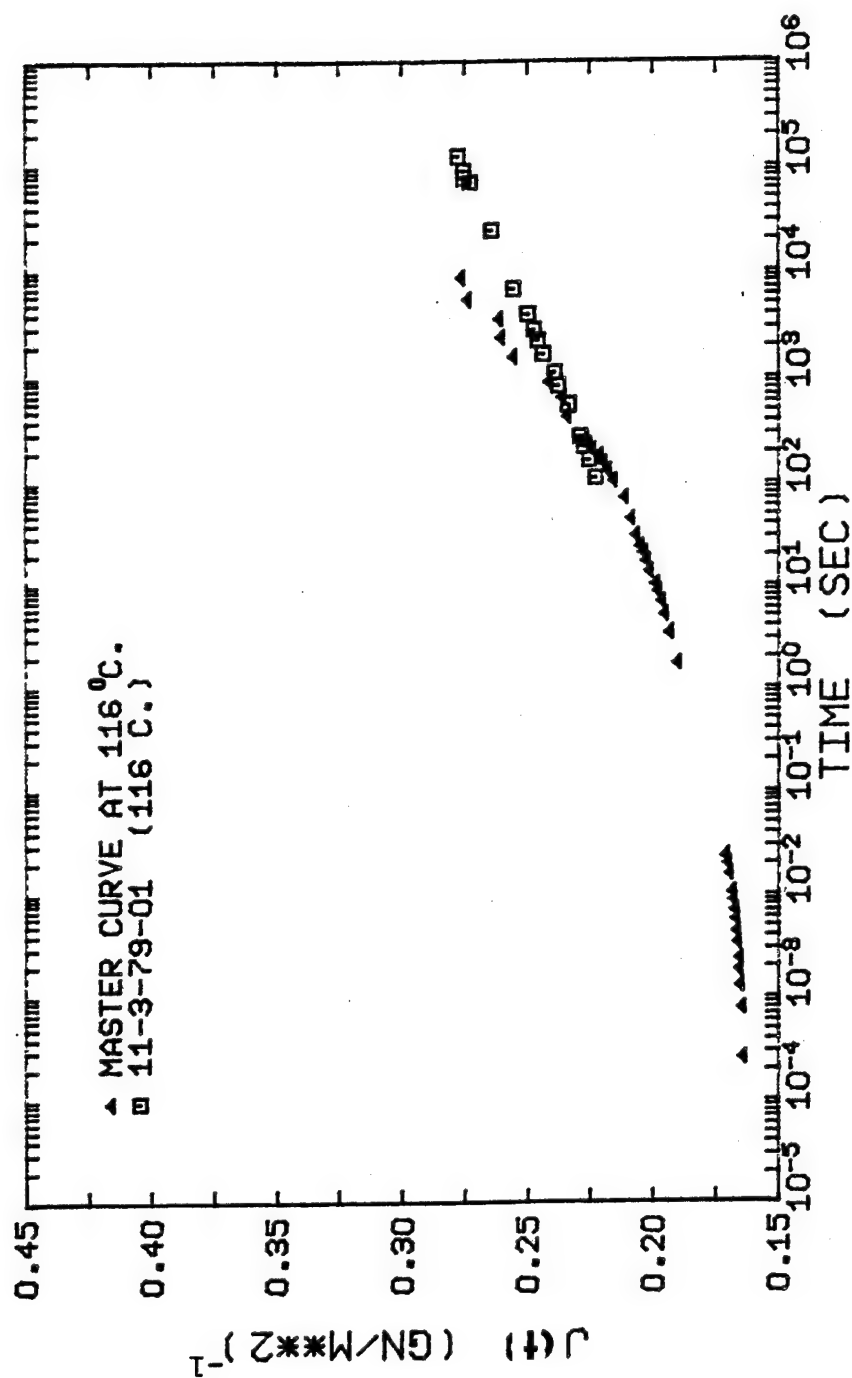


Figure D.2-1 The creep of the virgin resin at 116°C versus the prediction of the master curve

APPENDIX E

ERROR ANALYSIS

The purpose of this section is to identify the sources of experimental error (or uncertainty) and to estimate the effects of accumulated errors on quantities computed as functions, $f(x_1, x_2, \dots, x_n)$, of the directly measured variables, x_1, x_2, \dots, x_n . Accumulated errors are estimated from the arbitrary, but traditional, relationship:

$$\Delta f_{\pm} = \sum_i \left| \frac{\partial f}{\partial x_i} \right| |\Delta x_i|_{\pm} \quad (\text{E-1})$$

These estimates of accumulated error are pessimistic in the sense that larger values for Δf are obtained than would be from the "Law of Propagation of Errors"; viz,

$$\Delta f^2 = \sum_i \left(\frac{\partial f}{\partial x_i} \right)^2 (\Delta x_i)^2 \quad (\text{E-2})$$

Creep Characterization

The creep compliance is computed from the relationship:

$$J(t) = \epsilon(t)/\sigma_0 \quad (E-3)$$

where σ_0 is the (fixed) stress and $\epsilon(t)$ is the strain measured at time t . The stress, in turn, is given by

$$\sigma_0 = W_0/S \quad (E-4)$$

where W_0 is the applied load and S is the cross-sectional area of the specimen. From equation E-2, the estimate for the accumulated error of ΔJ is given by

$$\Delta J = \frac{S(\Delta\epsilon(t))}{W_0} + \frac{\epsilon(t)S(\Delta W_0)}{W_0^2} + \frac{\epsilon(t)(\Delta S)}{W_0} \quad (E-5)$$

The cross-sectional area, S , is given by

$$S = xy \quad (E-6)$$

where x is the width of the specimen and y is the thickness.

Each dimension was measured by a digital micrometer with an instrument error of $\pm 1 \times 10^{-4}$ in. (2.54×10^{-6} m).

This instrument error was chosen as the error in the measurement: $\Delta x = \Delta y = 1 \times 10^{-4}$ in. (2.54×10^{-6} m). From equation E-1,

$$\Delta S = (x + y)\Delta x \quad (E-7)$$

Typical specimen dimensions for the creep testing were $x = 0.75$ in. and $y = 0.0133$ in., so that

$$\Delta S = (.75 + .0133)(1 \times 10^{-4}) = 0.763 \times 10^{-4} \text{ in.}^2$$

$$\text{or } 4.92 \times 10^{-8} \text{ m}^2$$

The weights used to provide the constant stress for the creep experiments were weighed with a beam balance having an instrument error of ± 0.5 g. In terms of pounds-force (and newtons), the uncertainty in the load is

$$\Delta W_o = 1.1 \times 10^{-3} \text{ lbf} \quad (4.9 \times 10^{-3} \text{ N})$$

The uncertainty in the strain is not symmetric. The upper limit on the uncertainty, $\Delta \epsilon_+$, is controlled by the instrument error of the Vishay P350A strain recording device. The strain can be measured to the nearest 5 ± 10^{-6} in./in. The lower bound on the uncertainty, $\Delta \epsilon_-$, is controlled by the error in the alignment of the mounted strain gage and the alignment of the specimen in the creep grips. The application of the strain gage and the insertion of the creep specimen in the grips requires hand-to-eye coordination. The limitations on the error are dependent upon the talent and the experience of the operator.

After several trials, it was found that the strain gage could be aligned to within 5° of any predetermined axis. The same error was assumed to apply to the alignment of the specimen in the creep grips. Choosing an average case for the error is difficult, but the worst case situation can be identified.

The worst case situation is shown in figure E-1. The strain gage is misaligned from the specimen axis by the angle β and the specimen axis is misaligned from the axis of gravitational force by the angle ϕ . The worst case situation occurs when the strain gage is misaligned from the gravitational axis by the angle $(\phi - \beta)$. If $\phi = \beta$, the errors in misalignment can cancel.

Choosing 5° as the worst possible angle for both angles, the strain gage can be misaligned by as much as 10° resulting in a measured strain that is less than the true strain (the strain measured along the gravitational axis, Micro-Measurements Inc. (1977)). The uncertainty is always negative; therefore, if the maximum error in the worst case situation is greater than the instrument error ($5 \mu\epsilon$), then the maximum error is the proper negative error limit, $\Delta\epsilon_-$.

The difference between the measured and true strain

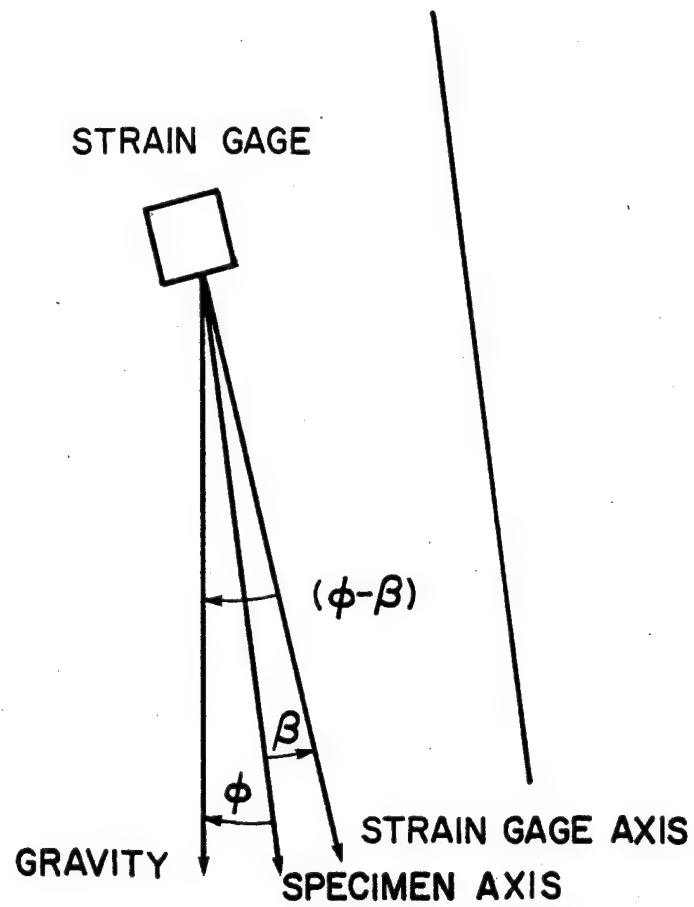


Figure E-1 Worst case misalignment for the maximum strain error in creep experiments

is expressed in terms of a correction offset, n .

$$\begin{array}{c} \text{True} \\ \text{Strain} \end{array} = \begin{array}{c} \text{Measured} \\ \text{Strain} \end{array} + n \quad (\text{E-8})$$

The correction offset can be calculated from the following equation (Micro-Measurements, Inc. (1977)):

$$n = (\epsilon_p - \epsilon_q) [\cos(2(\phi - \beta)) - \cos(2\phi)] / 2 \quad (\text{E-9})$$

where

ϵ_p = maximum strain (ϵ_1 for tensile stress)

ϵ_q = minimum strain (ϵ_2 for tensile stress)

The two strains are related by the Poisson's ratio for the 3501-6 resin,

$$\epsilon_q = -\nu \epsilon_p \quad (\text{E-10})$$

A brief calculation of the experimental error for the worst case situation is shown below. The strain data at 60 sec. for specimen 7-10-79-04 are used: $J(60) = 1590 \mu\epsilon$, angle ϕ is 5° , and angle β is -5° (or vice versa). The Poisson's ratio is listed in table 3.1-1.

$$n = (1590 + (.38 \times 1590)) [\cos(2 \times 10^\circ) - \cos(10^\circ)] / 2 \quad (\text{E-11})$$

$$n = -49 \mu\epsilon \quad (E-12)$$

The correction offset n at the worst case situation is the negative error limit in the strain. Since it is greater than $5 \mu\epsilon$, it is the proper limit that should be used in the calculation of the uncertainty of the creep compliance. Note that the negative error limit is a function of time and it would have to be recalculated for every data point being considered. The fixed error limits for specimen 7-10-79-04 at 60 sec. are expressed as

$$\Delta\epsilon(60) = \begin{cases} +5 \times 10^{-6} \text{ in./in.} \\ -49 \times 10^{-6} \text{ in./in.} \end{cases}$$

The fixed uncertainties ΔA , ΔW_0 , and $\Delta\epsilon$ can be substituted into equation E-5 in order to calculate the experimental error in the creep compliance. The sample calculation presented here uses the creep data at 60 sec. from specimen 7-10-79-04. The results of the calculation are:

$$\Delta J(60) = \begin{cases} +1.8 \cdot 10^{-3} \text{ (GN/m}^2\text{)}^{-1} \\ -6.6 \cdot 10^{-3} \text{ (GN/m}^2\text{)}^{-1} \end{cases}$$

The creep compliance at 60 sec. is $0.174 \text{ (GN/m}^2\text{)}^{-1}$ so that the percent error is given as +1.04% and -3.89%.

The reduced compliance defined in section 4.2.2 ($J_r = J(t)/J_0$) is the creep compliance divided by the initial creep compliance at zero time (as determined by the Voigt-Kelvin model). Since the same initial stress, σ_0 , is implied in both compliances, the reduced compliance is also the ratio of the strain at time t divided by the instantaneous elongation at zero time, $\epsilon(t)/\epsilon_0$. Using this form of the reduced compliance results in an expression for determining the experimental error for the reduced compliance. Substituting $\epsilon(t)/\epsilon_0$ into equation E-1 yields

$$\Delta J_r = \Delta \epsilon(t)/\epsilon_0 + \epsilon(t)(\Delta \epsilon_0)/(\epsilon_0)^2 \quad (E-13)$$

An example calculation is shown below. The experimental data is taken from the creep experiment on specimen 7-5-79-01. The values of the parameters used to calculate ΔJ_r were:

$$\epsilon_0 = 1840 \text{ } \mu\epsilon$$

$$\epsilon(t) = 2457 \text{ } \mu\epsilon \quad (t = 272,400 \text{ sec})$$

$$\Delta \epsilon(t) = \begin{cases} +5 \text{ } \mu\epsilon \\ -57 \text{ } \mu\epsilon \end{cases} \quad (t = 272,400 \text{ sec})$$

$$\Delta \epsilon_0 = +5 \text{ } \mu\epsilon$$

$$J_r = 1.335 \text{ at } 272,400 \text{ sec}$$

The error limits on $\Delta\epsilon(272,400)$ were computed from equation E-9. The error limits on $\Delta\epsilon_0$ were taken as the 95% (nonlinear) confidence limit fit of the Voigt-Kelvin model (see appendix G). The substitution of these quantities into equation E-13 yields:

$$J_r = \begin{cases} +0.007 & (0.5\%) \\ -0.035 & (2.6\%) \end{cases}$$

Dynamic Mechanical Characterizations

Substitution of the definition of the complex dynamic mechanical modulus (equation 3.2-1) into equation E-1 yields the following expression for the estimate of the error:

$$\Delta|E| = 0.20 \left(\frac{\Delta L}{S(A \cdot D - K)} + \frac{L(\Delta S)}{S^2(A \cdot D - K)} + \frac{L \cdot A(\Delta D)}{S(A \cdot D - K)^2} + \frac{L(\Delta K)}{S(A \cdot D - K)^2} \right) \quad (E-14)$$

where L = gage length of specimen (cm)
 S = cross-sectional area (cm²)
 D = dynamic force variable
 K = dynamic force constant
 A = integral constant (equals 1)
 0.2 = conversion factor to GN/m²

Each of the individual uncertainties is calculated below.

The gage length of the specimen was measured with adjustable calipers using a micrometer to measure the spacing between the calipers. The micrometer had an instrument error of 1×10^{-2} cm (0.0039 in.).

The uncertainty in the area was determined from equation E-7. Using average specimen dimensions of 5×10^{-1} cm for the width and 1.8×10^{-2} cm for the thickness, the uncertainty, ΔS , is 1.34×10^{-4} cm².

The method used to determine the error constant, K , and the associated uncertainty, ΔK , was based on the instructions given in the Operator's Manual for the Rheovibron (Toyo Measurements, Inc. (1969)). The error constant is the correction for the dynamic force, D . The elasticity in the grips and transducers of the Rheovibron induce error in the dynamic force reading. In effect, K is the correction which is equal to the value of D at zero specimen length. The value of K is unique for each polymer and set of grips, and it is a function of temperature. At constant temperature, the value of K can be determined from equation 3.2-1. The complex dynamic modulus, $|E|$, is a linear function of the specimen length, L . Rearranging equation 3.2-1 and solving for D gives

$$D = K + 0.20 L / (|E|S) \quad (E-15)$$

For a constant cross-sectional area S , D is a linear function of the length of the specimen. By measuring D while varying L , the value of K becomes the ordinate intercept of a straight line through the data. The complex modulus is also assumed to be independent of specimen length.

Three tests were run to determine K . For each test, the dynamic force D was measured at room temperature (25°C) while varying L . The same specimen was used for each data point by shortening the specimen after each measurement. This procedure ensured that the cross-sectional area was the same throughout the test. The results for two tests on specimens RH-15 and RH-16 are given in figure E-2. These tests represent the value of K for the virgin resin which was tested on the Rheovibron without the new improvements made on the grip-transducer assembly (see section 3.3). A linear least squares straight line was fit to the data for each test. The ordinate intercept for each line determines K . The square root of the variance in the parameter K was chosen as the value of ΔK . The average value of K and ΔK were: $K = 25 + \Delta K$ with $\Delta K = 2.5$. In figure E-3, a single test was performed on

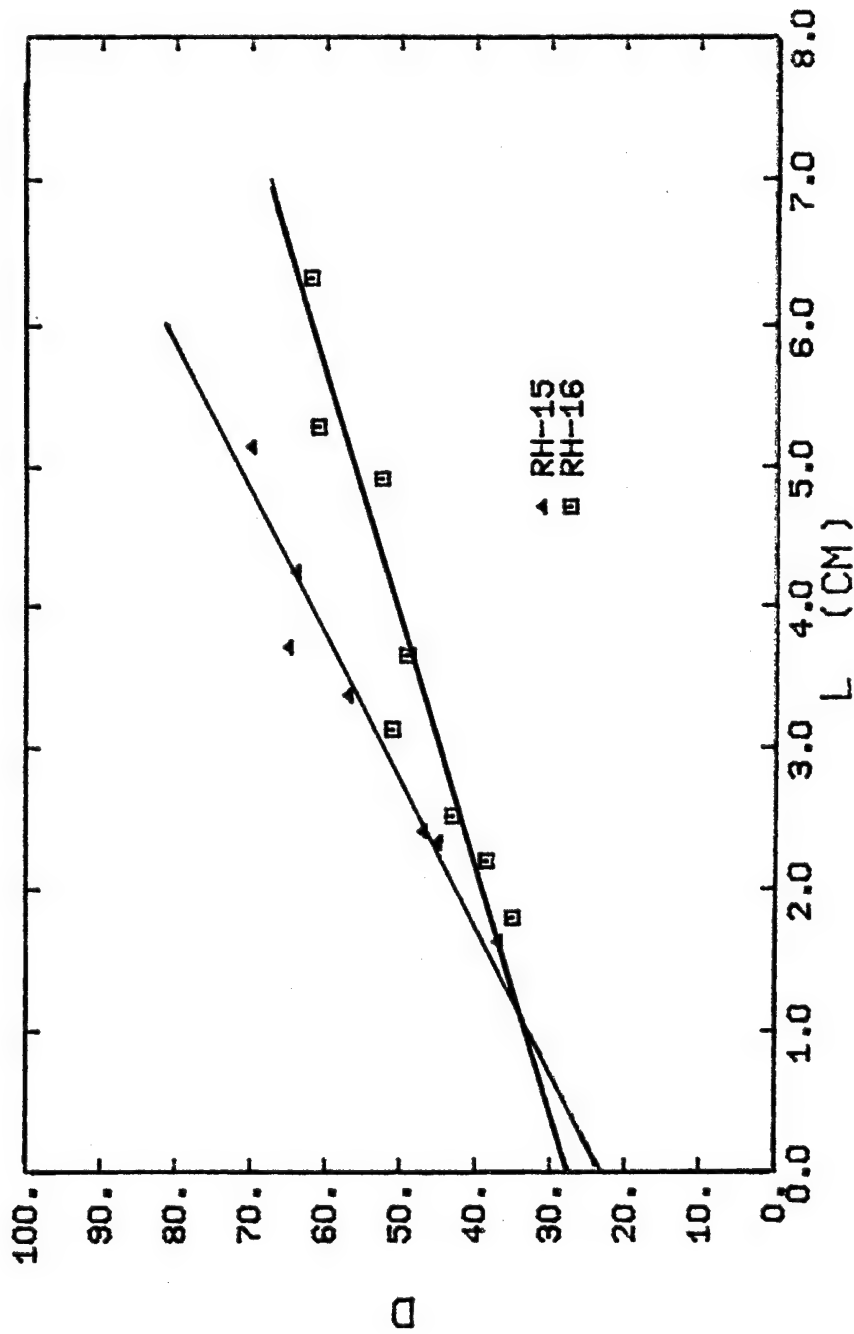


Figure E-2 Two computations for the value of the force constant, K , for the 3501-6 resin (tests without improvements)

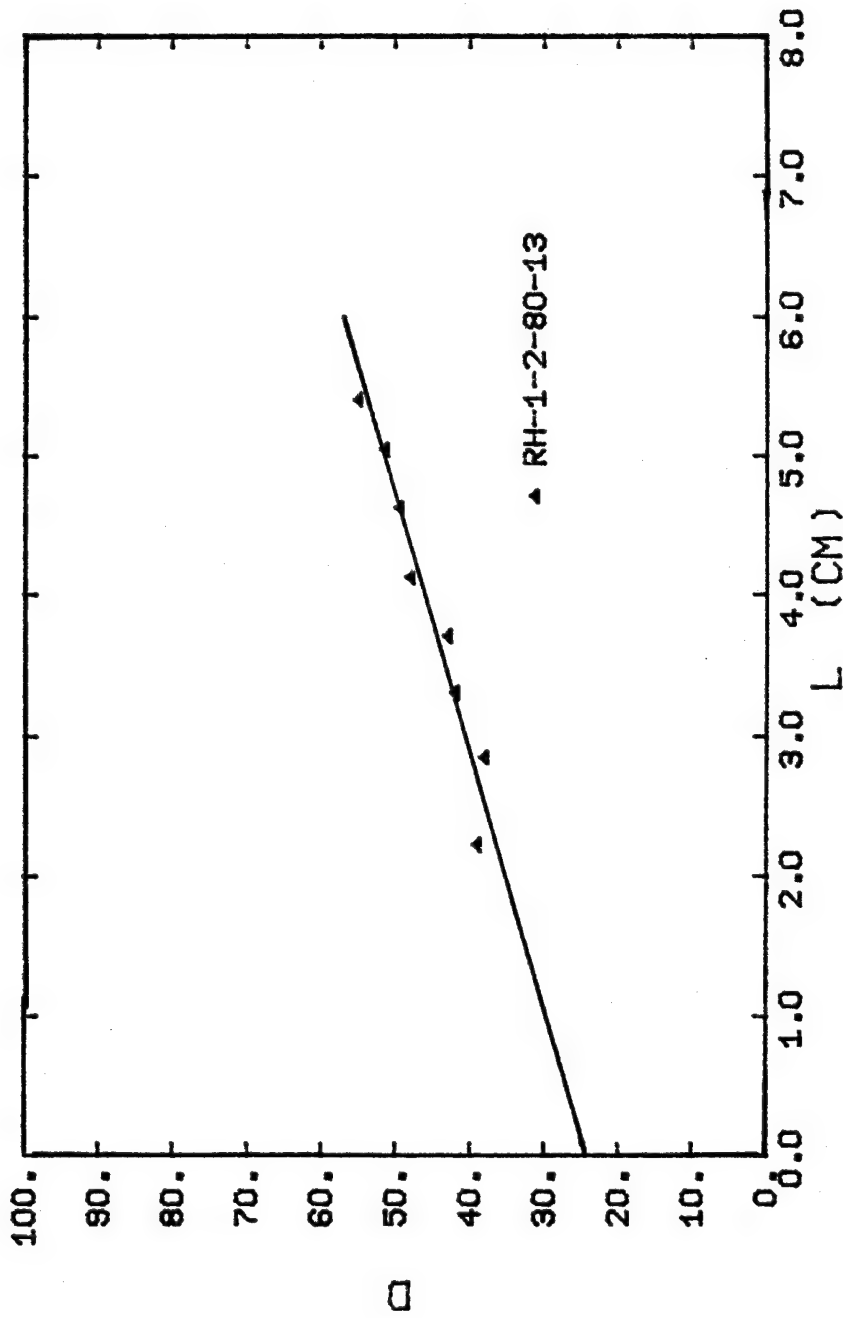


Figure E-3 The computation for the value of the force constant, K , for the 3501-6 resin (tests with the new improvements)

on the Rheovibron with the new improvements in the grip-transducer assembly. The results of the linear least squares fit were: $K = 24 + \Delta K$ with $\Delta K = 2.4$. The presence of the new improvements did not make a difference in the value of K because the value in each set of tests is not significantly different from the other. A value of $K = 25$ was used in all dynamic mechanical property calculations.

The values of the parameters in table E-1 represent the specimen dimensions and the dynamic mechanical behavior of a typical specimen. Substituting these quantities into equation E-14 gives the experimental error in the complex dynamic modulus: $\Delta|E| = \pm 0.32 \text{ GN/m}^2$.

At higher temperatures, K decreases slightly with increasing temperature. The value of K was not recomputed at these higher temperatures, however. The dynamic force, D , increases rapidly near the glass transition temperature making K negligible by comparison. Assuming K is a constant with increasing temperature does not create any significant error in the calculation of the complex dynamic modulus. Using K as a constant, the experimental error in the complex dynamic modulus was calculated at 150° and 250°C . The values of $\Delta|E|$ at three temperatures are:

TABLE E-1
DATA FOR THE SAMPLE CALCULATION OF THE FIXED
EXPERIMENTAL ERROR IN THE DYNAMIC MODULUS

ΔL (cm)	$1. \times 10^{-2}$
ΔS (cm ²)	1.34×10^{-4}
ΔD	0.5
ΔK	2.5
ΔE (GN/m ²)	3.70
L (cm)	5.5
S (cm ²)	8.5×10^{-3}
K	25.
D	60.

$$\Delta|E|(25^\circ) = 0.32 \text{ GN/m}^2 \quad (8.5\%)$$

$$\Delta|E|(150^\circ) = 0.14 \text{ GN/m}^2 \quad (5.3\%)$$

$$\Delta|E|(250^\circ) = 0.0026 \text{ GN/m}^2 \quad (1.8\%)$$

The percentage errors in parentheses are based on the mean complex dynamic modulus curves. The percent errors were calculated from the values of the complex dynamic modulus given in Figure 5.2-1. The mean curve for the virgin resin was used. In the last calculation at 250°C, the value of D is 897, which is much larger than the value of 60 used in the calculation at 25°C.

APPENDIX F
EFFECTS OF AGING ON CREEP

The creep behavior of polymeric materials may vary with the age of the sample. Such "aging effects" have been documented by Struik (1978) who proposes that the aging phenomena can be explained in terms of the following "free volume" concept. When a polymer is rapidly cooled to below its glass transition temperature, the molecules cannot undergo conformational rearrangements rapidly enough to achieve equilibrium (i.e., minimum free energy) structures. This non-equilibrium state results in an "excess" free volume. However, even at temperatures well below the glass transition temperature, some segmental mobility can occur so that the system can drift towards the equilibrium structures and the associated smaller free volumes. The rate of decrease of the free volume is non-linear; the molecular mobility decreases as the free volume decreases so that the rate of decrease in the free volume tends to zero as the free volume asymptotically approaches equilibrium.

As the material ages, the free volume decreases

and tends to restrict the mobility of the chain segments. The restricted mobility tends to increase the modulus and retard the creep behavior. Struik (1978) proposes that the principal of time-temperature superposition can be used to superimpose creep curves obtained at one temperature for samples with different aging times, t_e . By analogy to time-temperature superposition, the horizontal shift factor may be used to characterize an "aging" shift factor. Under these arguments, the value of the creep compliance, as measured at a specific time, should be smaller for specimens that have been aged for longer periods of time. These arguments further suggest that the retardation times for aged samples will be larger than the retardation times for fresh samples. Consequently, the value of τ_1 , as computed under the assumption of the Voigt-Kelvin model, should increase with the age of the specimen.

The specimens used in this work were aged from 23 to 172 days. The age of selected specimens is given in table F-1. The duration of the creep test of the various specimens is also included in table F-1. With the exception of specimen 7-10-79-04, the duration of the creep test is less than two percent of the age of the sample.

TABLE F-1
AGE OF ROOM TEMPERATURE CREEP SPECIMENS

Specimen No.	Age (days)	Test Duration (days)
7-5-79-01	136	3.16
7-5-79-02	122	0.18
12-11-79-01	23	0.34
12-11-79-05	34	0.29
6-29-79-02	136	0.110
7-10-79-04	97	6.83
4-4-79-02	172	0.27

The value of τ_1 is plotted against the age of the sample in figure F-1. The value of the creep compliance (as measured at 60 seconds and 22.5°C) is plotted versus the age of the sample in figure F-2. In both cases the scatter in the data caused by batch-to-batch variation masks the detection of any significant trends. Evidently, aging effects in the time scales considered are less significant than the variation in the material properties caused by batch-to-batch variation.

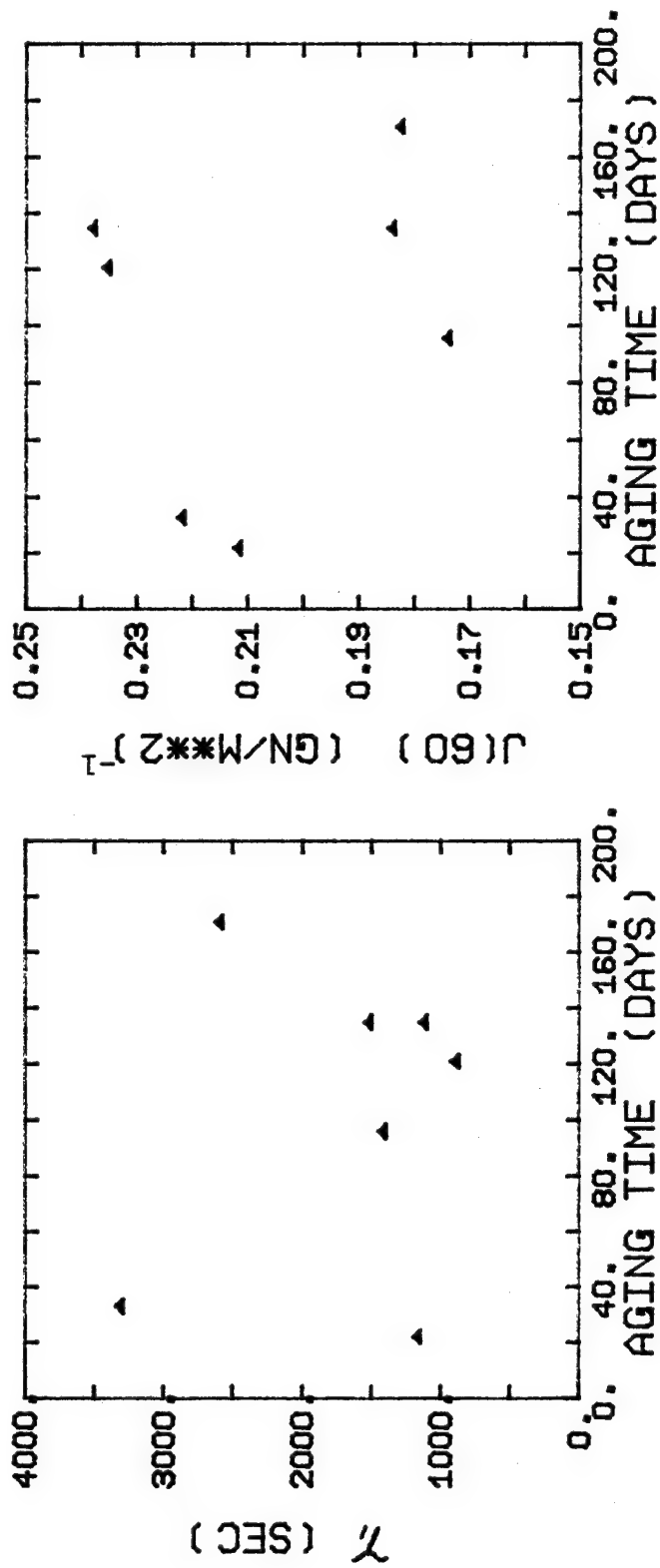


Figure F-1 The retardation time plotted against the aging time of the specimen

Figure F-2 The creep compliance at 60 sec. plotted against aging time

APPENDIX G
COMPARISONS OF VISCOELASTIC MODELS

The creep data for the eleven creep tests on the 3501-6 resin were fitted to the Voigt-Kelvin model (equation 2.1.2-12) and the power law model (equation 2.1.3-2) with a nonlinear least squares (NLLS) computer program (University of Delaware Computing Center library program). The creep data used to fit the viscoelastic models were taken from the primary or viscoelastic creep zone (the first thirty thousand seconds). The results of the curve fitting exercise are listed in tables 4.2.2-1 (Voigt-Kelvin model) and 4.2.2-2 (power law model) along with the standard estimate of error for each fit. Examples of how the models compare with the actual creep behavior are given in figures 4.2.2-2 and 4.2.2-8.

The comparison of figures 4.2.2-2 and 4.2.2-8 shows that, qualitatively, both models appear to give nearly equivalent representations of the creep behavior. However, a quantitative measure of the relative "goodness" of the curve fits may be judged by a standard "F-score" test; viz,

$$F\text{-Score} = s_I^2 / s_{II}^2 \quad (s_{II} < s_I) \quad (G-1)$$

where

s_I^2 = square of the standard estimate of error
for model I,

s_{II}^2 = square of the standard estimate of error
for model II.

A determination of a significant difference between the models can be judged by comparing the F-Score to tabulated values of the "F-Distribution" at the $(1-c)100\%$ confidence level:

$$F\text{-Score} > F_{1-c/2}(v_I, v_{II}) \quad (G-2)$$

with

$$v_I = n - p_I - 1, \text{ and}$$

$$v_{II} = n - p_{II} - 1.$$

Parameter n is the number of data points and p is the number of parameters of the model used to fit the data. If the criteria of equation G-2 is satisfied, then a significant difference between the models is demonstrated at the $(1-c)100\%$ confidence level. In this event, the model corresponding to the smaller estimate of error (s_{II}) may be judged as the "best fit" in the sense of minimizing

the standard estimate of error. If the F-test indicates no significant difference, then the simpler model (with fewer parameters) is usually preferred.

Values of the statistical variables for a typical room temperature creep test are:

$$n = 18$$

$$s_{II}^2 = 3.57 \cdot 10^{-8} \quad (\text{Power Law Model})$$

$$v_{II} = 15$$

$$s_I^2 = 7.73 \cdot 10^{-8} \quad (\text{Voigt-Kelvin Model})$$

$$v_I = 14$$

Accordingly, the value of the F-Score is 2.17; the critical value of the F-distribution at 99% confidence is 3.66.* Consequently, no significant difference is demonstrated between the two models.

Similar comparisons for the eleven creep tests are summarized in table G-1.

The comparisons given in table G-1 show that a consistent distinction between the two models is marginal even at the relatively weak 95% confidence level (for a

*Beyer, 1966; Bethea, et al., 1975; Korn and Korn, 1961.

TABLE G-1
SUMMARY OF F-SCORE TESTS

Specimen No.	Temperature (°C)	n	F-Score	Critical Values 95%	Critical Values 99%
7-10-79-04	22.8	18	1.47	2.46	3.66
12-11-79-01	22.5	19	2.17	2.43	3.49
12-11-79-05	21.2	19	2.24	2.43	3.49
11-3-79-01	116.	13	2.40	3.13	5.26
4-6-79-02	23.5	22	2.39	2.19	3.06
6-29-79-02	23.8	17	6.68	2.51	3.75
6-29-79-01	79.0	18	1.97	2.46	3.57
5-29-79-03	103.	17	1.05	2.51	3.75
7-5-79-01	23.8	20	4.21	2.30	3.34
7-5-79-02	23.5	19	1.35	2.43	3.49
12-11-79-06	21.2	18	4.66	2.46	3.57

majority of the tests). Thus the use of the 3-parameter power law model could be justified as a convenient device for data storage and retrieval. On the other hand, the 4-parameter Voigt-Kelvin model appears to yield more realistic extrapolations to "zero" time behavior. In addition, the analogy of the Voigt-Kelvin model to the behavior of a mechanical system of springs and dashpots provides a traditional (but nonetheless artificial) view for interpreting the role of the parameters.

Estimates for the Voigt-Kelvin parameters associated with the retardation time, τ_1 , the "parallel dashpot" viscosity, η_1 , and the "long-term" viscosity, η_0 , at various temperatures are illustrated in figures G-1 through G-6. In figures G-1 through G-3, the variation of τ_1 , η_1 and η_0 with temperature for all batches is presented. In figures G-4 through G-6, the variation of τ_1 , η_1 and η_0 with temperature for the single batch case is presented. The last three curves have been included to show the effect of batch-to-batch variation on the results. The single batch case is discussed in section 4.2.2.A. For all the batches, both the retardation time, τ_1 , and the long-term viscosity, η_0 , appear to be insensitive (within the error range) to temperature variations between 20°C and 100°C. The insensitivity of the retardation time implies (within

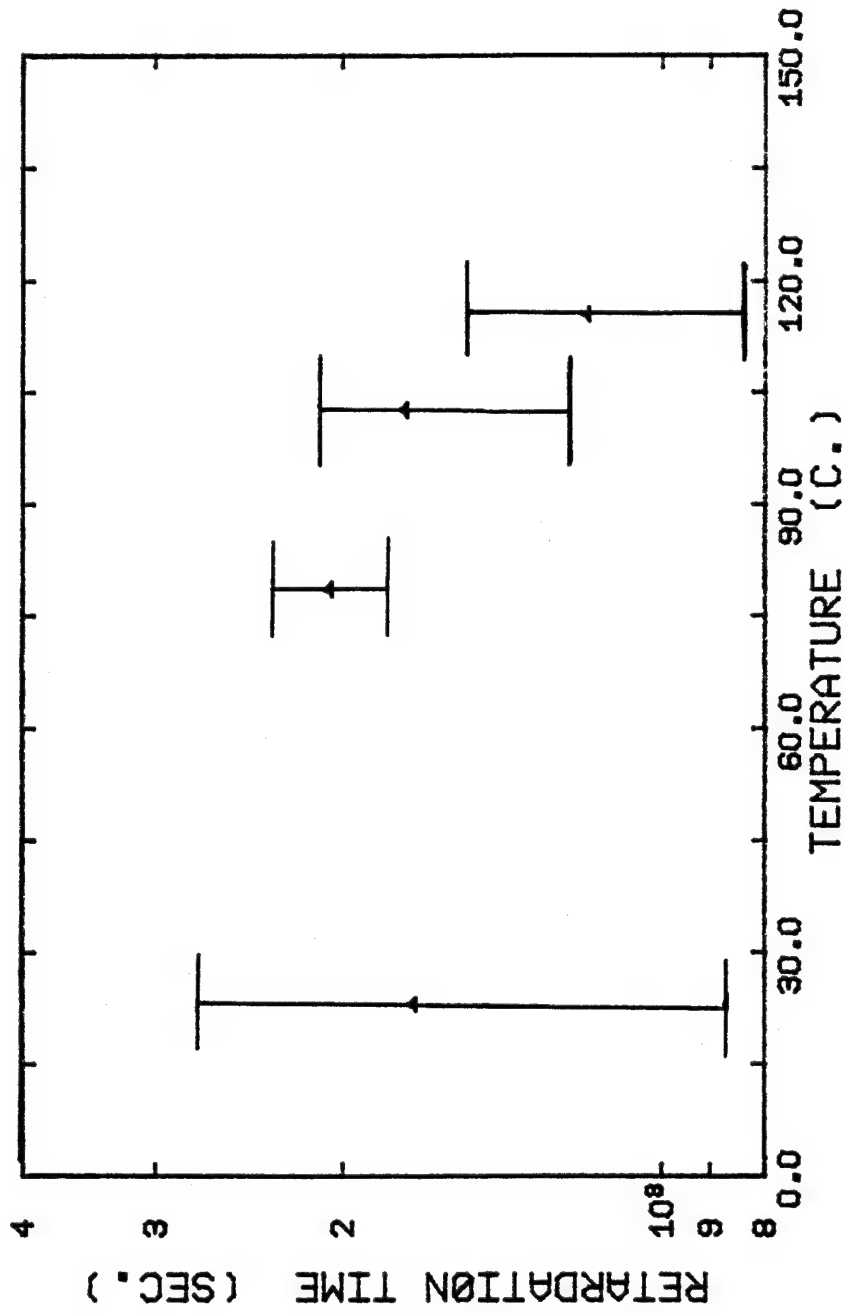


Figure G-1 Retardation time vs. temperature for all batches

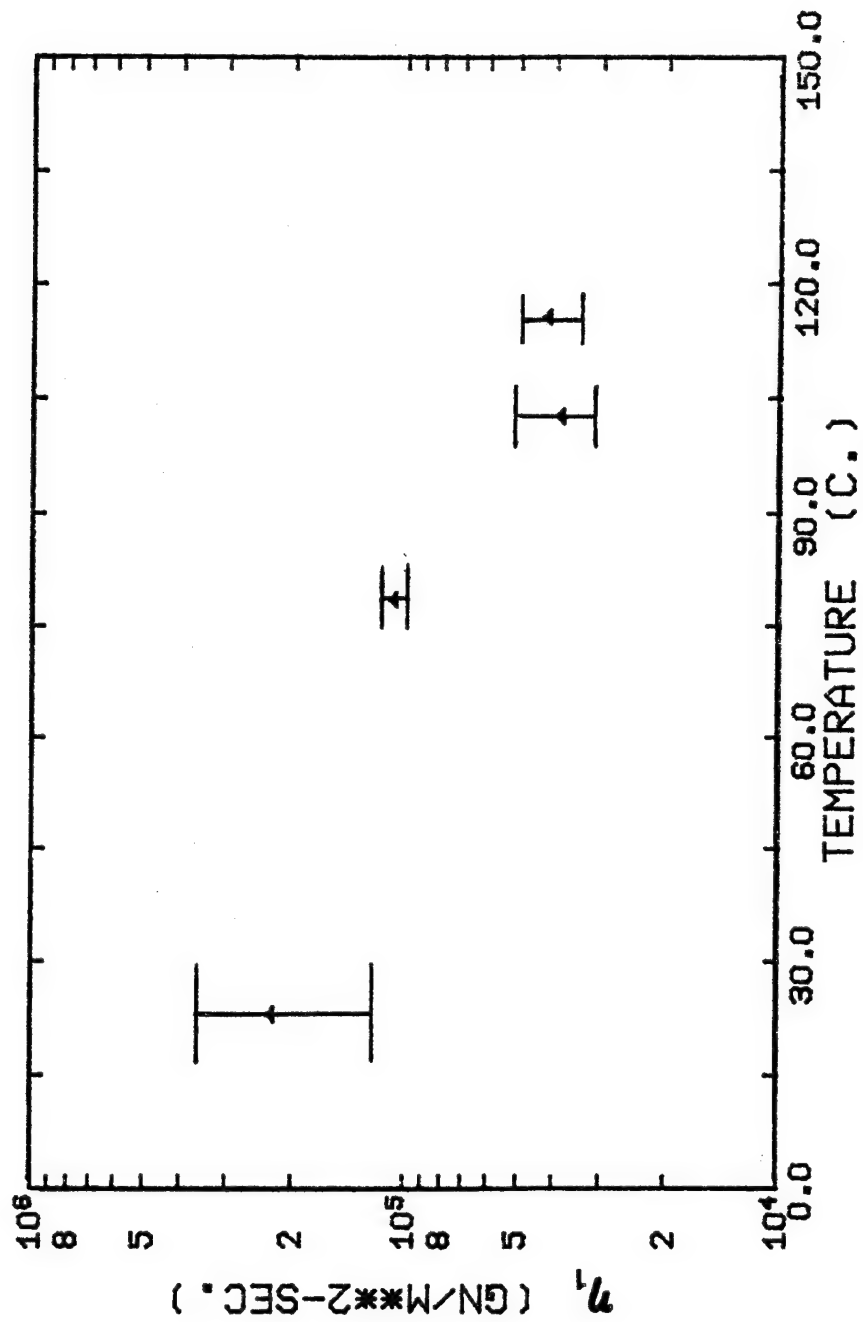


Figure G-2 The parallel dashpot viscosity vs. temperature for all batches

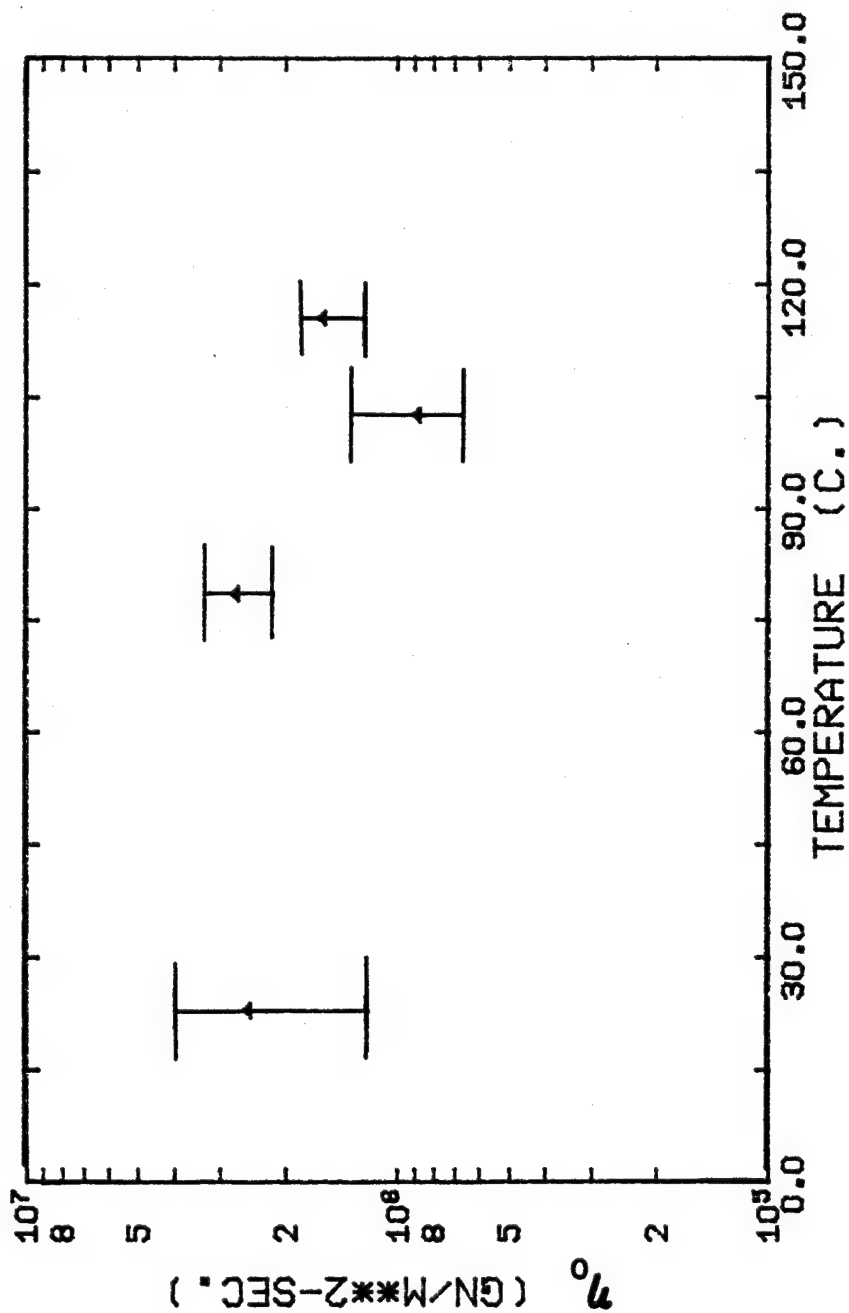


Figure G-3 The long term dashpot viscosity vs. temperature for all batches

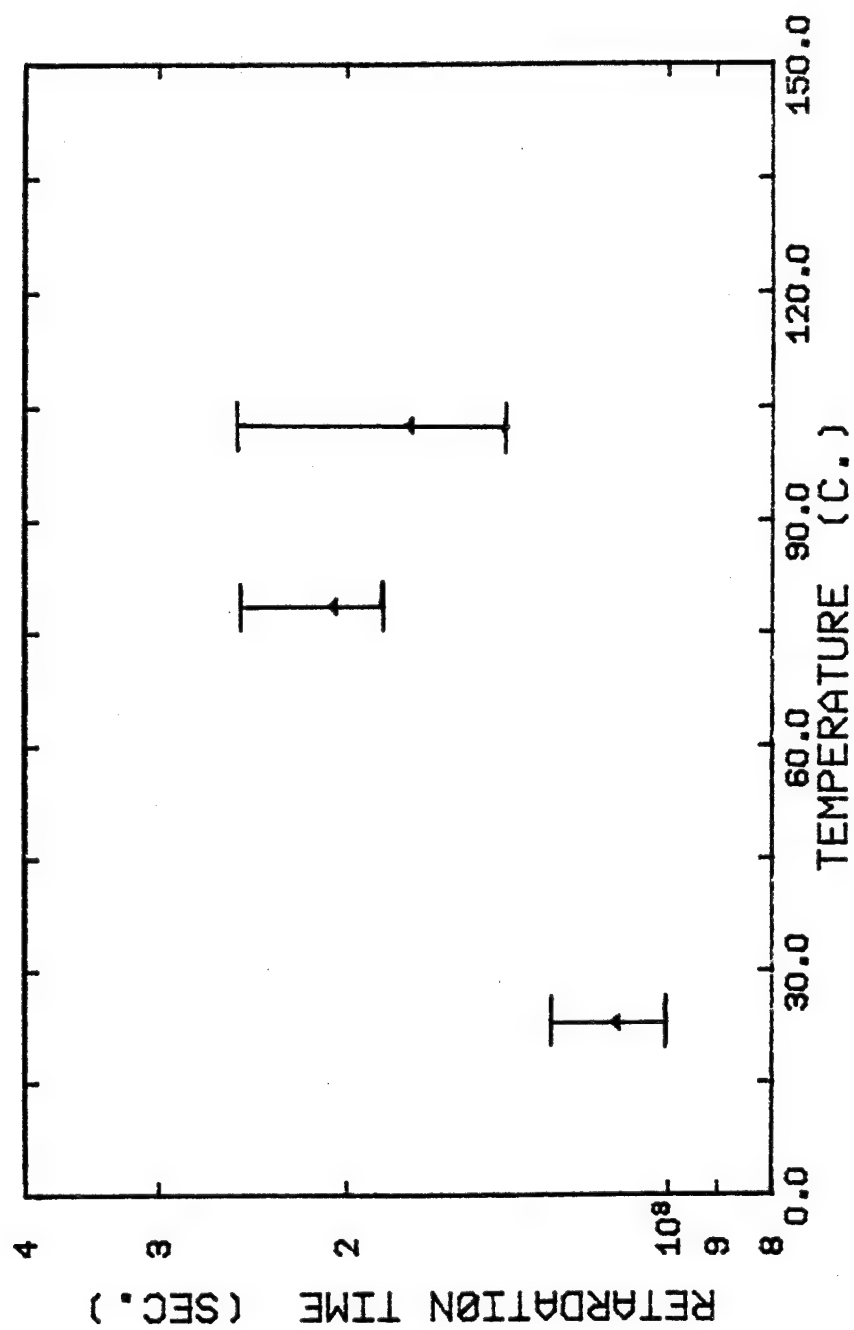


Figure G-4 Retardation time vs. temperature for batch 6-29-79-00

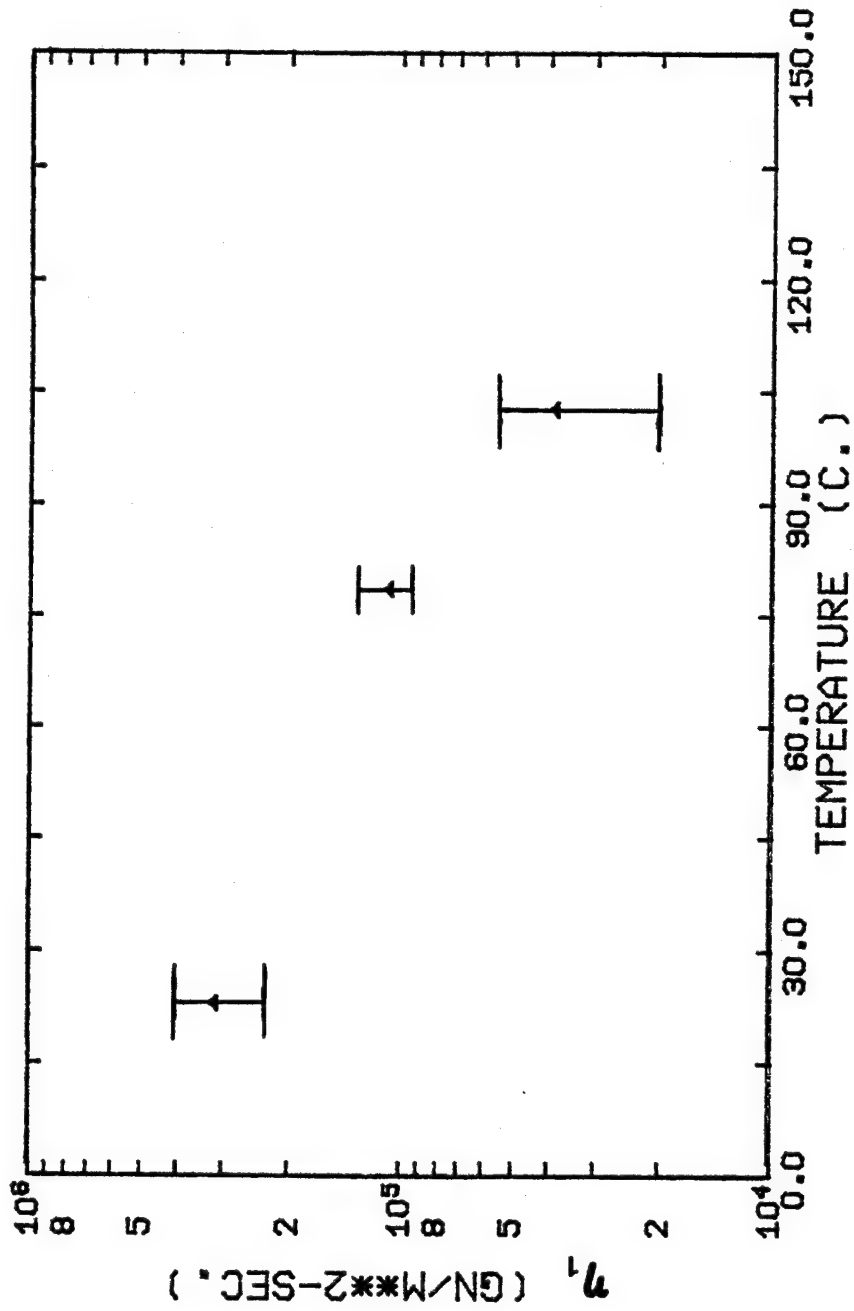


Figure G-5 The parallel dashpot viscosity vs. temperature for batch 6-29-79-00

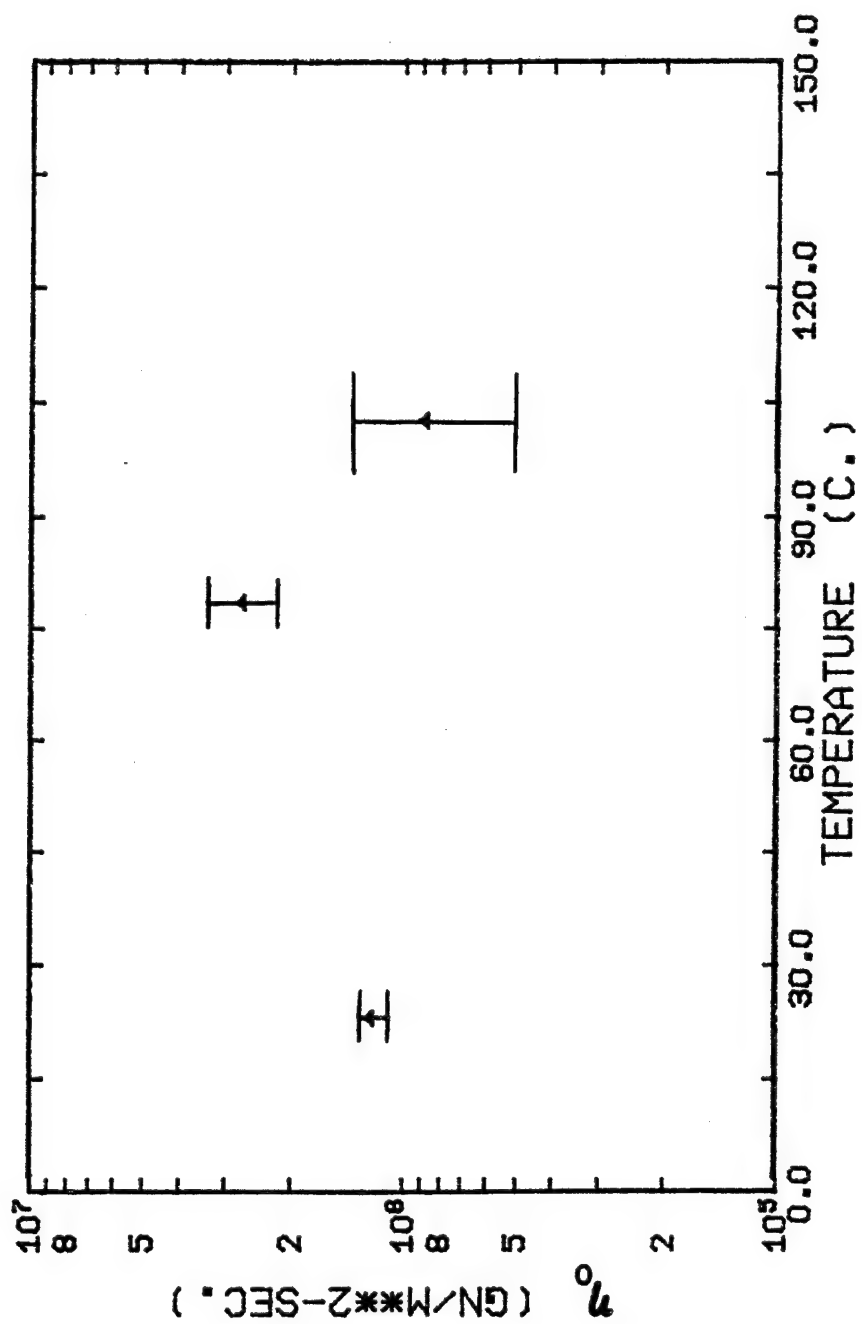


Figure G-6 The long term viscosity vs. temperature for batch 6-29-79-00

the context of the mechanical analogue) that the viscosity of the parallel dashpot and the associated "spring" modulus exhibit essentially the same dependence on temperature. It is not evident that these interpretations based on mechanical analogues provide insight to the molecular mechanisms underlying the creep phenomena.

The 4-parameter Voigt-Kelvin model could not be extended to fit the entire range of the creep data. The NLLS routine would not converge when creep data taken in excess of thirty thousand seconds was added to the data base. As noted in section 4.2.1, the long term creep behavior in the tertiary creep zone tends to "level out" as if an equilibrium compliance were being approached. This behavior implies that the term t/η_0 should be deleted from the Voigt-Kelvin model. The behavior of the resulting 3-parameter Voigt-Kelvin model is illustrated in figure G-7.

The deterioration of the overall quality of the fit is evident upon comparison with the fit obtained by the 4-parameter model illustrated in figure 4.2.2-2. The 3-parameter form of the Voigt-Kelvin model gives extrapolated values for J_0 which are much larger than the error estimates for J_0 . This truncated model smooths out the transition between the primary and secondary creep zones

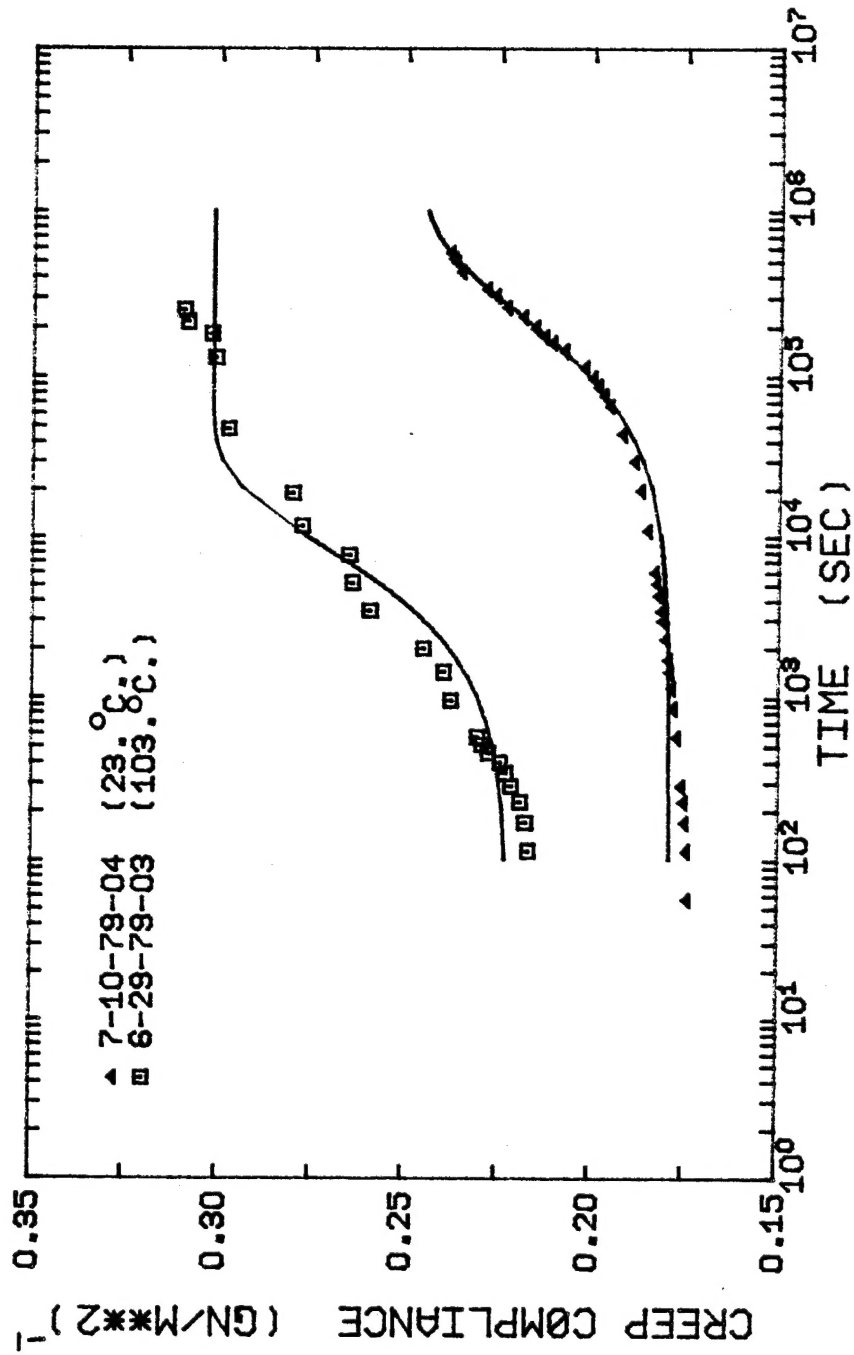


Figure G-7 The Voigt-Kelvin model vs. the creep data of the 3501-6 resin over the entire time range of the test

and predicts an equilibrium compliance at shorter times. These results indicate that the 3-parameter Voigt-Kelvin model can at best provide a lower limit to creep behavior.

In contrast, the 3-parameter power law model adequately represents the data at short times (as shown in figure G-8). At long times, the 3-parameter model tends to overestimate the creep behavior. Neither model could be used to fit creep data taken at temperatures in excess of 100°C.

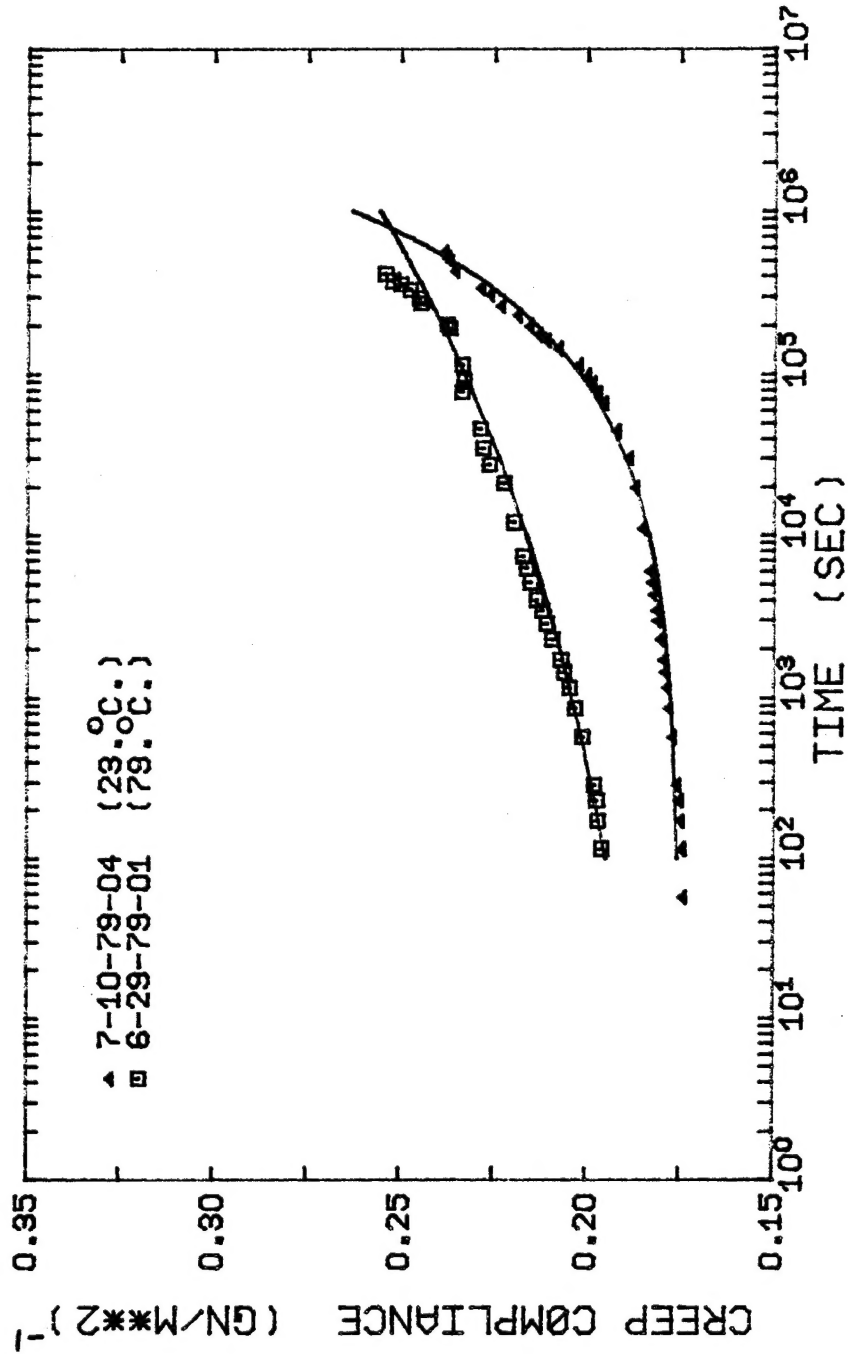


Figure G-8 The power law model vs. the creep data of the 3501-6 resin over the entire time range of the test